UNIVERSITY OF LONDON THESIS

Degree PhD Year 2007 Name of Author BUCHAN, Nina Elizabeth

The Regulation Of Convergent Extension During Gastrulation In Zebrafish

Nina Elizabeth Buchan

In submission for the degree
of Doctor of Philosophy
November 2007

Department of Anatomy & Developmental Biology
University College London

ProQuest LLC
789 East Eisenhower Parkway
P.O. Box 1346
Ann Arbor, MI 48106-1346

Declaration

I, Nina Elizabeth Buchan, confirm that the work presented in this thesis is my own. Where information has been derived from other sources, I confirm that this has been indicated in the thesis.

Acknowledgements

I would like to thank my primary supervisor Dr. Masa Tada, secondary supervisor Prof. Steve Wilson, post-doc. Dr. Masa Kai and former PhD student and friend Dr. Filipa Carreira-Barbosa. I am indebted to Chi-Bin Chien (Utah, USA); Sam England and the Adams lab (Cambridge, UK); the Heisenberg lab (Dresden, Germany); Vicky Prince (Chicago, USA); Miguel Concha and Andy Oates. I would also like to thank our 2004 undergraduate student Christine Yang and our new RA Kyoko Takatsu for work on *airbag*; the UCL Data Analysis team; the Irving Lab; the Clarke Lab; the Developmental Genetics Labs, CRUK; Isaac Bianco for his limitless honesty and contribution to work on *Slit* and *Robo*; Tom Hawkins for consistent sound advice; Matthias Carl and Jenny Regan for sharing their enormous laterality knowledge; and the rest of the Wilson lab past and present for their continued support and friendship.

Special thanks to Susan Evans, Les Dale, Karl Swann, Dave Whitmore, Martin Stanton & Marg Glover for much-appreciated help, advice and inspiration; Carole Wilson & the UCL Zebrafish Facility staff past and present, without whose hard work none of this would be possible; and lastly but most importantly, Wilson Lab miracle-worker Doreen Bailey, a true friend whose capacity for providing tea and listening to me whinge surely ought to earn her some sort of medal.

That I am able to complete this Ph.D. after the experiences of the past four years is a tribute to the amazing friends and family who have gone to extraordinary lengths to inspire and support me. From the bottom of my heart, thank you to: Mum, Dad & Carl, Martin Dooyes, Sam Arthur, Mabel, Polly Smith, Kate Hopwood & family, Emily & Rob Baulk, Matt Harwood, Dee Harding, Paul Spendley, Chris Copperwheat, Alex Ullermayer, Janette Harper, Bob & Sarah Fitzsimmons, Caz Frener, Will Norton, Carol Irving, Kyoko Hashimoto, Rachel Joynes, Ellen Dickens, Ian Warren, Nina Lyon, Helen Simons & family, Caroline Frener, Allan Witherick, Dorothy & Kor Newhouse, Edna & Sandy Buchan, Peter, Kirsten, Anja & Maja Buchan and the rest of the Buchans, Bakers & Bardens, Derek Dudley, Wendy Birch & the DR staff, Lynn, Freda & Jan, Rosemary Fletcher, Karen Greenway, Jim Maple, Sue Robinson, John Batten, Joe McFadden and Al Bowley.

It is also a tribute to those amongst my friends and family who died before their time, whose lives enriched my own and whose loss made me struggle harder: amongst them Jon Fitzsimmons, Chris Andrew, Brian Ruth and Peter Fitzsimmons. I owe the biggest debt of all to my Mum, best friend and reason for all my endeavours, who died suddenly aged 56 on 2nd March 2006. I dedicate this thesis to her.

Bravado

Have I not walked without an upward look
Of caution under stars that very well
Might not have missed me when they shot and fell?
It was a risk I had to take -- and took.

Robert Frost

Abstract

Coordinated cell movements during zebrafish gastrulation shape the embryo, forming three germ layers and establishing the embryonic body plan. Through convergent extension (CE) movements, mesodermal and neurectodermal cells intercalate at the dorsal midline, extending the anteroposterior axis. CE has been shown to be regulated by non-canonical Wnt signalling, homologous to planar cell polarity (PCP) signalling in *Drosophila*. In this thesis, I undertook several different approaches to understand the molecular mechanisms by which non-canonical Wnt/PCP signalling regulates CE.

Firstly, I characterised the novel PCP gene *pk1b*, one of three zebrafish homologues of the PCP gene *prickle* (*pk*). *pk1a* was shown to regulate CE. Like *pk1a*, *pk1b* is expressed during gastrulation. Abrogation of *pk1b* function enhances CE defects in the non-canonical Wnt/PCP pathway mutants *silberblick/wnt11* (*slb*) and *trilobite/stbm* (*tri*).

Secondly, I investigated the hypothesis that non-canonical Wnt signalling interacts with the *Drosophila* axon-pathfinding ligand Slit and its transmembrane receptor Robo in regulating CE. The zebrafish homologues *slit1a*, *slit2*, *slit3*, *robo1*, *robo2* and *robo3* are expressed during gastrulation, while gain of function of *slit2* in zebrafish was shown to severely disturb CE movements. Abrogation of *slit1a*, *slit2*, *robo2* and *robo3* function via morpholino knockdown and a dominant-negative approach yielded CE phenotypes in wildtype embryos and enhanced CE defects on non-canonical Wnt/PCP mutant/morphant backgrounds, suggesting that non-canonical Wnt/PCP and Slit/Robo signalling pathways cooperate in the context of CE.

Finally, I characterised a mutant identified in a screen for dominant enhancers of *slb* that we have provisionally named *airbag* (*abg*). Homozygous *abg* embryos exhibit a slightly shorter body axis and thickened yolk extension. The *pk1a, pk1b* and *stbm* morphant phenotypes are enhanced on the *abg* background. I explored the *abg* phenotype in contexts separate to CE prior to the mapping of this mutation.

Table of Contents

Index of Figures

Chapter One

Chapter Two

Chapter Three

Chapter Four

Chapter Five

Chapter Six

Index of Tables

Index of Abbreviations

Used in this thesis, alphabetically arranged.

abl	*abelson*
abg	*airbag* mutant (also known as *EnhC132*)
ANC	Actin nucleating centre
AP	Alkaline phosphatase
arm	*armadillo* (also known as *ß-catenin* in vertebrates)
ast	*astray* mutant
BBR	Boerringer blocking reagent
BCR	Blastocoel roof
bHLH	basic helix-loop-helix
BMP	Bone morphogenetic protein
bp	base-pairs, bases
BPL	Blastoporal pigment line
Bra	Brachyury
C	C-terminus or carboxy terminus
CA	Constitutively active
Ca^{2+}	Calcium
CamKII	Ca^{2+}/Calmodulin-Dependent Kinase II
CAAX	prenylation motif
Cdc42	*cell division cycle 42*
cDNA	complementary DNA
CE	Convergent Extension
chd	*chordin*
chm	*choroideremia* mutant
CIIS	C-terminal prenylation motif
cmlc2	*cardiac myosin light chain 2*
CNS	Central nervous system
comm	*commissureless*
cyc	*cyclops* mutant
Da	Daltons

daam1	*dishevelled-associated activator of morphogenesis*
DAB	3,3' Diaminobenzidine
dak	*dackel* mutant
DEP	Domain of modular Dsh protein
DIG	Digoxygenin
din	*chordino*
DIX	Domain of modular Dsh protein
dlx3	*distal-less homeobox 3*
DNA	deoxyribonucleic acid
DMZ	Dorsal marginal zone
Dpf	Days post fertilisation
dkk	*dickkopf*
DMSO	Dimethyl sulfoxide
DN	Dominant negative
dpp	*decapentaplegic*
dsh	*dishevelled*
DTT	Dithiothreitol
dub	*duboraya* mutant
ECD	Extracellular domain
ECL	Enhanced chemiluminescence
E. coli	*Escherichia coli*
EGF	Epidermal growth factor
ena	*enabled*
ENU	Ethylnitrosourea
EMT	Epithelial-to-mesenchymal transition
emx1	*empty spiracles homeobox 1*
EST	Expressed sequence tag
EVL	Enveloping layer
ext2	*exostosin2*
FGF	Fibroblast growth factor
fmi	*flamingo* (also known as *starry night* (*stan*) and *celsr*)
FN	Fibronectin

foxa3	*forkhead box a3* (also known as *fkd2* or *forkhead2*)
fy	*fuzzy*
fz	*frizzled*
g	grams
GFP	Green fluorescent protein
gsc	*goosecoid*
GSK-3	*glycogen synthase kinase 3*
GTP	Guanosine triphosphate
H_2O	Water
H_2O_2	Hydrogen peroxide
hep	*hemipterous mutant*
HEPES	4-(2-hydroxyethyl)-1-piperazineethanesulfonic acid
hgg1	*hatching gland 1*
HI	Heat-inactivated
hmgcr1b	*3-hydroxy-3-methylglutaryl-Coenzyme A reductase 1b*
Hpf	Hours post fertilisation
HS	Heperan sulphate
HSPG	Heperan sulphate proteoglycan
Hyb	Hybridisation buffer
ICD	Intracellular domain
ICM	Intermediate cell mass
Ig	Immunoglobulin
in	*inturned*
IMZ	Involuting marginal zone
JNK	Jun N-terminal Kinase
k	kilo
kny	*knypek/glypican4/6* mutant
KOH	Potassium hydroxide
KV	Kupffer's vesicle
l	litres
LB	Luria-Bertani culture broth
LIM	Domain found in and named after Lin 11, Islet-1 and Mec 3 genes

LWR	Length-to-width ratio
m or μ	micro
M	Moles, molar
MAB	Maleic acid buffer
MAPK	Mitogen-activated protein kinase
MHB	Midbrain-hindbrain boundary
MIB	Mediolateral intercalation behaviour
MIFs	Mesoderm inducing factors
mil	*miles apart* mutant
MO	morpholino
mRNA	messenger RNA
mwh	*multiple wing hairs*
MZ	Maternal-zygotic
n	nano
N	N-terminus or amino terminus
NaOAc	Sodium hydroxyacetate
NGS	Normal goat serum
NSB	Notochord-somite boundary
NTD	Neural tube defect
nVII	Facial or seventh cranial nerve
ntl	*no-tail*
NTP	nucleoside triphosphate
OD	Optical density
ord	*off-road/flamingo2* mutant
p	pico
papc	*paraxial protocadherin*
pax2.1	*paired box gene 2.1*
PBS	Phosphate-buffered saline solution
PCP	Planar cell polarity
PCR	Polymerase chain reaction
PDGF	Platelet derived growth factor
PDZ	Domain of modular Dsh protein

PET	Domain found in and named after Prickle, Espinas and Testin
PFU poly	DNA polymerase originating from *Pyrococcus furiosus*
PGCs	Primordial germ cells
PI3K	Phosphoinositide 3-kinase
PIP_3	Phosphoinositide 3,4,5-trisphosphate
pk	*prickle*
PK	Proteinase K
PKB	Protein kinase B
PKC	Protein kinase C
ppt	*pipetail/wnt5b* mutant
ptc	*patched*
PTU	1-phenyl-2-thiourea
PFA	Paraformaldehyde
R	Rhombomere (hindbrain)
R	Rhabdomere (fly eye)
REP	Rab escort protein
RGD	Arg-Gly-Asp sequence contained within FN
Rig-1	*retinoblastoma inhibiting gene 1*
RNA	ribonucleic acid
Robo	Roundabout
ROCK	Rho-associated kinase
RPE	Retinal pigment epithelium
RPM	Revolutions per minute
RT PCR	Real-time PCR
rx3	*retinal homeobox gene 3*
S1P	Sphingosine-1-phosphate
SB	Splice-blocking
scl	*stem cell leukaemia*
SDS PAGE	sodium dodecyl sulfate polyacrylamide gel electrophoresis
shh	*sonic hedgehog*
slb	*silberblick/wnt11* mutant
smad	SMA and MAD family gene, *Drosophila*

SMO	Spemann-Mangold Organiser
smo	*smoothened*
smu	*smoothened* mutant
sna	*snail*
spaw	*south-paw*
sple	*spiny-legs*
SSC	sodium chloride/sodium citrate solution
STATs	Signal Transducers and Activators of Transcription
stbm	*strabismus* (encoded by *trilobite* mutant; also known as *van gogh*)
Taq poly	DNA polymerase originating from *Thermus aquaticus*
Tcf-3	*transcription factor 3*
TGF-ß	Transforming growth factor beta
TM	Transmembrane
tri	*trilobite/stbm* mutant
UV	Ultraviolet
V	Volts
VAZ	Vegetal alignment zone
VegT	Vegetal T-Box (also known as *antipodean*, *xombi* and *brat*)
Vg1	Vegetal 1
Wg	Wingless
Wnt	Wg and Int family genes, *Drosophila*
WT	Wildtype
X	*Xenopus*
Xnr	*Xenopus* nodal-related
YFP	Yellow fluorescent protein
YSL	Yolk syncytial layer
zw3	*zeste-white 3*

Chapter One

General Introduction

Defining Gastrulation

The developing embryo is comprehensively rearranged during *gastrulation*, a series of highly coordinated movement and patterning events. Different species come in a wealth of shapes and sizes and the physical strategies used to bring about gastrulation vary widely across the animal kingdom. The spherical blastulae of the zebrafish, *Danio rerio*, and the African claw-toed frog, *Xenopus laevis*, are transformed from simple cell masses atop a nutritive yolk to three concentric germ layers surrounding an internalised yolk through a combination of internalisation, epiboly and convergent extension movements. The ectoderm is outermost, giving rise to the epidermis and neural tissues; the mesoderm lies beneath this, giving rise to the muscles, skeleton, heart, blood and urogenital system, while the endoderm is innermost, giving rise to the gut and associated organs.

Maternally provided determinants guide the embryo through early cleavages prior to the activation of the zygotic genome at the mid-blastula transition. Microtubule driven asymmetries in determinants provide positional information key to the creation of the dorsoventral axis and organising centres responsible for patterning the embryo. Concurrently, the forming mesoderm passes under the blastoderm margin, while epiboly movements spread the germ layers, covering and internalising the yolk. In this way, patterning events are intimately related to cell movements during gastrulation. However, the genetic regulation of cell movements during gastrulation is less well understood.

In this thesis, I analyse the expression and function of *pk1b*, a novel splice variant of *pk1*, one of three zebrafish orthologues of the *Drosophila* planar cell polarity gene *prickle* (*pk*) and a known regulator of zebrafish convergent extension movements. I investigate the role of zebrafish orthologues of the *Drosophila* axon pathfinding genes *slit* and *robo*, now understood to be critical to many instances of directed cell migration in both vertebrate and invertebrates, in the regulation of zebrafish convergent extension movements. Additionally, I characterise the phenotype of a novel convergent extension mutant, here provisionally named *airbag* (*abg*), that enhances the impaired convergent extension movements of the zebrafish *silberblick/wnt11* (*slb*) mutant. Using a variety of approaches, I aim to further our understanding of the genetic regulation of convergent extension movements during zebrafish gastrulation.

Vertebrate Gastrulation Movements

Gastrulation Movements in *Xenopus laevis*

Much of our knowledge of gastrulation movements was gained through the study of Amphibian cell and tissue movements in the African claw-toed frog, *Xenopus laevis*. Rapid, *ex utero* development of large, spherical embryos, in which rapidly dividing cells of the pigmented animal pole sit atop slowly dividing vegetal yolk cells, make *Xenopus* a model well suited to the study of gastrulation (Developmental Biology: Gilbert, 2000; From Egg to Embryo: Slack, 1991).

Bottle Cell Formation

Gastrulation movements begin rearranging the *Xenopus* blastula at stage 10. Historically, the initiation of gastrulation was thought to be the formation of a depression approximately 180° from the site of sperm entry at the site of blastopore formation, in the superficial vegetal *involuting marginal zone* (*IMZ*) (Gilbert, 2000; Hardin & Keller, 1988). There, *bottle cells* acquire a characteristic bottle shape in a two-step process of apicobasal elongation followed by apical constriction, the mechanism of which is poorly understood. The shape changes that define bottle cells could be cell autonomous; alternatively, they could be initiated by environmental stimuli such asymmetrical exposure to the alkaline fluid of the *blastocoel*, a fluid filled cavity in the animal hemisphere, to which their basal but not apical surfaces are exposed (Hardin & Keller, 1988; Keller *et al.*, 2003). Dense fibres visible at the apical pole of bottle cells could provide evidence of a contractile mechanism capable of altering the cytoarchitecture in response to such environmental stimuli (Keller *et al.*, 2003). Pigment accumulates in the apical poles of bottle cells, allowing their visualisation first as a grey pit in the IMZ, then, as bottle cell formation spreads in a dorsal to ventral wave around the marginal zone to form the *blastoporal groove*, as a circumferential pigmented line demarcating the blastopore lip, known as the *blastoporal pigment line* (*BPL*) (Hardin & Keller, 1988).

It was hypothesised that bottle cells invade the blastocoel, stimulated by the alkalinity of the blastocoel fluid, and in doing so initiate mesoderm involution by dragging firmly adherent surrounding tissues with them. However, excising bottle cells during early gastrulation results in normal gastrulation movements in these embryos: only part of the peripheral archenteron which bottle cells normally give rise to is lacking (Hardin & Keller, 1988). Bottle cells do assist in the initiation of involution at the IMZ, but their role is context dependent. In culture, isolated bottle cells contract

autonomously but uniformly, implying their characteristic bottle shape is imposed upon them by resistance from surrounding tissues (Hardin & Keller, 1998). Bottle cell contraction *in vivo* is resisted by the bulk of the vegetal cell mass whilst increased cell adhesion amongst bottle cells creates an anchored centre, distorting surrounding tissues (Hardin & Keller 1988; Keller *et al.*, 2003). These forces are amplified by the cytoskeletal alignment brought about by apicobasal elongation at bottle cell formation (Keller *et al.*, 2003). The outcome is that adjacent tissues are deformed by bottle cell formation, and the IMZ is displaced vegetally (Hardin & Keller, 1988). This distortion generated at the blastopore lip creates *hoop stress* that will drive the internalisation of the yolk and contribute to mesoderm involution, two major goals of gastrulation (Keller *et al.*, 1992; Keller *et al.*, 2000; Winklbauer & Keller, 1996).

The expression of constriction behaviour by bottle cells is channelled by resistance from surrounding tissues to provide the force for dramatic cell rearrangements. However, bottle cells are unique to amphibians, and although reminiscent of invagination of the mesoderm and endoderm during *Drosophila* gastrulation, bottle cell formation may not be a reliable indication of the initiation of gastrulation in all species (Hardin & Keller, 1988; Keller *et al.*, 2003; Leptin, 1995).

Vegetal Rotation

Tissue movements initiated at the onset of gastrulation, such as active, intrinsic movements within the vegetal cell mass, drive the future endoderm to undergo *vegetal rotation*, bringing about internalisation of the yolk and resulting in a passive rotation of the outer marginal zone (Keller *et al.*, 2003; Winklbauer & Schürfeld, 1999). The significance of these endodermal movements was

overlooked in the past, misinterpreted as single cell ingression of endodermal cells or as passive movements resulting from forces generated at the IMZ (Keller *et al.*, 2003).

Vegetal rotation carries the former vegetal-most endoderm of the blastula into a new location beneath the blastocoel roof of the gastrula's animal hemisphere, where it will become the prospective anterior mesendodermal structure known as the *cleft of Brachet*. Vegetal rotation movements concomittantly bring the forming mesoderm into position beneath the *blastocoel roof* (*BCR*) in a manner complementary to the constriction of the blastopore lip, facilitating the directional migration of the forming mesoderm internally across the blastocoel roof (Keller *et al.*, 2003; Winklbauer & Schürfeld, 1999). These movements presage subsequent gastrulation movements but are independent of bottle cell formation, the historically accepted visible onset of gastrulation. Vegetal rotation has important consequences for the movement and patterning events to follow, both in terms of the tissues that are brought into apposition with one another, and the inductive signals that are distributed by them, and because of this, vegetal rotation has become known as *the cryptic internal onset of gastrulation* (Nieuwkoop & Florschütz, 1950: cited in Keller *et al.*, 2003).

Mesoderm Induction

Mesoderm formation is thought to be the major driving force of gastrulation. Mesoderm inducing signals originate from the vegetal mass, where vegetal blastoderm cells release inductive signals that act upon the equatorial cells of the animal hemisphere, instructing them to adopt a mesodermal fate and establishing a belt of mesoderm at the equator of the embryo (Conlon & Smith, 1999; Green *et al.*, 1992; Harland & Gerhart, 1997; Kimelman *et al.*, 1992; Kurth & Hausen, 2000). 'The *TGF-ß*, *FGF* and *Wnt* pathways are critical for mesoderm induction, activating downstream signal transducers

including the *smad*, *MAPK* and *ß-catenin* pathways (Amaya *et al.*, 1993; Dale *et al.*, 1993; Dyson & Gurdon, 1997; Green *et al.*, 1992; Heasman, 1997; Heasman, 2006; Kimelman *et al.*, 1992; Kurth & Hausen, 2000; Schulte-Merker *et al.*, 1994). In the past, *TGF-ß* and *FGF* superfamily members were thought to activate these downstream pathways and initiate mesoderm induction and axis specification by means of anteroposterior or dorsoventral gradients; however, evidence for the existence of such gradients was elusive (Heasman, 1997; Heasman, 2006; Kimelman *et al.*, 1992; Kurth & Hausen, 2000; Lustig *et al.*, 1996).

The *TGF-ß* superfamily member *activin* is capable of inducing a spectrum of mesodermal cell types from cultured blastoderm cells in a dose-dependent manner (Green *et al.*, 1992). *FGFs* are not capable of inducing the same spectrum of mesodermal cell types *in vitro*, but instead alter the dose parameters necessary for each *activin*-induced mesodermal cell type (Green *et al.*, 1992). Signalling pathways such as the Wnt signalling pathway could also contribute to this local regulation of *activin*-based mesoderm induction (Christian *et al.*, 1992), and together these interactions fine-tune the activation of downstream pathways key to the graded induction of mesodermal types (Green *et al.*, 1992).

VegT is a maternally provided signal inherited by vegetal cells that activates endoderm specific genes, *mesoderm inducing factors* (*MIFs*) such as *Xnr5* and *Wnt8*, and the BMP/Wnt antagonist *cerberus* (Heasman, 2006; Kofron *et al.*, 1999; Xanthos *et al.*, 2001). Only *Xnr*s, not *FGFs* or *activin*, are sufficient to rescue both the endodermal and mesodermal functions of *VegT* when its expression is abrogated, so it is through *Xnrs* that *VegT* orchestrates mesoderm induction (Agius *et al.*, 2000; Heasman, 2006; Kofron *et al.*, 1999; Xanthos *et al.*, 2001). The *TGF-ß* family member *Vg1* shares *VegT*'s ability to activate the BMP antagonists *chordin*, *noggin* and *cerberus*, but is insufficient to

rescue *VegT* loss of function (Heasman, 2006). Downstream of *Xnrs*, T-Box genes such as *Xenopus Brachyury* (*XBra*) are expressed equatorially, where they regulate zygotic FGF signalling and feed back in a regulatory loop to modulate their expression. Although required for normal embryonic development, the role of *activin* in this chain of interactions is complicated: *activin* regulates the expression of dorsal zygotic genes such as *chordin* and *goosecoid*, and loss of function of *activin* results in elevated levels of *Xnr2*, suggesting that *activin* normally negatively interacts with *Xnrs* (Heasman, 2006; Piepenburg *et al.*, 2004). Loss of function of *activin* also results in decreased levels of the *Vg1*-related *derriere*, which in turn regulates the expression of specific pro-mesodermal *FGFs*. Through this complex network of events, *Xnrs*, *activin*, *derriere*, *Vg1* and many other factors cause the activation of signal transducers, transcriptional activators and repressors and cell cycle regulators in prospective mesodermal cells.

Mechanisms that antagonise mesoderm induction restrict mesoderm formation to the equatorial region, allowing the ectoderm to take a different path. Wnt genes, believed to be the original dorsal determinants, come to be expressed on the future dorsal side of the embryo in response to the localisation of maternally provided factors. At mesoderm induction, expression of *wnts* such as *wnt11* in the prospective dorsal side of the embryo restricts the expression of *BMP* antagonists such as *noggin* and *chordin*, excluding *BMP* expression from the dorsal animal quadrant of the embryo with the result that *BMP*-expressing regions of the ectoderm adopt an epidermal fate, while in the dorsal animal region, *BMP* antagonists and FGF signalling combine to induce a non-epidermal, neural specification.

Promiscuity of mesoderm inducing signals and their receptors has made interpretation of the molecular mechanisms of mesoderm induction difficult (Conlon & Smith, 1999; Harland & Gerhart,

1997; Heasman, 1997; Heasman, 2006). What is certain is that the induction of mesoderm is intimately related with the onset of gastrulation movements: local overexpression zygotic *VegT* in the animal hemisphere results in ectopic bottle cell formation and invagination of the epithelium, resembling events at the blastopore lip at the onset of gastrulation (Kurth & Hausen, 2000; Lustig *et al.*, 1996). Furthermore, treating animal cap explants (see Symes & Smith, 1987 for details on animal cap assay) with *activin in vitro* generates cell movement and rearrangement that results in their elongation, a mode of cell behaviour associated with gastrulation movements (Conlon & Smith, 1999; Harland & Gerhart, 1997). It is therefore difficult to separate movement and patterning when considering gastrulation.

Mesoderm Involution

Genes downstream of both mesoderm induction and blastopore lip formation collaborate to drive mesoderm involution at the IMZ. The BPL demarcates a hoop of constricted bottle cells above which the distorted IMZ bulges and is compelled by factors including the position of the marginal zone on the spherical embryo, the balance of constriction forces and of resistance from the vegetal mass, to roll in on itself or *involute* (Hardin & Keller, 1988; Keller *et al.*, 1992; Keller *et al.* 2000). Involution at the IMZ continues in a dorsal to ventral wave, prospective head mesoderm involuting first, followed by axial mesoderm, and ventral-most mesoderm involuting last (Winklbauer & Keller, 1996). Following this, involuting mesoderm undergoes active, directional migration along the blastocoel roof towards the animal pole as a cohesive group of cells of *involuting identity*, incapable of reintegrating with mesoderm of *pre-involuting identity*. Cell division does not account for the movement of the mesoderm during gastrulation: only early involuting anterior mesoderm shows mitotic divisions as gastrulation progresses, whereas there is no proliferation in dorsal, later involuting mesoderm (Saka

& Smith, 2001). The outcome of involution is that the mesoderm comes to lie between the ectoderm and endoderm, a process vital not only for the developing body plan of the embryo but also because the forming mesoderm is brought into proximity with new tissues, on which later signalling events will rely.

Epiboly

Epiboly movements spread rearranging embryonic tissues over the yolk with the aim of closing the blastopore. The contractile force created by IMZ-driven tissue distortion is balanced by resistance from the vegetal cell mass (Hardin & Keller, 1988). Active cell intercalation in both the neurectoderm and mesoderm becomes essential for the completion of gastrulation. In the first half of gastrulation, radial intercalation during epiboly helps compress the germ layers as they spread over the vegetal mass, generating fewer cell layers of greater surface area (Shih & Keller, 1992a; Wilson & Keller, 1991). The resulting extension of tissues is biased towards the anteroposterior axis to cover the yolk.

It is unclear to what extent cell proliferation contributes to epiboly movements, although mitotic divisions occur in ectodermal tissue throughout gastrulation (contrary to dorsal involuting mesoderm), while pre-gastrulation inhibition of the cell cycle results in severely disrupted gastrulation movements. Although mesoderm involution is not dependent on cell division, it is possible that epiboly is compromised by low cell number (Cooke, 1973: cited in Saka & Smith, 2001). Time-lapse analyses of cultured mesodermal explants reveal that radial cell stirring and repacking, resulting in deep mesodermal cells integrating superficially to create a thinner array, is prevalent soon after the initiation of gastrulation but decreases towards the middle of gastrulation, when it is superseded by *mediolateral intercalation behaviour* (*MIB*) (Wilson & Keller, 1991).

Convergent Extension

During late gastrulation, cells of the presumptive somitic and notochordal mesoderm and of the future spinal cord and hindbrain in the posterior neural plate actively intercalate with their neighbours, converging on the dorsal midline. These evolutionarily conserved movements, termed *convergent extension* (*CE*) movements, are used reiteratively throughout development, in processes as diverse as gastrulation, and neurulation, to narrow an array of cells in one axis and subsequently extend them in the anteroposterior axis (Wallingford *et al.*, 2002a). In the context of gastrulation, convergent extension movements contribute to the extension of the embryonic body along the anteroposterior axis.

CE requires major changes in cell shape, adhesion and motility, summarised in the following steps: polarisation, alignment, protrusivity, traction and intercalation. At the start of CE in *Xenopus*, mesodermal cells are not polarised and frequently extend filoform projections in random orientations that are progressively pruned through *contact inhibition* as CE proceeds, leaving only mediolaterally orientated projections (Shih & Keller, 1992a; Shih & Keller, 1992b). Highly polarised along the mediolateral axis, these cells exhibit *bipolar protrusive activity* (Keller, 2000; Shih & Keller, 1992a; Shih & Keller, 1992b). In the neurectoderm, cells display heterogeneous protrusive behaviours depending on their proximity to the axial mesoderm. Observation of *deep neural explants* (neurectoderm without underlying mesoderm) revealed that superficial neural ectodermal cells show *monopolar protrusivity* directed towards the notoplate-floorplate region in the dorsal midline (Elul *et al.*, 1997; Elul & Keller, 2000; Keller *et al.*, 2000). *Deep neural-over-mesoderm explants* demonstrated that deeper neurectodermal cells show a bipolar protrusivity more reminiscent of

mesodermal cells (Elul *et al.*, 1997; Elul & Keller, 2000). This raises the possibility that the mesoderm may be capable of organising cell behaviours in the overlying neurectoderm (Elul & Keller, 2000).

In two dorsolateral groups of cells in the anterior mesoderm, cells express mediolaterally orientated bipolar protrusive behaviour, termed MIB. *Shaved open-faced explants* (open-faced deep mesoderm-on-endoderm, superficial mesoderm removed), and *deep [mesodermal] cell explants* (deep mesoderm minus underlying endoderm), allowed the visualisation of mesodermal cell behaviours during CE in a way that resembles the situation *in vivo* as closely as possible (Shih & Keller 1992a; Shih & Keller, 1992b). MIB spreads medially and posteriorly throughout the mesoderm, in an arc known as the *vegetal alignment zone* (*VAZ*) (Shih & Keller, 1992b). Cells in this region undergo autonomous shape changes, elongating by reducing their *length to width ratio* (*LWR*), and through this elongation are forced into alignment with one another (Keller *et al.*, 2000; Shih & Keller, 1992a; Shih & Keller, 1992b). The mesoderm stiffens as cells actively exert traction on their neighbours, using their projections to pull themselves between their neighbours and intercalate (Keller *et al.*, 2000; Shih & Keller, 1992a; Shih & Keller, 1992b). Bipolar protrusivity results in a more promiscuous style of intercalation, with a high degree of neighbour exchange (Keller *et al.*, 2000). Arcs of mesodermal stiffening and MIB progress medially and posteriorly, deforming surrounding tissues and contributing significantly to the remodelling of the embryo during gastrulation.

Shaved single layer *deep neural explants* have shown that neurectodermal cells also exhibit MIB autonomously but without the dramatic LWR changes seen in the mesoderm (Elul *et al.*, 1997; Elul & Keller, 2000). Neurectodermal cells display bursts of MIB and intercalate episodically, and perhaps because of this, generation of force and tissue stiffening during neurectodermal MIB is considered to have less of an impact on the distortion of surrounding tissues compared to the mesoderm (Elul *et*

al., 1997; Keller *et al.*, 2000). Although isolated neurectodermal explants intercalate promiscuously, experiencing high levels of neighbour exchange, neurectodermal cells in persistent contact with the mesoderm intercalate conservatively with their immediate neighbours (Elul & Keller, 2000). Furthermore, cells outside the notoplate-floorplate region pull between one another and intercalate, but cells of the notoplate-floorplate region adhere to and are towed by underlying converging mesodermal structures such as the notochord, corroborating the idea that through vertical expression of inductive signals and/or adhesion molecules, the mesoderm is capable of influencing neurectodermal cell behaviour during CE (Elul *et al.*, 1997; Elul & Keller, 2000; Keller *et al.*, 2000).

Mediolaterally orientated intercalation spreads throughout the marginal zone in these tissues, and it is this convergence rather than directional migration that creates a mediolaterally narrower array of cells (Keller *et al.*, 2000). Furthermore, the contribution of cell division to CE in *Xenopus* is considered to be negligible: cells of the post-involuting dorsal mesoderm undergo no mitotic division in the second half of gastrulation, and the rounding up typical of dividing cells is at odds with the cell polarisation, alignment and protrusive behaviours necessary for CE (Holtfreter, 1942: cited in Shih & Keller, 1992a; Cooke 1973: cited in Saka & Smith, 2001). Intercalation in the notochordal mesoderm is however assisted by a process known as *boundary-capture*, where cells that come into contact with the future *notochord-somite boundary* (*NSB*) exchange bipolar for monopolar protrusivity and intercalate within the boundary, extending it anteroposteriorly and encouraging neighbouring cells to follow suit (Keller *et al.*, 2000; Shih & Keller, 1992a; Shih & Keller, 1992b). As a consequence intercalation in the *dorsal marginal zone* (*DMZ*) and boundary-capture, both the mesoderm and neurectoderm extend in the anteroposterior axis (Elul *et al.*, 1997; Keller, 2000; Shih & Keller 1992a). Cells undergoing CE perceive the balance of force and resistance within tissues and retain the capability to retract their projections and move to areas of low traction to maintain tissue-wide

integrity (Keller *et al.*, 2000; Shih & Keller, 1992a). However, the mechanism of this perception is unclear, as CE does not depend upon the underlying endoderm or secreted substrate (Elul *et al.*, 1997; Shih & Keller 1992a; Winklbauer & Keller, 1996). Despite the paradox of simultaneously stiffened yet highly motile tissues, these observations suggest that alignment, MIB and the balance of forces and resistance provided by neighbouring tissues are interdependent in convergent extension. The mechanism of this interdependence is unknown, but it has been suggested that both planar and vertical signals generate this coordination. Factors regulating cell adhesion in both the mesoderm and neurectoderm such as Integrins and Protocadherins are candidates for these planar signals, while planar and vertical signals of mesodermal origin, for instance originating from Spemann's organiser or from the NSB, could influence the mesoderm in the plane of the tissue and potentially the overlying neurectoderm (Elul et al., 1997; Keller, 2000; Shih & Keller 1992b).

In summary, the endoderm in *Xenopus* that will form the archenteron invaginates and rotates while coincidentally, forming mesoderm involutes at the IMZ yielding three concentric germ layers. Epiboly thins these tissues through radial intercalation and spreads them vegetally over the vegetal mass. Posteriorly progressing arcs of MIB in both the mesoderm and neurectoderm during CE results in mediolateral intercalation in the dorsal midline, extending the anteroposterior axis. These movements generate hoop stress at the blastopore lip with the result of closing the blastopore, completing gastrulation and creating the basic body plan of the embryo.

Gastrulation Movements in the Zebrafish, *Danio rerio*

Zebrafish are a simple yet versatile model organism with wide applications in the field of developmental biology. Inexpensive to maintain and breed, these Teleost fish have a relatively short

generation time, reaching sexual maturity between three and six months of age. Zebrafish breed in a photoperiodic manner, a typical pair producing a few hundred spherical embryos every "sunrise", conditions that are easily mimicked. Surrounded by a protective chorionic membrane, zebrafish embryos undergo rapid *ex utero* development, making their harvest easy, fast and ethical, and facilitating observation and manipulation from the single cell stage.

Superior optical transparency, which can be prolonged with the pigment inhibitor PTU (see Appendix One), makes zebrafish embryos ideal for the complex *in vivo* imaging and cell tracking techniques now central to studies in gastrulation. Although zebrafish are not suited to the classical 'cut and paste' experiments of *Xenopus*, microinjection of mRNA or antisense oligonucleotide morpholinos, mosaic analysis of cell autonomy by cell transplantation, even dissociated cell culture, are equally possible (Nasevicius & Ekker, 2000; The Zebrafish Book, Westerfield, 2000). Furthermore, evolutionary conservation of key developmental genes links zebrafish genetics with established model organisms including *Drosophila*, *Xenopus*, and mammals. Mutagenesis screens in zebrafish have already yielded a large amount of information about the genetic control of developmental events, making zebrafish an adaptable and important tool in furthering our understanding of vertebrate development.

The Onset of Gastrulation in Zebrafish

Strategies used by cells to bring about gastrulation movements are similar in *Xenopus* and zebrafish, despite their evolutionary separation. In the zebrafish blastula, dividing *deep cells* of the embryonic blastoderm are covered by an *enveloping layer* (*EVL*) and sit on top of a dense yolk or *yolk syncytial layer* (*YSL*) containing nutrients and maternally provided signals necessary to begin development

which unlike *Xenopus,* consists of a large syncytium rather than individual yolk cells (Kane *et al.*, 1996; Kane *et al.*, 2005; Shimizu *et al.*, 2005). Zebrafish blastula cells are loosely distributed, undergo undirected short-range movements and change shape randomly, but when gastrulation begins cells compact together, increasing cell density (Concha & Adams, 1998). Epiboly movements, the first morphogenetic movement in Teleost organisms, spread this coherent sheet vegetally over the yolk cell (Kane *et al.*, 1996; Kane *et al.*, 2005). These movements are dependent on the cell autonomous, morphological division of the epiblast into an *exterior layer* and an *interior layer*, without which, the radial intercalations that spread and thin tissues undergoing epiboly occur abnormally (Kane *et al.*, 2005). Epiboly is also dependent upon the YSL, deep cells of the blastoderm and the EVL undergoing movements together: uncoupling of epibolic movements between these layers has lethal consequences for the embryo (Kane *et al.*, 2005; Shimizu *et al.*, 2005).

Mesoderm Involution in Zebrafish

The internalisation of the mesoderm begins at 50% epiboly or shield stage, although in zebrafish, migration of the mesendoderm under the *blastoderm margin* (the zebrafish equivalent of the blastopore lip) is achieved through a mode of movement known as *emboly*, less cohesive than involution in *Xenopus* but more coordinated than the single cell ingression of avian and mammalian embryos (Carmany-Rampey & Schier, 2001; Solnica-Krezel, 2005). In order to ingress in this way, prospective mesendodermal cells undergo an *epithelial-to-mesenchymal transition* (EMT) and begin behaving cell autonomously (Carmany-Rampey & Schier, 2001; Montero *et al.*, 2005). Axial mesenchymal cells that will give rise to structures like the notochord ingress as a tight group, while migrating paraxial mesenchymal cells are less closely associated (Montero *et al.*, 2005).

Convergent Extension in Zebrafish

During late gastrulation, convergent extension movements shape the zebrafish gastrula as in *Xenopus*. The morphogenetic outcome of zebrafish convergent extension – mediolateral narrowing and subsequent anteroposterior extension in the mesoderm and neurectoderm – closely resembles that of *Xenopus*. Explants of tissues undergoing CE from *Xenopus* and zebrafish both exhibit autonomous elongation, suggesting that like in *Xenopus*, zebrafish convergent extension is an active, force producing process that occurs autonomously within tissues (Tada *et al.*, 2002). However in *Xenopus*, extension is a direct consequence of convergence, brought about by mediolaterally biased bipolar protrusive behaviour pulling cells between one another, boundary capture anchoring converging cells at the midline, and cell repacking distributing these accumulating cells along the anteroposterior axis. In contrast in zebrafish, convergence and extension are separable. Mesodermal extension begins prior to convergence, driven by the animal migration of internalising mesoderm during early gastrulation (Sepich *et al.*, 2005). Cells converge upon the shield via directed cell migration from more lateral positions and undergo intercalation and rearrangement only when they reach the dorsal midline (Glickman *et al.*, 2003; Sepich *et al.*, 2005). Directed convergence in zebrafish begins slowly in ventrolateral regions, accelerating around the time of yolk plug closure and peaking at the start of somitogenesis (Jessen *et al.*, 2002; Sepich *et al.*, 2002). Similarly to *Xenopus*, cells in the dorsal midline become mediolaterally elongated and exhibit protrusive behaviour in the mediolateral axis, although the significance of the orientation of protrusive behaviour remains poorly understood, exemplified in *Xenopus*, where bipolar protrusivity in the mesoderm contrasts with monopolar protrusivity in the neurectoderm, yet convergent extension occurs in both tissues (Wallingford *et al.*, 2002a). In *Xenopus*, boundary-capture at the notochord-somite interface

contributes to intercalation at the midline after convergence and intercalation begins, however there is no evidence for similar cell behaviour at the NSB in zebrafish (Elul *et al.*, 1997; Elul & Keller, 2000).

Mitotic cell divisions occur throughout gastrulation in both zebrafish and *Xenopus*, but the contribution these divisions make to the extension of the body axis is an issue of contention. In the zebrafish blastula, divisions are randomly orientated, but as gastrulation progresses, cell division becomes polarised and most divisions are *planar*, occurring in the plane of the tissue, perpendicular to the orientation of elongation (Gong & Fraser, 2004, consistent with the observations of Concha & Adams, 1998). This is in opposition to the long-held idea that the mitotic spindle of dividing cells aligns with the long axis of the cell due to constraints of cell shape (Gong & Fraser, 2004). In the past, it was considered unlikely that planar cell division contributes significantly to extension of the anteroposterior axis, as normal gastrulation movements occur even when cell division is blocked (Kessel, 1960: cited in Concha & Adams, 1998). More recently, it was shown that most epiblast cells in the zebrafish gastrula divide orthogonally to the plane of elongation, and that disruption of key signalling events during gastrulation results not only in convergent extension defects but in randomised cell polarity and division orientation (Gong & Fraser, 2004). The significance of these cell divisions to the extension of the anteroposterior axis remains to be elucidated.

Despite the many differences between convergent extension in *Xenopus* and zebrafish, common elements in the behaviour of cells undergoing CE in both organisms, such as mediolateral alignment and intercalation, imply that aspects of convergent extension, and potentially their genetic regulation, are evolutionarily conserved.

Anterior Migration of the Prechordal Plate

In both *Xenopus* and zebrafish, convergent extension is not the sole cell movement extending the anteroposterior axis during gastrulation. CE is assisted by active, anterior migration of the head mesoderm (Wallingford *et al.*, 2002a). In wildtype fish embryos, *prechordal plate* cells migrates anteriorly in the dorsal midline towards the animal pole, where they contribute to the embryonic *polster*, part of the prospective *hatching gland* (Kilian *et al.*, 2003). Anterior migration of prechordal plate cells is fast from the onset of gastrulation but decreases relative to other tissues towards the end of gastrulation (Kilian *et al.*, 2003).

In the past, it was thought that anteriorly migrating ventral medial neural tissue (the presumptive hypothalamus) physically split the common eyefield into two separate retinae (England *et al.*, 2006; Hirose *et al.*, 2004; Varga *et al.*, 1999). Dynamic imaging studies have provided no evidence that this is the case (England *et al.*, 2006). However the anterior migration of the prechordal plate is key to the development of a bilateralised eyefield in an inductive sense, as if anterior migration is compromised and the prechordal plate does not migrate far enough anteriorly, the patterning of overlying neural tissues is disturbed. In the case of the eyefield, retinal fusion results, demonstrating how a primary defect in movement can affect patterning secondarily (Heisenberg *et al.*, 1996; Heisenberg & Nüsslein-Volhard, 1997; Woo & Fraser, 1995).

Posterior Body Morphogenesis

The conserved movements that create anterior body structures during gastrulation are thought to occur as part of a primary program of development. Those that create posterior body structures such as the tailbud and yolk extension immediately after gastrulation at *bud stage* are thought to occur

secondarily and not merely as a continuation of gastrulation movements (Kanki & Ho, 1997; Marlow *et al.*, 1998). A combination of gastrulation movements and tailbud-specific movements create the tail in four steps: *bud formation*, *extension*, *protrusion* and *tail eversion* (Kanki & Ho, 1997; Marlow *et al.*, 1998). During the final stages of gastrulation, the blastoderm is spread over the yolk to the degree where dorsal and ventral blastoderm margins meet at the site of future tail development. At this dorsoventral boundary, *anterolateral divergence* and *subduction* occur (Kanki & Ho, 1997; Marlow *et al.*, 1998; Marlow *et al.*, 2004). In subduction, posterior prospective tailbud cells move beneath anterior prospective tailbud cells, a type of movement not seen during gastrulation movements as opposing sides of the blastoderm margin do not meet until gastrulation is complete (Marlow *et al.*, 2004). Subduction movements place superficial posterior prospective tailbud cells deeper within the tailbud and help segregate the restricted cell lineages characteristic of the tailbud (Kanki & Ho, 1997; Marlow *et al.*, 1998). The posterior-most part of the tailbud then becomes anchored to the yolk, forcing the extending tailbud to protrude (Kanki & Ho, 1997). Cell division in the anteromedial but not the posterior-most tip of the forming tail contributes to the extension of the tail, contrary to gastrulation, where orientated cell divisions occur throughout but gastrulation movements proceed normally if cell division is blocked (Kanki & Ho, 1997; Kessel, 1960: cited in Concha & Adams, 1998). At tail eversion, the tail physically separates from its anchor point, and both cell division and repacking within the forming tail extend it away from the yolk while maintaining its circumference (Kanki & Ho, 1997). Finally, the notochord extends from its dorsal anterior site of creation during gastrulation into the tail to assist eversion, offering an explanation for the short and malformed tails of some convergent extension mutants, in which patterning, cell proliferation and cell death are normal (Kanki & Ho, 1997; Marlow *et al.*, 1998).

In summary, the evolutionary distance between *Xenopus* and zebrafish is responsible for small differences in the cell movements employed to achieve gastrulation in each. However, spherical fish and frog embryos both face the common problem of internalising the forming mesoderm and spreading germ layers vegetally to cover the yolk, and they solve them by using similar strategies of epiboly and convergent extension. Sophisticated imaging techniques have exploited the transparency and superior genetics of zebrafish to build upon the foundation of knowledge derived from *Xenopus* gastrulation movements.

The Genetic Regulation of Gastrulation Movements

Planar Cell Polarity: from *Drosophila* to Vertebrates

The fruit fly *Drosophila melanogaster* is valued as a developmental model because it is inexpensive and simple to maintain and breed and has a short generation time, despite the fact that *Drosophila* larvae are relatively small and are unsuitable for many classic embryological techniques due to their opacity and hard cuticle. However, developmental genes and developmental processes in the fly are evolutionarily conserved in many species, including humans, mice and *Xenopus*, and the completion of sequencing of the *Drosophila* genome ensured that *Drosophila* became a key tool in investigating developmental genetics and the evolution of developmental mechanisms (Developmental Biology: Gilbert, 2000; Principles of Development: Wolpert *et al.*, 1998).

One of the central aims of developmental biology is to understand how long range patterning is coordinated within the embryo to link pattern at the cellular level to the tissue level. This is of particular relevance to the generation of pattern in a given plane, termed *tissue polarity* or *planar cell polarity* (*PCP*), crucial *in vivo* for the development of arrays of polarised structures such as hairs

whose function is dependent upon both an inherent asymmetry and tissue level polarity in the plane of the tissue. The need for a system suitable for observation of PCP led to the establishment of three epidermal regions in *Drosophila* as models for *planar level morphogenesis*. The *sensory bristles* of the thorax and abdomen, the *wing hair cells* of both the pupa and adult, and the *ommatidia* of the eye each exhibit a stereotypically ordered array of hairs or *trichomes* orientated in a common direction (Adler, 2002; Wehrli & Tomlinson, 1995; Wong & Adler, 1993). The generation and underlying genetic regulation of polarity was more recently implicated in vertebrate PCP, such as inner ear hair cell polarity, where polarised behaviour in the plane of the tissue drives mediolateral intercalation during convergent extension. The genetic mechanisms employed in these varied examples of PCP may in fact represent a universal polarity pathway.

PCP in *Drosophila*: Sensory Bristles, Wing Hair Cells & Ommatidia

Sensory bristles are orientated arrays of asymmetric hair bundles that protrude from the apical surface of cuticular cells and function as *mechanoreceptors* responsive to stimuli like vibration or pressure in a given plane. On the cuticular surface of the *Drosophila* thorax and abdomen, these hairs are orientated posteriorly, while on the appendages, they point distally (Adler, 2002; Eaton *et al.*, 1996). Sensory bristles form from groups of four cells, one of which will differentiate into the hair shaft, and these groups experience planar cell polarity both at tissue level and in the internal asymmetry of each hair bundle (Eaton, 1997). Similarly, in both the pupal and adult wing of *Drosophila*, each wing cell bears one distally orientated hair (Adler, 2002; Wong & Adler, 1993). Adult wing hairs are composed of F-actin and microtubules and are initiated asynchronously in patches throughout the wing from *prehairs*, subcellular F-actin rich regions localised at the distal vertex of hexagonal pupal wing cells (Adler, 2002; Eaton *et al.*, 1996; Wong & Adler, 1993). Both uniform

hexagonal cell shape and restriction of prehair actin polymerisation to the distal vertex contribute to the regulation of the number and even spacing of adult wing hairs (Eaton *et al.*, 1996; Wong & Adler, 1993).

In the fly eye, the establishment of PCP is more complex. The compound eye of *Drosophila* is composed of polarised subunits known as ommatidia, which differentiate in a wave of morphogenesis delineated by a *morphogenetic furrow* that sweeps across the eye from posterior to anterior (Wehrli & Tomlinson, 1995). Each ommatidium comprises approximately 20 cells, including eight *photoreceptors* and associated *pigment cells*, *corneal cells* and *sensory bristles* or *trichomes*. The photoreceptor cells each contain a dark *rhabdomere*, which allows their visualisation and numbering in retinal cross section. While photoreceptors R7 and R8 are central and unaffected by ommatidial polarity, photoreceptor cells R1 to R6 are arranged in an asymmetrical trapezoid shape that adopts one of two *chiral* forms (Wehrli & Tomlinson, 1995). In a wildtype fly, the rhabdomeres in each trapezoid arrangement display a characteristic polarity (Wehrli & Tomlinson, 1995). The chirality of each ommatidium is reliant upon the R3/R4 cell fate decision, and chirality is perturbed when patterning events in the eye are disrupted (Wehrli & Tomlinson, 1995). The eye is divided into dorsal and ventral halves by an equator, across which dorsal-ventral mirror image symmetry exists. In this way, ommatidial polarity also exists on several levels, at the cellular level, within each R1-R6 trapezoid group, and across the equator of the tissue (Adler, 2002; Wehrli & Tomlinson, 1995).

The Genetic Control of PCP in *Drosophila*

The existence of a distinct genetic pathway controlling planar cell polarity, distinct from the genes that regulate hair, trichome and ommatidial differentiation, is supported by the fact that mutations in tissue

polarity genes never affect their patterning, only their orientation within the plane of the epithelium (Adler, 2002; Wong & Adler, 1993). Disruption of these genes does not randomise all aspects of hair, trichome and ommatidia orientation however: rather, each mutation creates a characteristic disturbance of planar cell polarity.

Ommatidia and trichomes, sensory bristles and wing hair cells are developmentally, structurally and functionally different from one another, but all experience disturbance of hair orientation with mutations in a group of genes known as the *tissue polarity genes*. Core tissue polarity genes, including *frizzled* (*fz*), encoding a seven-pass transmembrane receptor, *dishevelled* (*dsh*), encoding a modular protein containing DEP, PDZ and DIX domains, *strabismus* (*stbm:* also known as *van gogh* or *vang*), encoding a four-pass transmembrane protein, *flamingo* (*fmi*: also known as *starry night* or *stan*), encoding a transmembrane protocadherin, and *prickle* (*pk*), encoding a LIM domain containing cytoplasmic protein, were shown through loss of function analysis to be important for different aspects of PCP in the wing, cuticle and eye (Axelrod, 2001; Axelrod *et al.*, 1998; Tree *et al.*, 2002; Wehrli & Tomlinson, 1995; Wong & Adler, 1993). The protein products of these genes respond to a graded PCP signal of unknown identity that causes a local imbalance in Frizzled (Fz) distribution, resulting in increased Fz at the distal vertex of cells (Axelrod, 2001; Axelrod *et al.*, 1998; Strutt, 2001). Dishevelled (Dsh) translocates to the membrane in a manner that is dependent on its DEP domain, and molecular components of the pathway such as Pk, Stbm and Fmi colocalise asymmetrically at the interface between cells, where they form self-organising complexes at the cell membrane (Axelrod, 2001; Tree *et al.*, 2002). In a feedback loop where downstream elements are required for the reactivation of upstream elements, an undetectable initial asymmetry is amplified and communicated in the plane of the tissue.

What is the identity of the initial signal that causes Fz distribution to become imbalanced? In a number of cell fate specification events in both invertebrate and vertebrate development, Fz proteins act as receptors for Wnts, secreted ligands of the *Drosophila* Wingless (Wg) family of glycoproteins (Fig. 1.1A; Cadigan & Nusse, 1997). Wnt ligands binds to Fz receptors, which utilise the DIX and PDZ domains of Dsh to antagonise factors such as Zeste-White3 (Zw3; known as GSK-3 in vertebrates) that normally target the transcriptional regulator Armadillo (Arm; β–catenin in vertebrates) for destruction (Axelrod *et al.*, 1998; Cadigan & Nusse, 1997). In the presence of certain Wnts, degradation of Armadillo/β–catenin is prevented, allowing it to interact with transcription factors like Tcf-3, leading to transcriptional regulation of target genes (Cadigan & Nusse, 1997). This has become known as *canonical Wnt signalling* and is best known for regulating cell decision-making during axis specification in vertebrates (Cadigan & Nusse, 1997). During PCP, Fz interacts with Dsh through its DEP domain, recruiting it to the membrane in a divergent Armadillo/β–catenin independent pathway primarily concerned with cell polarity (Axelrod, 2001; Axelrod *et al.*, 1998). However, in the context of *Drosophila* PCP, no Wnt ligand has been identified as the ligand for Fz and the identity and mode of distribution of the graded signal that initiates PCP signalling remains unknown (Axelrod, 2001; Axelrod *et al.*, 1998). Fz unusually functions both autonomously and non-autonomously during the reception, transduction and propagation of PCP signalling, illustrated by the ability of mutation or mosaicism to affect either or both aspects of its function (Krasnow & Adler, 1994; Vinson & Adler, 1987). Although two species of *fz* RNA exist in the fly, heatshock activation of each in transgenic flies revealed that only one of the two *fz* species encodes a protein that acts both autonomously and non-autonomously (Krasnow & Adler, 1994). During PCP in the wing, early overexpression (more than 6 hours before prehair initiation) of this *fz* causes a severe disturbance to polarity across the tissue, while overexpression immediately prior to prehair formation causes polarity

defects in individual cells, suggesting that non-autonomous signalling is required early in PCP to communicate the initiation of polarity across the tissue, while autonomous signalling is required later, establishing cytoskeletal polarity within each cell (Krasnow & Adler, 1994; Krasnow *et al.*, 1995).

The "early", cell non-autonomous function of Fz in the *Drosophila* wing is an instructive transmission of polarity, asymmetrically localised Fz acting intercellularly to recruit molecular components of the pathway to asymmetric subcellular locations (Krasnow & Adler, 1994). The seven-pass atypical cadherin Fmi becomes localised to the proximal/distal interfaces between cells, while cortical Pk protein becomes localised at the proximal edge of the cell (Tree *et al.*, 2002; Usui *et al.*, 1999). Pk non-autonomously antagonises Fz in neighbouring cells by binding to the DEP domain of Dsh and preventing its recruitment to the membrane, restricting both Fz and Dsh to the distal edge of the cell (Tree *et al.*, 2002). In this way, Fz and Dsh accumulate distally in each cell at the interface between high and low levels of Pk, and from this position transfer polarity across the tissue, amplifying the initial asymmetry (Tree *et al.*, 2002). However, this relationship is not straightforward: Fz function does not require Pk, and Pk does not appear to act in a linear pathway with Fz and Dsh (Krasnow *et al.*, 1995; Tree *et al.*, 2002). In the absence of Pk, asymmetry cannot be propagated, but in the $pk^{pk\text{-}sple}$ mutant wing where polarity is disturbed, cortical translocation of Dsh still occurs, supporting the idea that intercellular and intracellular PCP signalling are intimately linked but separately regulated (Tree *et al.*, 2002).

This *domineering non-autonomy* of Fz in the *Drosophila* wing is dependent upon the presence of the four-pass transmembrane protein Fuzzy (Fy) in responding cells, supported by the fact that the gain of function of Pk is blocked by mutations in *fy* (Lee & Adler, 2002). Non-autonomously acting Fz antagonises Fy in neighbouring cells, limiting Fy activity to the distal vertex of the wing hair cell

(Collier & Gubb, 1997). The *Drosophila fy* mutant grows multiple wing hairs from many sites at the cell periphery, suggesting Fy normally restricts hair formation to the correct location in the cell (Collier & Gubb, 1997; Lee & Adler, 2002; Wong & Adler, 1993). In turn, Fy and the putative transmembrane protein Inturned (In) positively regulate the downstream protein Multiple-wing-hairs (Mwh) (Collier & Gubb, 1997; Park *et al.*, 1996; Wong & Adler, 1993). *Drosophila mwh* mutants produce many wing hairs of different sizes per cell, all initiated from the cell periphery (Wong & Adler, 1993). *mwh*'s larger primary and accompanying smaller, secondary prehairs belie the role of Mwh in stabilising the actin cytoskeleton in advance of hair formation where Fy is active (Park *et al.*, 1996, Lee & Adler, 2002; Wong & Adler 1993).

The "late" Fz function is autonomous, independent of In and Fy, and results in the reorganisation of the actin cytoskeleton, although the exact mechanism by which Fz/Dsh signalling initiates cytoskeletal rearrangement is unclear (Krasnow & Adler, 1994; Lee & Adler, 2002). Fz levels are unaffected in *dsh* mutants, while increasing levels of Dsh can compensate for loss of function of Fz in the fly wing, suggesting that Dsh is a positive mediator of Fz activity (Krasnow *et al.*, 1995). If Fz recruits Dsh to the membrane as part of its autonomous function to participate in a receptor complex, what are its targets? DEP domains, like that of Dsh, exist in a number of proteins identified as regulators of GTPases and G-protein signalling, supporting the theory that cytoskeletal reorganisation downstream of Fz could be mediated by members of the *rho* family, like Rho, Rac1 and Cdc42 (Axelrod *et al.*, 1998; Ponting & Bork, 1996).

Significantly, the *fy* and *in* phenotypes are reminiscent of mutations in the *rho* family of small GTPases, known to regulate cytoskeletal components (Eaton *et al.*, 1996; Krasnow & Adler, 1994; Lee & Adler, 2002; Wong & Adler, 1993). Disrupting the function of Cdc42 or Rac1 severely disables

the generation of PCP, although while dominant negative Cdc42 affects actin polarization and subsequent outgrowth of wing hairs, dominant negative Rac1 produces multiple apolar hairs per cell, indicative of a failure to restrict hair outgrowth to the distal vertex of the cell (Eaton *et al.*, 1996). However, drugs such as latrunculin or cytochalasin that disrupt the actin cytoskeleton do not produce phenotypes identical to *in* or *fy* mutants, indicating that the relationship of *in* and *fy* with the actin cytoskeleton is not straightforward (Lee & Adler, 2002). These distinct phenotypes provide evidence that the cytoskeletal reorganization initiated by Fz/Dsh signalling can be subdivided into several responses utilizing different subsets of the cytoskeleton (Eaton *et al.*, 1996). These facts suggest cytoskeletal polarity is correlated with prehair formation, but this correlation is poorly understood despite the distal subcellular localisation of prehair formation and the distal orientation of wing hairs (Wong & Adler, 1993).

In summary, planar patterning of regularly repeating hairs, bristles and ommatidia in *Drosophila* is genetically regulated by the Fz/Dsh signalling pathway, distinct from the canonical Wnt/Armadillo pathway. Asymmetric recruitment to the cell membrane of factors downstream of PCP signalling influences the actin cytoskeleton, restricting pre-hair development to the correct location in each cell across the epithelium, and when this is disrupted, stereotypical disturbances to planar cell polarity ensue. This planar polarisation may be analogous to the polarised cell behaviour driving vertebrate gastrulation movements, and may in fact represent a universal mechanism for the tissue-wide regulation of polarised cell behaviour.

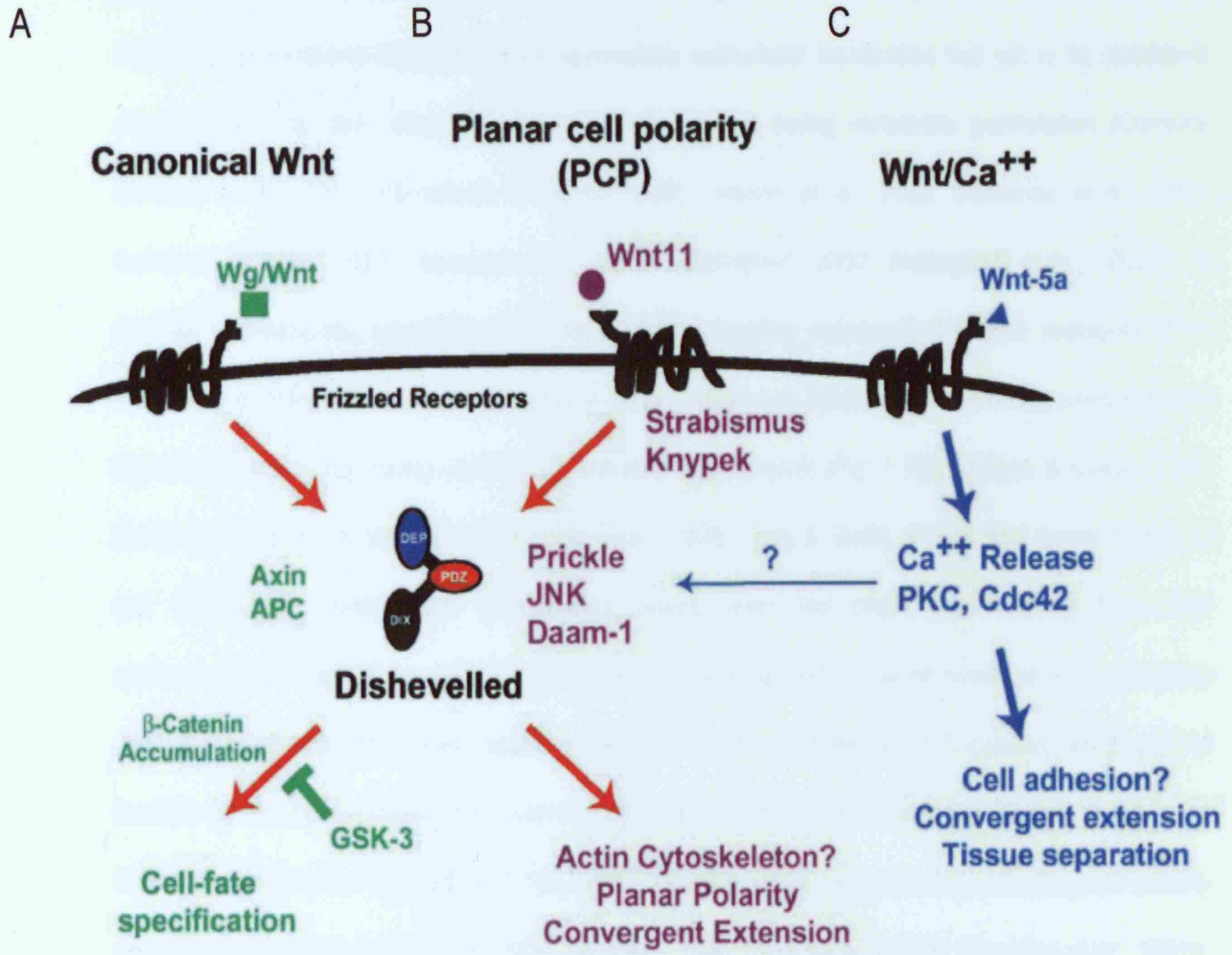

Figure 1.1

Schematic representations of the canonical Wnt, non-canonical Wnt and Wnt/Calcium signalling pathways.

A: the canonical Wnt signalling pathway. Secreted canonical Wnt ligand binds to Fz receptors and utilises the DIX and PDZ domains of Dsh to prevent the destruction of the transcriptional activator ß-catenin, allowing the activation of target genes involved in the specification of cell fate. B: non-canonical Wnt ligand binds to Fz receptors and utilise the PDZ and DEP domains of Dsh to activate downstream effectors of cell polarity and movement via mechanisms that remain poorly understood. C: Wnt ligands bind to Fz receptors stimulating the release of calcium from intracellular stores and activating downstream effectors of cell polarity and cell movement via mechanisms yet to be elucidated (adapted from Wallingford *et al.*, 2002a).

Non-Canonical Wnt Signalling Regulates Vertebrate CE

Molecular components of the *Drosophila* PCP pathway are evolutionarily conserved in vertebrates and although evidence supporting their asymmetric subcellular localisation has yet to be published, orthologues of *fz*, *dsh*, *stbm*, *pk* and *fmi* are expressed during vertebrate gastrulation (Carreira-Barbosa *et al.*, 2003; Formstone & Mason, 2005; Jessen *et al.*, 2002; Sumanas *et al.*, 2001; Sumanas & Ekker, 2001; Veeman *et al.*, 2003; Wallingford, 2000; Wallingford *et al.*, 2002b). In contrast to *Drosophila*, where the ligand for the PCP signalling pathway is unknown, members of the Wnt family of glycosylated secreted proteins were identified as ligands for Fz in a *non-canonical Wnt signalling pathway* regulating vertebrate gastrulation movements (Fig. 1.1B; Cadigan & Nusse, 1997; Du *et al.*, 1995; Ku & Melton, 1993; Smith *et al.*, 2000; Tada & Smith, 2000). Wnt family members can be loosely divided into two classes based upon the phenotype resulting from their overexpression. Gain of function of *canonical wnts* such as *wnt1* or *wnt8* results in a dorsalisation phenotype and induces ectopic axes through Dsh-mediated inhibition of ß-catenin, while gain of function of ß-catenin-independent, *non-canonical wnts* such as *wnt4* or *wnt5*, intrinsic to both the Wnt/PCP and Wnt/Ca^{2+} pathways (1.1C), affect a number of diverse processes including cell polarity and migration (Cadigan & Nusse, 1997; Du *et al.*, 1995; Ku & Melton 1993; Slusarksi *et al.*, 1997b; Westfall *et al.*, 2003). Some Wnt ligands, such as *wnt11*, are known to function in both the canonical and non-canonical Wnt signalling pathways and play a significant part in both PCP and dorsoventral axis specification: the interplay between these pathways adds another layer of complexity to Wnt signalling in vertebrates (Harland & Gerhart, 1997; Kofron *et al.*, 2007; Tao *et al.*, 2005).

Xwnt11 is maternally provided in the vegetal hemisphere of the oocyte and is zygotically expressed in a crescent in the dorsal marginal zone during early gastrulation and in two ventrolateral domains in

the neurectoderm as gastrulation progresses (Ku & Melton, 1993; Saka *et al.*, 2000). *Xwnt11* was discovered in a screen for downstream targets of the T-box transcriptional activator *Xenopus Brachyury* (*XBra*), and functions through a non-canonical pathway distinct from the canonical Wnt/ß-catenin pathway responsible for cell fate decisions (Cadigan & Nusse, 1997; Saka *et al.*, 2000; Smith *et al.*, 2000; Tada & Smith, 2000). It was established that *XBra* is required for normal gastrulation movements in *Xenopus* (Conlon *et al.* 1996; Conlon & Smith 1999). Overexpression of *Xenopus Brachyury* results in anteroposteriorly truncated embryos with ectopic mesodermal cell populations (Cunliffe & Smith, 1992; Saka *et al.*, 2000). Screening for direct targets of *XBra* revealed these defects to be separable, and that *Xwnt11* was responsible for the movement element of these defects (Heisenberg, Tada *et al.*, 2000; Tada & Smith, 2000). The C-terminally truncated, dominant negative form of *Xwnt11*, *dn-wnt11*, selectively inhibits the function of the non-canonical Wnt signalling pathway and injection of this construct creates embryos in which patterning is normal but gastrulation movements are severely impaired (Heisenberg, Tada *et al.*, 2000; Tada & Smith, 2000). These defects can be rescued by overexpression of non-canonical *wnts* such as *wnt11*, but not by overexpression of the canonical *wnt8* (Smith *et al.*, 2000).

Orthologues of the seven-pass transmembrane Wnt receptor Frizzled are in vertebrates, as in *Drosophila,* employed in both the ß–catenin dependent pathway controlling cell fate decisions and the ß–catenin independent pathway controlling morphogenetic movements (Sumanas *et al.*, 2001; Sumanas & Ekker, 2001). Ventral overexpression of Fz orthologues in *Xenopus* results in induction of a secondary axis, but in a subset of Fz orthologues, loss of function leads to gastrulation defects (Sumanas *et al.*, 2001; Sumanas & Ekker, 2001). Loss of function of *Xfz2* produces embryos with short and undulating notochords, highly reminiscent of loss of function of *wnt5* (Sumanas *et al.*, 2001). Loss of function of *Xfz7* yields severe convergent extension defects, reminiscent of dominant

negative Wnt, Fz or Dsh (Sumanas *et al.*, 2001; Sumanas & Ekker, 2001). This suggests that Wnt, Fz and Dsh function as part of the same pathway but that Fz2 and Fz7 are involved in different aspects of this pathway (Sumanas *et al.*, 2001; Sumanas & Ekker, 2001).

The modular protein Dsh is conserved in vertebrates, and as in *Drosophila*, utilises distinct protein-protein binding domains to participate in both the patterning of the axes and morphogenetic movements (Wallingford, 2000). In quiescent *Xenopus* cells, *Xdsh-GFP* is localised to the cytoplasm, while in cells actively undergoing convergent extension, *Xdsh-GFP* becomes localised to the cell membrane, where by an unknown mechanism it stabilises cellular protrusions (Wallingford, 2000). When *Xdsh* function is disrupted by use of a dominant negative form of *dishevelled* known as *Xdd1*, cells undergoing CE fail to elongate or align correctly, and severely compromised gastrulation movements result (Sokol, 1996; Wallingford, 2000).

Parallel and downstream components of Wnt/Dsh signalling suggest how non-canonical Wnt signalling is transduced and which molecules effect the changes on cell behaviour and polarity critical to gastrulation movements. The transmembrane protein Stbm is also conserved in vertebrates and is considered to function in a pathway to parallel but capable of modulating Wnt/Dsh signalling (Jessen *et al.*, 2002; Sepich *et al.*, 2000). Stbm bears four putative transmembrane domains and a PDZ domain contained in a long cytoplasmic tail (Jessen *et al.*, 2002; Park & Moon, 2002). Similarly to PCP in *Drosophila*, Stbm is capable of influencing the subcellular localisation of components of the non-canonical Wnt signalling pathway during zebrafish gastrulation (Park & Moon, 2002). Previously, it was shown that discrimination between the activation of the non-canonical Wnt and canonical Wnt signalling pathways occurred at the level of Dsh: the capability of Dsh to selectively activate these pathways, dependent on the combination of Wnt ligand and Fz receptor, is domain-dependent.

(Boutros *et al.*, 1998). The DEP domain of Dsh is specific to non-canonical Wnt signalling and activates downstream JNK signalling (Boutros *et al.*, 1998). It is now thought that the recruitment of Dsh-GFP to the cell membrane during non-canonical Wnt signalling promoting downstream phosphorylation of c-Jun, a member of the JNK signalling cascade, occurs in the presence of Stbm in a PDZ-domain dependent manner (Park & Moon, 2002). Stbm may therefore act as a positive regulator of non-canonical Wnt signalling with an output in JNK-mediated cytoskeletal reorganisation, although the exact molecular basis of Stbm's interaction with Wnt/Dsh signalling is unknown.

Orthologues of the *Drosophila* divergent class LIM domain containing protein Prickle, also considered to function in a parallel pathway to Wnt/Dsh signalling, are conserved in vertebrates (Carreira-Barbosa *et al.*, 2003; Hunter & Rhodes, 2005; Veeman *et al.*, 2003; Takeuchi *et al.*, 2003; Wallingford *et al.*, 2002b). LIM domain containing proteins are a functionally disparate family that share the ability to undergo multiple protein-protein interactions through multifunctional, cysteine/histidine rich *LIM domains*, facilitating the assembly of heterogeneous multiprotein complexes vital to processes throughout the cell (Bach, 2000; Dawid *et al.*, 1998; Hunter & Rhodes, 2005). LIM domains bind two zinc molecules, creating *zinc finger motifs*, that exist alone in the protein as in *LIM only* or *LMO proteins*, transcriptional regulators in processes including cell type differentiation and oncogenesis; or alongside domains of divergent function, such as homeodomains as in *LIM-HD proteins*, predominantly nuclear transcriptional activators integral to the *Shh*, *FGF*, *wnt* and *TGF-β* signalling pathways; Kinase domains as in *LIM-K proteins*, that phosphorylate key proteins in cytoskeletal organisation and motility; and a variety of other domains including PDZ, SH3 and GAP domains in *divergent class LIM proteins*, involved in processes as diverse as cell adhesion, trafficking between cell compartments, regulation of cytoskeletal architecture, transcriptional regulation and establishing cell polarity (Arber *et al.*, 1998; Bach, 2000; Dawid *et al.*, 1998; Hunter & Rhodes, 2005). Prickle

belongs to this divergent class of LIM domain containing proteins: while a role in cytoskeletal reorganisation is highly plausible, this has yet to be identified.

The output of *Drosophila* PCP signalling is the subcellular localisation and manufacture of an actin prehair, although the exact interactions that take place between PCP signalling pathway components and cytoskeletal regulators such as Rho, Rac, and Cdc42, belonging to the Rho family of GTPases, are unclear (Eaton *et al.*, 1996; Krasnow & Adler, 1994; Lee & Adler, 2002; Wong & Adler, 1993). Both canonical and non-canonical Wnt and Frizzled orthologues such as *wnt1*, *wnt11*, *fz1* and *fz7*, are capable of activating RhoA by inducing Dsh to form a complex with Daam1, a novel member of the Formin homology family of proteins recognised as regulators of cell polarity in a number of systems (Habas *et al.*, 2001). This was not the case for canonical-only Wnt and Frizzled orthologues or for truncated Dsh constructs where the non-canonical specific domains were deleted, implying a direct correlation with RhoA activation and cell polarity created by non-canonical Wnt signalling (Habas *et al.*, 2001). The Daam1 complex interacts with the Rho activators, Rho-GEFs, to reorganise the cytoskeleton through the formation of actin stress fibres (Habas *et al.*, 2001).

Cell adhesion is dynamic throughout gastrulation but until recently the relationship between Wnt/PCP signalling and the regulation of cell adhesion was poorly understood. Vertebrate orthologues of the *Drosophila* seven-pass transmembrane protocadherin Flamingo (Fmi), also known as Starry Night (Stan), bear a unique combination of transmembrane domains, cadherin repeats, EGF-like repeats and laminin-G binding sites that potentially mean cell adhesion and signalling could meet in one molecule (Chae *et al.*, 1999; Formstone & Mason, 2005; Usui *et al.*, 1999). During PCP in the *Drosophila* wing, Fmi responds to Fz asymmetry by becoming localised to the proximal/distal interfaces between cells (Usui *et al.*, 1999). Morpholino abrogation of Fmi function leads to defects in

both axis extension and epiboly: while it is possible speculate that adhesion proteins like Fmi facilitate cell-cell communication or create cell-cell integrity, the exact molecular function Fmi during vertebrate morphogenesis is unclear (Formstone & Mason, 2005). It was demonstrated that Wnt11 activity was capable of conferring cohesion between anteriorly migrating prechordal plate cells during zebrafish gastrulation movements by regulating the subcellular localisation of E-Cadherin (Ulrich *et al.*, 2005). More recently however, it was shown that Wnt11 directly regulates cell-cell contact by recruiting Fz7 to the membrane of neighbouring cells in a Fmi-dependent manner (Witzel *et al.*, 2006)

Other Signalling Pathways Involved in the Regulation of CE

Loss of function of individual components of the non-canonical Wnt signalling pathway affects different aspects of convergent extension; however, although impaired, convergent extension movements still occur. This is in part due to factors external to the non-canonical Wnt signalling pathway that play an important part in the regulation of cell movements during zebrafish gastrulation.

The embryonic shield, situated on the future dorsal side of the gastrula and equivalent to the Spemann-Mangold Organiser (SMO) in *Xenopus*, acts as an organising centre in the zebrafish gastrula. Genes expressed in the shield during gastrulation, such as the TGF-ß family members *noggin* and *chordin*, are best known for their role in dorsoventral axis specification. However, more recently it was shown that BMPs, members of the TGF-ß superfamily involved in the specification of ventral fates during axis determination, are capable of altering calcium-dependent cell adhesion by destabilising intercellular cadherin-anchored lamellipodia (von der Hardt *et al.*, 2007). As a consequence, migrating lateral mesodermal cells are driven dorsally during gastrulation independently of both axis specification and non-canonical Wnt signalling (von der Hardt *et al.*, 2007).

STATs (for Signal Transducers and Activators of Transcription) are also active in the shield during early gastrulation (Sepich *et al.*, 2005; Yamashita *et al.*, 2002). Loss of function of *STAT3* does not however result in aberrant cell fate specification: instead, *STAT3*-MO was discovered to non-autonomously impair the dorsally orientated directed migration of lateral cell populations before midgastrula stage (Yamashita *et al.*, 2002). This early lateral convergence is thought to promote convergent extension movements during late gastrulation. However, early lateral convergence is unaffected in the zebrafish non-canonical Wnt signalling mutants *tri* and *kny* (Sepich *et al.*, 2005). Similarly, the expression patterns of components of the non-canonical Wnt signalling pathway are unaffected by loss of function of *STAT3*, and STAT3 signalling occurs normally in the zebrafish *slb/wnt11* mutant (Miyagi *et al.*, 2004; Yamashita *et al.*, 2002). This implies that STAT3 regulates cell movements at the onset of gastrulation independently of non-canonical Wnt signalling, although recent evidence suggests that STAT3 signalling activates Dishevelled-Rho signalling through an as yet unidentified signalling cascade (Miyagi *et al.*, 2004).

STAT3 is also required for the anterior migration of prechordal plate cells during late gastrulation (Sepich *et al.*, 2005; Yamashita *et al.*, 2002). STAT3 cell autonomously targets LIV1, a zinc transporter protein essential for *endothelial to mesenchymal transition* (*EMT*) in processes involving cell movement during both embryonic and adult life (Yamashita *et al.*, 2004). In turn, LIV1 regulates the subcellular localisation of Snail, bringing about EMT in organiser cells during zebrafish gastrulation (Yamashita *et al.*, 2004). However, loss of function of LIV1 severely reduces the anterior migration of organiser cells while Snail is expressed in both axial and paraxial mesendoderm, suggesting that other mechanisms contribute to the regulation of the anterior migration of prechordal plate cells.

Phosphoinositide 3-Kinase (PI3K), known to function downstream of the PDGF signalling pathway in processes such as cell proliferation, vesicle trafficking and chemotaxis, has been shown to specifically regulate the anterior migration of prechordal plate cells in zebrafish (Montero *et al.*, 2003). PI3K activity causes recruitment of Protein Kinase B (PKB) to the leading edge of polarised cells, where it binds to Phosphoinositide 3,4,5-trisphosphate (PIP_3) initiating a phosphorylation cascade that ultimately results in the phosphorylation of Myosin and subsequent polarisation of the cytoskeleton (Chung *et al.*, 2001; Montero *et al.*, 2003; Stephens *et al.*, 2002). Loss of function of PI3K using the PI3K inhibitor LY294002 almost completely abolished cell polarity and orientated pseudopodial and filopodial projections in prechordal plate cells (Montero *et al.*, 2003). However, the direction of cell migration was unaffected, indicating that our understanding of the regulatory mechanisms underlying the anterior migration of the prechordal plate is far from complete (Montero *et al.*, 2003). The zebrafish mutant *miles apart* (*mil*), isolated as part of screen for dominant suppressors of *silberblick*, carries a mutation in the Sphingosine-1-phosphate (S1P) receptor, a component of the PI3K signalling pathway known to regulate the anterior migration of the prechordal plate during zebrafish convergent extension movements (Montero *et al.*, 2003). *mil* embryos exhibit *cardia bifida*, a failure of the bilateral heart primordia to fuse in the midline (Matsui *et al.*, 2006). *mil* mutants also display impaired anterior migration of the prechordal plate, potentially linking cell migration during gastrulation with the cell migration of bilateral primordia towards the midline during the organogenesis of unpaired organs (Kai M. & Tada M., unpublished data; Matsui *et al.*, 2005; Matsui *et al.*, 2006; Ober *et al.*, 2004; Warga & Nüsslein-Volhard, 1999).

The *dickkopf* (*dkk*) family of secreted proteins are known as 'head inducers" for their role in antagonising the posteriorising influence of Wnts in the neural plate (Erter *et al.*, 2001, Glinka *et al.*, 1998, Kawano & Kypta, 2003, Kiecker & Niehrs, 2001a and Lekven *et al.* 2001: cited in Caneparo *et*

al., 2007). Secreted by cells of the organiser, they inhibit Wnt signalling by binding to Frizzled co-receptors such as LRP5/6 (Mao *et al.*, 2001: cited in Caneparo *et al.*, 2007). However, both loss of function and gain of function of *dkk1* impair gastrulation movements: loss of function of *dkk1* accelerates the internalisation and rostral migration of the mesoderm, while gain of function of *dkk1* retards both mesoderm internalisation and convergent extension (Caneparo *et al.*, 2007). Surprisingly, the role of *dkk1* in the regulation of convergent extension movements is independent of canonical Wnt signalling, but interaction with non-canonical Wnt signalling is not excluded as *dkk1* binds not only to LRP5/6 but also to *knypek/glypican in vivo*, effectively bridging canonical and non-canonical Wnt signalling (Caneparo *et al.*, 2007).

The JNK signalling pathway is best known for the transcriptional regulation of target genes such as the *TGF-ß* family member *decapentaplegic* (*dpp*) in the orchestration of the "zippering-up" of the *amnioserosa* during *dorsal closure* in *Drosophila* (Jacinto *et al* 2001; Jacinto & Martin, 2001; Kaltschmidt *et al.*, 2002). Recently, it was elucidated that JNK signalling interacts with planar cell polarity proteins in the formation of *actin nucleating centres* (*ANCs*) in migrating leading edge cells, facilitating the focal accumulation of actin around adherens junctions that eventually becomes incorporated into exploratory, actin-based protrusions such as filopodia (Kaltschmidt *et al.*, 2002). Molecular components of planar cell polarity signalling, such as Fz and Dsh, were discovered to change their subcellular localisation during dorsal closure, becoming progressively localised to adherens junctions (Kaltschmidt *et al.*, 2002). The *Drosophila* mutant *hemipterous* (*hep*) lacks JNK-kinase, and in *hep* mutants, cells elongate normally but the localisation of PCP proteins and subsequent ANC formation is decreased (Kaltschmidt *et al.*, 2002). However, repressors of JNK signalling must operate in cells of the amnioserosa for normal dorsal closure to occur. In the

Drosophila mutant *hindsight*, JNK signalling is no longer repressed in the amnioserosa, and dorsal closure comes to a standstill (Jacinto & Martin, 2001).

Overexpression of *dpp* rescues mutants for JNK signalling, implying that JNK signalling operates through *dpp* (Chen *et al.*, 2002, Hou *et al.*, 1997, Jacinto *et al.*, 2002; Riesgo-Escovar & Hafen, 1997; Sluss & Davis, 1997). *Drosophila* Rho-family GTPases mutants exhibit defective dorsal closure; however, overexpression of dominant negative *cdc42* produces a phenotype similar to *dpp* pathway mutants but dissimilar to JNK pathway mutants (Genova *et al.*, 2000; Jacinto *et al.*, 2002; Ricos *et al.*, 1999). Another potential mediator between JNK signalling and the cytoskeleton and is the small GTPase Rho1. Embryos overexpressing ROCK or Rho-associated kinase show defective dorsal closure due to improper assembly of the myosin component of the actinomyosin cable (Jacinto *et al.*, 2002; Mizuno *et al.*, 2002). Rho1 may also interact with factors that regulate actin localised to adherens junctions, such as the tyrosine kinase *abelson* (*abl*) and its target, the modulator of actin dynamics *enabled* (*ena*) (Grevengoed *et al.*, 2001; Jacinto *et al.*, 2002). In this way, the molecular building blocks of the cytoskeleton could be altered in response to upstream planar cell polarity signalling.

Calcium (Ca^{2+}) signalling has been proposed as a possible downstream effector of Wnt/Fz signalling, and a Wnt/Ca^{2+} pathway has been implicated in the regulation of morphogenetic movements (Fig. 1.1C; Sheldahl *et al.*, 2003; Slusarski *et al.*, 1997a; Slusarski *et al.*, 1997b). XWnt5a, but not XWnt8, was found to stimulate the release of intracellular calcium in the presence of the Fz2 receptor, via G-protein-linked receptor activation of the phosphatidylinositol signalling pathway (Slusarski *et al.*, 1997a; Slusarski *et al.*, 1997b). Interfering with Wnt/Ca^{2+} signalling resulted in the expansion of expression domains of markers such as *krox20*, reflecting impaired morphogenetic movements

(Slusarski *et al.*, 1997b). Wnt/Fz signalling activates Protein Kinase C (PKC), causing it to translocate to the cell membrane in a G-protein dependent manner, an event that is blocked by the presence of dominant negative *Xwnt11* (Kuhl *et al.*, 2000; Sheldahl *et al.*, 1999). Wnt/Fz signalling also activates Ca^{2+}/Calmodulin-Dependent Kinase II (CamKII), an enzyme shown to be upregulated on the future ventral side of the embryo during axis specification (Kuhl *et al.*, 2000). Overexpression of a constitutively active form of CamKII ventralised *Xenopus* embryos, while loss of function of CamKII yielded a dorsalisation phenotype, indicating that CamKII normally antagonises dorsal fates and promotes ventral fates in the early embryo in a manner dependent upon non-canonical Wnt signalling (Kuhl *et al.*, 2000). More recently, it was discovered that the non-canonical specific PDZ and DEP domains of Dsh were sufficient to activate both PKC and CamKII downstream of Wnt/Fz signalling (Sheldahl *et al.*, 2003). Furthermore, Dsh is capable of stimulating Ca^{2+} flux independently of G-protein linked signalling (Sheldahl *et al.*, 2003). Therefore, the non-canonical Wnt and Wnt/Ca^{2+} signalling pathways experience considerable overlap, but despite evidence linking Wnt/Ca^{2+} signalling components such as PKC with non-canonical Wnt signalling, the extent of this overlap and the mechanisms by which it is achieved in the context of convergent extension movements during gastrulation have yet to be elucidated (Sheldahl *et al.*, 2003).

The environment upon which gastrula cells rearrange plays an active role in regulating cell behaviour (Marsden & DeSimone, 2001). The migration of the forming mesoderm is dependent upon the secretion of extracellular matrix proteins by pre-involuting mesodermal cells of the blastocoel roof, creating a stable interface upon which migration occurs (Winklbauer & Keller, 1996; Ramos *et al.*, 1996). *RGD peptides* block the *RGD sequence* (Arg-Gly-Asp) of FN (a region of FN important for IMZ cell binding), rendering endogenous FN inactive. Use of these FN inhibitors demonstrated that cohesion between involuting mesodermal cells, involuting as opposed to pre-involuting mesodermal

identity, and adhesion and migration on the BCR, can occur independently of FN in *Xenopus* (Winklbauer & Keller, 1996). However, loss of function of FN in *Xenopus* was shown to randomise the orientation of cellular protrusions while increasing their number with the result of impairing convergent extension movements (Davidson *et al.*, 2006). Furthermore, FN is known to be critical for the radial intercalations that thin and spread tissues during epiboly (Marsden & DeSimone, 2001). Members of the Integrin superfamily of receptors are thought to mediate contact between migrating cells and Fibronectin in a manner that recruits Dsh to the cell membrane, connecting the changes to cell polarity and cell adhesion generated by non-canonical Wnt signalling with the interaction of migrating cells with their environment during gastrulation (Ramos *et al.*, 1996; Marsden & DeSimone, 2001).

Zebrafish Non-Canonical Wnt Signalling Mutants

Zebrafish mutants exhibiting convergent extension defects provide insight into the genetic regulation of gastrulation movements both through their relationship with the non-canonical Wnt signalling pathway and the characteristic range of morphogenetic defects to which these mutations give rise.

silberblick (*slb*)

The zebrafish convergent extension mutant *silberblick* (*slb*) (German: squint) was discovered during a large scale ENU mutagenesis screen performed at the Max Planck Institut für Entwicklungsbiologie in Tübingen, Germany in 1996 (Fig. 1.2B; see Materials & Methods; described in Driever *et al.*, 1996; Haffter *et al*, 1996; Solnica-Krezel *et al.*, 1996). The primary defect of *slb* is a gastrulation defect, resulting in a shortened anteroposterior axis and malformed polster at 10hpf (part of the anterior prechordal plate which will contribute to the hatching gland), both defects the result of reduced

convergent extension movements (For an exploration of convergent extension phenotypes, see Appendix Two; Heisenberg *et al*, 1996; Heisenberg & Nüsslein-Volhard, 1997; Heisenberg, Tada *et al.*, 2000). However, before the mutation was mapped, *slb* was grouped with mutants in which forebrain patterning is disrupted, based upon its partially penetrant secondary neurectodermal defect in the separation of the retinae (Heisenberg *et al*, 1996; Heisenberg & Nüsslein-Volhard, 1997). It is now widely accepted that, unlike ventral CNS patterning mutants such as *cyclops* (*cyc*) where lack of *nodal* signalling leads to cyclopia due to deletion of ventral CNS structures, cyclopia in *slb* arises as a consequence of impaired convergent extension reducing the anterior migration of tissues with important inductive roles in CNS patterning, not by preventing the physical splitting of the eyefield by the ventral CNS as was once erroneously thought (England *et al.*, 2006; Heisenberg *et al.*, 1996; Heisenberg & Nüsslein-Volhard, 1997; Sampath *et al.*, 1998; Woo & Fraser, 1995).

wnt11 expression is strongly downregulated in *slb* embryos, whereas in wildtype embryos, *wnt11* is expressed in the germ ring during early gastrulation and in the paraxial head mesoderm and anterior neurectoderm during late gastrulation (Heisenberg, Tada *et al.*, 2000). Wnt11 was a good candidate for *slb* as previous work in *Xenopus* demonstrated that XWnt11 regulates gastrulation cell movements through a pathway distinct from canonical Wnt signalling (Saka *et al.*, 2000; Smith *et al.*, 2000; Tada & Smith, 2000). In both the slb^{tx226} and slb^{tx216} alleles of *silberblick*, a premature stop codon is introduced into the gene, creating in non-functional proteins (Heisenberg, Tada *et al.*, 2000). The *slb* phenotype is rescued by overexpressing *wnt11* mRNA (Heisenberg, Tada *et al.*, 2000; Ulrich *et al.*, 2003). It was confirmed that *slb* encodes the secreted glycoprotein ligand Wnt11 (Heisenberg, Tada *et al.*, 2000; Ulrich *et al.*, 2003).

Cells in *slb* embryos move more slowly and appear less well directed than in wildtype embryos, and unlike in wildtype embryos, where cell processes are preferentially orientated in the direction of migration, the orientation of cell processes is disturbed in *slb* (Heisenberg, Tada *et al.*, 2000; Ulrich *et al.*, 2003). As a consequence, midline intercalation during convergent extension is reduced in *slb*, visible in mediolaterally expanded and anteroposteriorly reduced expression domains of key markers during gastrulation (Fig. 1.2H & L; Appendix Two; Heisenberg, Tada *et al.*, 2000). Reduced anterior migration of prechordal plate cells is highlighted by *hgg1* expression, showing the misshapen prechordal plate to be situated posterior to the anterior border of the neural plate in *slb*. The expression domains of *ntl* in the notochord and *dlx3* at the anterior border of the neural plate in *slb* show mediolateral expansion and anteroposterior reduction relative to wildtype embryos, reflecting reduced convergent extension in both anterior and posterior regions of the embryos (Heisenberg, Tada *et al.*, 2000). But *wnt11* is expressed paraxially, suggesting it is required non-autonomously at range for normal midline cell behaviour during CE (Heisenberg, Tada *et al.*, 2000; Tada *et al.*, 2002). Transplanted wildtype cells do not undergo CE more efficiently than *slb* host cells, confirming this non-autonomous role (Heisenberg, Tada *et al.*, 2000).

To confirm whether non-canonical signalling acted downstream of Wnt11 was a more complex task, as overexpression of full length *dsh* mRNA results in a dorsalisation phenotype due to the activation of both canonical and non-canonical Wnt signalling (Heisenberg, Tada *et al.*, 2000; Tada *et al.*, 2002). However, it was possible to rescue *slb* using an N-terminally truncated form of *dsh* known as *dsh-ΔN*, which bears the domains necessary for non-canonical signalling (PDZ, DEP) but lacks the domain specific to canonical Wnt signalling (DIX), meaning that this construct only activates Wnt/PCP signalling (Heisenberg & Tada, 2000). Furthermore, a specific inhibitor of non-canonical signalling,

the truncated form of *dsh* known as *dsh-DEP+*, yielded a CE phenotype reminiscent of *slb* when over-expressed in wildtype embryos (Heisenberg, Tada *et al.*, 2000; Tada *et al.*, 2002).

pipetail (*ppt*)

The recessive zebrafish *pipetail* (*ppt*) mutant was originally isolated as part of the Tübingen ENU mutagenesis screen (Fig. 1.2C; Appendix Two; Driever *et al.*, 1996; Haffter *et al.*, 1996; Hammerschmidt *et al*, 1996). Although *ppt* mutants were named and grouped with mutants for tail development based upon their tail morphogenesis phenotype, the primary defect in *ppt* is a gastrulation defect (Hammerschmidt *et al*, 1996; Killian *et al.*, 2003). *ppt* embryos exhibit an anteroposteriorly shortened body axis, a tailbud that fails to extend away from the yolk and a thicker, shorter, malformed yolk extension (Hammerschmidt *et al.*, 1996). Accompanying these defects is a secondary malformation of the skull that results in poorly differentiated head cartilages and compressed skeletal structures (Hammerschmidt *et al.*, 1996). Analysis of markers for tailbud differentiation such as *eve1* showed that the developing tail was patterned normally in *ppt* embryos (Hammerschmidt *et al.*, 1996). However, expression of *ntl* at the end of gastrulation revealed a compressed and undulating notochord, while expression of *myoD* showed the somites to be mediolaterally expanded, both due to impaired convergent extension (Hammerschmidt *et al.*, 1996).

ppt encodes zebrafish *wnt5b* (Rauch *et al.*, 1997; Stoick-Cooper *et al.*, 2007). Maternally provided and zygotically expressed from the onset of gastrulation, *wnt5* is expressed in both epiblast and hypoblast cells in the germ ring, restricting to the posterior axial and paraxial mesendoderm by tailbud stage (Kilian *et al.*, 2003). This domain of *wnt5b* expression in the posterior mesendoderm is adjacent to the domain of *wnt11* expression in anterior paraxial mesendodermal cells (Kilian *et al.*,

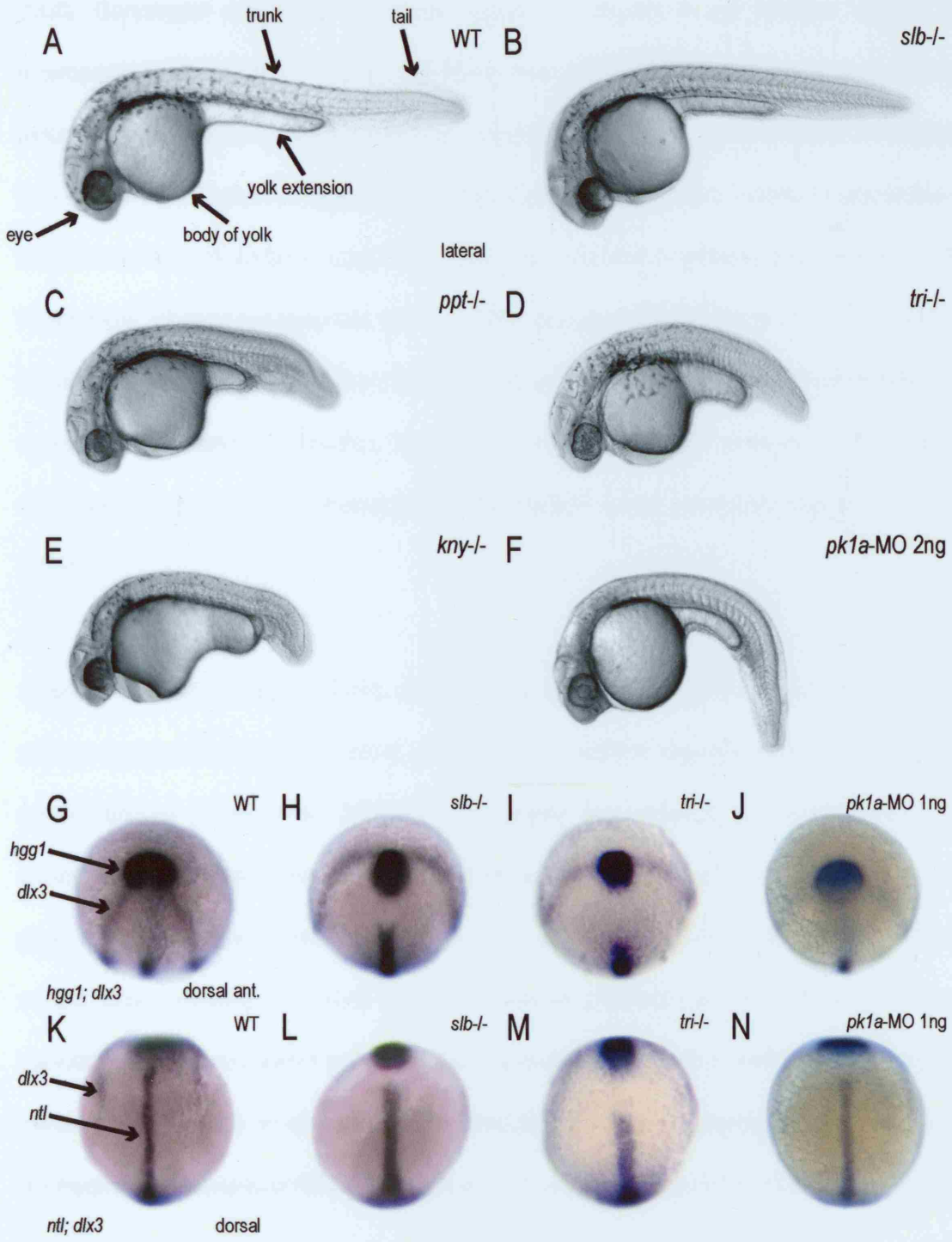

Figure 1.2
Zebrafish convergent extension mutants.

Fig. 1.2A-F: the effect of reduced convergent extension movements on anteroposterior body length at 24h in zebrafish non-canonical Wnt signalling mutants and morphants. A: wildtype; B: *silberblick/wnt11* (*slb-/-*); C: *pipetail/wnt5b* (*ppt-/-*); D: *trilobite/stbm* (*tri-/-*); E: *knypek/glypican* (*kny-/-*); and F: *prickle1a* (*pk1a*) morphant (2ng). 1.2G-N: *in situ* hybridisation at tailbud stage for the mesodermal markers *ntl* and *hgg1* and the neurectodermal marker *dlx3* in *slb-/-* (H & L); *tri-/-* (I & M); and *pk1a* morphant embryos (1ng *pk1a*-MO; J & N), highlighting both mesodermal and neurectodermal defects in convergent extension movements relative to wildtype embryos (G & K). (images B-D, G, H, K & L adapted from Kilian *et al.*, 2003, courtesy of M. Tada).

2003). Convergent extension in posterior regions is reduced in *ppt* embryos, leading to an anteroposterior shortening of the body axis (Kilian *et al.*, 2003). This is supported by anteroposteriorly reduced, mediolaterally expanded expression of *ntl* in the notochord, and mediolateral expansion of *dlx3* in the neural plate of *ppt* embryos (Kilian *et al.*, 2003). Biotin labelled transplanted cells redistributed less efficiently on a *ppt* host background compared to wildtype cells (Kilian *et al.*, 2003). Furthermore, labelling *ppt* morphant cells with either cytosolic or membrane bound GFP revealed that in *ppt*, cells are more rounded than their wildtype equivalents and show fewer projections of less coordinated orientation, suggesting that loss of function of *wnt5b* prevents cells adopting the mediolaterally bipolar shape necessary for cell intercalation during convergent extension (Kilian *et al.*, 2003).

Anterior migration of the prechordal plate, marked by *hgg1* expression, is indistinguishable from wildtype in *ppt* embryos, in contrast to *slb/wnt11* where anterior migration of the prechordal plate is greatly reduced (Kilian *et al.*, 2003). This suggested that *ppt/wnt5b* is required for convergent extension in the posterior mesoderm and neurectoderm (Kilian *et al.*, 2003). However, the prechordal plate of *ppt:slb* double mutants is more severely malformed and posteriorly situated than either mutant alone, implying that *wnt5* is also capable of affecting cell movements in the anterior mesoderm and neurectoderm but is partially functionally redundant to *wnt11* (Kilian *et al.*, 2003). Hence, overexpression of *wnt5b* mRNA can partially rescue the prechordal plate phenotype of *slb*, but much larger amounts of RNA are necessary to do so compared to *wnt11* (Kilian *et al.*, 2003).

The *ppt/wnt5b* phenotype resembles loss of function of *frizzled2* (*fz2*), a *fz* linked to the non-canonical Wnt signalling pathway (Kilian *et al.*, 2003; Sumanas *et al.*, 2001). Loss of function of *fz2* did not significantly enhance the *ppt* phenotype, suggesting that *fz2* acts downstream of *wnt5b*, while loss of

function of *fz2* in *slb* leads to a greatly enhanced phenotype, suggesting that *wnt11* and *fz2* are in parallel pathways (Kilian *et al.*, 2003; Sumanas *et al.*, 2001). The expression domain of *fz2* overlaps with *wnt5b* expression during gastrulation, while expression of another *fz* associated with non-canonical Wnt signalling, *fz7*, overlaps with *wnt11* expression (El-Messaoudi & Renucci, 2001; Kilian *et al.*, 2003). Local production of these non-canonical Wnt ligands, or equally differential Fz receptor expression creating specific domains of competence, could be responsible for functions of Wnt5b and Wnt11 distinct to specific anteroposterior levels of the embryo (Kilian *et al.*, 2003).

trilobite (*tri*)

The recessive zebrafish convergent extension mutant *trilobite* (*tri*) was originally isolated in the Boston chemical mutagenesis screen (Fig. 1.2D; Appendix Two; Driever *et al.*, 1996; Haffter *et al.*, 1996; Hammerschmidt *et al.*, 1996; Solnica-Krezel *et al.*, 1996). *tri* embryos exhibit severe shortening of the anteroposterior axis, resulting in embryos than are rounder at tailbud stage relative to typically ovoid wildtype embryos (Hammerschmidt *et al.*, 1996; Sepich *et al.*, 2000). At 24hpf, *tri* embryos resemble a trilobite, exhibiting a characteristic shortened anteroposterior axis and ventrally curled body. Unlike *silberblick* however, retinal fusion is atypical in *tri* embryos, only a proportion of tri^{tk50f} clutches showing mild fusion of the eyes (Heisenberg & Nüsslein-Volhard, 1997).

Anteroposterior compression and mediolateral expansion of the expression domains of several key markers was evident in *tri*, reflecting reduced convergent extension rather than a transformation of cell fate (Fig. 1.2I & M; Hammerschmidt *et al.*, 1996; Sepich *et al.*, 2000). While the ventral markers *bmp2b*, *bmp4* and *eve1* and the dorsal markers *gsc* and *din* showed dorsoventral patterning to be unaffected in *tri*, *ntl* expression at tailbud stage showed the notochord to be shorter in the

anteroposterior axis and mediolaterally broader, while both *papc* and *myoD* expression in the paraxial mesoderm and somites respectively were indistinguishable from wildtype except for expansion in the mediolateral axis resulting from impaired convergent extension (Appendix Two; Hammerschmidt *et al.*, 1996; Sepich *et al.*, 2000). There was no alteration in the expression of either the canonical Wnt *wnt8*, or interestingly, the non-canonical Wnts *wnt5* and *wnt11*, although the eye phenotype of *slb* is strongly enhanced in *tri*:*slb* double mutants, suggesting that *tri* might function in the same pathway or in a parallel pathway to Wnt11 (Heisenberg & Nüsslein-Volhard, 1997; Sepich *et al.*, 2000). More recently it was ascertained that, unlike *slb*, the defects in *tri* cannot be rescued by injection of *dsh-ΔN* or *rho-kinase2* mRNAs, adding weight to the theory that *tri* acts to modulate non-canonical Wnt signalling in the regulation of gastrulation movements in a parallel pathway to Wnt11 (Jessen *et al.*, 2002).

The zebrafish homologue of the *Drosophila* PCP gene *strabismus* (*stbm*) is mutated in *tri* (Jessen *et al.*, 2002). *stbm* is maternally provided and zygotic expression is ubiquitous in early wildtype embryos until segmentation, where *stbm* is upregulated in anterior neural tissues (Park & Moon, 2002). Overexpression of *stbm* mRNA on a wildtype background severely inhibits convergent extension movements, creating cyclopic embryos with a dramatically reduced anteroposterior body length, ventral curling of the body, bunched and blocky somites and a malformed yolk extension (Jessen *et al.*, 2002). Conversely, overexpression of *stbm* is capable of rescuing the convergent extension phenotype of homozygous *tri* mutant embryos (Jessen *et al.*, 2002). Injection of a morpholino against *stbm* (*stbm*-MO) in wildtype embryos recapitulates the convergent extension defects of *tri*, and this morpholino knockdown of *stbm* enhances the phenotype of homozygous *tri* mutants, resulting in cyclopic embryos that are greatly shortened in the anteroposterior axis and whose yolk extension is barely distinguishable from the yolk (Jessen *et al.*, 2002).

The *tri* mutation causes a number of alterations in cell behaviour relative to wildtype. In *tri*, cells undergoing convergent extension movements in the paraxial ectoderm fail to elongate properly, have a reduced LWR and do not mediolaterally align as successfully as comparable cells in wildtype gastrulae (Jessen *et al.*, 2002). Cell tracking analysis revealed the speed of convergence in *tri* embryos compared to wildtype embryos (Jessen *et al.*, 2002; Sepich *et al.*, 2000). In wildtype, ventrolateral cell movements are initially slow, speeding up at tailbud stage as the yolk plug is closing, then decelerating as somite formation begins (Jessen *et al.*, 2002; Sepich *et al.*, 2000). In contrast in *tri*, initial ventrolateral convergence is indistinguishable from wildtype but cells converge much more slowly around yolk plug closure and the start of segmentation (Jessen *et al.*, 2002; Sepich *et al.*, 2000). The direct result of this reduction in speed of convergence movements is that the blastoderm is thinner at the animal pole in *tri* embryos because of the delayed anterior extension of the mesoderm (Sepich *et al.*, 2000). Transplanted *tri* cells failed to revert to wildtype elongation or alignment in wildtype hosts, revealing these defective behaviours to be cell autonomous (Jessen *et al.*, 2002).

prickle (*pk*)

A zebrafish *prickle* mutant has yet to be generated. However, two orthologues of the *Drosophila* divergent class LIM-domain-containing protein have been identified, *pk1a* and *pk2* (Carreira-Barbosa *et al.*, 2003; Veeman *et al.*, 2003). Both zebrafish *pk1a* and *pk2* are expressed in tissues undergoing morphogenesis during gastrulation. *pk1a* has been shown to be maternally provided (Carriera-Barbosa *et al.*, 2003). Zygotic expression of *pk1a* begins dorsally in the pre-gastrula embryo, spreading through the germ ring during early gastrulation and restricting to migrating mesodermal cells as involution occurs (Carreira-Barbosa *et al.*, 2003; Veeman *et al.*, 2003). At the end of

gastrulation, *pk1a* is expressed paraxially in posterior neurectodermal and in pre-somitic mesodermal cells, and at the lateral border of the neural plate in a manner similar to *wnt11* expression (Carreira-Barbosa *et al.*, 2003; Veeman *et al.*, 2003). Zygotic *pk2* expression also begins dorsally and spreads around the blastopore lip, leading to a diffuse expression in the mesoderm and neurectoderm as gastrulation progresses, this expression restricting to the axial mesoderm at tailbud stage (Veeman *et al.*, 2003). Expression of *pk1a* and *pk2* persists after gastrulation in both neural and mesodermal structures although it has not been determined whether this complementary expression of vertebrate *prickle* genes reflects the kind of cooperation between *pk* isoforms evident in *Drosophila* (Gubb *et al.*, 1999; Veeman *et al.*, 2003).

Loss of function analysis of *pk1a* and *pk2* using morpholinos was used to dissect their involvement in the regulation of morphogenetic movements (Carreira-Barbosa *et al.*, 2003; Veeman *et al.*, 2003). *pk1a*-morphants (Fig. 1.2F) display an anteroposteriorly shortened, mediolaterally widened neural plate and notochord during gastrulation, resulting in a characteristic craniocaudally shortened and ventrally curled body axis at pharyngula stage (Appendix Two; Carreira-Barbosa *et al.*, 2003; Veeman *et al.*, 2003). Although it is unclear how the curly tail down phenotype relates to defective gastrulation movements, shortening of the body axis is highly reminiscent of gastrulation mutants like *slb*, *ppt* and *tri*. *pk2*-morphant embryos show similar but less severe gastrulation defects, while coinjection of *pk1a*-MOa and *pk2*-MOa does not significantly enhance the phenotype relative to single *pk* morphants, suggesting that *pk1a* and *pk2* are not functionally redundant (Veeman *et al.*, 2003).

In *pk1a* morphants at the end of gastrulation, the expression domains of neural markers such as *dlx3*, *pax2.1*, *krox20* and mesodermal markers like *ntl*, *hgg1*, *sna2* and *papc* are anteriorly shortened and

mediolaterally expanded while anteroposterior and dorsoventral patterning remains unaffected, characteristic of defective convergent extension movements (Fig. 1.2J & N; Appendix Two; Carreira-Barbosa *et al.*, 2003). *bmp2b* and *chd* expression show dorsoventral patterning to be unaffected in *pk1a*-morphants (Carreira-Barbosa *et al.*, 2003). *sna2* and *papc* expression patterns respectively show the head and pre-somitic mesoderm to be mediolaterally expanded due to reduced convergence (Carreira-Barbosa *et al.*, 2003). Likewise, expression of *dlx3* reveals a mediolaterally expanded neural plate, and within the neural plate, *pax2.1* in the prospective midbrain and *emx1* in the prospective telencephalon show expansion in the mediolateral axis (Carreira-Barbosa *et al.*, 2003). *ntl* expression reveals the notochord to be mediolaterally expanded and anteroposteriorly shortened, while *hgg1* expression reveals that anterior migration of the prechordal plate is impaired (Carreira-Barbosa *et al.*, 2003).

Gain of function analyses add further support to the idea that zebrafish *pk* regulates CE. Overexpression of *pk1a* in wildtype results in severe but variable disturbances to normal morphogenesis, ranging from a mediolaterally broader neural plate to twisted notochord (Veeman *et al.*, 2003). Furthermore, transplanted *pk1a* overexpressing cells showed an impaired ability to undergo convergence and extension, integrating less efficiently into the anteroposterior axis of the host for reasons not fully understood (Carreira-Barbosa *et al.*, 2003; Heisenberg, Tada *et al.*, 2000).

In *Drosophila* pupal wing cells, Prickle protein is localised to the distal edge of the cell, where it is thought to prevent the recruitment of Dsh protein to the cortical region. As a result the accumulation of Fz and Dsh at the membrane is restricted to the proximal edge of the cell, influencing the location of prehair formation through an unknown mechanism (Tree *et al.*, 2002). Without *pk* function Fz and Dsh remain symmetrically distributed and planar polarity is lost (Tree *et al.*, 2002). Similarly in

zebrafish, *pk1a* is capable of functionally interacting with the *fz/dsh* pathway in the context of vertebrate convergent extension. Loss of *pk1a* function was discovered to enhance the convergent extension defects of *slb* and *ppt* (Carreira-Barbosa *et al.*, 2003). In *slb* embryos injected with *pk1a*-MO, the anterior migration of the prechordal plate was more severely impaired than in *slb* mutants or *pk1a*-morphants alone (Carreira-Barbosa *et al.*, 2003). Likewise, in *ppt* embryos injected with *pk1a*-MO, the somites were more severely mediolaterally expanded and anteroposteriorly reduced than in *ppt* mutants or *pk1a*-morphants alone (Carreira-Barbosa *et al.*, 2003). *pk1a*-MO also enhances the CE defects of *tri* embryos, resulting in a severely shortened body axis and compressed somites (Carreira-Barbosa *et al.*, 2003).

Surprisingly, overexpression of *pk1a* mRNA does not rescue the phenotypes of established CE mutants like *silberblick* (*slb*), instead enhancing the severity of CE defects (Carriera-Barbosa *et al.*, 2003). This suggests that the amount of *pk* is critical for the regulation of CE, and anything more or less compromises CE. Despite the symmetrical cytoplasmic subcellular localisation of *pk1a* in the cells of the zebrafish gastrula, it is possible that, similarly to *Drosophila* PCP, *pk1a* acts to disrupt Dsh/Fz complex formation during CE. While increasing Fz7 levels has no effect on Pk1a, increasing Pk1a levels results in lower levels of Dsh (Carreira-Barbosa *et al.*, 2003).

knypek (*kny*)

knypek (Polish: shorty) was isolated in the 1996 Boston screen and classified as a mutant in which cellular rearrangements during gastrulation occurred abnormally (Fig. 1.2E; Driever *et al.*, 1996; Haffter *et al.*, 1996; Solnica-Krezel *et al.*, 1996; Topczewski *et al.*, 2001). Similarly to the *trilobite* mutant, cell tracking assays revealed anteroposterior extension of the body axis to be strongly

reduced in homozygous *kny* embryos as a result of impaired convergent extension movements, leading to mediolaterally broader somites and partial retinal fusion (Appendix Two; Solnica-Krezel *et al.*, 1996; Topczewski *et al.*, 2001). *kny* encodes *glypican*, a *heparan-sulphate proteoglycan* (*HPSG*) known to be involved in cell adhesion and expressed ubiquitously during gastrulation (Topczewski *et al.*, 2001). *kny:slb* double mutants show greatly enhanced convergent extension defects in a dose-dependent fashion, indicating that *kny* and *slb* interact in the context of gastrulation movements (Topczewski *et al.*, 2001). *kny/tri* double mutants are considered the strongest convergent extension mutants (Marlow *et al.*, 1998). Overexpression of *kny* mRNA enhances non-canonical Wnt signalling, suggesting that *kny* is a positive regulator of the non-canonical Wnt signalling pathway during morphogenesis (Topczewski *et al.*, 2001).

In summary, the cloning of genetic mutants and generation of morphants for zebrafish orthologues of *Drosophila* of core PCP genes connects interactions at the molecular level with cell behaviour, tissue-level behaviour and morphology. Aspects of mutant and morphant phenotypes less obviously related to impaired convergent extension movements highlight research directions that could potentially provide future insight into the genetic interactions underlying gastrulation cell behaviour.

PCP Signalling Outside Gastrulation in Vertebrates

Introduction

Growing evidence suggests that non-canonical Wnt signalling participates in cell migration events where patterning remains unaffected not just during gastrulation but at many points during development. Such observations add credence to the theory that PCP signalling represents a

generalised pathway for the regulation of cell movement, and the diverse range of developmental processes regulated by non-canonical Wnt signalling highlights the clinical significance of this pathway. There are clear parallels between *Drosophila* PCP and non-canonical Wnt signalling outside gastrulation in vertebrates: orientated hair arrays in ciliated structures throughout vertebrate development bear close resemblance to arrays of hairs in the fly that acquire their polarity through PCP signalling.

Planar cell polarity in vertebrates is evident in the inner ear, where rows of mechanosensory stereocilia are orientated in the plane of the epithelium, allowing them to respond to mechanical stimuli in a specific plane and convey information to the brain about balance, gravity or acceleration (Davies *et al.*, 2005; Lewis & Davies, 2002). Planar cell polarity in the vertebrate inner ear, similarly to the *Drosophila* wing or eye, exists on three levels: in the intrinsic asymmetry of the actin filament core that comprises each stereocilium, in the relationship of this asymmetry with neighbouring cells and globally in the epithelium (Davies *et al.*, 2005; Lewis & Davies, 2002). Core *Drosophila* PCP genes, such as *fz* and *fmi*, are evolutionarily conserved in vertebrates and are thought to function in the establishment of PCP in the vertebrate inner ear analogously to their function in PCP in *Drosophila* (Davies *et al.*, 2005; Lewis & Davies, 2002). The zebrafish *choroideremia* (*chm*) mutant, in which inner ear hair cells are extremely depleted in combination with swim bladder defects, pericardial oedema and retinal degeneration, encodes Rab Escort Protein 1 (REP1), crucial for the post-translational prenylation of members of the Rab-GTPase subfamily of the Ras family of G-proteins (Starr *et al.*, 2004).

Rab-GTPases are known to participate in vesicular transport (Starr *et al.*, 2004; Zerial & McBride, 2001). The subcellular localisation of Drosophila PCP genes is critical for the propagation of planar

cell polarity (Axelrod, 2001; Strutt, 2001; Tree *et al.*, 2002). Despite a lack of evidence demonstrating the asymmetric subcellular localisation of vertebrate Wnt/PCP proteins *in vivo*, expression of *Drosophila* Pk in vertebrate cells did show asymmetric accumulation, suggesting that the importance of subcellular localisation is evolutionarily conserved (Ciruna *et al.*, 2006). Protein prenylation is key to the function of Rabs in vesicular transport, and may also be important for the targeting and trafficking of vertebrate analogues of PCP proteins, for instance in the regulation of convergent extension movements. During zebrafish gastrulation, Wnt11 and Rab5c were demonstrated to interact in the regulation of E-Cadherin endocytosis, suggesting that non-canonical Wnt signalling modulates cell cohesion in prechordal mesendodermal cells by influencing vesicular trafficking (Ulrich *et al.*, 2005). Moreover, zebrafish orthologues of *Drosophila pk* bear a C-terminal prenlyation motif in the form of the CIIS sequence (Veeman *et al.*, 2003). While the CIIS motif is dispensable for the function of *pk* orthologues in the context of convergent extension, it is possible to speculate that this prenylation motif relates to the trafficking and subcellular localisation of *pk* orthologues (Veeman *et al.*, 2003). In support of the importance of this post-translational protein modification to directed cell migration, prenylation was more recently shown to be necessary for the migration of *primordial germ cells* (*PCGs*) into the developing zebrafish gonad (Thorpe *et al.*, 2004).

Kupffer's vesicle, a ciliated organ situated near the extending tailbud in the early zebrafish embryo, bears an inherent chirality that creates directional flow of fluid and signalling molecules around the embryo (Essner *et al.*, 2005). Disruption of cilia structure in the KV abolishes the directional fluid flow critical for the establishment of initial left/right asymmetry (Essner *et al.*, 2005; Kramer-Zucker *et al.*, 2005). Furthermore, cilia driven fluid flow is essential for the normal organogenesis of unpaired organs situated at the midline during gastrulation, such as the zebrafish kidney and brain: cilia defects that abolish fluid flow cause abnormal fluid retention that distends the forming kidney and

brain, leading to cystic kidneys and hydrocephaly (Kramer-Zucker *et al.*, 2005). Recently it was shown that zebrafish morphant *duboraya* (*dub*), in which the cilia in Kupffer's vesicle are fewer in number and incorrectly formed, has laterality, organogenesis and convergent extension defects (Oishi *et al.*, 2006). Upon examination, the non-canonical *frizzled2* morphant was discovered to share phenotypic features with *dub* morphants, including asymmetrical somitogenesis, disturbed heart laterality and abnormal heart development, prompting for the future an investigation into whether polymerisation of F-actin in cellular projections like cilia is an output of non-canonical Wnt signalling common to both Kupffer's vesicle formation and gastrulation movements (Oishi *et al.*, 2006; Sumanas *et al.*, 2001).

During vertebrate *neurulation*, a series of coordinated movements roll and fuse the neural plate into a tube known as the *neural tube*, which will give rise to the brain and spinal cord (Copp *et al.*, 2003). When neurulation occurs incorrectly, an *open neural tube* results, the basis of a spectrum of *neural tube defects* (*NTDs)* of varying axial location and severity that are amongst the most common birth defects in mankind, at an estimated 1/1000 births (Ciruna *et al.*, 2006; Copp *et al.*, 2003). The mouse mutants *loop-tail*, *crash* and *spin-cycle* exhibit defects in neural tube formation and encode components of the non-canonical Wnt signalling pathway (Copp *et al.*, 2003; Curtin *et al.*, 2003; Kibar *et al.*, 2001). A mutation in *tri/stbm* (known as *vangl2* in the mouse) is the basis of the *looptail* mutant, while two separate missense mutations in *fmi/stan* (known as *celsr1* in the mouse) underlie the *crash* and *spin-cycle* mouse mutants (Copp *et al.*, 2003; Curtin *et al.*, 2003; Kibar *et al.*, 2001). In these mouse mutants, impaired convergent extension movements result in an anteroposteriorly shorter, mediolaterally wider neural plate, and as a consequence, forming neural folds that normally fuse in the midline to form the neural tube are too far apart to do so (Copp *et al.*, 2003; Ybot-Gonzalez *et al.*, 2007). Both neural tube defects and convergent extension defects are evident in mice doubly mutant

for *dishevelled1* (*dvl1*) and *dishevelled2* (*dvl2*), while a loss of polarisation in neural keel cells that abolishes the orientation of cell division, causing daughter cells to be extruded from the forming neurepithelia, may underlie the neural tube defects in the *MZtri* mutant (Ciruna *et al.*, 2006; Wang *et al.*, 2006). Interestingly, neural tube defects also result from gain of function of dominant-negative *Rho kinase 2* (*dnRok2*) in zebrafish (Copp *et al.*, 2003; Marlow *et al.*, 2002). In both vertebrates and invertebrates, Rho-associated kinases (ROCKs) are used reiteratively in processes involving cell polarity and rearrangement: for instance in *Drosophila*, ROCKs are known to influence actin bundle formation during PCP in the wing (Marlow *et al.*, 2002; Winter *et al.*, 2001). Correlating these defects with non-canonical Wnt signalling not only provides insight as to the nature of the cellular effectors of the pathway, but may also influence clinical practice related to NTDs.

Exploring the applications of non-canonical Wnt signalling outside gastrulation in this way could further our knowledge of the common molecular interactions controlling cell polarity and movement, and potentially offer explanations for hitherto inexplicable aspects of non-canonical mutant or morphant phenotypes: for instance, laterality disturbances, heart defects or neural tube defects. In the following section I intend to focus on one area outside gastrulation particularly relevant to this thesis: Slit/Robo signalling.

PCP Signalling & Axon Pathfinding

During the formation of the *Drosophila* CNS, 90% of axons project across the midline to the contralateral side of the nervous system, creating a bilaterally symmetrical, ladder-like scaffold of axon commissures. The construction of this scaffold relies upon an intricate balance of attractive and repulsive axon guidance cues secreted by glial cells of the midline mesectoderm. Multiple long-range

diffusible and short-range contact-mediated guidance cues are thought to interact with axonally-expressed receptors to form a complex system by which appropriate commissure formation is promoted, inappropriate midline crossing is prevented, and erroneous crossing or recrossing are corrected (Kidd *et al.*, 1998; Seeger *et al.*, 1993; Tear *et al.*, 1996).

A novel transmembrane receptor of the Immunoglobulin superfamily, Roundabout (Robo), and a novel cell surface protein Commissureless (Comm), were discovered in a large-scale screen in *Drosophila* for mutants in which axon pathfinding across the CNS midline occurred abnormally while patterning in the CNS remained undisturbed (Kidd *et al.*, 1998; Seeger *et al.*, 1993; Tear *et al.*, 1996). In *robo* mutants, axons that normally project longitudinally instead cross and recross the midline (Kidd *et al.*, 1998a; Kidd *et al.*, 1998b; Seeger *et al.*, 1993). Conversely, in *comm* mutants, axons extend briefly towards the midline but retract with the result that almost no CNS commissures form (Seeger *et al.*, 1993; Tear *et al.*, 1996). These findings imply that Robo and Comm are involved in complementary aspects of growth cone guidance during midline crossing, a process distinct from other migratory events along axon trajectories (Seeger *et al.*, 1993; Tear *et al.*, 1996). The simplest interpretation of these phenotypes is that *comm* encodes a component of a chemoattractant pathway, while *robo* encodes a component of a chemorepellent pathway. In this model, migrating axons are free to cross the midline inappropriately in the absence of *robo* as the necessary repulsion is lacking, while in the absence of *comm*, repulsive mechanisms dominate, explaining why axons do not cross the midline. However, this model does not explain why *comm:robo* double mutants share the same phenotype as embryos singly mutant for *robo* (Seeger *et al.*, 1993; Tear *et al.*, 1996).

A better explanation is that *comm* functions to suppress *robo*, preventing commissural axons from responding to *robo*-mediated repulsion before they have crossed midline (Seeger *et al.*, 1993; Tear *et*

al., 1996). Indeed, when *comm* is overexpressed, a *robo*-like phenotype results and *robo* expression in the neurepithelium is greatly reduced (Kidd *et al.*, 1998b). *robo* is expressed at the surface of the growth cone as opposed to other regions of the axon in support of its role as a guidance receptor, while *comm* is expressed on the surface of midline glial cells (Kidd *et al.*, 1998a; Tear *et al.*, 1996). Axons that never normally cross the midline strongly express *robo* at the growth cone surface at all times, leaving *robo* free to act upon putative midline repellent cues (Kidd *et al.*, 1998a; Kidd *et al.*, 1998b). Axons that do normally cross the midline upregulate *robo* expression at the growth cone surface only after midline crossing has occurred: prior to midline crossing, *robo* is only weakly expressed at the cell surface as it is sequestered away from the growth cone surface in vesicles within the cell (Kidd *et al.*, 1998a; Kidd *et al.*, 1998b). Significantly, Comm is transferred from glial cells to axons once they have crossed the midline, where it is later visible in vesicles (Tear *et al.*, 1996). Whether directly or indirectly, *comm* is thought to regulate this internalisation of *robo* in these axons as part of an intricate mechanism to prevent axons lingering at the midline once they have crossed (Kidd *et al.*, 1998b).

The large secreted glycoprotein Slit was shown to act as a ligand for the transmembrane receptor Roundabout (Robo) (Brose *et al.*, 1999; Kidd *et al.*, 1999). Slit was first identified in *Drosophila*, where it is expressed at high levels by a subset of midline neurepithelial cells adjacent to growing neurons (Rothberg *et al.*, 1988). In the *Drosophila slit* mutant, the CNS axons scaffold is collapsed as migrating neurons enter the midline but cannot leave (Battye *et al.*, 1999; Kidd *et al.*, 1999; Rothberg *et al.*, 1988). This indicates that Slit normally functions as a chemorepellent cue in axon guidance in *Drosophila* (Battye *et al.*, 1999; Kidd *et al.*, 1999).

Slit and Robo orthologues are known to be structurally and functionally conserved in a number of vertebrates and invertebrates (Bedell *et al.*, 2005; Challa *et al.*, 2001; Challa *et al.*, 2005; Dalkic *et al.*, 2006; Fricke *et al.*, 2001; Hutson *et al.*, 2001; Kidd *et al.*, 1998a; Lee *et al.*, 2001; Park *et al.*, 2003; Yeo *et al.*, 2001; Zallen *et al.*, 1998). The zebrafish mutant *astray* (*ast*) carries a mutation in vertebrate *robo2* and was originally identified in a screen for mutants in which retinotectal axon pathfinding occurred abnormally (Karlstrom *et al.*, 1996; Fricke *et al.*, 2001; Hutson & Chien, 2002). In *ast* mutants, pathfinding errors approaching and exiting the CNS midline occur more frequently and are less likely to be corrected than in wildtype (Hutson & Chien, 2002). Likewise, loss of function of the *robo3 variant 1* (*robo3v1*) isoform of zebrafish *robo3* resulted in the misdirection of motor axon projections from the spinal cord (Challa *et al.*, 2005). Conversely, the vertebrate *robo* orthologue *magic roundabout* (*robo4*) is not expressed in neuronal tissues and does not regulate axon pathfinding (Bedell *et al.*, 2005; Huminiecki *et al.*, 2002; Park *et al.*, 2003). *robo4* is expressed in the vascular endothelium at sites of active angiogenesis in mice and zebrafish, where it inhibits the migration of endothelial cells during angiogenesis in a manner analogous to axon pathfinding (Bedell *et al.*, 2005; Huminiecki *et al.*, 2002; Park *et al.*, 2003). The function of vertebrate orthologues of *Drosophila robo* in the construction of structures as diverse as neuronal scaffolds and vascular networks raises the possibility that the Robo receptor is employed reiteratively in the control of directed cell migration throughout development.

To date, no homologue of *Drosophila comm* has been identified in vertebrates. However, an equivalent mechanism of the cytoplasmic sequestering of the Robo receptor, critical to preventing premature Slit receptivity away from the *Drosophila* CNS midline, may have been identified in vertebrates. *Rig-1/Robo3* is a mouse orthologue of *Drosophila robo* distantly related to other murine *robo* orthologues, originally discovered in a screen for genes upregulated in *retinoblastoma* deficient

mice (Yuan *et al.*, 1999). In the mouse, *Rig-1* expression is visible in the forebrain and spinal cord and also in non-neural tissues in the head, where it overlaps with the expression of murine *robo1* (Camurri *et al.*, 2004). More recently, it was discovered that expression of *Rig-1* in precrossing mammalian commissural neurons reduced their sensitivity to the Slit ligand in a manner analogous to the interaction between Comm and Robo in *Drosophila* (Sabatier *et al.*, 2004). In *Rig-1* knockout mice, premature sensitivity to Slit chemorepellent activity resulted in a lack of commissures throughout the CNS, a phenotype highly reminiscent of the *Drosophila commissureless* mutant (Sabatier *et al.*, 2004). This phenotype is partially rescued in *Rig-1:robo1* double mutant mice but not at all in *Rig-1*: *robo2* double mutants, suggesting that Rig-1 suppresses Robo1's ability to respond to the Slit signal *in vivo* (Sabatier *et al.*, 2004). This could indicate that vertebrate Slit/Robo signalling has evolved an alternate Comm-like mechanism to prevent premature Slit-mediated repulsion.

The role of vertebrate orthologues of *Drosophila slit* in axon guidance is not straightforward: the *slit* cue has been shown to act at both short and long range, and as both a chemorepellent and a chemoattractant (Brose *et al.*, 1999; Kidd *et al.*, 1999; Wang *et al.*, 1999). Like *Drosophila slit*, undergo post-translational modification in the form of proteolytic processing, yielding C- and N-terminal fragments that both function during development (Brose *et al.*, 1999). While the 55-60kDa C-terminal fragment (Slit2-C) is sufficient to rescue the fly *slit* mutant, the larger 140kDa N-terminal fragment (Slit2-N) has been shown to be involved not only in axon repulsion in flies and in vertebrates, but also in axon branching in vertebrates (Brose *et al.*, 1999; Kidd *et al.*, 1999; Wang *et al.*, 1999). Slit2-C is highly diffusible, whereas Slit2-N is more closely associated with the cell surface membrane, prompting speculation that Slit2-C mediates long-range functions while Slit2-N mediates short-range functions (Brose *et al.*, 1999).

Four *slit* orthologues, *slit1a*, *slit1b*, *slit2* and *slit3*, have been identified in zebrafish, each sharing a high degree of homology with *Drosophila slit* but intriguingly, expressed prior to axonogenesis (Hutson *et al.*, 2003; Yeo *et al.*, 2001). *slit2* and *slit3* are not reported to be expressed maternally, while zygotic expression of *slit2* and *slit3* starts at midgastrula stage (Yeo *et al.*, 2001). As gastrulation proceeds, *slit2* expression becomes restricted to the axial mesoderm and neurectoderm and the anterior border of the neural plate, while *slit3* expression becomes restricted to the axial mesoderm and neurectoderm and the prechordal plate (Yeo *et al.*, 2001). Two isoforms of *slit1*, *slit1a* and *slit1b*, are expressed ubiquitously between the 16-cell stage and dome stage, implying that these *slits* are maternally provided, but their expression profile during gastrulation is unknown (Hutson *et al.*, 2003).

Six *robo* orthologues have been identified in zebrafish: *robo1*, *robo2*, *robo2_tv2*, *robo3v1*, *robo3v2* and *robo4* (Bedell *et al.*, 2005; Challa *et al.*, 2001; Challa *et al.*, 2005; Dalkic *et al.*, 2005; Lee *et al.*, 2001). Both *robo2* and *robo3* exist as two isoforms with distinct expressions and functions during development, known as *robo2* (also known as *robo2 variant 1* or *robo2_tv1*) and *robo2 variant 2* (*robo2_tv2*), and *robo3 variant 1* (*robo3v1*) and *robo3 variant 2* (*robo3v2*) respectively (Challa *et al.*, 2005; Dalkic *et al.*, 2006). Of these zebrafish orthologues, *robo1*, *robo2, robo3v1* and *robo3v2* are reported to be maternally provided (Challa *et al.*, 2005). Zygotic *robo1* starts to be expressed at midgastrula stage and continues to be expressed ubiquitously during gastrulation (Challa *et al.*, 2001; Lee *et al.*, 2001). *robo2* starts to be expressed towards the end of gastrulation (Challa *et al.*, 2001; Lee *et al.*, 2001). The newly described splice variant of *robo2*, *robo2_tv2*, does not start to be expressed until 24hpf (Dalkic *et al.*, 2006). Meanwhile, both *robo3v1* and *robo3v2* are expressed during gastrulation: *robo3v1* is only weakly expressed during early gastrulation but peaks at 10hpf, while *robo3v2* is expressed most strongly during early gastrulation and diminishes towards the

completion of gastrulation (Challa *et al.*, 2005). Interestingly, of the two variants of *robo3*, *robo3v1* structurally resembles an "authentic" *robo* receptor, while *robo3v2* is structurally more reminiscent of the murine *robo* orthologue *Rig-1*, thought to act in a manner similar to *Drosophila* Comm (Challa *et al.*, 2005; Sabatier *et al.*, 2004). However, despite *robo3v2* lacking a canonical signal sequence, both *robo3v1* and *robo3v2* are expressed at the cell surface, and the significance of their structural diversity remains unclear (Challa *et al.*, 2005). *robo4* expression in the notochord is first visible during late gastrulation and persists until the 23 somite stage, at which time *robo4* begins to be expressed in the forming heart and vasculature, supporting its role in endothelial cell migration and angiogenesis (Bedell *et al.*, 2005).

Gain of function of *slit2* in zebrafish causes impaired convergent extension movements and cyclopia, suggesting that *slit2* has an early role in directed cell migration in a process distinct from axon guidance (Yeo *et al.*, 2001). Furthermore, loss of function of *robo3v2* in zebrafish results in a reduction of the anteroposterior axis highly reminiscent of impaired convergent extension movements (Challa *et al.*, 2005). These facts, combined with the expression of *slit* and *robo* orthologues during gastrulation, prompted the following questions. Does the repellent ligand Slit act through its axon pathfinding receptor Robo in the regulation of gastrulation movements, for instance as a component of a universal mechanism of cell migration? If so, how does Slit/Robo signalling integrate with the non-canonical Wnt signalling pathway known to regulate convergent extension movements?

A generalised cell migration defect that perturbs many types of cell movements in the embryo, for instance both during gastrulation and axon pathfinding, is plausible when it is considered that disturbances to cell migration outside the context of gastrulation movement have been observed in *trilobite* and *pk1a* morphants (Bingham *et al.*, 2002; Carreira-Barbosa *et al.*, 2003; Jessen *et al.*,

2002). *pk1a* and *tri* are expressed in the hindbrain during neuronal migration, and *prickle* and *trilobite* cooperate in the regulation of hindbrain branchiomotor (nVII) neuron migration (Carreira-Barbosa *et al.*, 2003; Jessen *et al.*, 2002). The tangential migration of facial (nVII) hindbrain branchiomotor neurons into posterior rhombomeres is slower and less well directed in *tri* (Bingham *et al.*, 2002; Jessen *et al.*, 2002). Like the gastrulation defect of *tri*, this neuronal migration phenotype can be rescued by overexpression of *stbm* mRNA (Jessen *et al.*, 2002). However, *tri* acts non-autonomously in branchiomotor neuron migration: transplanted wildtype motor neurons did not migrate normally in *tri* host rhombomeres, but the abnormal migration of transplanted *tri* neurons was rescued on a wildtype host background (Jessen *et al.*, 2002). In *pk1a* morphants, branchiomotor neuron migration was similarly reduced, while *pk1a*-MO greatly enhanced the migration defects of *tri* heterozygotes, confirming that *pk1a* and *tri* cooperate in the regulation of branchiomotor neuron migration (Carreira-Barbosa *et al.*, 2003). As branchiomotor neuron migration is normal in *slb*, *ppt* and *kny* embryos, and injection of the PCP specific dominant negative form of *dsh*, *Xdd1*, has no effect on branchiomotor neuron migration in wildtype embryos, it has been proposed that this process is regulated independently of non-canonical Wnts (Bingham *et al.*, 2002; Jessen *et al.*, 2002).

In this thesis, I explore a significant collaboration between axon guidance genes and non-canonical Wnt signalling components in the regulation of convergent extension movements during gastrulation to understand potential elements of a universal mechanism for directed cell migration. In Chapter Three of this thesis, I characterise the novel *pk1* splice variant, *pk1b*. I show that *pk1b* is expressed during gastrulation in a manner dissimilar to zebrafish *pk1a*. In Chapter Four, I show that the Slit2 ligand acts through Robo2 and Robo3v2 receptors in the regulation of convergent extension movements during zebrafish gastrulation. I undertake a more thorough examination of the expression of key zebrafish *slit* and *robo* orthologues throughout gastrulation, then using both loss of function

and gain of function approaches, I demonstrate a role for Robo2 and Robo3v2 in convergent extension movements. Subsequently in Chapter Five, I show that Slit/Robo signalling interacts with zebrafish orthologues of the *Drosophila* PCP gene *prickle*. Finally in Chapter Six, I characterise a novel convergent extension mutant generated as part of screen for enhancers of the *silberblick/wnt11* (*slb*) phenotype.

Chapter Two

Materials & Methods

Fish Maintenance & Techniques

General Care

Adult zebrafish were kept in an aquarium system supplied by Aquatic Habitats according to the guidelines set out in The Zebrafish Book (Westerfield, 2000). Fish were kept at optimal stocking density (40 per 10L tank) and frequent stock-taking ensured that, where possible, two or three reliable breeding pairs of each line from the current generation were available for use, while a new generation, for instance six months younger, was being raised to take their place when older carriers became less reliable. A departmental breeding rotation system was in place to produce AB x TU strain wildtype embryos every morning, while mutants were paired individually in breeding boxes the night before embryos were required. Embryos were kept in Fish Medium in plastic 90mm Petri dishes at 28.5°C (see Appendix One for Fish Medium details) and staged according to standard references such as Kimmel *et al.*, 1995. To maintain the transparency of the fish for observation past 24hpf, 2ml of 25X stock solution of the pigment inhibitor 1-phenyl-2-thiourea (PTU) was added to the Fish Medium in the Petri dish (approximately 50ml; final concentration of PTU therefore in the range of 1X) prior to the start of pigmentation. Fry were humanely culled in the lab by overdose of the anaesthetic Tricaine (MS222: Sigma) and never kept beyond 5dpf in line with Home Office recommendations. Procedures such as culling adult fish or finclipping were performed by the UCL Zebrafish Facility staff on our behalf.

Enhancers of *slb*: Screen Strategy

A number of mutants that act as enhancers or suppressors of the *silberblick* phenotype were isolated as part of a chemical mutagenesis screen performed in 2001/2002 in collaboration with the Heisenberg Lab at the Max Planck Institute in Dresden (Figure 2.1: based upon the 1996 screen in which many mutants, including *slb*, *tri*, *ppt* and *kny*, were identified. See Appendix Two; Haffter *et al.*, 1996, Driever *et al.*, 1996; Mullins *et al.*, 1994; Solnica-Krezel *et al.*, 1996). To generate these mutants, fertile adult *slb* males were treated with Ethylnitrosourea (ENU; Sigma), a mutagenic agent that generates point mutations in sperm DNA (see The Zebrafish Book: Westerfield, 2000). Mutagenised males were then crossed with untreated wildtype females of the strain TL. Progeny of the first mating were discarded to avoid fertilisation with residual sperm produced before mutagenesis. Progeny of the next mating, the F1 generation, were 100% heterozygous for *slb* plus several novel, ENU-induced mutations. These F1 fish were raised to adulthood where they were randomly incrossed to yield screenable F2 generation embryos. F2 generation embryos were fixed at tailbud stage and scored for enhancement of the *slb* phenotype through *in situ* hybridisation for the *dlx3*, *hgg1* and *ntl* markers. F2 parents whose progeny did show an enhancement of the convergent extension defects of *slb* were then outcrossed with TL for two generations to eliminate *slb*, creating carriers heterozygous solely for the mutation of interest. In this medium-scale screen, we screened 354 genomes and two mutants were identified, homozygous embryos of which showed a phenotype.

Dissection, Fixation & Storage of Embryos

Embryos younger than 10hpf and still inside their chorionic membrane were fixed directly and dechorionated afterwards. For unhatched embryos older than 10hpf, it was necessary to

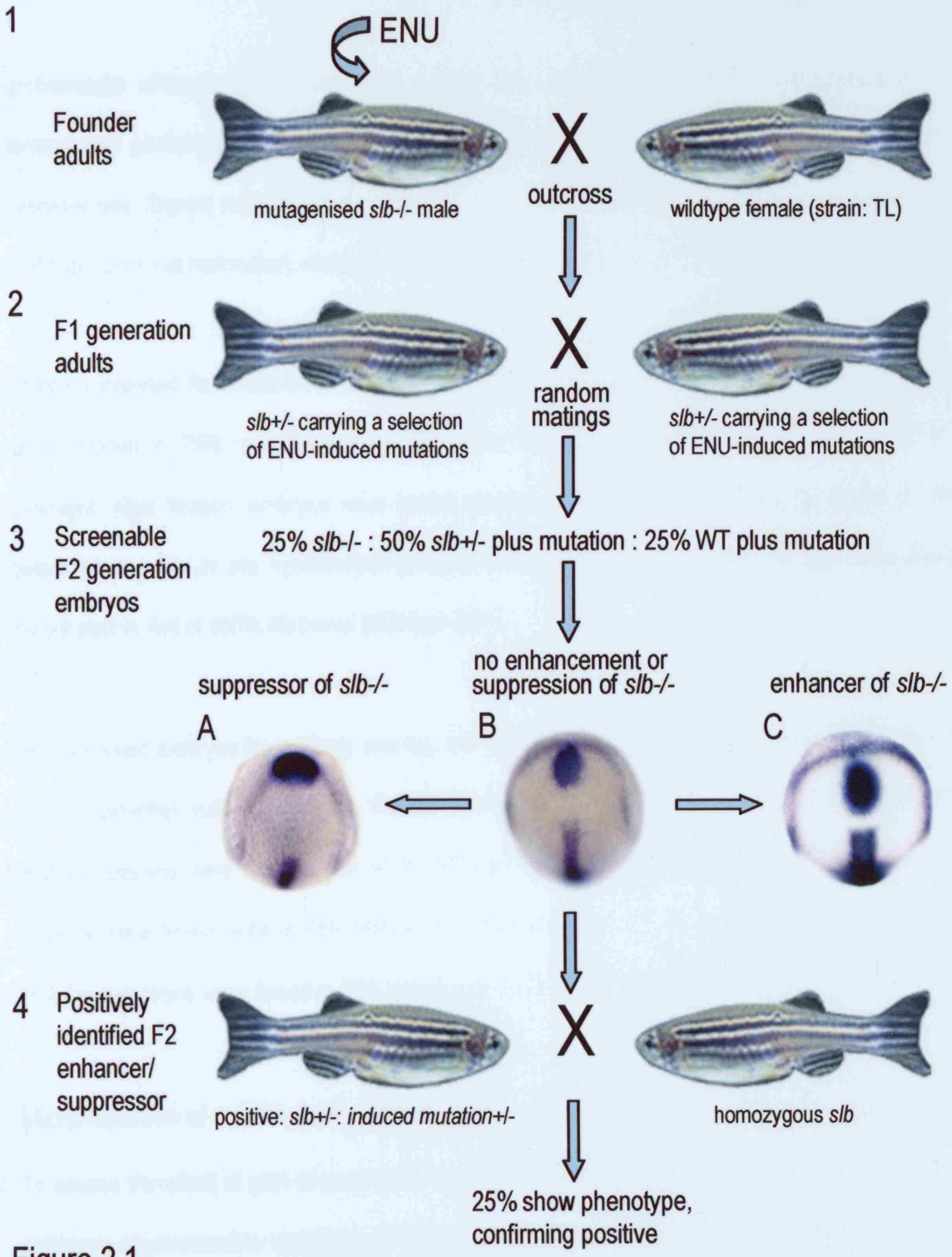

Figure 2.1

Screen strategy: generation of dominant enhancers and suppressors of the *silberblick/wnt11* (*slb-/-*) phenotype.

1. ENU-mutagenised founder *slb-/-* males were outcrossed with wildtype females of the strain TL to yield F1 generation adults 100% heterozygous for *slb* and each carrying a selection of ENU-induced mutations. 2. F1 fish were randomly incrossed. 3. The F2 progeny screened by *in situ* hybridisation for the mesodermal markers *ntl* and *hgg1* and the neurectodermal marker *dlx3* to screen for potential enhancement (C) or suppression (A) of the convergent extension defects of *slb-/-* (B). 4. Positively identified carriers of a mutation enhancing or suppressing the *slb-/-* phenotype were crossed with *slb-/-* carriers, and if 25% of the progeny showed the enhanced/suppressed phenotype, the positive identification was confirmed.

dechorionate embryos before fixation to ensure they are completely fixed. Dechorionation with forceps was performed on a dissection plate (see Appendix One) consisting of 1% Agarose for everyday use (Sigma) topped with a small volume of 1X PBS (OXOID), to minimise damage to the embryos. Once dechorionated, embryos were collected in 1.5ml Eppendorf tubes ready for fixation.

Embryos intended for whole-mount *in situ* hybridisation were fixed in 1ml of 4% Paraformaldehyde (PFA; Sigma) in PBS (see Appendix One), either at room temperature for 2 hours or at 4°C overnight. After fixation, embryos were rinsed several times in PBS to remove all traces of PFA before starting the *in situ* hybridisation protocol, or where necessary, fixed embryos were stored dehydrated in 1ml of 100% Methanol (BDH) at -20°C.

Dechorionated embryos for antibody staining with the acetylated tubulin antibody were fixed with 1ml of 20% Dimethyl sulfoxide (DMSO; Sigma) in Methanol at 4°C overnight. All other embryos for antibody staining were fixed in 1ml of 4% PFA as for *in situ* hybridisation. DMSO/Methanol-fixed embryos were rinsed twice in 75% Methanol in PBS and stored in 1ml of 100% Methanol at -20°C. PFA fixed embryos were rinsed in PBS and stored in 1X PBS at 4°C.

Micro-Injection of mRNA & Morpholino *in vivo*

To assess the effect of gain of function through mRNA over-expression, or loss of function through antisense oligonucleotide morpholinos (Nasevicius & Ekker, 2000), I used a Picospritzer III, 3-axis micromanipulator and glass capillary needle pulled on a P-87 Micropipette puller (Sutter Instruments) to micro-inject approximately 1nl of mRNA or morpholino into live embryos, either in the centre of the

yolk directly under the cell at the single-cell stage, ensuring even distribution during subsequent cell divisions, or into specific cells to label a population of cells at later stages.

Embryos collected immediately after laying at 9:30am were lined up against the edge of a glass slide (BDH) in a plastic Petri dish lid using a 3ml graduated plastic pastette, excess fish medium removed so that embryos were held in place by capillary action. Then, using Eppendorf Microloader pipette tips, around 4µl of RNA or morpholino was loaded into a glass capillary needle. I calibrated the volume to be micro-injected by snapping the needle with clean forceps at high magnification and, using a graticule slide, altering the injection interval in microseconds until 10 pedal clicks produced a droplet 2 graticule units in diameter (approximately 2nl). Prior to injecting, I compared droplet size to embryo size to check that the volume was not too large for the yolk or cell to contain: normally 2 pedal clicks (approximately 1nl) was appropriate. After each embryo was injected and the row was completed, I checked whether fluid was still flowing out of the needle to confirm that every embryo received the dose. The injected embryos were then rinsed off the slide with a pastette and placed in a clean, labelled Petri dish for incubation at 28°C.

Imaging: Fixed Specimens

I observed and photographed fixed specimens by placing them in a drop of 90% glycerol on a depression slide (BDH) against a white background. A plastic needle was used to orientate the embryos. To photograph, I used a Leica DFC320 digital camera and software on a Nikon SMZ1500 dissection microscope. Images were subsequently optimised using Adobe Photoshop CS1.

Imaging: Live Photography

Live specimens for observation and photography were first anaesthetised in a low concentration solution of Tricaine in Fish Medium to reduce movement, then viewed with transmitted light in a drop of 2.5% Methyl Cellulose in Fish Medium (see Appendix One) on a depression slide. A plastic needle was used to orientate the embryos. To photograph, I used a Leica DFC320 digital camera and software on a Nikon SMZ1500 dissection microscope. Images were subsequently optimised using Adobe Photoshop CS1.

Imaging: *in vivo* Time-Lapse Movies

For time-lapse imaging, embryos were first dechorionated on a pre-warmed dissection plate made with 1% Agarose in Hank's Embryonic Medium (see Appendix One). Healthy dechorionated embryos intended for confocal time-lapse microscopy were mounted on a glass coverslip (BDH) in a bead of 1% Agarose (Type VII low-melt; Sigma) in Hank's Embryonic Medium, and orientated such that the region of interest faced the coverslip. To achieve this, low-melt Agarose aliquots in a 1.5ml Eppendorf tubes were heated in a 50°C heat block until melted, but cooled slightly before mounting to prevent damage to the live embryos. To mount each embryo, I took a small volume of warm Agarose in a flame-polished glass pipette into which I sucked the chosen embryo. I put embryo and Agarose back into the warm aliquot to reduce the amount of Fish Medium diluting the Agarose. I then sucked up Agarose and embryo and placed on the coverslip in a small bead. I orientated each embryo quickly using a hair loop before the bead cooled, then left the beads to set. Meanwhile I "drew" rectangular watertight chambers on to glass slides with a syringe filled with Silicon Grease (RS). I filled these chambers with pre-warmed Hank's Embryonic Medium, then pressed the coverslips, mounted

embryos facing inwards, against the Silicon Grease to form a sealed chamber where the Agarose bead was bathed in warm embryo medium and the region of interest faced upwards. This chamber could then be safely immersed in a Petri dish of distilled water for *in vivo* imaging. Time-lapse movies were captured through a 63X water immersion lens on a Leica DMLFS confocal fluorescence microscope. Subsequently, images were processed in ImageJ software.

Imaging: Subcellular Localisation of Venus-Pk1b *in vivo*

To visualise the subcellular localisation of the Venus-Pk1b protein (Venus is a YFP derivative; shared with the Wilson Lab by Atushi Miyawaki) relative to Membrane-RFP at shield and tailbud stages, it was necessary to inject a low concentration of each mRNA to avoid an overexpression phenotype. Firstly, I combined a subthreshold but clearly visible dose of *venus-pk1b* mRNA (300pg) with *membrane-RFP* mRNA (100pg) and co-injected this mixture into a single cell between the 2 and 8-cell stage (see Micro-Injection of mRNA & Morpholino *in vivo* for injection protocol) to visualise the subcellular localisation mosaically on a wildtype background. Secondly, I combined *venus-pk1b* and *membrane-RFP* mRNAs at these doses with a subthreshold dose (100pg) of one of the following experimental mRNAs: *fz7* or *stbm*. I mounted and photographed z-sections through these embryos at between 40% epiboly and shield stage using the confocal microscope (see Imaging: *in vivo* Time-Lapse Movies section for protocol). Finally, to put this subcellular localisation in context, I injected *membrane-RFP* mRNA (100pg) at the 1-cell stage to ubiquitously label the cell membrane, and injected *venus-pk1b* mRNA (300pg) into a single cell at the 8-cell stage to yield mosaic expression. At the 2-somite stage I mounted these embryos in a dorsal orientation to visualise by confocal microscopy any relationship between the subcellular localisation of Venus-Pk1b relative to landmarks

such as the notochord-somite boundary. Localisation was visualised through a 63X water immersion lens on a Leica DMLFS confocal fluorescence microscope. Images were subsequently optimised using Adobe Photoshop CS1.

Molecular Techniques

Linearisation of Template DNA for Microinjection mRNA or Riboprobe Manufacture

Before the *in vitro* transcription of ribonucleic acids, template DNA contained within a vector must be linearized via restriction digest at unique restriction sites upstream of the 5' end of the insert. Based upon Sambrook *et al.*, 1989, I typically linearized 5µg of template DNA in a total reaction volume of 50µl as follows:

5µg Template DNA

10µl Restriction Buffer optimal for enzyme(s) (Boehringer Mannheim)

2µl Restriction Enzyme(s) (Promega)

Ultra-pure H_2O to 50µl

This reaction was incubated in a 37°C water bath for 3 hours. The linearized DNA was then extracted by adding 1 volume of Phenol/Chloroform/Isoamyl Alcohol 25:24:1 (Sigma), vortexing and centrifuging at 13,000 RPM for 10 minutes. After spinning, the hydrophilic supernatant containing the linearized DNA was carefully removed and placed in a fresh autoclaved 1.5ml Eppendorf tube. To precipitate the DNA, 1/10 volume of NaOAc (Sigma) and 2 volumes of 100% Ethanol (BDH) were added and the reaction chilled at -80°C for a minimum of 30 minutes. The reaction was then spun at

13,000 RPM in a refrigerated centrifuge at 4°C for 20 minutes, after which time the DNA was visible as an opaque pellet on the back of the tube. The supernatant was carefully removed and replaced with 2 volumes of 70% Ethanol in H_2O to wash the pellet, and spun again at 13,000 RPM for 20 minutes at 4°C. The supernatant was again carefully removed and the pellet dried either by vacuum drying or by evaporation, before resuspension in the desired volume of H_2O.

in vitro Transcription: Riboprobe Manufacture

Based upon Sambrook *et al.*, 1989, manufacture of probe for *in situ* hybridisation took place in a total volume of 20µl as follows:

1µg linear DNA

7.5µl Ultra-pure H_2O

4µl 5X Transcription Buffer (Promega)

2µl DTT (Promega)

2µl DIG RNA Labelling Mix (Roche Diagnostics)

0.5µl RNasin (Promega)

2µl RNA Polymerase (Promega)

This reaction was incubated in a 37°C water bath for 2 hours. After this, 1µl of DNase (Promega) was added for every 1µg of template DNA, and the reaction was incubated at 37°C for a further 20 minutes. The DNase was then heat-inactivated in a 70°C heat block for 10 minutes. As the DIG label segregates to the hydrophobic/organic proportion during Phenol/Chloroform/Isoamyl Alcohol

extraction, it was not possible to purify riboprobe in this way. Instead, the probe was column-purified (Amersham): the total reaction volume was made up to 50µl by the addition of 30µl of ultra-pure H_2O, then passed through a pre-prepared column to remove any free DIG, template DNA, enzymes, etc. Eluate from the column containing the pure probe was stored 1:1 with Formamide (Sigma).

PROBE	REFERENCE	VECTOR	LINEARISE	TRANSCRIBE
ntl	Schülte-Merker *et al.*, 1994	pBS	HindIII	T7
hgg1	Vogel & Gerster, 1997	Unknown	Xho1	T3
dlx3	Ekker *et al.*, 1992	pBS	EcoR1	T7
papc	Yamamoto *et al.*, 1998	Unknown	Apa1	T3
sna2	Thisse *et al.*, 1995	Unknown	Xho1	T7
pax2.1	Takeuchi *et al.*, 2003	Unknown	Unknown	Unknown
rx3	Loosli *et al.*, 2003	pBS SK	Xba1	T7
chd	Miller-Bertoglio *et al.*, 1997	Unknown	Not1	SP6
bmp2b	Nikaido *et al.*, 1997	pBS KS-	EcoR1	T3
GATA1	Detrich *et al.*, 1995	Unknown	Xba1	T7
foxA3/ fkd2	Odenthal & Nüsslein-Volhard, 1998	Unknown	Apa1	T7
scl	Gering *et al.*, 1998	pBS	Ecor1	T7
cmlc2	Yelon *et al.*, 1999	Unknown	Not1	T3
pk1a	Carreira-Barbosa *et al.*, 2003	pBS	EcoR1	T3
pk1b	Unpublished	pBS	EcoR1	T3
pk2	Veeman *et al.*, 2003	pBS	Unknown	Unknown
slit1a	Hutson *et al.*, 2003	pBSII SK+	HindIII	T3
slit2	Yeo *et al.*, 2001	pBS	Xho1	T3
slit3	Yeo *et al.*, 2001	pBS	Xho1	T3
robo1	Lee *et al.*, 2001	pBS	HindIII	T7
robo2	Lee *et al.*, 2001	pBSII SK+	Xho1	T3
robo3v1	Lee *et al.*, 2001	pBS	HindIII	T7
robo4	Bedell *et al.*, 2004	pBS SK-	BamH1	T7

Table 1. *in situ* hybridisation probes used in this thesis.

Neat probe was stored at –20°C, to be diluted in Hybridisation Buffer before *in situ* hybridisation. Where the optimum dilution for a probe was unknown, a trial hybridisation with a provisional dilution of 1/100 helped calibrate a suitable working concentration.

I assessed the quality of the riboprobe by RNA Gel Electrophoresis. 1µl of probe plus 4µl of ultra-pure H_2O was denatured for 5 minutes in a 70°C heat block, then put on ice for 2 minutes. After the addition of 2µl of 6X Agarose Loading Dye, the sample was loaded immediately on to a 0.8% Agarose Gel containing 1µl of Ethidium Bromide. The gel ran at 100V for approximately 30 minutes before visualisation under UV light.

in vitro Transcription: mRNA for Micro-Injection

For large transcripts, I used Message Machine T7 and SP6 Kits (Ambion) according to their standard protocols to boost mRNA yield and quality; otherwise I used a protocol based upon Sambrook *et al.*, 1989 to manufacture mRNA for *in vivo* micro-injection. Transcription took place in a total reaction volume of 50µl as follows:

5µg linear DNA, made up to 26.5µl with ultra-pure H_2O

10µl 5X Transcription Buffer

5µl DTT

4.5µl NTP Cap Mix (NEB; see Appendix One)

1µl RNasin (Promega)

3µl RNA Polymerase (Promega)

This reaction was incubated in a 37°C water bath for 30 minutes before the addition of 2.5µl 10mM uncapped GTP (Roche Diagnostics) to promote extension of the transcripts. With very long

transcripts, it is possible to add 2.5µl of 20mM GTP. The reaction was incubated for 1 hour at 37°C before 5µl DNase was added, then incubated for a further 30 minutes at 37°C.

The RNA was extracted by adding one volume of Phenol/Chloroform/Isoamyl Alcohol, vortexing and centrifuging at 13,000 RPM for 10 minutes. The supernatant containing the RNA was placed in a fresh autoclaved Eppendorf tube before a second purification step: a pre-prepared column (Clontech) in a 4°C refrigerated centrifuge at 2000 RPM for 5 minutes. To precipitate, 1/10 volume of NaOAc and 2 volumes of 100% Ethanol were added to the eluate and the RNA chilled at -80°C for a minimum of 30 minutes. The precipitated RNA was spun for 20 minutes at 13,000 RPM in a 4°C refrigerated centrifuge, after which the RNA could be seen as an opaque pellet. The supernatant was removed and the pellet washed with 2 volumes of 70% Ethanol in ultra-pure H_2O at 4°C for 20 minutes at 13,000 RPM. The supernatant was removed and the pellet dried by evaporation on ice before resuspension in the desired volume of H_2O.

The amount and quality of RNA transcribed was assessed in two ways. Firstly, I looked at the intensity and smearing of the band produced during RNA Gel Electrophoresis. 1µl of probe plus 4µl of ultra-pure H_2O was denatured for 5 minutes in a 70°C heat block, then put on ice for 2 minutes. 2µl of 6X Agarose Loading Dye was added and the RNA was loaded immediately on to a 0.8% Agarose Gel containing 1µl of Ethidium Bromide. The gel ran at 100V for approximately 30 minutes before visualisation under UV light. Secondly, I measured the Optical Density (OD) of the RNA using a spectrophotometer to compare the concentration and quality of 1/40 dilutions of RNA against distilled water.

Cloning of *pk1b*

The novel *pk1* gene *pk1b* was cloned by Masa Tada according to the protocol outlined in Carreira-Barbosa *et al.*, 2003. An EST clone with high homology to *Xenopus pk* was used as a probe to screen a gastrula cDNA library (Lambda ZAP) and isolate a full-length cDNA for *pk1b*. The positive clones were converted into pBS SB(-). An antisense probe for *pk1b* for *in situ* hybridisation was manufactured by linearising pBS-*pk1b* with EcoR1 and transcribing with T3 (Table 1). Morpholinos and mRNA were manufactured based upon maps provided by Vicky Prince, University of Chicago.

Morpholino Preparation

A preliminary examination of *slit*-MOs was possible using 10µl aliquots of 10ng/nl stock solutions of *slit1a*-MO, *slit1b*-MO, *slit1*-SBMO *slit2*-MO and *slit3*-MO generously supplied by Chi-Bin Chien, University of Utah. Subsequently, we ordered *slit1a*-MO and *slit2*-MO based upon the published sequence of these morpholinos, and they were supplied by GeneTools as a 300mM lyophilised powder and resuspended in 300µl 1X HEPES buffer (Appendix One) yielding a 4mM stock solution that was stored at -80°C. A 20µl aliquot of an 8ng/nl stock solution of *pk1b*-MOb was kindly provided by Vicky Price, University of Chicago. According to the published sequences, we ordered *robo2*-MO, *robo3v1*-MO and *robo3v2*-MO from GeneTools and resuspended these in HEPES buffer also (Challa *et al.*, 2005; Hutson & Chien, 2002). Aliquots of 4mM stock solutions of *pk1a*-MO and *pk1b*-MOa were provided by Masa Tada and Filipa Carreira-Barbosa. The morpholinos used in this thesis are listed in Table 2.

MORPHOLINO	TYPE	SEQUENCE	REFERENCE
pk1a-MO	ATG	GCCCACCGTGATTCTCCAGCTCCAT	Carreira-Barbosa *et al.*, 2003
pk1b-MOa	ATG	GGCAGTAGCGAATCTGTGTTGAAGC	Unpublished
pk1b-MOb	SB	ttaatgaaactcacCAATATTCTCT	Unpublished
slit1a-MO	ATG	gACAACATCCTCCTCTCgCAggCAT	Zolessi *et al.*, 2006
slit1b-MO	ATG	GCTCGGTGTCCGGCATCTCCAAAAG	Zolessi *et al.*, 2006
slit1-SBMO	SB	GAAATAAACTCACAGCCTCTCGGTG	Unpublished
slit2-MO	ATG	CATCACCgCTgTTTCCTCAAgTTCT	Unpublished
slit3-MO	ATG	TATATCCTCTGAGGCTGATAGCAGC	Unpublished
robo2-MO	ATG	TCCTGTCATAGTCCACATCCACACC	Hutson & Chien, 2002
robo3v1-MO	ATG	CCCTAAAAGCGCTACAATCCACCTG	Challa *et al.*, 2005
robo3v2-MO	ATG	CTCTTCTTTAGCAGCGGAGGGGACG	Challa *et al.*, 2005

Table 2. Sequence information for morpholinos used in this thesis.

Construct Manufacture

With the assistance of Masa Tada, I manufactured a series of constructs for *in vivo* micro-injection to investigate the effect of perturbation of *robo2*, *robo3v1* and *robo3v2* function on the regulation of convergent extension (Figure 2.2). The Robo3v2(ECD/TM)-GFP construct features the extra-cellular and transmembrane domains of Robo3v2 but lacks the intracellular domain (2.2A). The Lyn-Robo2(ICD)-GFP, Lyn-Robo2(ICD) (unlabelled), Lyn-Robo3(ICD)-GFP and Lyn-Robo3(ICD) (unlabelled) constructs feature the membrane localisation sequence of the Lyn tyrosine kinase enzyme ('Lyn') to create artificially membrane-anchored versions of the intracellular domain of Robo2 and the intracellular domain common to both variants of Robo3 lacking their respective extracellular domains (2.2B-E). The Lyn membrane localisation sequence:

GGATCCAATATGGGATGTATTAAATCAAAAAGGAAAGACGAATTC

BamH1 EcoR1

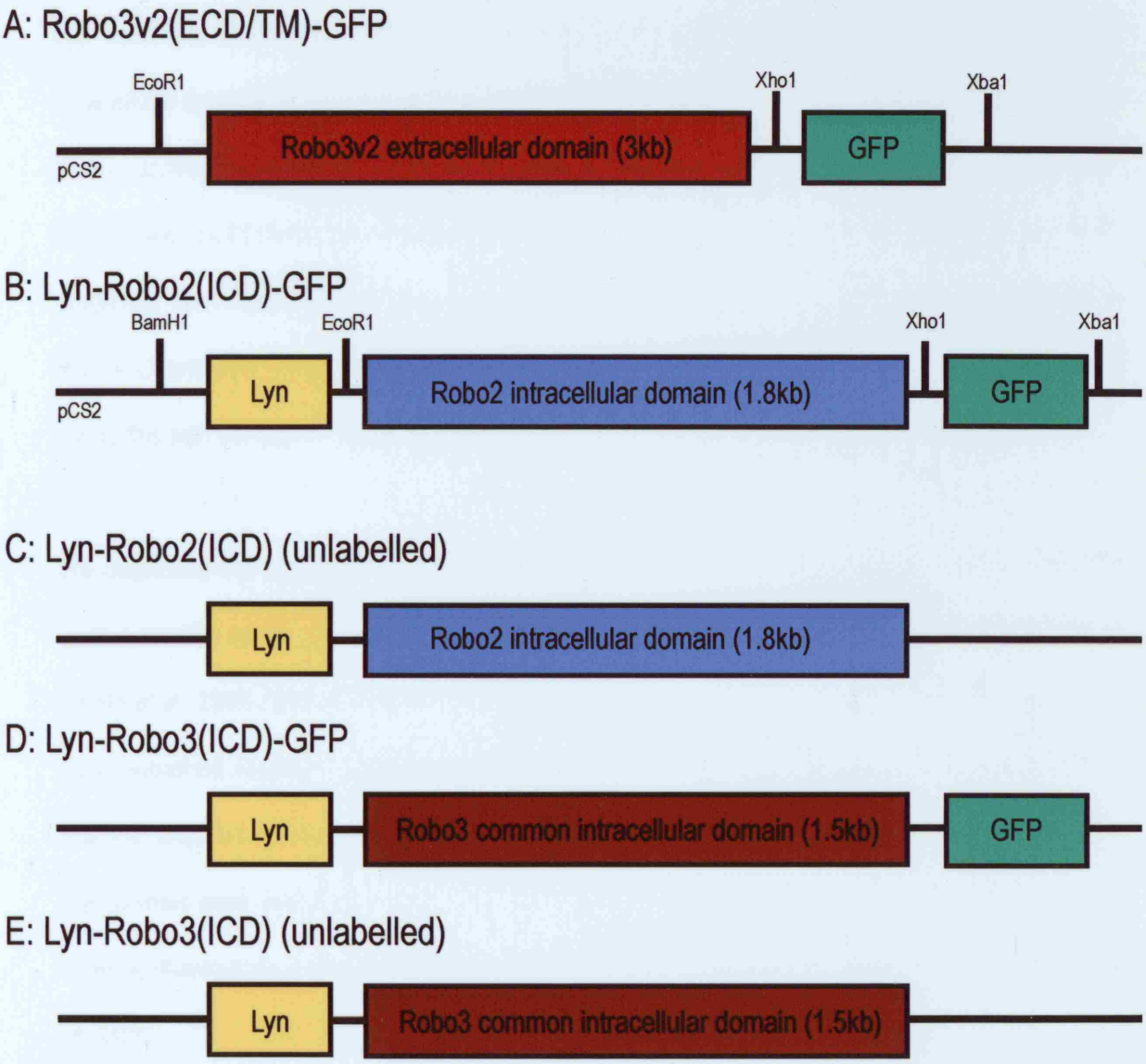

Figure 2.2

Structure and manufacture of Robo constructs.

A: the Robo3v2 extracellular/transmembrane domain (ECD/TM) constuct, annotated to show details of the manufacture of this construct. B-F: the membrane-anchored Robo intracellular domain (ICD) constructs. B: the Lyn-Robo2(ICD)-GFP construct, annotated to show details of the manufacture of all four Robo (ICD) constructs; C: an unlabelled version of the Lyn-Robo2(ICD) construct; D: the Lyn-Robo3(ICD)-GFP construct; E: an unlabelled version of the Lyn-Robo3(ICD) construct. These constructs are in the pCS2+ vector.

Primer Design & PCR

We used the Polymerase Chain Reaction (PCR) to amplify extracellular/transmembrane and intracellular domains from full-length Robo DNA templates. pBS-Robo2 and pSPORT-Robo3v1 were kindly supplied by Chi-Bin Chien (University of Utah) and from these we produced full-length pCS2-Robo2 and pCS2-Robo3v1 constructs. We manufactured full-length pCS2-Robo3v2 by PCR-amplifying the Robo3v2-specific region using the *robo3v2s2* and *robo3v2a2* primers (see Table 3) from a C-terminally truncated pBS-Robo3v2-Myc construct kindly supplied by Christine Beattie and fusing this with the region common both Robo3 variants obtained from full-length pCS2-Robo3v1.

We diagnosed the two variants of Robo3 using the common antisense primer *robo3coma1* and the variant-specific sense primers *robo3v1s* and *robo3v2s* based upon the sequences published in Challa *et al.*, 2005. Primers designed to amplify domains of interest from these templates were based upon published sequence information obtained from the NCBI website (Table 3). It was necessary that the amplified domains joined seamlessly with the 3' GFP label where appropriate: to achieve this, primers were designed to incorporate an Xho1 site at the 3' end of the amplified region. Primers were synthesized by Invitrogen and Sigma and stored as 100mM stock solutions in ultra-pure water at –20ºC.

Although each reaction was individually titred, PCR was performed in a reaction volume of 25µl on an Eppendorf Mastercycler PCR machine (94ºC; 60ºC; 72ºC for 30-35 cycles) based on the following protocols:

Using Taq Polymerase (Promega):

1µl Template DNA

2.5µl $MgCl_2$ (Promega)

1.5µl $MgCl_2$-free buffer (Promega)

0.5µl dNTP

1µl primer (s) (10µM stock)

1µl primer (a) (10µM stock)

17µl Ultra-Pure H_2O

0.5µl Taq Polymerase

Using PFU Polymerase (Stratagene):

1µl Template DNA

2.5µl 10X PFU buffer (Stratagene)

0.5µl dNTP

1µl primer (s) (10µM stock)

1µl primer (a) (10µM stock)

18.5µl Ultra-Pure H_2O

0.5µl PFU Polymerase (Stratagene)

1µl of the 25µl PCR product was then analysed by RNA Gel Electrophoresis.

TOPO Cloning & Vector Preparation

PCR products were cloned directly in to the multiple cloning site of the pCRII-TOPO vector using the TA Cloning Kit (Invitrogen). Once each domain of interest was in the TOPO vector, it was necessary to prepare the backbone of the Robo constructs. We used pCS2-Fmi-GFP and pCS2-Lyn-Fmi-GFP, constructs manufactured by Masa Tada and Filipa Carreira-Barbosa, as the basis for our Robo constructs (Thesis: Carreira-Barbosa F.). In the pCS2-Fmi-GFP construct, Fmi exists between the EcoR1 and Xho1 sites, while GFP is between the Xho1 and Xba1 sites. Similarly in the pCS2-Lyn-Fmi-GFP construct, Lyn exists between BamH1 and EcoR1 sites, Fmi between EcoR1 and Xho1 sites, and GFP between the Xho1 and Xba1 sites.

PRIMER	SENSE/ ANTISENSE	SEQUENCE	AMPLIFIES	TO MAKE
robo2ces1	S	GGAATTCTACTGGAGG AGGAAGAAGAGA	Robo2 ICD from pBS-Robo2	Lyn-Robo2(ICD)-GFP
robo2cxa1	A	CCTCGAGTAACTCTCC GGAAAACTGCGC	Robo2 ICD from pBS-Robo2	Lyn-Robo2(ICD)-GFP
robo3v2s2	S	CGCGGAATTCGAGAT GCTGCGTTACCTGATA	Robo3v2-specific region	pCS2-Robo3v2 (full-length)
robo3v2a2	A	ATCACGTGGCACTGCA ATTGG	Robo3v2-specific region	pCS2-Robo3v2 (full-length)
SP6 promoter primer	S	CCCAAGCTTGATTTAG GTGAC	Robo3 ECD from pCS2-Robo3v2	Robo3v2(ECD)-Venus
Robo3v2A3	A	TGTGTGTCGACGCAGT AGATCCACACGCTGAA	Robo3 ECD from pCS2-Robo3v2	Robo3v2(ECD)-Venus
robo3INTRAs1	S	GGAATTCTACTGCCGA CGCAAGAAGAGA	Robo3 ICD from pSPORT-Robo3v1	Lyn-Robo3(ICD)-GFP
robo3-a1	A	GGTCGACTCTCATCTC ATCATTTCTCTT	Robo3 ICD from pSPORT-Robo3v1	Lyn-Robo3(ICD)-GFP
robo3coma1	A	TACGACTGACGGCCTC GCCCAAGT	common primer	Diagnosis
robo3v1s	S	GCCCGTGACATGAAC GTTGGAG	Robo3v1-specific region	Diagnosis
robo3v2s	S	CCTACAGGAGAGAGA GGGAGAAAG	Robo3v2-specific region	Diagnosis

Table 3. Primers used in the manufacture and diagnosis of *robo* constructs.

To make the Robo3v2(ECD)-GFP construct, we PCR amplified the ~3kb Robo3v2-specific extracellular domain of pCS2-Robo3v2 (full-length) using the *SP6 promoter* and *robo3v2A3* primers (Table 3) and cloned this into a pre-prepared pCS2-GFP backbone (Figure 2.2).

To make the pCS2-Robo3(ICD) constructs, we performed a 3-hour restriction digest with EcoR1 and Xho1 of both the pCS2-Lyn-Fmi-GFP construct to prepare it as a vector by discarding the Fmi insert, and of the pCRII-TOPO-Robo3(ICD) construct to prepare the new insert: the PCR-amplified 1.5kb intracellular domain common to both Robo3 variants. Subsequently, we made the Lyn-Robo3(ICD) (unlabelled) from the Lyn-Robo3(ICD)-GFP construct by excising the ~1.5kb Lyn-Robo3(ICD) fragment in a 3-hour restriction digest with BamH1 and Xho1. We then transferred this fragment into the pCS2+ vector correspondingly prepared with BamH1 and Xho1, leaving the GFP behind (Figure 2.2).

To make Lyn-Robo2(ICD)-GFP, we released the Robo3(ICD) from the Lyn-Robo3(ICD)-GFP construct through a 3-hour digest with EcoR1 and Xho1, and replaced this with the PCR-amplified 1.8kb intracellular domain of Robo2, obtained by digest of pCRII-TOPO-Robo2(ICD) with EcoR1 and Xho1. To produce the Lyn-Robo2(ICD) (unlabelled) construct, we excised the ~1.8kb Lyn-Robo2(ICD) fragment from the Lyn-Robo2(ICD)-GFP construct by restriction digest with BamH1 and Xho1 and cloned it into the pCS2+ vector correspondingly prepared with BamH1 and Xho1, leaving the GFP behind (Figure 2.2).

In each instance, we ran these digests on 1% Agarose gels, then using a UV Transilluminator, cut insert and vector bands of the appropriate size from the gels with a clean scalpel blade. We extracted the insert and vector DNA using the Gel Extraction Kit (Qiagen). We calibrated the relative amounts of insert and vector DNA to use in the ligation of the constructs post-extraction by running 1µl insert and vector DNA side by side on a gel.

Ligation

We ligated Robo insert DNA with the digested pCS2-Venus and pCS2-Lyn-GFP backbones in the following reactions (total reaction volume of 20µl):

Insert DNA

Vector DNA

4µl 5X T4 DNA Ligase Buffer (Invitrogen)

1µl T4 DNA Ligase (Invitrogen)

Ultra-Pure H_2O to 20µl

The relative amounts of insert and vector DNA were calibrated for each individual reaction depending on the recovery of DNA from the Gel Extraction Kit. We also performed a control ligation each time where Insert DNA was excluded. These reactions were carried out at 4°C overnight.

Transformation & Innoculation

We transformed my ligations into XL-10 gold strain E. coli competent cells for amplification. We defrosted aliquots of competent cells on ice and gently added 2µl of each ligation to 25µl cells. After incubation on ice for 15mins, we heatshocked the bacteria at 42°C for 30secs to induce plasmid uptake, then added 300µl LB culture medium and incubated at 37°C for 15-30mins. After this, we plated out 100µl of each ligation on to Agar + Ampicillin plates and incubated plates upside down in a 37°C incubator overnight.

Large constructs such as pCS2-Robo2 (full-length), pCS2-Robo3v1 (full-length) and pCS2-Robo3v2 (full-length) required electroporation to be taken up by DHIOB competent cells (home–made). We added 2µl of each ligation to 50µl thawed electrocompetent cells and immediately transferred the mixture to an electroporation cuvette. The cuvette was tapped to prevent air bubbles before inserting it into a BioRad Electroporator. We pulsed the bacteria according to the Electroporator's standard setting for bacteria, then transferred the electrocompetent cells to a round-bottomed 15ml tube, added 500µl LB culture medium and placed the culture in the shaken incubator at 37°C for 1 hour. After this, we plated 100µl on to Agar + Ampicillin plates and incubated the plates upside down in a 37°C incubator overnight.

The next morning, we collected the plates, wrapped them in Nescofilm and stored them at 4°C until the evening, when we prepared ten round-bottomed tubes each containing 2ml of LB and 50ug/ml Ampicillin. We picked ten colonies with wooden toothpicks, innoculated each round-bottomed tube and transferred the cultures to the 37°C shaken incubator for overnight incubation.

DNA Extraction

Where possible, we selected positive clones by PCR analysis using primers outlined in Table 3. We then extracted the construct DNA from the bacterial cultures using the Mini-Prep Kit (Qiagen), after which we further diagnosed the constructs via restriction digest. We injected the constructs as DNA and visualised GFP expression (for labelled constructs) on a fluorescence dissection microscope. Once satisfied that the constructs were made correctly, we linearised each construct using Not1 and used the linearised DNA as a template to manufacture mRNA for *in vivo* micro-injection using SP6

polymerase (for protocols, see sections on Linearisation, *in vitro* Transcription of mRNA and Micro-Injection).

Detection of mRNA and Protein

Whole-mount *in situ* Hybridisation

Whole-mount *in situ* hybridisation took place over three days. During day one, stored dechorionated embryos in 100% Methanol must be progressively rehydrated by washing on a shaker at room temperature in 1ml of 75%, 50% then 25% Methanol in PBS Tween (0.1%) (see Appendix One). Rehydrated embryos (and freshly dechorionated embryos in PBS that were not stored in 100% Methanol) then underwent three 15 minute shaken washes at room temperature with 1ml PBS Tween (0.1%). After this, embryos post-10hpf required treatment with 10µg/ml Proteinase K (PK) in PBS at room temperature to permeabilise them for deeper probe penetration (exact time depends on stage of embryo: e.g. 20 minutes for 24hpf embryos, 1 hour for 60hpf embryos). After treatment, excess PK was removed by three PBS Tween (0.1%) rinses, followed by post-fixation in 1ml of 4% PFA for 30 minutes at room temperature. Excess PFA was rinsed off with three PBS Tween (0.1%) washes. Embryos were then pre-hybridised in a 69°C heat block for 2 hours with 500µl Hybridisation (Hyb+) Buffer (see Appendix One). After pre-hybridisation, this Hyb+ Buffer was replaced with approximately 300µl of DIG-labelled riboprobe diluted in Hyb+ (see Molecular Techniques: *in vitro* Transcription: Riboprobe Manufacture for probe manufacture protocol) and hybridised overnight at 69°C. Probes used or referred to in this thesis are detailed in Table 3.

At the start of day two, probe was recovered for re-use. Excess non-specifically bound probe was progressively washed off in 1ml of 100%, 75%, 50% then 25% Hyb- Buffer (see Appendix One) in SSC Tween (0.1%) solution in the 69°C heat block. The embryos then underwent two 30 minute washes in 1ml of 2X SSC Tween (0.1%) at 69°C, followed by two 30 minute washes in 1ml of 0.2X SSC Tween (0.1%) at 69°C. Subsequently, the embryos were cooled for ten minutes at room temperature in 1ml of fresh Maleic Acid Buffer plus 0.1% Triton (MABT), then blocked for 2 hours at room temperature in 1ml of 2% Boerringer Blocking Reagent in MABT (BBR), to which 10% heat-inactivated goat serum (HI NGS) and 0.1% Triton was added. Hybridisation with 1ml of a 1/4000 dilution of anti-DIG-AP (Alkaline Phosphatase) antibody (Roche Diagnostics) diluted in MABT plus 10% HI NGS took place at 4°C overnight.

Day three consisted of eight 1-hour MABT washes on a shaker at room temperature to reduce non-specific antibody binding. Embryos were placed in 1ml Staining Buffer containing Levamisol (see Appendix One), an inhibitor of natural alkaline phosphatase activity that ensures staining is specific. Staining Buffer was replaced with 500µl BM Purple (Boehringer Mannheim), a substrate that turns from clear to purple when metabolised by alkaline phosphatase. The embryos were then transferred to 25-well plates for shaken colour development, during which time light must be excluded from the samples. When colour development was optimal, embryos were rinsed thoroughly in Staining Buffer and post-fixed in 4% PFA, either for 20 minutes at room temperature or (more usually) overnight at 4°C. After post-fixation, embryos were rinsed in PBS to remove traces of PFA, then transferred progressively into 30%, 50%, 75%, 80% then 90% glycerol in PBS for scoring, photographs and storage at 4°C. In this thesis, embryos exhibiting both mesodermal, prechordal mesodermal and

neurectodermal convergent extension defects similarly to the mutant *silberblick/wnt11* (*slb*) (see Introduction, Fig. 1.2H & L) were classified as having 'severe CE defects', while embryos in which cell movements were less severely affected or affected in fewer tissues, more reminiscent of *pk1a* morphants (1.2J & N), were classified as having 'moderate' CE defects'. These classifications are explored further in Appendix Two.

Whole-Mount Antibody Staining

Antibody staining took place over three days and was based upon protocols outlined in Wilson *et al.*, 1990 and MacDonald *et al.*, 1995. During the first day, embryos were bleached prior to staining for 10 minutes at room temperature in 100% Methanol to which 10µl of 30% H_2O_2 had been added. After this, the embryos were progressively rehydrated by washing in 75%, 50% then 25% Methanol in PBS. These rehydrated embryos were washed three times in PBS Triton (0.5%), then treated with 1.5µg/ml Proteinase K in PBS, to permeabilise their surfaces for deeper staining. After this, the PK was thoroughly rinsed off the embryos with PBS Triton (0.5%) then the embryos were post-fixed in 4% PFA. Excess PFA was rinsed off with PBS Triton (0.5%), then the embryos were blocked for 2 hours on a shaker at room temperature in 1ml of a blocking buffer comprising PBS Triton (0.5%) containing 10% HI NGS and 1% DMSO. The embryos were incubated overnight at 4°C with the primary antibody diluted in this blocking buffer.

Day two consisted of eight 1 hour washes in PBS Triton (0.5%) to remove excess, non-specifically bound primary antibody, followed by blocking for two hours on the shaker at room temperature in 1ml

of PBS Triton (0.5%) blocking buffer with 10% HI NGS and 1% DMSO added. Embryos were then incubated at 4°C overnight with a secondary antibody diluted in this blocking buffer.

Day three began with eight 1-hour washes in PBS Triton (0.5%) to reduce excess, non-specifically bound secondary antibody. After washing in 1X PBS to remove excess detergent, embryos were placed in 3,3' Diaminobenzidine (DAB) liquid in PBS for 20 minutes at room temperature (see Appendix One). This was replaced with DAB liquid in PBS activated by the addition of 30% H_2O_2, the embryos transferred to 4-well plates, and light excluded from the samples while the stain developed. Once stained, embryos were rinsed thoroughly in PBS to remove traces of DAB and post-fixed in 4% PFA for 30 minutes at room temperature. Excess fix was rinsed off the embryos by thoroughly rinsing in PBS. Finally, the stained embryos were bleached to refine the staining in a solution of KOH/H_2O_2 for 30 minutes at room temperature. Bleach was rinsed off by washing with PBS, then the stained embryos were ready to be transferred progressively into 30%, 50%, 75%, 80% then 90% glycerol in PBS for scoring, photographs, and storage at 4°C.

Western Blotting

To confirm that my putative dominant negative constructs Lyn-Robo2(ICD)-GFP and Lyn-Robo3(ICD)-GFP were producing a protein product within injected embryos, I performed a Western. To better design this experiment, I estimated the sizes of the protein products of these constructs based upon the molecular weight of their constituent amino acids (See Appendix Two) and came up with the following predicted sizes in kDa:

Robo2(ICD) = 626 amino acids = approx. 69kDa

Robo3(ICD) = 502 amino acids = approx. 55kDa

Lyn + GFP = total approx. 25kDa

Therefore:

Lyn-Robo2(ICD)-GFP = approx. 94kDa

Lyn-Robo3(ICD)-GFP = approx. 80kDa

Western Blotting takes place over several days. Ahead of time, I micro-injected 20 wildtype embryos with 100pg of *lyn-robo2(ICD)-GFP* mRNA, and 20 wildtype embryos with 100pg of *lyn-robo3(ICD)-GFP* mRNA and incubated them at 28°C until they reached 40% epiboly. I placed these embryos on a warmed dissection plate made from 1% Agarose in Hank's Embryonic Medium filled with a little fresh Hank's medium. I dechorionated the embryos and deyolked them with a Tungsten needle, leaving the blastoderm caps, which I collected with a glass pipette and transferred to a 1.5ml Eppendorf tube. After removing any excess medium, I resuspended the caps in 25µl 4X Sample Buffer (see Appendix One) and boiled them at 95°C in a heat block for 10 minutes, before storing them at -20°C until ready to begin blotting.

On the first day of blotting, I loaded 10µl (roughly equivalent to 3 blastoderm caps) into a 10% SDS PAGE gel (see Appendix One), the interface between upper and lower gels made with my predicted protein band sizes in mind. I ran this gel between 50 and 100V, after which I soaked it in 1X Blotting Buffer (see Appendix One) for 1 minute. I transferred the protein bands on to Hybond membrane electrically, using a Biorad Semi-Dry Transblotter set at 15V for 30 minutes. After this, I washed the

membrane 5-6 times in PBS Tween (0.1%) for 30 minutes, then on a shaker, blocked with a solution of 0.5% skimmed milk in PBS Tween (0.1%) for 2 hours at room temperature. I replaced this with a 1/500 dilution of the primary antibody, in this case rat anti-GFP, in 0.5% skimmed milk in PBS Tween (0.1%) for hybridisation overnight at 4°C.

On day two, I removed non-specifically bound antibody from the membrane by several long washes in PBS Tween (0.1%). I replaced this with a 1/5000 dilution of the secondary antibody, goat anti-rat HRP, in 0.5% skimmed milk in PBS Tween (0.1%) and left to hybridise at room temperature for 1 hour. I removed any non-specifically bound secondary antibody with extended PBS Tween (0.1%) washes, followed by washing once in 1X PBS to remove excess detergent. In the presence of H_2O_2, the HRP cap of the secondary antibody activated the substrate of the ECL Kit (Amersham), converting it into a fluorescent form that could then be visualised by exposing the membrane to photographic film. Exposure time varies: in the case of the *lyn-robo*(*ICD*) constructs, I exposed the membrane to the film for 30 seconds.

At a later date, I re-probed the membrane with a 1/200 dilution of the anti-ß-tubulin antibody in 0.5% skimmed milk in PBS Tween (0.1%) to provide a suitable loading control. I washed off excess anti-ß-Tubulin antibody with PBS Tween (0.1%) washes, then incubated with a 1/2000 dilution of the anti-mouse-AP antibody in 0.5% skimmed milk in PBS Tween (0.1%). I reduced the background again by long washes in PBS Tween (0.1%), then prepared the membrane for colour development by immersion in Staining Buffer. I developed the colour by replacing this with 7 volumes of Staining Buffer plus 1 volume of BM Purple, then re-photographed.

Chapter Three

pk1b regulates convergent extension movements in zebrafish.

Introduction

During the establishment of PCP in the *Drosophila* wing, the *pk* and *sple* isoforms of the *prickle* gene operate antagonistically and are not functionally redundant (Gubb *et al.*, 1999). Both overexpression and loss of function of the isoforms of *Drosophila prickle* causes perturbation of PCP, suggesting that the *pk* and *sple* isoforms exist in a necessary stoichiometric balance within the cell (Gubb *et al.*, 1999). Fz/Dsh signalling, and subsequently actin prehair formation, is confined to the distal vertex of wing hair cells by the asymmetrically localised, proximal inhibitory activity of Pk (Axelrod, 2001; Strutt, 2001; Tree *et al.*, 2002). Recruitment of PCP proteins to asymmetric complexes at the cell membrane in this way non-autonomously propagates cell polarisation in the plane of the epithelium, although the mechanisms by which symmetry is initially broken is poorly understood, as the translocation of PCP proteins such as Fz, Dsh, Pk or Stbm appears to be interdependent (Axelrod, 2001; Bastock *et al.*, 2003; Jenny *et al.*, 2003; Strutt, 2001; Tree *et al.*, 2002). Recently, it was suggested that the asymmetric subcellular localisation of the four-pass transmembrane protein Strabismus (Stbm) is responsible for the asymmetric recruitment of Pk to the cell membrane in *Drosophila* ommatidia (Jenny *et al.*, 2003). Furthermore, Stbm has been shown to bind to both Pk and Dsh and recruit them to the apicolateral cell membrane in the establishment of wing hair polarity in the fly, after which, Dsh is recruited to the cell membrane distally and Pk proximally, breaking the symmetrical distribution of PCP proteins (Bastock *et al.*, 2003). However initiated, a feedback loop is set in motion that acts to

progressively restrict Fz/Dsh signalling and downstream actin prehair formation to the distal edge of cells (Axelrod, 2001; Strutt, 2001; Tree *et al.*, 2002).

While no evidence exists to support the asymmetric localisation of the endogenous protein products of vertebrate orthologues of *Drosophila* PCP genes, *Drosophila* Pk labelled with GFP was shown to localise asymmetrically when artificially expressed in cells of the zebrafish neurula (Ciruna *et al.*, 2006), implying that the relationship between the subcellular localisation of vertebrate orthologues of *Drosophila* PCP gene products and their function is evolutionarily conserved. In support of this, Fz7 can recruit Dsh from its subcellular localisation in cytoplasmic vesicles to the cell membrane in a manner analogous to the recruitment of Dsh to the cell membrane during *Drosophila* PCP (Axelrod *et al.*, 1998; Carreira-Barbosa *et al.*, 2003). Similarly, while *venus-pk1a* localises uniformly throughout the cytoplasm of deep cells at 40% epiboly and this localisation does not change in response to *fz7* or *stbm* overexpression, Pk1a is capable of blocking the membrane recruitment of Dsh by Fz7 in a manner reminiscent of the restriction of Fz/Dsh complex formation in the *Drosophila* wing (Carreira-Barbosa *et al.*, 2003; F. Carreira-Barbosa & M. Tada, unpublished data).

Two orthologues of *Drosophila prickle* have been identified zebrafish to date, termed *pk1a* and *pk2* (Carreira-Barbosa *et al.*, 2003; Takeuchi *et al.*, 2003; Veeman *et al.*, 2003). Of these, *pk1a* is known to be maternally provided, while both *pk1a* and *pk2* are expressed in tissues undergoing morphogenesis during gastrulation. Zygotic *pk1a* expression begins n the future dorsal region of the pre-gastrula embryo, spreading anteriorly through the marginal zone after the onset of gastrulation movements and restricting to migrating mesodermal cells as involution occurs (Thesis: Carreira-Barbosa F., 2005; Carreira-Barbosa *et al.*, 2003; Veeman *et al.*, 2003). Between 90% epiboly and

tailbud stage, *pk1a* expression shifts from axial to paraxial tissues and is conspicuously absent from the dorsal midline (Carreira-Barbosa *et al.*, 2003). At the end of gastrulation, *pk1a* is expressed paraxially in posterior neurectodermal and in pre-somitic mesodermal cells, and at the lateral border of the neural plate in a manner similar to *wnt11* expression (Carreira-Barbosa *et al.*, 2003; Veeman *et al.*, 2003). While zygotic expression of *pk2* begins dorsally and spreads anteriorly through the marginal zone in a manner similar to *pk1a* expression, leading to a diffuse expression in the mesoderm and neurectoderm as gastrulation progresses, *pk2* expression restricts to the axial mesoderm by the end of gastrulation (Thesis: Carreira-Barbosa F., 2005; Veeman *et al.*, 2003).

Loss of function of *pk1a* and loss of function *pk2* results in disrupted convergent extension movements, but simultaneous loss of function of *pk1a* and *pk2* does not significantly enhance these convergent extension defects relative to loss of function of either *pk1a* or *pk2* alone, suggesting that these *pk* orthologues are not functionally redundant (Carreira-Barbosa *et al.*, 2003; Veeman *et al.*, 2003). Both loss of function and gain of function of components of the *Drosophila* PCP signalling pathway are known to cause defects in planar polarity. Similarly, both loss of function and gain of function of vertebrate orthologues of *Drosophila* PCP genes implicated in the regulation of convergent extension movements results in perturbation of cell polarity. For instance, gain of function of *pk1a* also results in morphological defects characteristic of impaired convergent extension movements: severe shortening of the body axis, malformation of the yolk extension and partial fusion of the eyes at 24hpf (Appendix Two; Carreira-Barbosa *et al.*, 2003).

Loss of function of *pk1a* is known to enhance the convergent extension defects of the zebrafish convergent extension mutant *silberblick/wnt11* (*slb*), suggesting that *pk1a*, considered to function in a

parallel pathway to Wnt11, is capable of modulating non-canonical Wnt signalling in the regulation of convergent extension during zebrafish gastrulation (Carreira-Barbosa *et al.*, 2003). Loss of function of *pk1a* is known to enhance the convergent extension defects of the *trilobite/stbm* (*tri*) mutant, also considered to function in a parallel pathway to Wnt11 and capable of modulating non-canonical Wnt signalling (Carreira-Barbosa *et al.*, 2003). The interaction between *pk1a* and *tri/stbm* in the context of convergent extension is dose dependent: loss of function of *pk1a* on the *tri+/-* background is sufficient to negate the remaining functional copy of *stbm*, recapitulating the *tri-/-* phenotype (Carreira-Barbosa *et al.*, 2003). Pk1a and Stbm also function in a pathway considered Wnt-independent in the regulation of facial (nVII) hindbrain branchiomotor neuron migration (Bingham *et al.*, 2002; Carreira-Barbosa *et al.*, 2003; Jessen *et al.*, 2002). However, other vertebrate orthologues of PCP genes known to regulate CE, such as Flamingo2/Celsr2 (Fmi2) and Frizzled3a (Fz3a), were recently shown to collaborate in the regulation of facial (nVII) hindbrain branchiomotor neuron migration (Wada *et al.*, 2006), suggesting that this Wnt-independent classification may require revision.

pk1b is a novel variant of *pk1* and was cloned in 2005 by Masa Tada from a gastrula cDNA library using the conserved N-terminus region as a probe (see Materials & Methods: Cloning of *pk1b*. Pk1b map and *pk1b*-MOs kindly provided by Vicky Prince, University of Chicago). *pk1b* has a longer N-terminus region but in other respects is structurally very similar to *pk1a* (Fig. 3.1; Carreira-Barbosa *et al.*, 2003; Veeman *et al.*, 2003). I characterised the expression and function of *pk1b* in the context of convergent extension movements. I also examined the interaction of *pk1b* with the convergent extension mutants *slb* and *tri*, with the aim of understanding how vertebrate *prickle* orthologues interact with one other and with non-canonical Wnt signalling in the regulation of convergent extension movements.

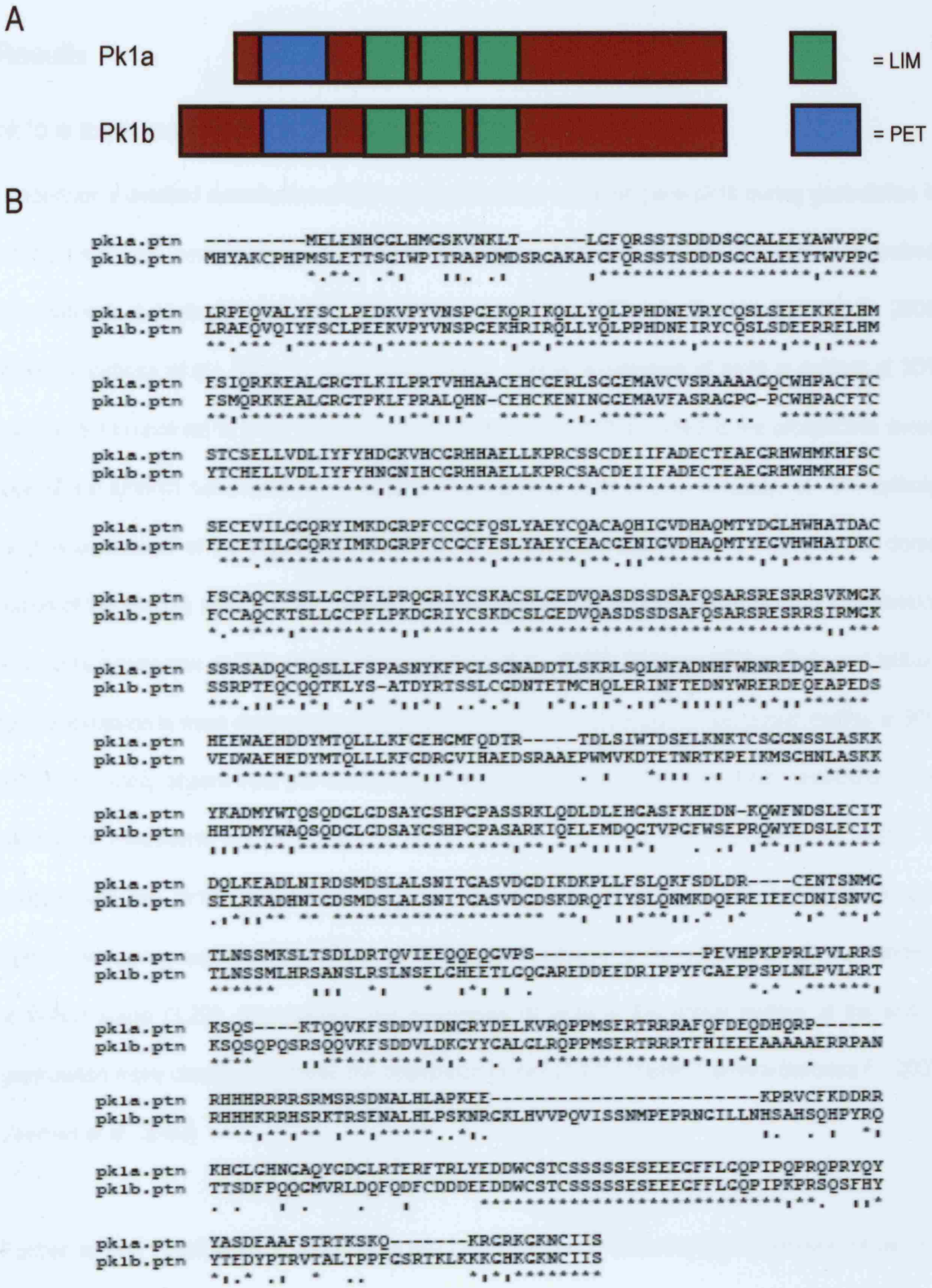

Figure 3.1

Pk1a and Pk1b proteins are structurally similar.

A: representation of the similarities in structure between Pk1a and Pk1b proteins; B: alignment of the amino acid sequences of the Pk1a and Pk1b proteins, highlighting similar regions (courtesy of M. Tada).

Results

pk1b is expressed during zebrafish gastrulation

I undertook a detailed examination of the expression of the novel *pk* gene *pk1b* during gastrulation in wildtype embryos, compared to the zebrafish orthologues *pk1a* and *pk2* (for information on probes, see Materials & Methods: Riboprobe Manufacture and Table 1; Thesis: Carreira-Barbosa F., 2005; Carreira-Barbosa *et al.*, 2003; Veeman *et al.*, 2003). Zygotic expression of *pk1b* is evident at 30% epiboly, but in contrast to *pk1a* (Fig. 3.2E), *pk1b* expression is not restricted to the prospective dorsal side of the embryo but expressed throughout the marginal zone (3.2A). Similarly, at 70% epiboly, *pk1b* is expressed at the blastopore margin (3.2B), while *pk1a* expression is limited to the dorsal region of the embryo (3.2F). In this respect, *pk1b* expression more closely resembles *pk2* expression than *pk1a* expression at 70% epiboly (3.2I; Veeman *et al.*, 2003). Between 90% epiboly and tailbud, *pk1a* expression is most dynamically expressed: strong *pk1a* expression in the dorsal midline at 90% (3.2G) is notably absent from the dorsal midline by tailbud stage, *pk1a* expression restricting to the pre-somitic mesoderm and the posterior neurectoderm (3.2H; Carreira-Barbosa *et al.*, 2003). In contrast with this, *pk1b* expression in the dorsal midline at 90% (3.2C) is not downregulated in axial tissues, remaining expressed in midline mesoderm and diffusely in the posterolateral neurectoderm at tailbud stage (3.2D). Interestingly, the expression of *pk1b* in the dorsal midline at the end of gastrulation more closely resembles the expression of *pk2* (3.2J) (Thesis: Carreira-Barbosa F., 2005; Veeman *et al.*, 2003).

Further to this, I performed a series of *in situ* hybridisations to examine the expression of *pk1b* in zebrafish mutants for components of the non-canonical Wnt signalling pathway. Although loss of

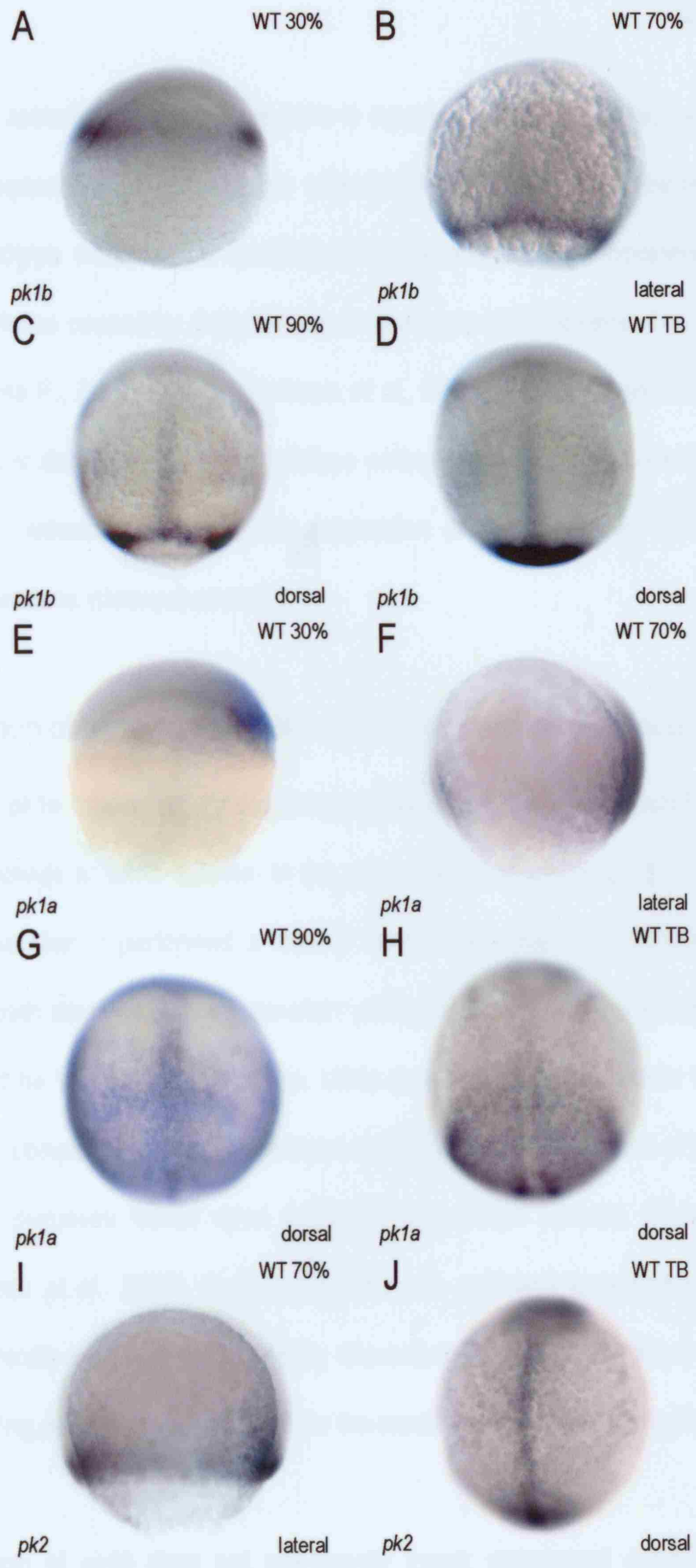

Figure 3.2

Expression of *pk1b* compared to *pk1a* and *pk2* expression during gastrulation.

Expression of *pk* orthologues in wildtype embryos. A-D: expression of *pk1b* at A: 30%; B: 70%; C: 90% and D: 100% epiboly. E-H: expression of *pk1a* at E: 30%; F: 70%; G: 90% and H: 100% epiboly. I & J: expression of *pk2* at 70% (I) and 100% (J) epiboly (images E-H: Carreira-Barbosa *et al.*, 2003; Thesis: Carreira-Barbosa, F.).

function of the zebrafish *pk* orthologue *pk1a* is reported to result in defective convergent extension movements, expression of *pk1a* in the *silberblick/wnt11* (*slb*) and *trilobite/stbm* (*tri*) mutants is identical to wildtype except for a mediolateral expansion and anteroposterior compression of the expression domains caused by defective convergent extension movement in these mutants (Thesis: Carreira-Barbosa F., 2005; Carreira-Barbosa *et al.*, 2003). Likewise, expression of *pk1b* in the *slb* and *tri* mutants is distinguishable from wildtype embryos only due to the mediolateral expansion and anteroposterior reduction of the midline expression of *pk1b* resulting from impaired convergent extension movements (data not shown).

Loss of function of *pk1b* causes mild convergent extension defects

Expression of *pk1b* differs from *pk1a* during gastrulation, and it is plausible to ask whether this dissimilarity extends to *pk1b* function in the orchestration of convergent extension movements. To answer this question, I performed a loss of function analysis of *pk1b* using two splice-blocking morpholinos, both singly and in combination: *pk1b*-MOa, designed by Masa Tada, and *pk1b*-MOb, kindly provided by Vicky Prince (Chicago, USA) (see Materials & Methods: Morpholino Preparation and Table 2). I compared the loss of function of *pk1b* with loss of function of *pk1a*, which I replicated for calibration purposes based upon published information (Thesis: Carreira-Barbosa F., 2005; Carreira-Barbosa *et al.*, 2003). 2ng of *pk1a*-MO was sufficient to reproduce the anteroposteriorly shortened, ventrally curled body axis highly characteristic of *pk1a* morphant embryos at 24hpf (Fig. 3.4B) while a 1ng dose was subthreshold for the creation of this phenotype (Table 4).

Loss of function of *pk1b* does not significantly impair convergent extension movements during zebrafish gastrulation in either the mesoderm or neurectoderm (Fig. 3.3; Table 4; For an exploration

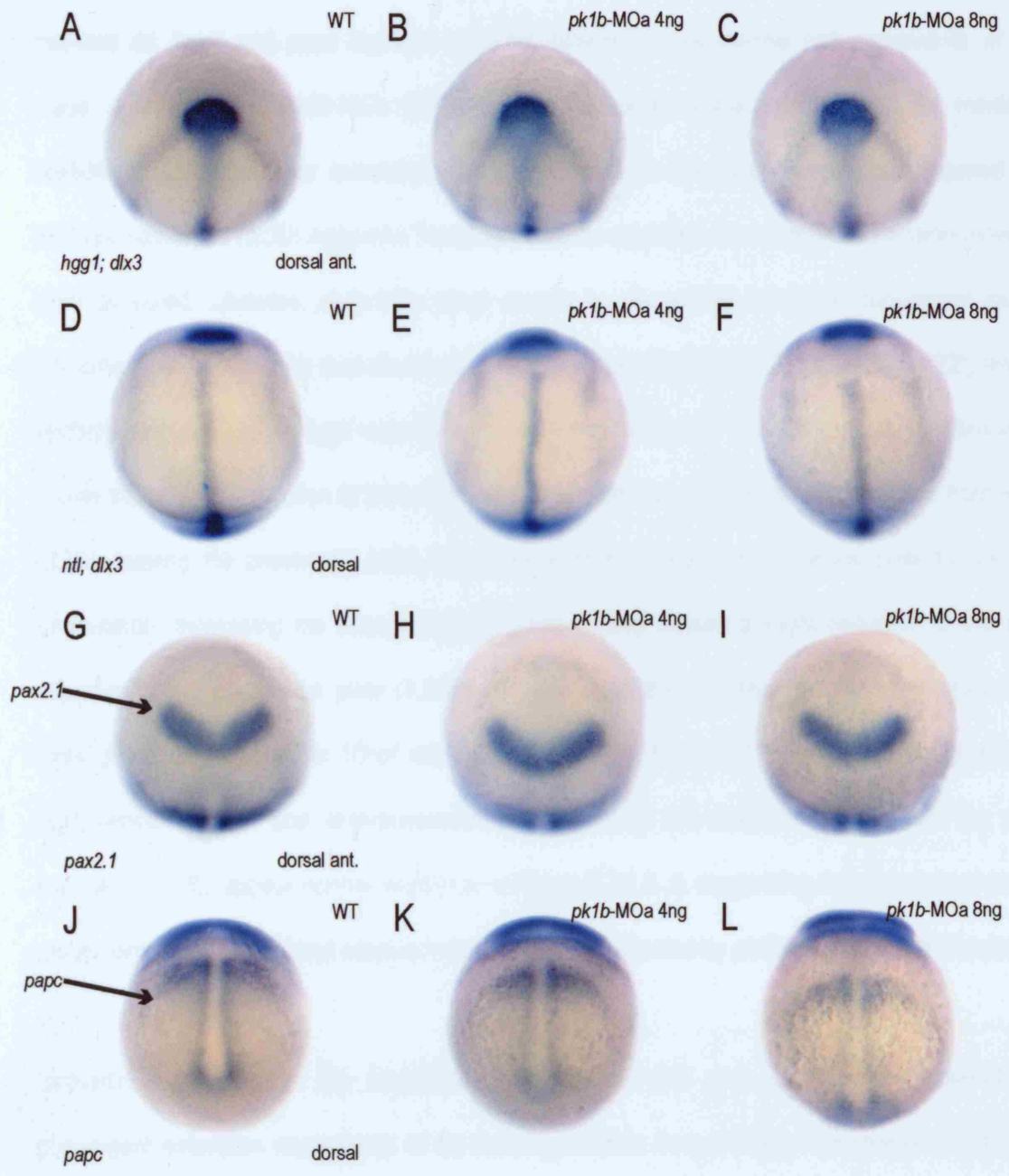

Figure 3.3

***in situ* hybridisation analysis of the effect of loss of function of *pk1b* on convergent extension.**

Expression of mesodermal markers *ntl*, *hgg1* and *papc* and neural markers *dlx3* and *pax2.1* in *pk1b* morphant embryos at the end of gastrulation. 4ng *pk1b*-MOa does not impair convergent extension movements (B, E, H & K); 8ng *pk1b*-MOa causes slightly reduced anterior migration of the prechordal plate but no major alterations to mesodermal and neurectodermal marker expression domains (C, F, I & L) relative to wildtype embryos (A, D, G & J), suggesting that other aspects of convergent extension are normal.

of convergent extension phenotypes, see also Appendix Two). *in situ* hybridisation analysis for the markers *ntl*, *hgg1* and *papc* highlight potential defects in mesodermal cell movements at tailbud stage. A 4ng dose of *pk1b*-MOa (3.3E) causes no morphological differences in the mediolateral breadth or anteroposterior extension of *ntl* expression in the axial mesoderm compared to the wildtype notochord (3.3D; Appendix Two), as would be expected if convergent extension movements were disrupted. Likewise, *pk1b*-MOa (4ng) causes no discernible defects in convergent extension movements in the paraxial mesoderm, marked by expression of *papc* (3.3K; 100%, n=22), relative to wildtype embryos (3.3J). *hgg1* expression in the prechordal plate of *pk1b* morphant embryos (3.3B) shows the anterior migration of this structure during gastrulation to be indistinguishable from wildtype (3.3A), leaving the prechordal plate fully anterior to the border of the neural plate by the end of gastrulation. Increasing the dosage of *pk1b*-MOa to 8ng causes a slight reduction in the anterior migration of the prechordal plate (3.3C) compared to wildtype (3.3A), leaving this structure slightly more posteriorly situated at 10hpf relative to the anterior border of the neural plate. However, the mediolateral breadth and anteroposterior length of both the notochord (3.3F) and the paraxial mesoderm (3.3L) appear normal relative to wildtype (3.3A & J), suggesting that convergent extension movements in both axial and paraxial mesoderm are unaffected by *pk1b* knockdown at this dose.

Similarly, expression of the neurectodermal markers *dlx3* and *pax2.1* show neurectodermal convergent extension movements to be indistinguishable from wildtype. Expression of *dlx3* at the border of the neural plate does not show the mediolateral expansion and anteroposterior shortening that typically results from impaired convergent extension movements, either at 4ng (3.3B & E) or 8ng (3.3C & F) doses of *pk1b*-MOa. Expression of *pax2.1* in the prospective MHB of *pk1b* morphant embryos shows no alteration in the size, shape or angle of the bilateral expression domains at either

4ng (3.3H) or 8ng (3.3I) doses of *pk1b*-MOa relative to wildtype *pax2.1* expression (3.3G). This not only shows that neurectodermal convergent extension movements are unaffected, but also that patterning in the future brain is normal as a result of *pk1b* loss of function. This contrasts greatly with loss of function of *pk1a*, where convergent extension movements are compromised in both the mesoderm and the neurectoderm (Carreira-Barbosa *et al.*, 2003).

PK MORPHANTS 24HPF	AMT (ng)	TOTAL	SEVERE CE DEFECTS %	MILD CE DEFECTS %	WT-LIKE %	DEAD %	MISC. %
WT+*pk1b*-MOa	2	23	-	-	100	-	-
WT+*pk1b*-MOa	4	92	-	-	98	1	1 non-specific
WT+*pk1b*-MOa	8	83	8	34	55	2	1 non-specific
WT+*pk1b*-MOb	4	27	-	96	-	4	-
WT+*pk1b*-MOb	8	91	-	95	1	4	-
WT+*pk1a*-MO	1	50	-	-	92	8	-
WT+*pk1a*-MO	2	53	96	4	-	-	-
WT+*pk1a*-MO +*pk1b*-MOa	*pk1a*: 1 *pk1b*: 2	98	96	-	1	3	-
WT+*pk1b*-MOa +*pk1b*-MOb	2 each	56	-	93	2	5	-
***slb*-/-+*pk1b*-MOa**	4	91	-	98	-	1	1 non-specific
***tri* inx+*pk1b*-MOa**	4	99	23	-	70	7	-
***tri* inx+*pk1b*-MOa**	8	43	21	-	60	19	-
***ord* inx+*pk1a*-MO**	2	42	-	90	-	7	2 non-specific
***ord* inx+*pk1b*-MOa**	4	28	-	-	100	-	-
***ord* inx+*pk1b*-MOa**	8	31	-	-	100	-	-
PK MORPHANTS: 10HPF (*hgg1, ntl & dlx3*)							
WT+*pk1b*-MOa	4	29	-	-	100	-	-
WT+*pk1b*-MOa	8	65	-	97	3	-	-
WT+*pk1b*-MOb	8	77	-	-	100	-	-
WT+*pk1a*-MO	1	11	-	100	-	-	-
WT+*pk1a*-MO +*pk1b*-MOa	*pk1a*: 1 *pk1b*: 2	25	-	60	40	-	-

Table 4. *pk1b* loss of function.

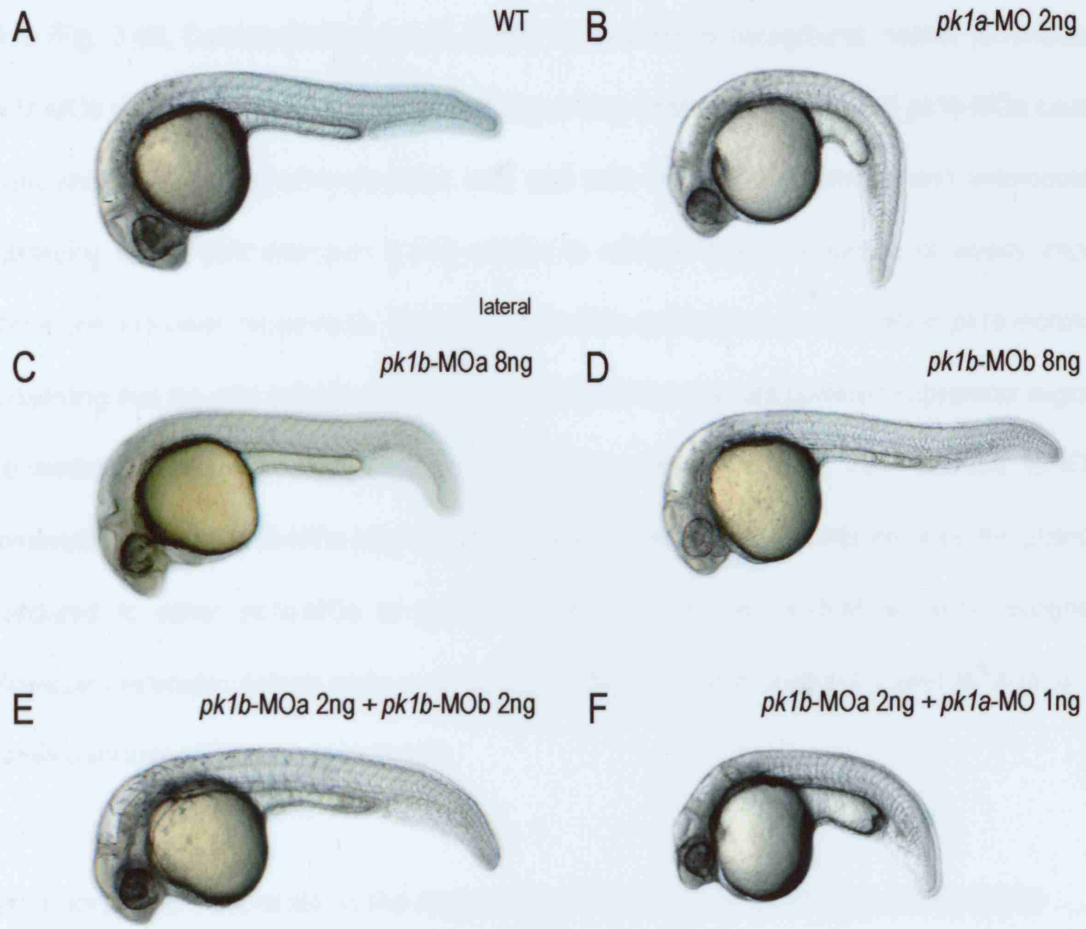

Figure 3.4

Loss of function of *pk1b* at 24hpf.

A: wildtype embryo; B: *pk1a* morphant emrbyo (2ng *pk1a*-MO); C: *pk1b* morphant embryo (8ng *pk1b*-MOa); *D: pk1b* morphant embryo (8ng *pk1b*-MOb); E: *pk1b* morphant embryo (a combination of 2ng *pk1b*-MOa and 2ng *pk1b*-SBMO); and F: enhanced convergent extension defects in the *pk1a* and *pk1b* double morphant (2ng *pk1b*-MOa plus 1ng *pk1a*-MO) relative to *pk1a* loss of function (B) and *pk1b* loss of function (C, D & E).

In support of these observations, loss of function of *pk1b* does not result in a significant shortening of the anteroposterior axis at 24hpf (Fig. 3.4C-E; Table 4), contrasting sharply with loss of function of *pk1a* (Fig. 3.4B; Carreira-Barbosa *et al.*, 2003). On a wildtype background, neither *pk1b*-MOa nor *pk1b*-MOb yields a discernible phenotype at 2ng or 4ng doses. An 8ng dose of *pk1b*-MOa causes a slight shortening of the anteroposterior axis and mild increase in diameter and anteroposterior shortening of the yolk extension (3.4C) relative to wildtype (3.4A), evidence of weakly impaired convergent extension movements. The separation of the eyefield occurs normally in *pk1b* morphants, suggesting that the mild defects arising from *pk1b* loss of function are confined to posterior regions of the embryo. 8ng of *pk1b*-MOb yields a phenotype indistinguishable from wildtype (3.4D). In combination, 2ng of *pk1b*-MOa plus 2ng of *pk1b*-MOb does not significantly enhance the phenotype compared to either *pk1b*-MOa or *pk1b*-MOb alone (3.4E). As *pk1b*-MOa yields recognisable convergent extension defects while, even at high doses, *pk1b*-MOb does not, I used *pk1b*-MOa for all subsequent loss of function experiments.

pk1a and *pk1b* cooperate in the regulation of convergent extension movements

The contrast between the expression pattern and loss of function phenotype of *pk1a* and *pk1b* raises the question of whether these *pk1* genes are capable of cooperation in the regulation of convergent extension movements. To address this, I examined the effect of simultaneous loss of function of *pk1a* and *pk1b* (Fig. 3.4; Table 4; Appendix Two), using subthreshold doses of each morpholino: a 1ng dose of *pk1a*-MO combined with a 2ng dose of *pk1b*-MOa. By using doses that would not individually create convergent extension defects in this way, I could be confident that any enhancement of convergent extension defects reflected a genuine interaction, not just the addition of two separate

phenotypes. I found that simultaneous loss of function of *pk1a* and *pk1b* resulted in a greatly enhanced phenotype relative to individual loss of function of either *pk1a* (3.4B) or *pk1b* (3.4C). In *pk1a:pk1b* double morphant embryos (3.4F), anteroposterior extension of the body axis is severely reduced in a manner comparable to the most severe convergent extension mutants, such as *trilobite/stbm* (*tri*) (see Introduction: Fig. 1.2D). As a consequence, somites in the trunk, whilst appearing to be patterned normally and exhibiting a normal horizontal myoseptum, are compressed in the anteroposterior axis. Furthermore, the yolk extension is severely malformed, thicker in diameter, anteroposteriorly shorter and less well separated from the body of the yolk. While there is no evidence of retinal fusion, the eyes are positioned more anteriorly than in wildtype embryos (3.4A), *pk1a* morphants (3.4B) or *pk1b* morphant embryos (3.4C), and the surrounding forebrain abnormally shaped. In combination, these defects are reminiscent of severely impaired convergent extension movements and reflect epistasis between *pk1a* and *pk1b*.

Gain of function of *pk1b* does not affect convergent extension movements

Although *pk1b* yielded almost no loss of function phenotype, both loss of function and gain of function of many vertebrate orthologues of *Drosophila* PCP genes results in characteristic disturbances to convergent extension. I overexpressed fluorescently labelled *venus-pk1b* mRNA on a wildtype background (Table 5). At 100pg, 200pg 300pf and 400pg doses, it was possible to detect the expression of Venus from 40% epiboly onwards by UV fluorescence microscopy, indicating that the *venus-pk1b* mRNA was correctly manufactured. However at 24hpf, *pk1b* overexpressing embryos were indistinguishable from wildtype controls at 100pg, 200pg, 300pg and 400pg doses. At 10hpf, *in situ* hybridisation analysis of *venus-pk1b* overexpressing embryos (300pg) using the mesodermal

markers *hgg1* and *ntl* and the neurectodermal marker *dlx3* showed convergent extension movements in both the mesoderm and neurectoderm to be indistinguishable from wildtype controls. To ascertain that the N-terminal Venus label was not interfering with the function of Pk1b, I also overexpressed unlabelled *pk1b* mRNA. Embryos overexpressing unlabelled *pk1b* (100pg) mRNA were also indistinguishable from wildtype embryos at 24hpf. This evidence suggests that gain of function of *pk1b* has no effect on convergent extension movements, in sharp contrast with overexpression of *pk1a* (Carreira-Barbosa *et al.*, 2003).

GAIN OF FUNCTION OF PK 24HPF	AMT (pg)	TOTAL	SEVERE CE DEFECTS %	MILD CE DEFECTS %	WT-LIKE %	DEAD %	MISC. %
WT+*pk1b*	100	87	-	-	94	3.5	2.5 non-specific
WT+*venus-pk1b*	100	40	-	-	100	-	-
WT+*venus-pk1b*	200	48	-	-	90	8	2 non-specific
WT+*venus-pk1b*	300	39	-	2.5	90	5	2.5 non-specific
WT+*venus-pk1b*	400	81	-	-	93	6	1 non-specific
GAIN OF FUNCTION OF PK: 10HPF (*hgg1; dlx3 & ntl*)							
WT+*venus-pk1b*	300	25	4	40	56	-	-

Table 5. *pk1b* gain of function.

Loss of function of *pk1b* weakly enhances the *slb* phenotype

To address whether, similarly to loss of function of *pk1a*, loss of function of pk1b was capable of enhancing the convergent extension defects of *silberblick/wnt11* (*slb*), I examined the effect of loss of function of *pk1b* on convergent extension in *slb-/-* embryos, using 4ng of *pk1b*-MOa (Fig 3.5; Table

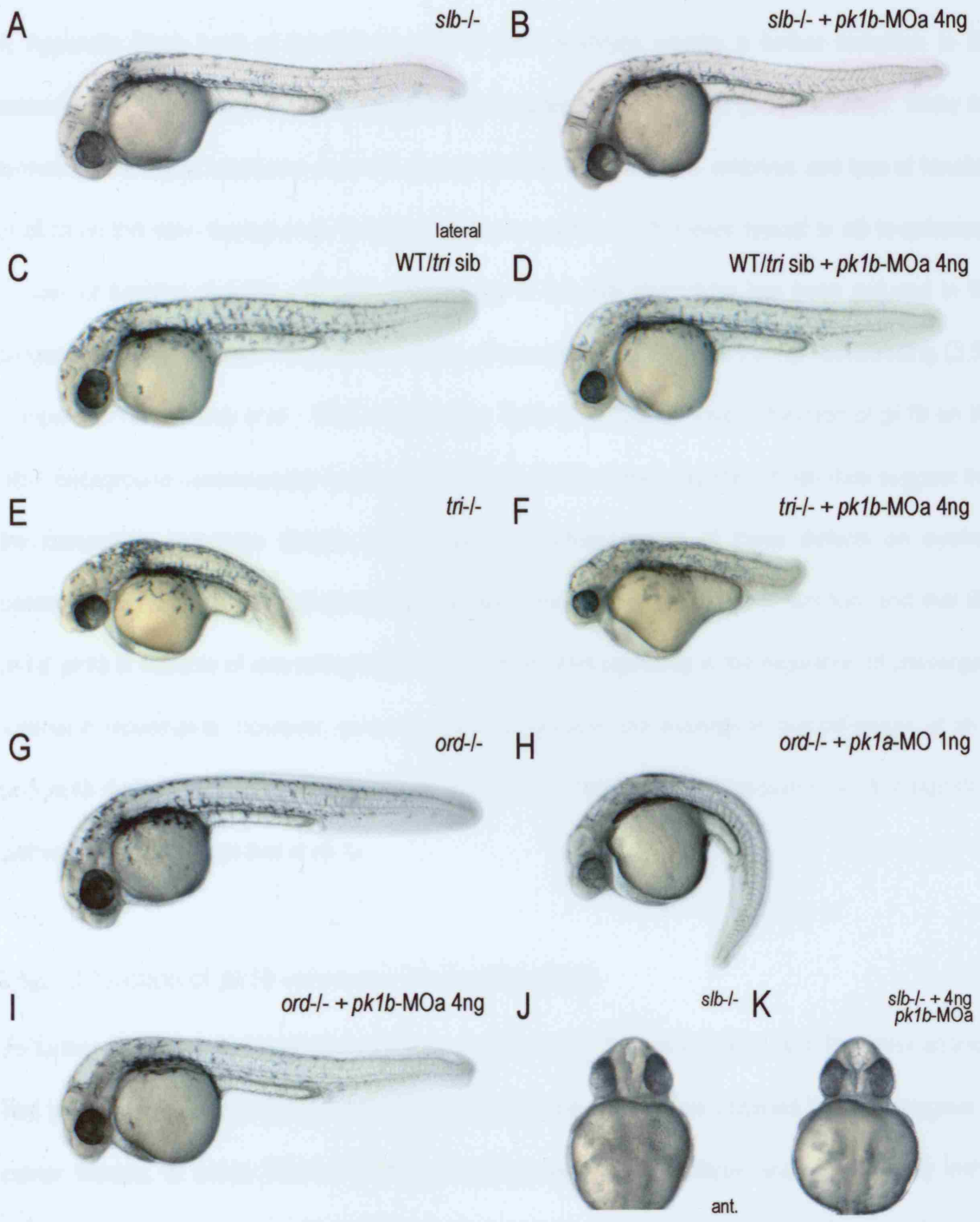

Figure 3.5

Loss of function of *pk1b* on the *silberblick*, *trilobite* and *off-road* mutant backgrounds.

An examination of the effects of *pk1b* loss of function on the convergent extension defects of *slb*, *tri* and *ord* at 24hpf. A: homozygous *slb* embryo; B: 4ng *pk1b*-MOa on homozygous *slb* background; C: typical sibling from a heterozygous *tri* carrier incross, genotypically WT or heterozygous for *tri*; D: *tri* sibling injected with 4ng *pk1b*-MOa; E: homozygous *tri* embryo; F: 4ng *pk1b*-MOa on homozygous *slb* background; G: homozygous *ord* embryo; H: 1ng *pk1a*-MO on homozygous *ord* background; I: 4ng *pk1b*-MOa on homozygous *ord* background; J: *slb-/-*, anterior view; K: 4ng *pk1b*-MOa on *slb-/-* background, anterior view.

4; Appendix Two). Loss of function of *pk1b* in *slb-/-* embryos causes a further reduction in the extension of the anteroposterior axis (Fig. 3.5B) compared to *slb-/-* alone (3.5A) at 24hpf. While the formation of the yolk extension does not appear to differ between *slb-/-* embryos and loss of function of *pk1b* on the *slb-/-* background, the defect in the separation of the eyes typical to *slb* is enhanced by loss of function of *pk1b*. Although the severity of the eye phenotype has been reduced in the progeny of our *slb* carriers through the creation of successive generations through outbreeding (3.5J; compare to Heisenberg *et al.*, 1996; Heisenberg, Tada *et al.*, 2000), loss of function of *pk1b* on the *slb-/-* background causes partial fusion of the retinae (3.5K). Taken together, these data suggest that the convergent extension defects and subsequent consequences of these defects on eyefield bilateralisation characteristic of *slb* are epistatically enhanced by *pk1b* loss of function, and that like *pk1a*, *pk1b* is capable of interacting with non-canonical Wnt signalling in the regulation of convergent extension movements. However, given the contrast between the expression and behaviour of *pk1a* and *pk1b* during gastrulation, the nature of *pk1b*'s interaction with the non-canonical Wnt signalling pathway may differ from that of *pk1a*.

Loss of function of *pk1b* enhances the *tri* phenotype

To further define the contrast between *pk1a* and *pk1b* and their relationship with the non-canonical Wnt signalling pathway, I examined *pk1b* loss of function in embryos obtained by heterozygous *tri* carrier incross, in which 75% of the clutch was phenotypically wildtype and genotypically either wildtype or *tri+/-*, and the remaining 25% was homozygous for *tri-/-* (Fig. 3.5; Table 4; Appendix Two). At 24hpf, loss of function of *pk1b* in homozygous *tri* embryos resulted in an enhancement of convergent extension defects relative to *tri-/-* or *pk1b* morphant embryos alone. 4ng of *pk1b*-MOa on

the *tri-/-* background (3.5F) caused further shortening of the already severely reduced anteroposterior axis of the *trilobite* mutant (3.5E). Coupled with this, loss of function of *pk1b* also further reduced the separation of the yolk extension from the body of the yolk, producing a yolk so malformed that the distinction between the body of the yolk and the yolk extension is lost. The separation of the eyes occurs normally in these embryos, supporting the idea that the defects of both *tri-/-* and *pk1b* morphants occur posteriorly on the body axis.

However unlike *pk1a*, loss of function of *pk1b* in heterozygous *tri* embryos does not cause an enhancement of convergent extension defects more pronounced than in *pk1b* morphants or *tri* heterozygotes alone at 10hpf. A 4ng dose of *pk1b*-MOa resulted caused only a slight shortening of anteroposterior body length in the *tri* heterozygote or wildtype proportion of the embryos (3.5D) compared to uninjected siblings (3.5C), suggesting that, dissimilarly to loss of function of *pk1a*, loss of function of *pk1b* on the *tri+/-* background is insufficient to recapitulate the *tri-/-* phenotype. In concert, these observations confirm that the genetic interaction between *pk1b* and known regulators of convergent extension movements such as *tri* or *slb* differs greatly from that of *pk1a*.

In contrast to *pk1a*, loss of function of *pk1b* does not enhance the *ord* phenotype

The zebrafish mutant *off-road* (*ord*) carries a mutation in *fmi2/celsr2*, one of three zebrafish orthologues of the *Drosophila* PCP gene *flamingo/starry night* (*fmi/stan*) identified to date (Thesis: Carreira-Barbosa F., 2005; Wada *et al.*, 2006). Vertebrate orthologues of *flamingo/starry night* (*fmi/stan*) encode atypical protocadherins, implying that the regulation of cell adhesion is one potential downstream effector of both PCP signalling and non-canonical Wnt signalling (Thesis:

Carreira-Barbosa F., 2005). Phenotypically wildtype at 24hpf, the *off-road* mutant acquired its name due to defective hindbrain facial (nVII) branchiomotor neuron migration, an aspect of its phenotype in common with zebrafish convergent extension mutants such as *trilobite/stbm* (*tri*) or *pk1a* morphant embryos (Bingham *et al.*, 2002; Carreira-Barbosa *et al.*, 2003; Jessen *et al.*, 2002; Thesis: Carreira-Barbosa F., 2005). Recently, *fmi2/celsr2* was shown to interact with *fz3a* in the regulation of branchiomotor migration, raising the possibility that the regulation of hindbrain facial (nVII) branchiomotor neuron migration is not so much Wnt-independent as previously thought, but Dsh-independent, the pathway diverging from non-canonical signalling after the Fz receptor (Wada *et al.*, 2006).

Loss of function of *pk1a* strongly enhances convergent extension defects in *ord-/-* mutants (Fig. 3.5; Table 4; Appendix Two). Injection of 1ng *pk1a*-MO on the homozygous *ord* background, a dose subthreshold for the creation of the characteristic *pk1a* morphant phenotype (see Fig. 3.4B), results in reduction of anteroposterior body length and ventral curling of the body axis (3.5H) relative to uninjected *ord-/-* embryos at 24hpf (3.5G). Additionally, the yolk extension is increased in diameter, shortened in the anteroposterior axis and generally less well separated from the body of the yolk. These facts suggest that *pk1a* is epistatic to *fmi2/celsr2* in the regulation of convergent extension movements.

In comparison, loss of function of *pk1b* in homozygous *ord* embryos does not enhance their convergent extension defects (Fig. 3.5; Table 4; Appendix Two). At 24hpf, a 4ng dose of *pk1b*-MOa on the homozygous *ord* background (3.5I) yielded a phenotype indistinguishable from *ord-/-* (3.5G) or *pk1b* morphants alone (3.4C). I concluded that, in contrast to *pk1a*, *pk1b* does not functionally

interact with *fmi2/celsr2* in the regulation of convergent extension movements. I cannot however exclude the possibility that *pk1b* interacts with *fmi2/celsr2* in the regulation of other processes, such as branchiomotor neuron migration.

At 40% epiboly, Venus-Pk1b localises to puncta at the cell membrane

In an attempt to understand the differences in expression and function I have observed between *pk1a* and *pk1b* in the regulation of convergent extension, I investigated the subcellular localisation of Pk1b at 40% epiboly using confocal microscopy (Fig. 3.6; Table 6 & 7; see Materials & Methods: Imaging: *in vivo* Time-Lapse Movies; Imaging: Subcellular Localisation of Venus-Pk1b *in vivo*). Pk1a was visualised by the addition of the YFP-derivative, Venus, to the N-terminus of the protein, because labelling Pk proteins at the C-terminus could interfere with the function of the CIIS motif, an evolutionarily conserved prenylation site (Carreira-Barbosa *et al.*, 2003; Veeman *et al.*, 2003). The translation of the Venus label was found to be extremely inefficient in this orientation: however, Western Blot analysis showed that the Venus-Pk1a was translated normally *in vivo*. Pk1b shares this CIIS motif, so like Venus-Pk1a, Pk1b is also labelled at the N-terminus, but the efficiency of Venus translation is improved in Pk1b, possibly due to less interference from the slightly longer N-terminus region of Pk1b compared to Pk1a. I co-injected 300pg of *venus-pk1b* mRNA with 100pg *membrane-RFP* mRNA in one cell between the 2 and 8-cell stages, providing a suitable intensity of fluorescence but yielding no visible gain of function phenotype. In this way, I created mosaic embryos where I could easily observe the subcellular location of Pk1b in green relative to the landmark of the cell surface membrane in red. I observed Pk1b localisation *in vivo* in both enveloping layer (EVL) cells and deep cells in the animal pole of ten wildtype embryos at 40% epiboly.

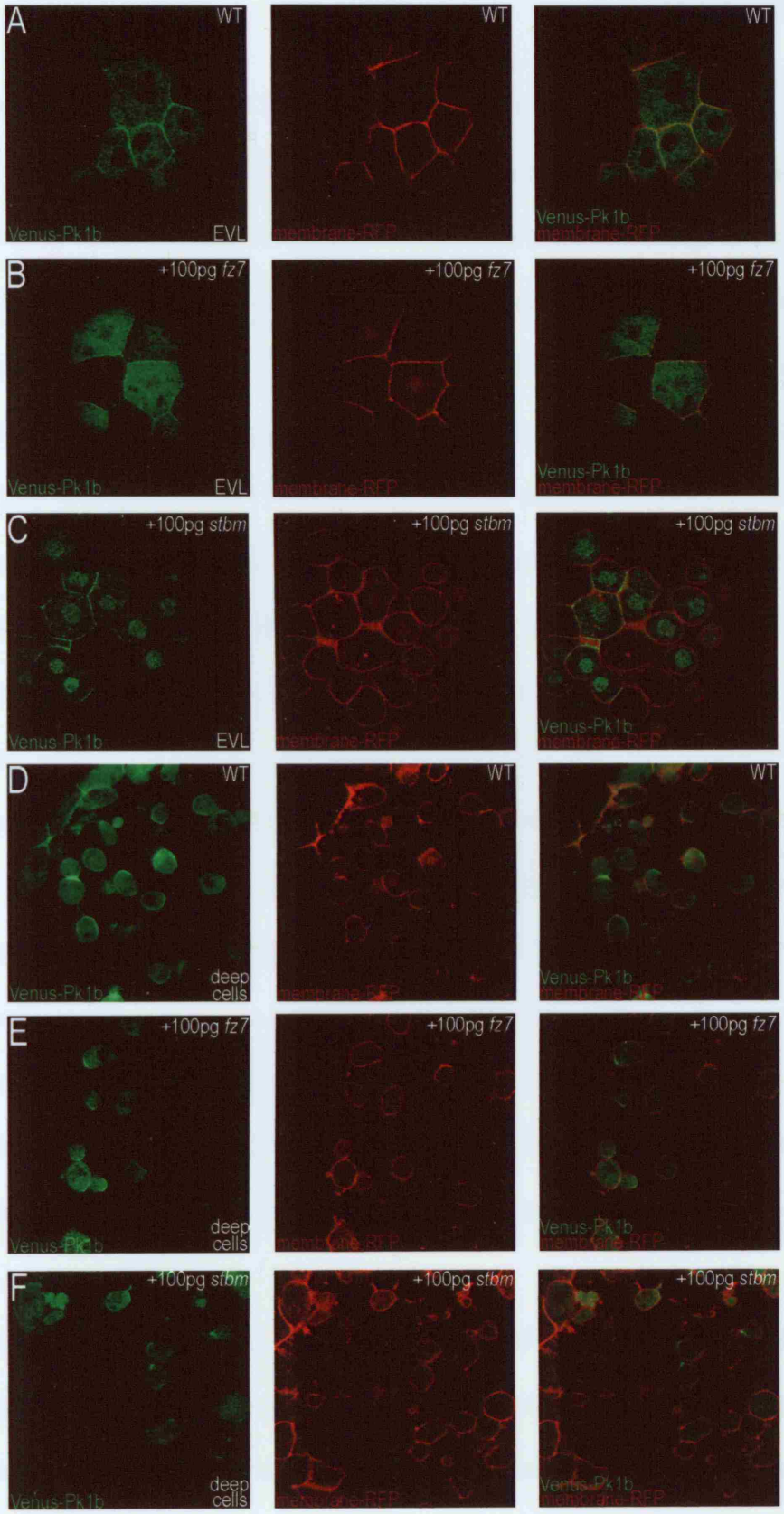

Figure 3.6

Subcellular localisation of Venus-Pk1b *in vivo*.

A-C: localisation of Venus-Pk1b (green) relative to membrane-RFP (red) in EVL cells in wildtype (A); WT+100pg *fz7* mRNA (B); and WT+100pg *stbm* mRNA (C). D-F: localisation of Venus-Pk1b (green) relative to membrane-RFP (red) in deep cells in wildtype (D); WT+100pg *fz7* mRNA (E); and WT+100pg *stbm* mRNA (F).

In wildtype embryos, expression of Venus-Pk1b was visible in the cytoplasm and at the cell membrane in both EVL and deep cells (Fig. 3.6; Table 7). In the majority of EVL cells observed (3.6A; 76% where n=313), Venus-Pk1b was localised at the interfaces between the large EVL cells, all cells also showing puncta within their cytoplasm (100%). In a large proportion of the deep cells I observed, Venus-Pk1b was localised to puncta at the cell membrane (3.6D; Table 6; 41% where n=732), and this proportion of cells greatly outnumbered the cells with punctate Venus-Pk1b localisation in the cytoplasm (22%). Expression of Venus-Pk1b in cytoplasmic puncta most likely corresponds with vesicles in the cytoplasm, and contrasts greatly with the uniform cytoplasmic localisation of Venus-Pk1a (Carreira-Barbosa *et al.*, 2003). Membrane localisation of Venus-Pk1b in deep cells is however complex: the membrane puncta I observed varied greatly in size, shape, number per cell and position within the cell. Although mosaic overexpression of *venus-pk1b* and *membrane-RFP* makes the observation of neighbouring cells difficult, I did observe both membrane localisation of Venus-Pk1b at the interface between neighbouring cells, and cells in which Venus-Pk1b was not at the interface between cells, implying that Pk1b is not exclusively situated at the interfaces between neighbouring cells. Intriguingly, at 40% epiboly, I saw no recognisable orientation of the membrane localisation of Venus-Pk1b with respect to any embryonic axis or landmark or any tissue movements as might be anticipated at the onset of gastrulation, in contrast with other PCP orthologues such as Dsh, known to be localised at cell-cell contacts in a Wnt11/Fz-dependent manner (Witzel *et al.*, 2006).

To ensure that this apparent lack of polarised localisation of Venus-Pk1b was not the result of observing embryos either before the onset of gastrulation at which time cell movements are more random, or without an appropriate landmark against which to compare their polarity, I tried a different approach. I injected 100pg *membrane-RFP* mRNA at the 1-cell stage to ubiquitously label the cell

membrane in red, and then mosaically expressed 300pg *venus-pk1b* mRNA in one cell at the 8-cell stage. I observed the dorsal aspect of the embryos at the 2-somite stage using confocal fluorescence microscopy, when the notochord-somite boundary (NSB) was clearly visible (Fig. 3.7; Table 8). In this way, I theorised that the landmark of the NSB would be visible in terms of the cell shapes outlined in Membrane-RFP, while mosaic Venus-Pk1b expression could be visualised within the notochord and in paraxial tissues, and any orientation of their membrane puncta with respect to the dorsal midline recorded. I examined axial and paraxial cells in six wildtype embryos: in most embryos, Venus-Pk1b appeared to be brightly expressed in other regions of the embryo but excluded from the dorsal midline, as if Pk1b was intrinsically refractory to this approach. In the embryos where it was possible to visualise Venus-Pk1b mosaically in axial and paraxial cells adjacent to the NSB, I was unable to observe any evidence that Pk1b is asymmetrically localised within cells in the dorsal midline (Fig. 3.7).

SUBCELLULAR LOCALISATION OF PK1B. DEEP CELLS	AMT (pg)	TOTAL EMBRYOS	TOTAL CELLS	CELLS WITH MEMBRANE LOCALISATION OF PK1B %	CELLS WITH MEMBRANE PK1B AT CELL INTERFACES %	CELLS WITH CYTOPLASMIC LOCALISATION OF PK1B %
venus-pk1b* + *membrane-RFP	*pk1b*: 300 *RFP*: 100	10	732	41	24	22
venus-pk1b* + *membrane-RFP* + *fr7	*pk1b*: 300 *RFP*: 100 *fr7*: 100	4	610	42	27	16
venus-pk1b* + membrane-RFP + *stbm	*pk1b*: 300 *RFP*: 100 *stbm*: 100	3	531	22	13	12

Table 6. Subcellular localisation of Venus-Pk1b in deep cells at 40% epiboly.

SUBCELLULAR LOCALISATION OF PK1B: EVL CELLS	AMT. (pg)	TOTAL EMBRYOS	TOTAL CELLS	CELLS WITH MEMBRANE LOCALISATION OF PK1B %	CELLS WITH MEMBRANE PK1B AT CELL INTERFACES %	CELLS WITH CYTOPLASMIC LOCALISATION OF PK1B %
***venus-pk1b* + membrane-RFP**	*pk1b*: 300 *RFP*: 100	10	313	76	76	100
venus-pk1b* + membrane-RFP + *fr7	*pk1b*: 300 *RFP*: 100 *fr7*: 100	4	83	88	88	100
venus-pk1b* + membrane-RFP + *stbm	*pk1b*: 300 *RFP*: 100 *stbm*: 100	3	206	66	66	32

Table 7. Subcellular localisation of Venus-Pk1b in EVL cells at 40% epiboly.

Venus-Pk1b localisation at 40% epiboly does not change in the presence of Fz7

I examined Venus-Pk1b localisation in response to Fz7 in both EVL and deep cells in the animal pole of 4 embryos *in vivo* by confocal fluorescence microscopy, using the following subthreshold doses of mRNA: 300pg *pk1b*-venus, 100pg *membrane-RFP* and 100pg *fz7* (unlabelled) (Fig. 3.6; Table 6 & 7). Venus-Pk1b localised to puncta within the cytoplasm and at the cell membrane in both EVL and deep cells in a manner indistinguishable from the localisation of Pk1b in wildtype embryos. In EVL cells, punctate localisation of Venus-Pk1b was visible in the cytoplasm of all cells observed (3.6B; 100%, n=83; Table 7), most likely reflecting Pk1b within vesicles, while localisation of Venus-Pk1b at the cell membrane was visible in the majority of EVL cells (88%), and always restricted to the interfaces between neighbouring cells. In the majority of deep cells observed, Venus-Pk1b was localised to puncta at the cell membrane (3.6E; Table 6; 42% where n=610), although Venus-Pk1b was visible in cytoplasmic puncta in a smaller proportion of cells (16%). I observed membrane localisation of Venus-Pk1b at the interfaces between neighbouring cells, but equally, I observed Venus-Pk1b localisation at the membrane in isolated cells, indicating that membrane localisation of Pk1b is not

exclusively restricted to the boundaries between neighbouring cells. As with the localisation of Venus-Pk1b in wildtype embryos, I was unable to observe any consistency in the size, shape, number or position of the puncta of Venus-Pk1b at the cell membrane, nor any recognisable orientation of these puncta with respect to any embryonic axis or moving tissue at the onset of gastrulation. From this, I conclude that the presence of Fz7 has no effect on the subcellular localisation of Pk1b, similarly to Pk1a (Carreira-Barbosa *et al.*, 2003). This contrasts with, for instance, Dsh, known to be localised at cell-cell contacts in a Wnt11/Fz-dependent manner (Witzel *et al.*, 2006).

SUBCELLULAR LOCALISATION OF PK1B: DEEP CELLS	AMT (pg)	TOTAL EMBRYOS	TOTAL AXIAL CELLS	AXIAL CELLS SHOWING ORIENTATED *Pk1B* EXPRESSION %	TOTAL PARAXIAL CELLS	PARAXIAL CELLS SHOWING ORIENTATED *PK1B* EXPRESSION %
venus-pk1b+ membrane-RFP	*pk1b*: 300 *RFP*: 100	6	179	0	153	0

Table 8. Subcellular localisation of *pk1b* at the 2-somite stage.

Venus-Pk1b localisation at 40% epiboly is altered in the presence of Stbm

I investigated the localisation of Venus-Pk1b in the presence of Stbm in both EVL and deep cells in the animal pole of 3 embryos *in vivo* by confocal fluorescence microscopy, using the following subthreshold doses of mRNA: 300pg *pk1b*-venus, 100pg *membrane-RFP* and 100pg *stbm* (unlabelled) (Fig. 3.6; Table 6 & 7). I observed punctate Venus-Pk1b localisation at the membrane and in the cytoplasm in both EVL and deep cells, but the proportions of cells displaying these puncta either at the membrane or in the cytoplasm subtly differed from Pk1b localisation in wildtype embryos

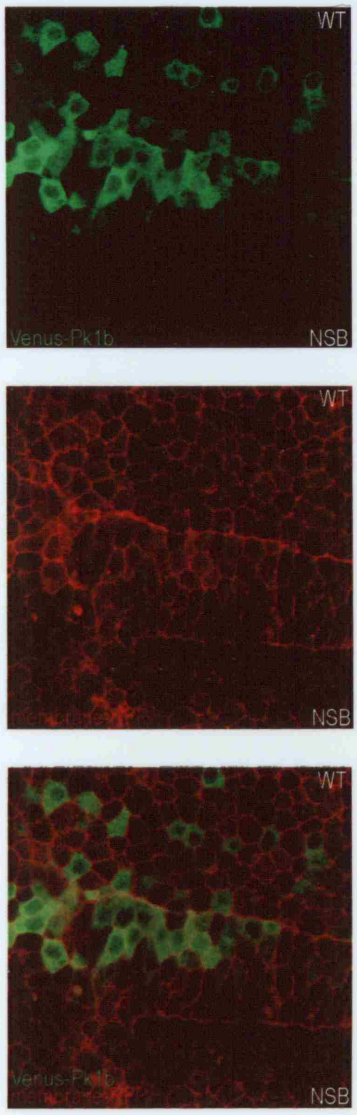

Figure 3.7

Subcellular localisation of Venus-Pk1b relative to the NSB at the 2-somite stage.

Mosaic expression of Venus-Pk1b (300pg) does not show asymmetric expression with respect to the notochord-somite boundary (NSB), visualised with ubiquitous expression of membrane-RFP (100pg).

or in the presence of Fz7. In EVL cells, the majority of cells showed membrane localisation of Venus-Pk1b at the interfaces between cells as in wildtype embryos (3.6C; Table 7; 66% where n=206). Cytoplasmic puncta were still visible in EVL cells, but in a much smaller proportion of cells than in wildtype (32%). Likewise, in deep cells, punctate localisation of Venus-Pk1b was evident both at the cell membrane (3.6F; Table 6; 22%, n=531) and within the cytoplasm (13%, n=531), but in both cases, in a greatly reduced number of cells compared to wildtype. As in wildtype embryos, despite the limitations of mosaic labelling, I was able to observe cells in which Venus-Pk1b was localised at cell-cell interfaces as well as cells where Venus-Pk1b was localised away from cell interfaces, implying that, unlike in EVL cells, Pk1b does not exclusively localise to the interfaces between neighbouring cells. Again, there was no detectable consistency in the size, shape, number per cell or position of the puncta observed in these embryos, and no recognisable orientation with respect to any embryonic axis or tissue.

Rather than a shift in localisation of Venus-Pk1b from the membrane to cytoplasmic vesicles, these data seem to reflect an overall downregulation of Pk1b in the presence of Stbm. These observations are at odds with the role of Stbm during *Drosophila* PCP signalling in the fly wing and eye: Stbm is thought to bind Pk and recruit it to the cell membrane at the proximal vertex of the cell where it antagonises Fz/Dsh signalling, restricting it to the distal vertex of the cell (Bastock *et al.*, 2003; Jenny *et al.*, 2003). These data also contrast with Pk1a, the localisation of which is indistinguishable from wildtype localisation in the presence of *stbm* (F. Carreira-Barbosa & M. Tada, unpublished data).

Discussion & Conclusion

Summary

In this chapter, I have shown while *pk1a* and *pk1b* expressions are similar during early gastrulation, *pk1b* expression diverges from *pk1a*, more closely resembling *pk2* expression than *pk1a* expression during late gastrulation (Carreira-Barbosa *et al.*, 2003; Veeman *et al.*, 2003). I have shown that loss of function of *pk1b* causes a mild defect in convergent extension movements, in contrast to loss function of *pk1a* (Carreira-Barbosa *et al.*, 2003). Moreover, the severe defects resulting from the simultaneous loss of function of both *pk1a* and *pk1b* suggest that these divergent *pk1* genes are epistatic and cooperate in the regulation of convergent extension.

To further characterise the difference between *pk1a* and *pk1b* function, I investigated the ability of *pk1b* to enhance the convergent extension defects of zebrafish mutants for components of the non-canonical Wnt signalling pathway and pathways considered parallel to the non-canonical Wnt signalling pathway. Similar to loss of function of *pk1a*, loss of function of *pk1b* enhanced the convergent extension defects of the *silberblick/wnt11* (*slb*) mutant, suggesting that *pk1b* can interact with the non-canonical Wnt signalling pathway (Carreira-Barbosa *et al.*, 2003). Loss of function of *pk1b* also enhanced the convergent extension defects of *trilobite/stbm* (*tri*), suggesting that like *pk1a*, *pk1b* can interact with *stbm* in the modulation of the non-canonical Wnt signalling pathway in the context of convergent extension movements (Carreira-Barbosa *et al.*, 2003). However, the phenotype resulting from *pk1b*'s enhancement of either *slb-/-* or *tri-/-* is less severe than that of *pk1a*, (Carreira-Barbosa *et al.*, 2003).

To attempt to explain the differences between *pk1a* and *pk1b* function during convergent extension, I compared the subcellular localisation of Venus-Pk1b with that of Venus-Pk1a (Carreira-Barbosa *et al.*, 2003; F. Carreira-Barbosa & M. Tada, unpublished data). Venus-Pk1a is localised uniformly throughout the cytoplasm at 40% epiboly, whereas in contrast, Venus-Pk1b in restricted to randomly orientated puncta at the cell membrane, and to a lesser extent, in the cytoplasm (Carreira-Barbosa *et al.*, 2003). Like Venus-Pk1a, Venus-Pk1b localisation is unaffected by presence of Fz7 (Carreira-Barbosa *et al.*, 2003). However, while Venus-Pk1a localisation is unchanged in the presence of Stbm, punctate expression of Venus-Pk1b both in the cytoplasm and at the cell membrane is evident in fewer cells.

Discussion

During the establishment of PCP in *Drosophila*, the accumulation of Fz protein to the distal vertex of wing hair cells is initiated by an unknown mechanism. Neighbouring cells respond to this local imbalance by asymmetrically recruiting PCP proteins into self-organising protein complexes at the cell membrane. The Prickle (Pk) protein exists as two, non-functionally redundant isoforms in the fly, known as *pk* and *sple* (Gubb et al., 1999). Pk protein localises to the proximal vertex of the cell, where it antagonises Fz/Dsh signalling by preventing the membrane recruitment of Dsh by Fz. As a result, PCP proteins such as Pk, Stbm and Fmi accumulate proximally within wing hair cells, while Fz and Dsh accumulate distally within wing hair cells. This creates cell polarity that is non-autonomously amplified and propagated across the wing in the plane of the epithelium, with the consequence of restricting Fz/Dsh signalling and downstream cytoskeletal reorganisation and actin prehair formation to the distal vertex of each wing hair cell (Axelrod, 1998; Gubb *et al.*, 1999; Krasnow & Adler, 1994; Lee & Adler, 2002; Strutt, 2001; Tree *et al.*, 2002; Wong & Adler, 1993). However, the relationship

between Pk and Fz/Dsh signalling is not straightforward. Pk does not act in a linear pathway with Fz and Dsh, and neither Fz function or Dsh recruitment is dependent upon Pk, but the propagation of the asymmetric localisation of PCP proteins is abolished by loss of function of *pk* (Krasnow *et al.*, 1995; Tree *et al.*, 2002). More recently, it was proposed that the Strabismus (Stbm) protein, a putative four-pass transmembrane protein known to be asymmetrically localised in the *Drosophila* wing and eye, bridges non-canonical Wnt signalling and this parallel pathway with its ability to bind and recruit both Pk and Dsh to the cell membrane in the propagation of PCP (Bastock *et al.*, 2003; Jenny *et al.*, 2003).

Drosophila PCP genes such as *fz*, *dsh*, *pk stbm* and *fmi* are evolutionarily conserved in vertebrates (Carreira-Barbosa *et al.*, 2003; Formstone & Mason, 2005; Jessen *et al.*, 2002; Sumanas *et al.*, 2001; Sumanas & Ekker, 2001; Veeman *et al.*, 2003; Wallingford, 2000; Wallingford *et al.*, 2002b). A ligand for the Fz receptor has yet to be identified in the *Drosophila* PCP signalling pathway: however in vertebrates, Wnts such as Wnt11 and Wnt5b act as ligands for a Fz/Dsh pathway distinct from the canonical Wnt signalling pathway involved in the specification of cell fate, known as the non-canonical Wnt signalling pathway (Axelrod *et al.*, 1998; Cadigan & Nusse 1997). Non-canonical Wnt signalling has been shown to orchestrate a number of morphogenetic processes analogous to *Drosophila* PCP, including the regulation of cell polarity and cell migration driving convergent extension movements during gastrulation in *Xenopus* and zebrafish (Ku & Melton, 1993; Saka *et al.*, 2000; Smith *et al.*, 2000; Sokol, 1996; Sumanas *et al.*, 2001; Sumanas & Ekker, 2001; Tada & Smith, 2000; Wallingford, 2000). Similarly to the *Drosophila* PCP signalling pathway, vertebrate orthologues of *pk*, *stbm* and *fmi* are considered to function in a parallel pathway capable of modulating non-canonical Wnt signalling in the regulation of gastrulation movements (Carreira-Barbosa *et al.*, 2003;

Formstone & Mason, 2005). Pk, Stbm and Fmi are also thought to function in the regulation of branchiomotor neuron migration (Carreira-Barbosa *et al.*, 2003; Jessen *et al.*, 2002; Wada *et al.*, 2006). This role is considered Wnt-independent: recently however, Frizzled3a and Fmi2/Celsr2 were shown to interact in branchiomotor neuron migration, suggesting that rather than Wnt-independent, the non-canonical Wnt signalling pathway and neuronal migration pathways diverge at some point downstream of the Fz receptor (Carreira-Barbosa *et al.*, 2003; Wada *et al.*, 2006).

Loss of function of *pk1b* on the wildtype background weakly impairs convergent extension movements. Although verification of the efficacy of *pk1b* loss of function, such as rescue of *pk1b* morphants by *pk1b* mRNA and confirmation of reduced *pk1b* levels in *pk1b* morphant embryos by RT PCR is yet to be done, the early indication is that loss of function of *pk1b* contrasts greatly with the effect of loss of function of *pk1a* on convergent extension movements (Carreira-Barbosa *et al.*, 2003; For an exploration of convergent extension phenotypes, see Appendix Two). This suggests that *pk1b* and *pk1a* may only be functionally redundant in certain contexts: a theory that only future cross-rescue of loss of function of one *pk1* orthologue by gain of function of the other will prove. However, incomplete functional redundancy is not unexpected for several reasons. Firstly, while *pk1a* and *pk1b* are expressed similarly in the marginal zone during early gastrulation, their expression diverges during late gastrulation: *pk1b* is expressed in the dorsal midline, while *pk1a* is expressed in the posterior neurectoderm and pre-somitic mesoderm but conspicuously absent from the dorsal midline at tailbud stage (Carreira-Barbosa *et al.*, 2003). The expression pattern of *pk1b* more closely resembles that of zebrafish *pk2* during gastrulation (Veeman *et al.*, 2003). Secondly, despite the similarity in structure of the protein products of *pk1a*, *pk1b* and *pk2*, simultaneous loss of function of *pk1a* and *pk2* suggested these *pk* orthologues are not functionally redundant (Carreira-Barbosa *et*

al., 2003; Veeman et al., 2003). Indeed, during PCP signalling in *Drosophila*, the *pk* isoforms *pk* and *sple* are not functionally redundant and cannot rescue each other's function (Gubb *et al.*, 1999). However, simultaneous loss of function of *pk1a* and *pk1b* caused convergent extension defects more severe and dissimilar in phenotype to loss of function of either *pk1a* or *pk1b* alone. Taken together, these facts suggest that zebrafish *pk* orthologues have discrete functions in the regulation of convergent extension movements.

The contrast between the enhancement of convergent extension defects in the zebrafish *silberblick/wnt11* (*slb*), *trilobite/stbm* (*tri*) and *off-road/fmi2* (*ord*) mutants caused by loss of function of either *pk1a* or *pk1b* supports the theory that these *pk1* genes have discrete functions in the context of the regulation of gastrulation movements. Loss of function of *pk1a* severely enhances the convergent extension defects of *silberblick*, while *pk1a* gain of function is capable of rescuing hyperactivation of the non-canonical Wnt signalling pathway resulting from *wnt11* overexpression, indicating that endogenous *pk1a* activity antagonises non-canonical Wnt signalling in a manner highly reminiscent of the role of Pk during *Drosophila* PCP (Carreira-Barbosa *et al.*, 2003). Conversely, loss of function of *pk1b* weakly enhances the convergent extension defects of *silberblick*, causing further shortening of the anteroposterior axis and enhancing the accompanying failure in eyefield bilateralisation (less pronounced in our *silberblick* carriers due to outbreeding). The defects arising from loss of function of *pk1b* in wildtype are confined to the posterior region of the body axis: although mild in comparison to loss of function of *pk1a*, the fact that loss of function of *pk1b* in *silberblick* can enhance the failure of eyefield separation of *silberblick* is evidence of a genetic interaction between *pk1b* and the vertebrate non-canonical Wnt signalling pathway. An investigation of the ability of *pk1b* gain of function to rescue the *wnt11* overexpression phenotype is necessary to dissect the nature of this interaction

compared with that of *pk1a*, although the contrast between *pk1a* and *pk1b* function is made apparent by the divergent manner in which the two *pk1* genes interact with other known regulators of convergent extension movements.

pk1a has been shown to interact with *stbm* in the regulation of both convergent extension movements via modulation of the non-canonical Wnt signalling pathway, and in a Wnt-independent manner, the migration of facial (nVII) branchiomotor neurons in the hindbrain (Carreira-Barbosa *et al.*, 2003; Jessen *et al.*, 2002). I have shown in this chapter that, similarly to *pk1a*, *pk1b* is capable of interacting with *stbm*. Loss of function of *pk1b* is known to reduce hindbrain facial (nVII) branchiomotor neuron migration in wildtype embryos, and confirmation of whether *pk1b* and *stbm* interact during neuron migration is necessary in the future. In the context of convergent extension movements, loss of function of *pk1b* enhances the defects of the *trilobite/stbm* (*tri*) mutant, further compressing the body of *tri-/-* embryos in the anteroposterior axis and abolishing the division between the body of the yolk and the yolk extension. While loss of function of *pk1b* enhanced the predisposition to cyclopia of the *silberblick* mutant, the defects of both homozygous *trilobite* and *pk1b* morphant embryos are confined to the posterior region of the body axis, explaining why loss of function of *pk1b* in *tri-/-* enhances the impaired convergent extension movements posteriorly without giving rise to cyclopia. This reflects epistasis rather than the addition of two unrelated phenotypes, but the nature of this functional interaction is different from that of *pk1a*.

The effect of loss of function of *pk1a* on the *trilobite* background contrasts with that of *pk1b* in two ways. Firstly, loss of function of *pk1a* in *tri-/-* embryos affects convergent extension movements much more severely than loss of function of *pk1b* (Carreira-Barbosa *et al.*, 2003). Secondly, loss of function

of *pk1a* enhances the convergent extension phenotype of heterozygous *tri* embryos with the result that they are indistinguishable from homozygous *tri*, suggesting that *stbm* and *pk1a* function in the same pathway in the context of the regulation of convergent extension (Carreira-Barbosa *et al.*, 2003). In effect, loss of function of *pk1a* is sufficient to cancel out the effects of one copy of the *stbm* gene. In comparison, loss of function of *pk1b* is insufficient to enhance the defects of heterozygous *tri* embryos, and while a genetic interaction genuinely occurs between *pk1b* and *stbm* in the regulation of convergent extension movements, *pk1b* activity is of less significance to this pathway than *pk1a*.

The contrast between *pk1a* and *pk1b* function during zebrafish gastrulation is most clear from their respective interactions with the *off-road/fmi2* (*ord*) mutant: while loss of function of *pk1a* generates convergent extension defects in *ord-/-* mutants, loss of function of *pk1b* meanwhile has no detectable consequence on convergent extension movements in *ord-/-* mutants. The *off-road/fmi2* (*ord*) mutant is phenotypically wildtype at 24hpf, but facial (nVII) branchiomotor neuron migration is disrupted in the hindbrain reminiscently of loss of function of *pk1a* on the *tri/stbm* mutant background (Carreira-Barbosa *et al.*, 2003). The role of PCP proteins such as *fmi2* in the regulation of branchiomotor neuron migration was considered to be Wnt-independent, but as recent data demonstrated that Fz3a and Fmi2 interact in branchiomotor neuron migration in zebrafish and Fz is the receptor for Wnt ligands, this may not be the case (Wada *et al.*, 2006). It is possible to speculate that a pathway responsible for the regulation of neuronal migration, featuring Stbm, Fmi and Pk orthologues, diverges from the non-canonical Wnt signalling pathway downstream of Fz. An examination of the effect of loss of function of *pk1b* on the ord background on facial (nVII) branchiomotor neuron migration is necessary to place *pk1b* in this pathway: however, in support of this role, loss of function of *pk1b* using a combination of *pk1b*-MOa and *pk1b*-MOb was discovered to reduce branchiomotor

neuron migration in a manner reminiscently of loss of function of *pk1a* on the *tri/stbm* mutant background (personal communication, V. Prince; Carreira-Barbosa *et al.*, 2003; Rohrschneider *et al.*, 2007).

To understand more about the events underpinning the divergent functions of *pk1a* and *pk1b* during zebrafish gastrulation, I examined the subcellular localisation of Venus-Pk1b compared to that of Venus-Pk1a at 40% epiboly (Carreira-Barbosa *et al.*, 2003). I demonstrated earlier in this chapter that overexpression of 300pg of *pk1b* caused no detectable gain of function phenotype, and that the addition of the Venus label at the N-terminus of the protein neither interfered with Pk1b function nor created any artefactual convergent extension phenotype. I found that Venus-Pk1b localised to puncta within the cytoplasm and at the cell membrane, many more cells showing membrane localisation than cytoplasmic localisation of Pk1b. Contrastingly, Venus-Pk1a localises uniformly throughout the cytoplasm at 40% epiboly, although the subcellular localisation of both Pk1a and Pk1b differs greatly from the highly asymmetric distribution of Pk during PCP signalling in *Drosophila*. I found no evidence of polarisation of Pk1b localisation with respect to any embryonic axis or tissue movement. It is possible that 40% epiboly was too early to observe polarisation in an orientation relevant to the tissue movements of gastrulation, but observation of polarised cells at the 2-somite stage relative to the recognisable landmark of the notochord-somite boundary failed to provide evidence of a consistent orientation of Pk1b localisation with respect to the anteroposterior and mediolateral axes of the cell. This pattern of subcellular localisation of Pk1b did not change in the presence of Fz7, consistent with published data on *pk1a* (Carreira-Barbosa *et al.*, 2003).

Recent data on PCP signalling in the *Drosophila* wing and eye suggested that Stbm was responsible for the asymmetric localisation of PCP proteins such as Dsh and Pk by directly binding these proteins and recruiting them to the membrane (Bastock *et al.*, 2003; Jenny *et al.*, 2003). In this chapter, I observed that fewer cells show punctate localisation of Venus-Pk1b protein at the cell membrane in the presence of Stbm, but this result is difficult to explain for several reasons. Firstly, the Venus-Pk1b that is no longer recruited to the cell membrane is not to be found in the cytoplasm either, suggesting that rather than a shift in subcellular localisation of Venus-Pk1b, there is less Venus-Pk1b overall. As I used identical doses of fresh mRNA for each experiment, I cannot explain this. Secondly, these data directly contradict the events of *Drosophila* PCP, extremely implausible given the many parallels between the function of *Drosophila* PCP proteins and their homologues in non-canonical Wnt signalling. In the case of the subcellular localisation of Dsh-GFP in the presence of Stbm, overexpression of *pk1a* reduced the amount of Dsh-GFP visible within the embryos, later confirmed as a downregulation by Western Blot analysis (Carreira-Barbosa *et al.*, 2003). While I tested for visible convergent extension defects at 24hpf and found none, I cannot rule out the possibility that a 300pg dose of Venus-Pk1b is causing a hidden gain of function phenotype that is somehow feeding back upon the pathway. I examined fewer embryos with *stbm* mRNA, and at this stage, my impression is that this result is artefactual: however, a more thorough analysis, possibly contrasting with the subcellular localisation of Venus-Pk1b in the *stbm* mutant *trilobite*, will be necessary to fully appreciate whether these components of PCP signalling influence each other's subcellular localisation.

Chapter Four

Slit acts through the Robo receptor in the regulation of convergent extension movements during zebrafish gastrulation.

Introduction

The secreted glycoprotein Slit is the repellent ligand for the Roundabout (Robo) receptor (Brose *et al.*, 1999). During commissure formation in the developing *Drosophila* CNS, the Robo receptor is sequestered away from the cell surface of pre-crossing axons by Commissureless (Comm): however, after crossing the CNS midline, Robo is freed by Comm and becomes expressed on the cell surface of migrating axons where it is free to bind Slit (Kidd *et al.*, 1998a; Kidd *et al.*, 1998b; Rothberg *et al.*, 1988; Seeger *et al.*, 1993; Tear *et al.*, 1996). Receipt of the Slit ligand repels post-crossing axons, helping them exit the midline and preventing errorial recrossing, a role that is evolutionarily conserved in vertebrates and invertebrates (Brose *et al.*, 1999; Challa *et al.*, 2005; Fricke *et al.*, 2001; Hutson & Chien, 2002; Kidd *et al.*, 1998; Marillat *et al.*, 2004; Sabatier *et al.*, 2004; Zallen *et al.*, 1998). Intriguingly, vertebrate orthologues of Slit and Robo start to be expressed before there are axons to guide (Camurri *et al.*, 2004; Challa *et al.*, 2001; Challa *et al.*, 2005; Dalkic *et al.*, 2006; Hutson *et al.*, 2003; Yeo *et al.*, 2001; Lee *et al.*, 2001).

The zebrafish *slit* orthologues *slit1a*, *slit1b*, *slit2* and *slit3* are expressed dynamically during gastrulation (Hutson *et al.*, 2003; Yeo *et al.*, 2001). Gain of function of *slit2* in zebrafish causes severe convergent extension defects by impairing the convergence of mesoderm upon the dorsal

midline during gastrulation (Yeo *et al.*, 2001). *slit2* overexpression also results in cyclopia, which in combination with convergent extension defects is a phenotype highly reminiscent of established convergent extension mutants such as *silberblick/wnt11* (*slb*) (Heisenberg *et al.*, 1996; Heisenberg, Tada *et al.*, 2000). While vertebrate Robo receptors are known to act as receptors for Slit ligands in the context of axon pathfinding (Brose *et al.*, 1999), it is not known whether the axially expressed Slit2 ligand functions through the Robo receptor to regulate specific aspects of cell behaviour during convergence, intercalation or extension during gastrulation.

Six orthologues of *Drosophila robo*, including splice variants, are known to exist in zebrafish: *robo1*, *robo2_tv1*, *robo2_tv2*, *robo3v1*, *robo3v2* and *robo4* (Bedell *et al.*, 2005; Challa *et al.*, 2001; Challa *et al.*, 2005; Dalkic *et al.*, 2006; Lee *et al.*, 2001). Of these, *robo1*, *robo2_tv1*, and two variants of *robo3*, *robo3v1* and *robo3v2* are expressed during zebrafish gastrulation (Bedell *et al.*, 2005; Challa *et al.*, 2001; Challa *et al.*, 2005; Dalkic *et al.*, 2006; Lee *et al.*, 2001). The predicted proteins encoded by *robo2* and *robo3v1* bear a signal peptide targeting them to the cell surface membrane, while the predicted protein encoded by *robo3v2* lacks a signal peptide in a manner reminiscent of the murine *robo3* orthologues *Rig-1*. This structural similarity between Robo3v2 and Rig-1 is of particular interest because Rig-1 was reported to act similarly to *Drosophila* Commissureless during vertebrate CNS formation, and no vertebrate orthologues or functional analogues of *comm* have been identified to date (Challa *et al.*, 2005; Lee *et al.*, 2001; Sabatier *et al.*, 2004; Yuan *et al.*, 1999). However, the authentic receptor Robo2 and the structurally divergent Robo3v1 and Robo3v2 isoforms each possess a transmembrane domain and are all expressed at the cell membrane *in vivo*, making them all potentially capable of receiving the *slit* signal (Challa *et al.*, 2005; Lee *et al.*, 2001).

No morphological defects were reported in the zebrafish MZ *robo2* mutant *astray* (*ast*) or in *robo3v1* morphant embryos generated using *robo3v1*-specific morpholino (Challa *et al.*, 2005; Fricke *et al.*, 2001). Contrastingly, loss of function of *robo3v2* using a *robo3v2*-specific morpholino resulted in aberrant development of the trunk and tail in a dose-dependent manner (Challa *et al.*, 2005). *in situ* hybridisation analysis of *robo3v2*-morphants revealed the expression domains of dorsal markers such as *ntl* or *gsc* to be expanded at the expense of ventral markers such as *scl*, while *krox-20* expression in the presumptive hindbrain and *papc* expression in the pre-somitic mesoderm were also mediolaterally expanded (Challa *et al.*, 2005). These observations were interpreted as a disruption of dorsoventral axis specification, but are in part reminiscent of convergent extension defects.

It is therefore possible to speculate that expression of both *slit* and *robo* orthologues prior to axonogenesis relates to a hitherto unidentified function of Slit/Robo signalling in midline cell behaviour during convergent extension, potentially mirroring the events of axon pathfinding in the CNS. In this chapter, I undertook both loss of function and gain of function approaches to address the question of whether Slit acts through specific Robo receptors in the regulation of convergent extension movements during zebrafish gastrulation.

Results

Zebrafish *slit* and *robo* orthologues are expressed during gastrulation

I undertook a more detailed characterisation of the dynamic expression of the *slit1* isoform *slit1a* through gastrulation by *in situ* hybridisation at a series of time points through gastrulation (for protocol, see Materials & Methods: *in situ* hybridisation). Secondly, to begin to address the question

of whether zebrafish orthologues of *Drosophila robo* act as a receptor for the Slit ligand during convergent extension, I explored the dynamic expression of the zebrafish *robo* orthologues *robo1, robo2 and robo3* by *in situ* hybridisation at a series of time points during gastrulation.

slit1 exists as two isoforms in zebrafish, *slit1a* and *slit1b*, of which *slit1b* expression was previously described (Hutson *et al.*, 2003). I characterised the expression of *slit1a* at 30%, 50% 70%, 90% and 100% epiboly during zebrafish gastrulation. At 30% epiboly *slit1a* expression was undetectable, consistent with observations that *slit* genes are not maternally provided (Hutson *et al.*, 2003; Yeo *et al.*, 2001). Ubiquitous low-level expression of *slit1a* begins at the midgastrula stage. As gastrulation proceeds, *slit1a* expression becomes restricted to cells accumulating within the shield (Figure 4.1A). At 70% epiboly, *slit1a* expression is broadly visible in the extending dorsal midline (4.1B). This expression of *slit1a* in the extending dorsal midline is perpetuated at 90% epiboly (4.1C). At tailbud stage, *slit1a* is most strongly expressed in the dorsal midline and at the lateral borders of the neural plate (4.1D). Although weak, the midline expression of *slit1a* is reminiscent of other *slit* orthologues in zebrafish, particularly *slit2* (Yeo *et al.*, 2001).

Ubiquitous expression of the zebrafish *robo* orthologues *robo1* and *robo2* is evident throughout gastrulation (4.1E-L). *robo1* is ubiquitously expressed at germ stage (4.1E). This ubiquitous expression remains unchanged at shield stage and 70% epiboly, and any increase in expression detectable in the shield or dorsal midline can be attributed to the accumulation of cells in these regions as dorsal convergence progresses (4.1F & G). At tailbud stage, *robo1* is expressed ubiquitously at low levels throughout the embryo (4.1H). *robo2* exists as two isoforms in zebrafish, *robo2* (also known as *robo2_tv1*) and *robo2_tv2* (Dalkic *et al.*, 2006; Lee *et al.*, 2001). Without variant

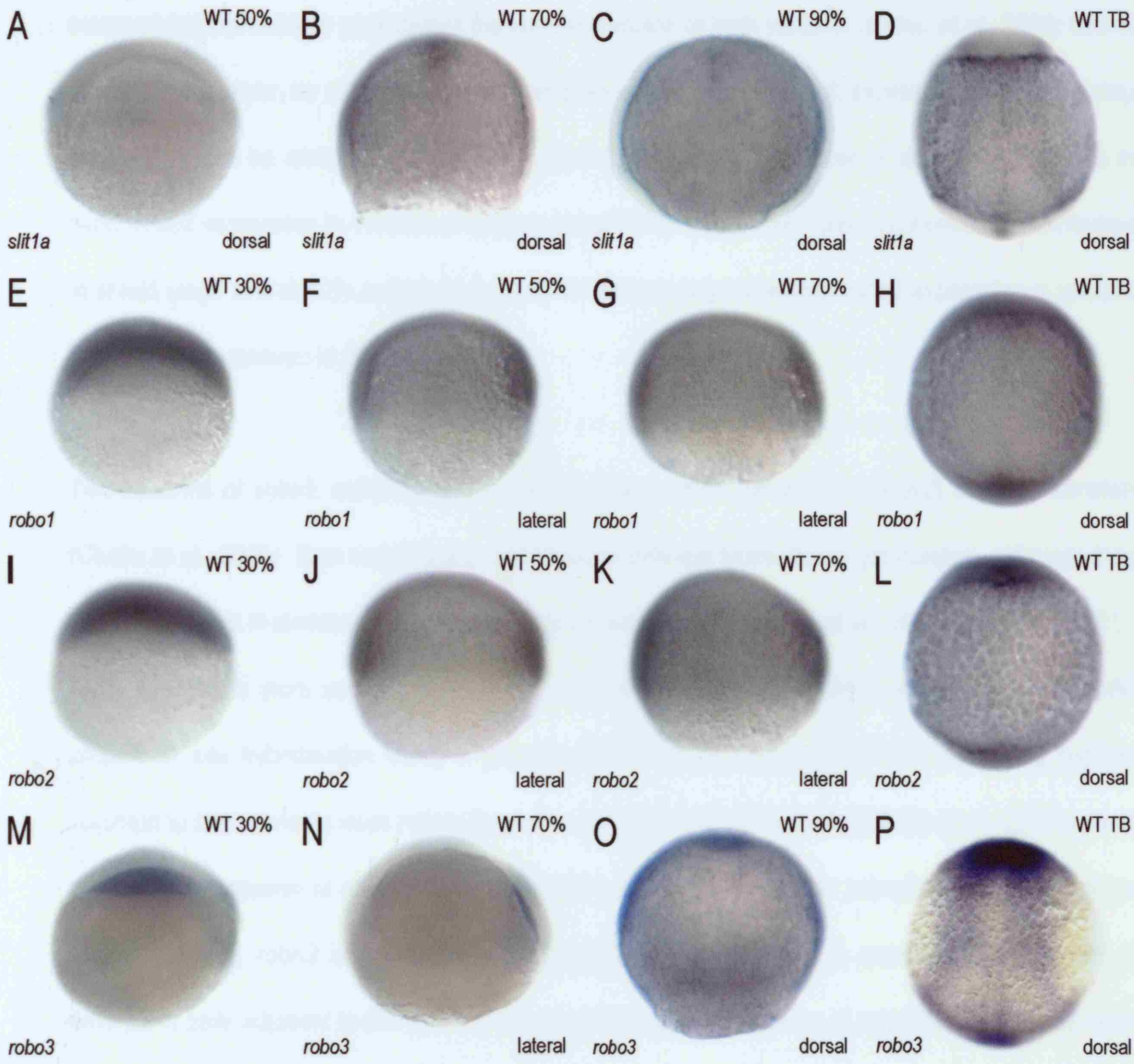

Figure 4.1

Zebrafish orthologues of *slit* and *robo* are expressed during gastrulation.

Fig. 4.1A-D: expression of *slit1a* in wildtype embryos, beginning at 50% epiboly (A), in the extending dorsal midline at 70% (B) and 90% (C) epiboly, finally becoming restricted to the dorsal midline and lateral border of the neural plate at tailbud stage (D). Fig. 4.1E-H: wildtype expression of *robo1*, ubiquitously expressed at 30% (E), 50% (F), 70% (G) and 100% (H) epiboly. 4.1I-L: wildtype expression of *robo2* (reflecting the *robo2* isoform *robo2_tv1*), ubiquitously expressed at 30% (I), 50% (J), 70% (K) and 100% (L) epiboly. Fig. 4.1M-P: *robo3* expression in wildtype embryos (reflecting the sum of the *robo3* variants *robo3v1* and *robo3v2*) is visible in a subset of cells at 30% epiboly (M) and, persisting in this layer, dorsally at 70% epiboly (N), becoming downregulated in the dorsal midline but remaining diffusely expressed in lateral regions by 90% epiboly (O). Restricting to dorsal anterior mesoderm and neurectoderm, the posterolateral borders of the neural plate and the interface between axial and paraxial mesoderm at tailbud stage (P), *robo3* expression remains absent from the midline at the end of gastrulation.

specific probes, *in situ* hybridisation using a generic probe derived from *robo2* but containing regions common to both variants must reflect the sum expression of both variants (Dalkic *et al.*, 2006; Lee *et al.*, 2001). However, as *robo2_tv2* expression does not begin until 24hpf, expression of *robo2* during gastrulation can be attributed to *robo2/robo2_tv1* (Dalkic *et al.*, 2006; Lee *et al.*, 2001). With this in mind, *robo2* expression is ubiquitous at germ stage (4.1I). Ubiquitous *robo2* expression is maintained at shield stage and at 70% epiboly (4.1J & K). At tailbud stage, low-level *robo2* expression is uniform throughout the embryo (4.1L).

Two isoforms of *robo3*, *robo3 variant 1* (*robo3v1*) and *robo3 variant 2* (*robo3v2*) exist in zebrafish (Challa *et al.*, 2005). Both variants are expressed at different times during gastrulation, although they differ only at the N-terminus and share a large common region (Challa *et al.*, 2005; Lee *et al.*, 2001). While *robo3v2* is more strongly expressed than *robo3v1* during gastrulation, without variant specific probes, *in situ* hybridisation using a generic probe derived from *robo3v1* but containing regions common to both variants must reflect the sum expression of both variants (Challa *et al.*, 2005; Lee *et al.*, 2001). Expression of *robo3* during gastrulation is distinct from other zebrafish *robo* orthologues. At 30% epiboly, *robo3* is not expressed ubiquitously: instead *robo3* is expressed in a subset of embryonic cells adjacent to the yolk (4.1M). At shield stage, expression of *robo3* remains in this layer but becomes restricted to the future dorsal side of the embryo (4.1N). At 90% epiboly, *robo3* is diffusely expressed in lateral regions and at the blastoderm margin, but appears to be absent from the extending dorsal midline (4.1O). At tailbud stage, *robo3* expression becomes restricted to dorsal anterior mesodermal and neurectodermal tissues, the posterolateral border of the neural plate and in two posterior stripes at the interface between paraxial and axial mesoderm, but is conspicuously absent from the dorsal midline (4.1P). This expression is dissimilar to other zebrafish *robo*

orthologues, but the transition from dorsal midline expression during late gastrulation to a complete absence from the dorsal midline at 100% epiboly bears similarity to the dynamic expression of *pk1a* at this time (Carreira-Barbosa *et al.*, 2003).

In addition to this, I examined the expression of *slit1a*, *slit2*, *slit3*, *robo1*, *robo2* (generic probe) and *robo3* (generic probe) in the zebrafish convergent extension mutants *silberblick/wnt11* (*slb*) and *trilobite/stbm* (*tri*) during gastrulation. The expression of zebrafish *slit* and *robo* orthologues is unaltered in *slb* and *tri* except for the mediolateral expansion of their expression domains resulting from impaired convergent extension movements in these mutants (data not shown).

Loss of function of *slit1a* causes convergent extension defects

Loss of function of *slit1a*, using 2ng of *slit1a*-MO, results in reduced convergent extension movements during gastrulation relative to wildtype (Fig. 4.2 & 4,3; Table 9; for probe and morpholino information see Materials & Methods: Tables 1 & 2). *in situ* hybridisation analysis of the mesodermal markers *ntl*, *hgg1* and *papc* and the neurectodermal markers *dlx3*, *rx3*, and *pax2.1* at tailbud stage shows convergent extension movements to be perturbed in both the mesoderm and neurectoderm of *slit1a* morphant embryos. The resulting phenotype is distinct from the convergent extension mutant *silberblick/wnt11* (*slb*) but bears some similarity to *pk1a* morphant embryos at tailbud stage (see Introduction: Figure 1.2H & L; J & N; convergent extension phenotypes defined in Appendix Two).

In the mesoderm, expression of *ntl* in the notochord reveals a weak reduction in the convergence and extension of the axial mesoderm, producing a notochord that is slightly expanded in the mediolateral

axis and slightly shorter in the anteroposterior axis in *slit1a* morphant embryos (Fig. 4.2F) relative to wildtype embryos (4.2E). Similarly, *papc* expression in the paraxial mesoderm shows a weak mediolateral expansion and anteroposterior reduction with a broader axial gap, corresponding to the mediolaterally expanded notochord, in *slit1a* morphant embryos (4.2N; 65% where n=17) relative to the paraxial mesoderm of wildtype embryos (4.2M; 100% where n=25). Further evidence of impaired mesodermal cell movements is revealed by the expression of *hgg1* in the prechordal plate. Anterior migration of the prechordal plate is weakly reduced in *slit1a* morphant embryos (4.2B): in contrast to wildtype embryos (4.2A) where the prechordal plate migrates beyond the anterior border of the neural plate, defective migration in *slit1a* morphant embryos causes the prechordal plate to be situated more posteriorly, one-third of the way across the border of the neural plate, at the end of gastrulation.

Expression of *dlx3* at the border of the neural plate reveals convergent extension in the neurectoderm to be strongly reduced, resulting in a neural plate that is expanded in the mediolateral axis and shortened in the anteroposterior axis (Fig. 4.2B & F) relative to the neural plate of wildtype embryos (4.2A & E). Although the neural markers *rx3* in the prospective eyefield and *pax2.1* in the prospective MHB are expressed normally, their expression domains show weak mediolateral expansion and anteroposterior compression in *slit1a* morphants (4.2J; 65% where n=17) relative to wildtype embryos (4.2I; 100% where n=25). This suggests that while convergent extension movements are perturbed in the neurectoderm, patterning in the brain and eye occurs normally in *slit1a* morphants.

Impaired neural and mesodermal convergent extension movements and impaired anterior migration of the prechordal plate in *slit1a* morphant embryos injected with 2ng *slit1a*-MO result in a consistent shortening of the anteroposterior axis at 24hpf (Figure 4.3B; Table 9) relative to wildtype embryos

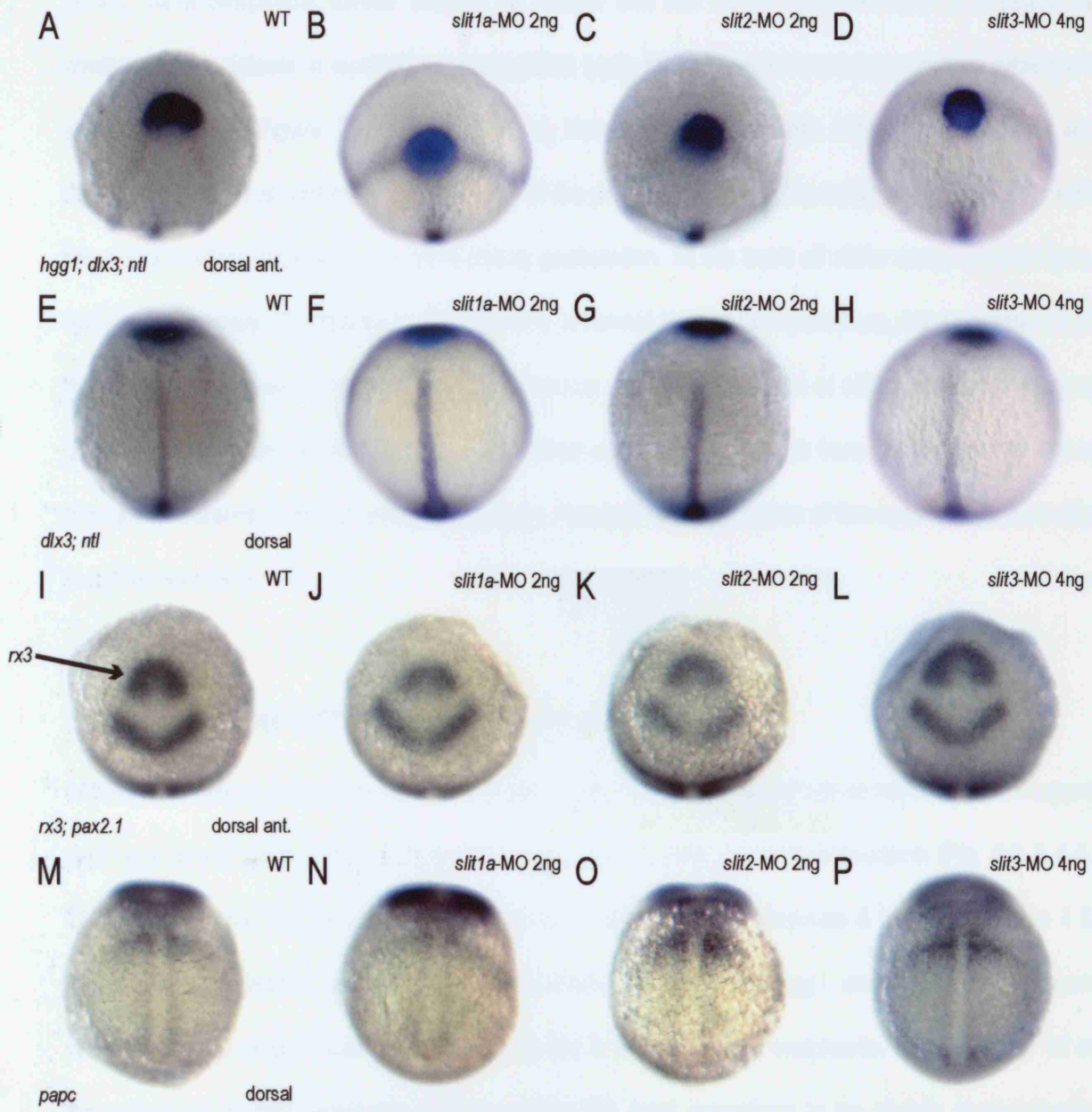

Figure 4.2

Weak convergent extension defects result from *slit1a*, *slit2* and *slit3* loss of function.

Fig. 4.2A-H: convergent extension movements in mesoderm relative to neurectoderm highlighted by *hgg1*, *dlx3* and *ntl* expression in the *slit1a* morphant (B & F), *slit2* morphant (C & G) and *slit3* morphant (D & H) relative to wildtype embryos (A & E). I-L: weak mediolateral expansion of *rx3* and *pax2.1* expression domains in the *slit1a* morphant (J), *slit2* morphant (K) and *slit3* morphant (L) relative to wildtype embryos (I). M-P: weak mediolateral expansion of *papc* expression in *slit1a* morphant (N), *slit2* morphant (O) but not *slit3* morphant embryos (P) relative to wildtype (M).

(4.3A). *slit1a* morphants exhibit variable tail flexion that can occur either ventrally or dorsally. In contrast to the defects in eyefield separation that typify the convergent extension mutant *silberblick* (see Introduction: Figure 1.2B; Appendix Two; Heisenberg *et al.*, 1996; Heisenberg, Tada *et al.*, 2000), the defects of *slit1a* morphants occur in the posterior region of the body axis, correlating with the dorsal midline expression of *slit1a* during gastrulation. In the trunk of *slit1a* morphant embryos, the somites appear structurally normal, bearing a normal horizontal myoseptum, but compressed in the anteroposterior axis relative to wildtype embryos. The yolk extension of *slit1a* morphant embryos is thicker in diameter, shorter in the anteroposterior axis and its extension from the body of the yolk is reduced compared to that of wildtype embryos. However, the separation of the eyes occurs normally in *slit1a* morphants.

Loss of function of *slit2* causes convergent extension defects

In contrast to *slit1a* morphants, loss of function of *slit2* using 2ng *slit2*-MO does not impair convergent extension movements in the neurectoderm to the same extent as in the mesoderm (Fig. 4.2 & 4,3; Table 9; Appendix Two; for probe and morpholino information see Materials & Methods: Tables 1 & 2). *in situ* hybridisation analysis of the mesodermal markers *ntl*, *hgg1* and *papc* reveals weak mesodermal convergent extension defects similar to those of *slit1a* morphants. Expression of *ntl* in the notochord of *slit2* morphant embryos shows the axial mesoderm to be slightly mediolaterally expanded and anteroposteriorly shortened (4.2G), relative to the notochord of wildtype embryos (4.2E), as a result of weakly reduced convergent extension movements. Likewise, expression of *papc* in the paraxial mesoderm shows weak mediolateral expansion and anteroposterior reduction as a result of *slit2* loss of function (4.2O; 78% where n=23) relative to wildtype controls (4.2M; 100%

where n=25), the mediolaterally wider axial channel of *slit2* morphant embryos corresponding with the mediolaterally expanded notochord. Expression of *hgg1* in the prechordal plate shows anterior migration of the prechordal plate to be only weakly perturbed: in contrast with *slit1a* morphants, the anterior migration of the prechordal plate of *slit2* morphants brings this structure almost fully across the anterior border of the neural plate by the completion of gastrulation (4.2C; Table 9), similarly to wildtype (4.2A), suggesting that *slit2* function is more significant in cell movements at the dorsal midline than in the migration of the prechordal plate.

Conversely to *slit1a* morphant embryos, neurectodermal convergent extension occurs relatively normally in *slit2* morphant. Although expression of *dlx3* at the border of the neural plate shows the neural plate to be mediolaterally broader in *slit2* morphant embryos (4.2C & G; Table 9) than in wildtype embryos (4.2A & E), the reduction in convergent extension appears less severe than that caused by loss of function of *slit1a* (4.2B). Both the prospective eyefield marker *rx3* and the prospective MHB marker *pax2.1* are normally expressed, but their expression domains are mildly expanded in the mediolateral axis and compressed in the anteroposterior axis as a result of *slit2* loss of function (4.2K; 78% where n=23) relative to control embryos (4.2I where 100%, n=25), exaggerating the midline gap between the right and left *pax2.1* expression domains. This suggests that impaired convergent extension movements account for the *slit2* morphant phenotype, leaving patterning of the brain and eye unaffected. Again, the visible convergent extension defects resulting from loss of function of *slit2* appear confined to posterior regions of the body axis, correlating with dorsal midline expression of *slit2* during late gastrulation (Yeo *et al.*, 2001). In this way, the *slit2* morphant phenotype is less similar to the *silberblick/wnt11* mutant and more reminiscent of (but

compromising convergent extension movements less severely than) the *pk1a* morphant at the end of gastrulation (see Introduction: Figure 1.2H & L; J & N; Appendix Two).

SLIT MORPHANTS: 24HPF	AMT (ng)	TOTAL	SEVERE CE DEFECT %	MILD CE DEFECT %	WT-LIKE %	DEAD %	MISC. %
WT+*slit1a*-MO	1	85	-	19	81	-	-
WT+*slit1a*-MO	2	41	-	93	-	2	5 non-specific
WT+*slit1a*-MO	4	30	7	93	-	-	-
WT+*slit1a*-SBMO	2	50	-	-	88	4	8 non-specific
WT+*slit1a*-SBMO	4	12	-	92	-	8	-
WT+*slit1b*-MO	2	19	-	63	-	26	11 non-specific
WT+*slit1b*-MO	4	18	-	72	-	28	-
WT+*slit2*-MO	1	13	-	100	-	-	-
WT+*slit2*-MO	2	24	-	-	92	8	-
WT+*slit2*-MO	4	69	65	29	-	-	6 non-specific
WT+*slit3*-MO	4	25	-	-	96	-	4 non-specific
WT+*slit1a*-MO +*slit2*-MO	2 each	51	-	63	-	-	37 eye/somite defects
WT+*slit1a*-MO +*slit3*-MO	*slit1a*: 1 *slit3*: 1	30	-	33	-	40	27 eye/somite defects
WT+*slit2*-MO +*slit3*-MO	2 each	51	-	8	92	-	-
SLIT MORPHANTS: 10HPF (*hgg1, ntl & dlx3*)							
WT+*slit1a*-MO	1	18	-	-	100	-	-
WT+*slit1a*-MO	2	17	-	-	100	-	-
WT+*slit1a*-MO	4	10	-	-	100	-	-
WT+*slit2*-MO	1	18	-	56	44	-	-
WT+*slit2*-MO	2	16	-	75	25	-	-
WT+*slit3*-MO	2	8	-	-	100	-	-
WT+*slit3*-MO	4	15	93	7	-	-	-

Table 9. Loss of function of zebrafish *slit* orthologues.

The primarily mesodermal convergent extension defects caused by loss of function of *slit2* (2ng *slit2*-MO) lead to a consistently anteroposteriorly shortened body axis at 24hpf (Figure 4.3C; Table 9)

relative to wildtype embryos (4.3A). Uniquely amongst *slit* morphants, *slit2*-MO caused a consistent ventrally curling of the body axis reminiscent of *pk1a* morphant embryos (see Introduction: Figure 1.2F) (Carreira-Barbosa *et al.*, 2003). Similarly to *slit1a* morphants, the defects caused by loss of function of *slit2* occur posteriorly on the body axis. In the trunk, the somites of *slit2* morphant embryos appear structurally normal, and exhibiting a normal horizontal myoseptum, but are compressed in the anteroposterior axis relative to wildtype. The yolk extension is abnormally thick in diameter, anteroposteriorly shorter and less well separated from the yolk than in wildtype embryos. Separation of the eyes occurs normally in *slit2* morphant embryos.

Loss of function of *slit3* causes transient convergent extension defects

slit3 loss of function, using 4ng *slit3*-MO, results in impaired convergent extension movements in both mesoderm and neurectoderm and along the entire body axis at the end of gastrulation (Fig. 4.2 & 4,3; Table 9; Appendix Two; for probe and morpholino information see Materials & Methods: Tables 1 & 2). In the mesoderm, expression of *ntl* in the notochord shows *slit3* loss of function to cause weak mediolateral expansion and anteroposterior shortening of the axial mesoderm (4.2H; Table 9) relative to wildtype embryos (4.2E). This weak mediolateral expansion and anteroposterior compression of the axial mesoderm is echoed in a mild mediolateral expansion and anteroposterior shortening of the paraxial mesoderm of *slit3* morphant embryos (4.2P; 100% where n=22) relative to wildtype embryos (4.2M; 100% where n=16) visualised by *papc* expression. Expression of the mesodermal marker *hgg1* reveals that the anterior migration of the prechordal plate is most strongly affected by *slit3* loss of function, correlating with the expression of *slit3* in the prechordal plate during late gastrulation (Yeo *et al.*, 2001). At the end of gastrulation, the prechordal plate of *slit3* morphant embryos has barely

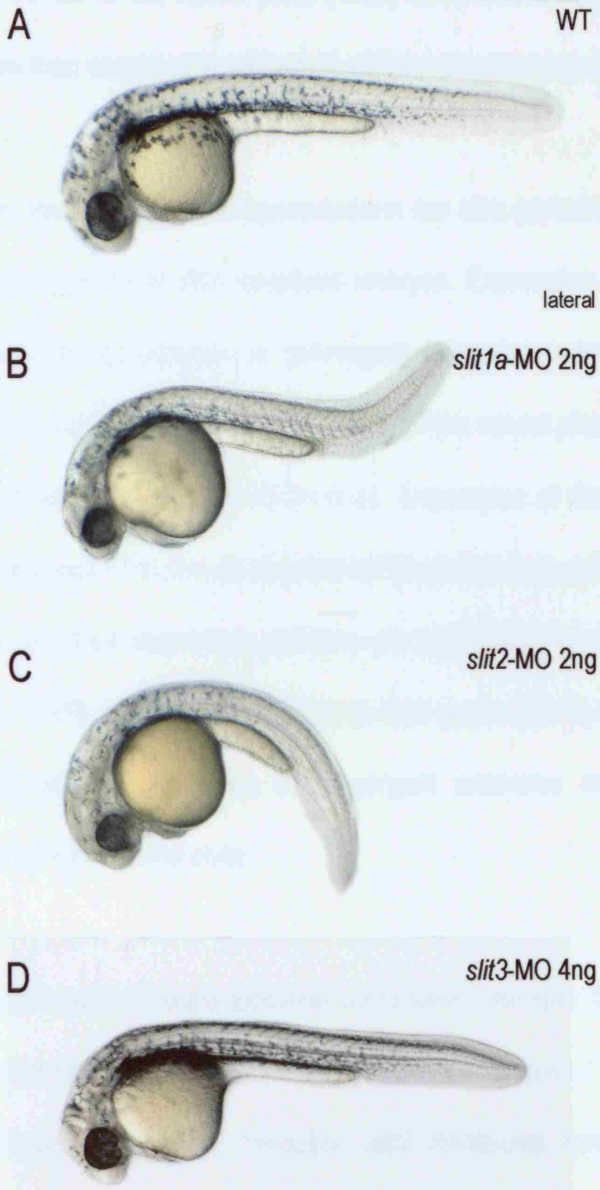

Figure 4.3

Reduced anteroposterior extension of the body axis at 24h caused by loss of function of *slit1a* and *slit2*, but not *slit3*.

Fig. 4.3A: 24h wildtype. Fig. 4.3B-D: the effect on anteroposterior extension of the body axis at 24h of individual *slit* morpholinos injected on a wildtype background. B: *slit1a* morphant. C: *slit2* morphant. D: *slit3* morphant.

crossed the anterior border of the neural plate (4.2D) compared to wildtype (4.2A), a reduction in migration more severe than observed in *slit1a* and *slit2* morphant embryos (4.2B and C respectively).

Convergent extension movements in the neurectoderm are also perturbed to a much greater extent in *slit3* morphants than in *slit1a* or *slit2* morphant embryos. Expression of *dlx3* at the border of the neural plate reveals a strong reduction in convergent extension movements that causes severe mediolateral expansion and anteroposterior shortening of the neural plate in *slit3* morphant embryos (4.2D & H) relative to wildtype embryos (4.2A & E). Expression of the neural markers *rx3* in the prospective eyefield and *pax2.1* in the prospective MHB confirm that patterning is occurring normally in the brain and eye, but their expression domains are mediolaterally expanded as a result of *slit3* loss of function (4.2L; 100% where n=22) relative to their expression in wildtype (4.2I; 100%; where n=16), corresponding with the reduction in convergent extension movements and subsequent mediolateral expansion of the neural plate.

Defects in both mesodermal and neurectodermal convergent extension throughout the body axis are reminiscent of the *silberblick/wnt11* mutant (see Introduction: Figure 1.2H & L; Heisenberg *et al.*, 1996; Heisenberg, Tada *et al.*, 2000). However, *slit3* morphants recover from these apparently transient convergent extension defects and by 24hpf, *slit3* morphant embryos (Figure 4.3D) are almost completely indistinguishable from wildtype embryos (4.3A), a slight reduction in anteroposterior body length the only remaining indication of these early defects.

Combinatorial loss of function of *slits* does not enhance convergent extension defects

I assessed the affect of *slit* loss of function by testing five morpholinos: *slit1a*-MO, *slit1b*-MO, *slit1* splice-blocking MO (*slit1*-SBMO), *slit2*-MO, and *slit3*-MO (Fig. 4.2 & 4,3; Table 9; Appendix Two; for probe and morpholino information see Materials & Methods: Tables 1 & 2). Of these, *slit1a*-MO, *slit2*-MO and *slit3*-MO caused convergent extension defects at 10hpf, of which, the defects caused by *slit1a*-MO and *slit2*-MO persisted until 24hpf, while *slit1b*-MO and *slit1*-splice-blocking-MO had a negligible effect on convergent extension movements at both tailbud stage and at 24hpf (Table 9). As *slit1a*, *slit1b*, *slit2* and *slit3* are all expressed during gastrulation (Hutson *et al.*, 2003; Yeo *et al.*, 2001), the transient mild convergent extension defects of *slit3* morphant embryos and the negligible effect of *slit1b*-MO and *slit1*-SBMO could reflect compensation by functionally redundant *slit* orthologues. I attempted to address this apparent functional redundancy through combinatorial knockdown of *slit* orthologues using the following combinations of morpholinos: *slit1a*-MO plus *slit2*-MO, *slit1a*-MO plus *slit3*-MO and *slit2*-MO plus *slit3*-MO (Table 9). This did not result in convergent extension defects of greater severity than any individual *slit* morpholino, implying that *slits* have distinct functions during zebrafish gastrulation.

Gain of function of *robo2* and *robo3 variant2* does not affect convergent extension

Before answering the question of whether *robo* and *slit* orthologues collaborate in the regulation of convergent extension movements, it was necessary to investigate gain of function of individual zebrafish *robo* orthologues: firstly, to check that receptor gain of function alone has no effect on convergent extension movements prior to co-overexpression with full-length *slit2* mRNA, and secondly, if a phenotype results from overexpression of individual *robo* orthologues, to calibrate

suitable subthreshold doses for co-overexpression. To achieve this, I individually overexpressed full-length *robo2*, *robo3v1* and *robo3v2* mRNAs (Fig. 4.5 & 4.6; Table 10; Appendix Two; see Materials & Methods: in vitro Transcription of mRNA for Micro-Injection, Construct Manufacture & Table 3 for details on full-length *robo* mRNAs).

SLIT & ROBO OVEREXPRESSION 24HPF	AMT.	TOTAL	SEVERE CE DEFECTS %	MILD CE DEFECTS %	WT-LIKE %	DEAD %	MISC. %
WT+*slit2*	100	6	-	-	100	-	-
WT+*slit2*	300	19	53	26	-	11	10 non-specific
WT+*robo2*	200	41	-	10	80	5	5 non-specific
WT+*robo3v1*	200	59	-	2	90	8	-
WT+*robo3v2*	100	85	-	9	79	12	-
WT+*robo3v2*	200	28	-	7	86	7	-
WT+*robo3v2*	300	32	-	-	75	19	6 non-specific
WT+*robo2+slit2*	100 each	30	-	70	-	20	10 non-specific
WT+*robo3v1+slit2*	100 each	38	-	8	63	24	5 non-specific
WT+*robo3v2+slit2*	100 each	58	29	66	-	5	-
SLIT & ROBO OVEREXPRESSION: 10HPF (*hgg1, ntl & dlx3*)							
WT+*slit2*	100	24	-	58	42	-	-
WT+*slit2*	300	27	22	48	30	-	-
WT+*robo2*	200	21	-	29	71	-	-
WT+*robo3v1*	200	22	32	50	18	-	-
WT+*robo3v2*	200	23	-	35	65	-	-
WT+*robo2+slit2*	100 each	23	13	61	26	-	-
WT+*robo3v2+slit2*	100 each	30	40	37	23	-	-

Table 10. Overexpression of zebrafish *slit* and *robo* orthologues.

in situ hybridisation analysis of the mesodermal markers *ntl* and *hgg1* and the neurectodermal marker *dlx3* at tailbud stage showed convergent extension movements to be largely unaffected in 200pg *robo2* overexpressing embryos (Fig. 4.5D & H; Table 10) relative to wildtype (4.5A & E). Consistently, overexpression of 200pg full-length *robo2* mRNA yielded no discernible morphological disturbances at 24hpf (80% where n=41). Likewise, *in situ* hybridisation analysis for the *ntl*, *hgg1* and *dlx3* markers revealed that overexpression of 200pg *robo3v2* mRNA had little effect on convergent extension movements (4.5J & N) relative to wildtype embryos (4.5A & E). Likewise, overexpression of 200pg full-length *robo3v2* mRNA caused no detectable morphological disturbances at 24hpf (86% where n=28; Table 10).

Gain of function of *robo3 variant1* causes transient convergent extension defects

At 24hpf, embryos overexpressing 200pg of full-length *robo3v1* mRNA are indistinguishable from wildtype (90% where n=59). However, *in situ* hybridisation analysis for the markers *ntl*, *hgg1* and *dlx3* at the end of gastrulation reveals transient but severe disturbances to convergent extension movements in 200pg *robo3v1* overexpressing embryos (Fig. 4.5I & M; Table 10) relative to wildtype (4.5A & E). Reminiscent of the *silberblick/wnt11* mutant, embryos overexpressing 200pg of full-length *robo3v1* mRNA display convergent extension defects in both mesoderm and neurectoderm along the entire body axis (see Introduction: Figure 1.2H & L; Appendix Two; Heisenberg *et al.*, 1996; Heisenberg, Tada *et al.*, 2000).

Expression of *ntl* in the notochord shows convergent extension movements to be reduced in the axial mesoderm of *robo3v1* overexpressing embryos, creating a notochord that is expanded in the

mediolateral axis and shortened in the anteroposterior axis (4.5M) compared to wildtype embryos (4.5E), *robo2* overexpressing embryos (4.5H) and *robo3v2* overexpressing embryos (4.5N). Anterior migration of the prechordal plate, highlighted by *hgg1* expression, is severely reduced in *robo3v1* overexpressing embryos in a manner highly reminiscent of *silberblick/wnt11*: in contrast to wildtype embryos (4.5A), the prechordal plate of embryos overexpressing 200pg of *robo3v1* has failed to migrate across the anterior border of the neural plate, and at the end of gastrulation is situated posterior to this landmark (4.5I). Furthermore, expression of *dlx3* at the border of the neural plate reveals strongly reduced neurectodermal convergent extension movements resulting in severe mediolateral expansion and anteroposterior compression of the neural plate in *robo3v1* overexpressing embryos (4.5I & M) relative to wildtype embryos (4.5A & E). This suggests not only that Robo3v1 does not behave like an "authentic" receptor, but also that the two variants of *robo3* are not functionally redundant in the context of the regulation of convergent extension movements during zebrafish gastrulation.

Zebrafish Robo orthologues functionally interact with Slit2 in the context of convergent extension

I tested the hypothesis that zebrafish Robos are capable of acting as receptors for Slit ligands in the context of convergent extension movements (Yeo *et al.*, 2001). Firstly, I calibrated subthreshold doses of the mRNAs to be co-overexpressed. 300pg of full-length *slit2* mRNA is sufficient to reproduce the published, dose-dependent gain of function phenotype: severe convergent extension defects and cyclopia (4.4C & D; Table 10; Appendix Two; Yeo *et al.*, 2001).

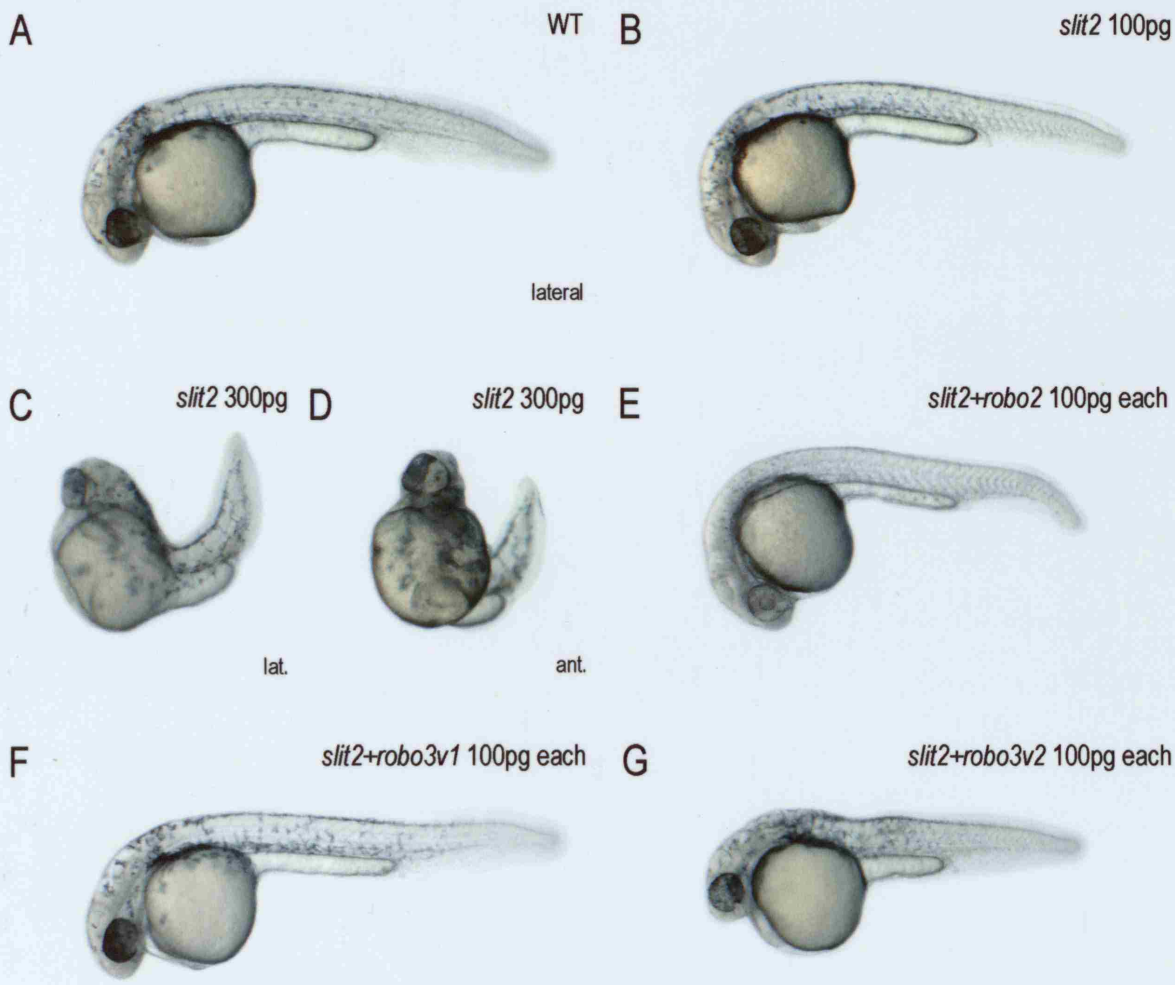

Figure 4.4

Robo2 and Robo3v2, but not Robo3v1, functionally interact with Slit2.

A: wildtype embryo at 24hph; B: *slit2* overexpression, subthreshold for convergent extension defects (100pg); C & D: *slit2* overexpression (300pg) causes severe convergent extension defects (C) and cyclopia (D) as described in Yeo *et al.*, 2001; E-G: co-overexpression of the *slit2* ligand and zebrafish *robo* orthologues. E: co-overexpression of *slit2* and *robo2* (both 100pg); F: co-overexpression of *slit2* and *robo3v1* (both 100pg); G: co-overexpression of *slit2* and *robo3v2* (both 100pg).

in situ hybridisation analysis reveals that overexpression of *slit2* mRNA (300pg) causes severe disturbances to the relative positions of the mesodermal markers *ntl* and *hgg1* and the neurectodermal marker *dlx3* at 10hpf (Fig. 4.5C & G). Prechordal plate migration, highlighted by *hgg1* expression, is severely impaired (4.5C), while mediolateral expansion of the neural plate, marked by *dlx3* expression, and the axial mesoderm, marked by *ntl* expression, reflects severely impaired convergent extension movements (4.5C & G). The severity of these defects is reminiscent of the convergent extension mutant *silberblick/wnt11* (*slb*) (see Introduction: Fig. 1.2H & L; Appendix Two). A 100pg dose of full-length *slit2* mRNA falls does not yield this severe phenotype at 24hpf (4.4B; Table 10) and does not produce severe convergent extension defects at 10hpf (4.5B & F), so is suitable for co-overexpression. As overexpression of 200pg of *robo2* and *robo3v2* full-length mRNAs caused no detectable phenotype and overexpression of 200pg of *robo3v1* yielded only a transient disturbance to convergent extension movements, a 100pg dose of each *robo* was guaranteed to produce no independent disturbances to morphology (data not shown). Any enhancement of convergent extension defects as a result of a functional interaction between ligand and receptor could clearly be distinguished from the mere addition of two unrelated overexpression phenotypes.

Robo2 functionally interacts with Slit2 in the context of convergent extension

Embryos co-overexpressing *robo2* and *slit2* are almost indistinguishable from wildtype at 24hpf. *robo2* and *slit2* co-overexpressing embryos (4.4E) are marginally shorter in the anteroposterior axis than control embryos (4.4A), although the separation of the eyes and yolk extension development occur normally in these embryos. However, *in situ* hybridisation analysis using the mesodermal markers *hgg1* and *ntl* and neurectodermal marker *dlx3* revealed transient but significant convergent

extension defects at tailbud stage (Fig. 4.5; Table 10). *ntl* expression in the notochord looks relatively normal (4.5O) relative to wildtype (4.5E), suggesting that the defects of *robo2* and *slit2* co-overexpressing embryos are confined to more anterior regions of the body axis. The expression of *dlx3* at the border of the neural plate of *robo2* and *slit2* co-overexpressing embryos (4.5K & O) shows the neural plate to be mildly expanded in the mediolateral axis and shorter in the anteroposterior axis relative to wildtype (4.5A & E), *slit2* overexpressing embryos (4.5B & F) or *robo2* overexpressing embryos (4.5D & H). Meanwhile, *hgg1* expression in the prechordal plate shows that the anterior migration of this structure across the border of the neural plate to be compromised, leaving the prechordal plate situated slightly posteriorly relative to the border of the neural plate by the end of gastrulation.

Convergent extension movements are impaired in *robo2* and *slit2* co-overexpressing embryos to a much lesser extent than in *robo3v2* and *slit2* co-overexpressing embryos. However, convergent extension defects are enhanced in these embryos at tailbud stage relative to the individual overexpression of either ligand or receptor. This suggests that *robo2* and *slit2* functionally interact in the context of the regulation of convergent extension movements, and that Robo2 acts as a receptor for Slit2 during zebrafish gastrulation.

Robo3v2 functionally interacts with Slit2 in the context of convergent extension

in situ hybridisation analysis of *robo3v2* and *slit2* co-overexpressing embryos at the end of gastrulation using the mesodermal markers *ntl* and *hgg1* and the neurectodermal marker *dlx3* reveals defects in the convergent extension movements of both mesoderm and neurectoderm (Fig. 4.5;

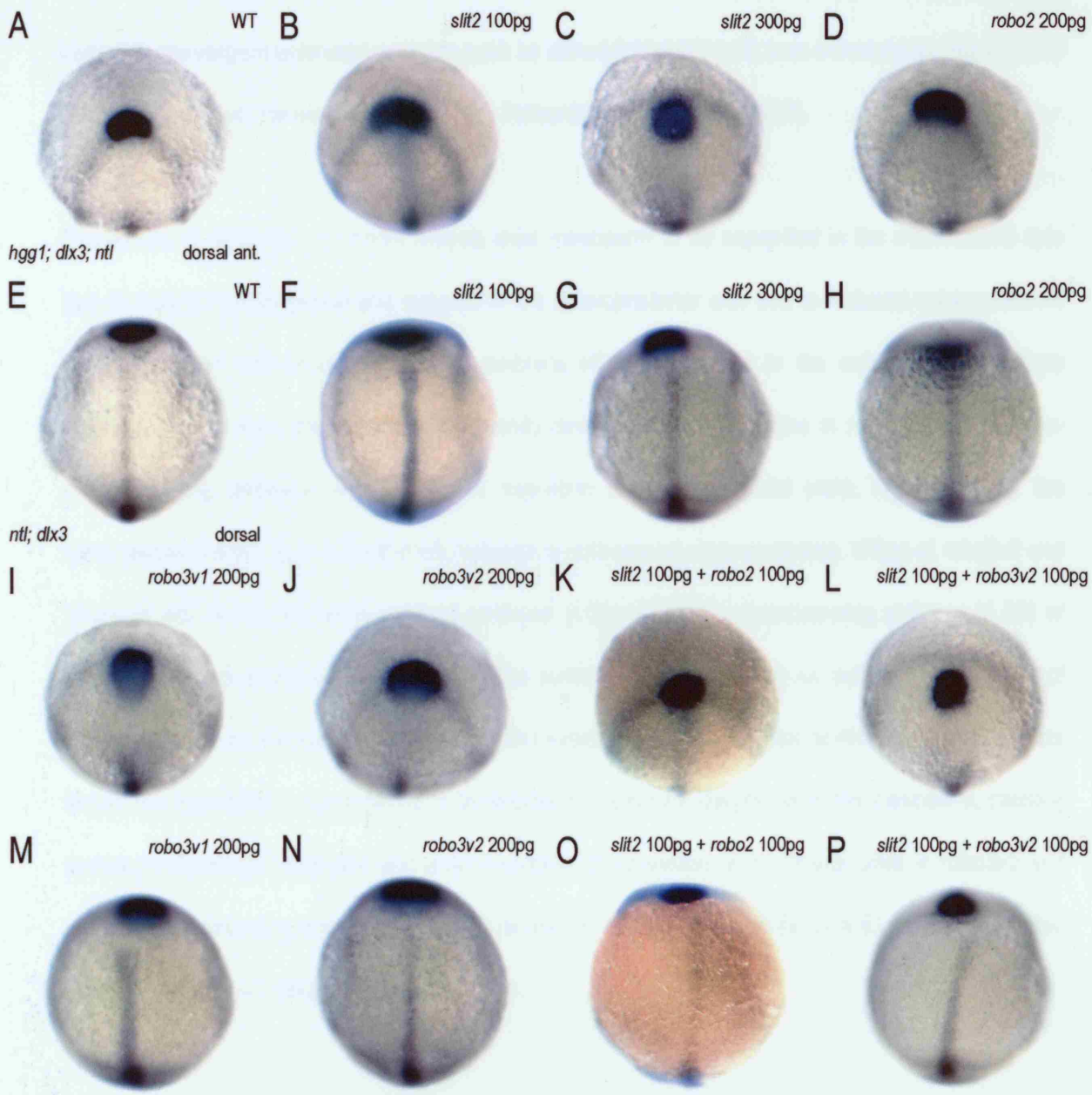

Figure 4.5

Robo2 and Robo3v2, but not Robo3v1, functionally interact with Slit2 in the regulation of convergent extension movements.

A & E: wildtype embryo; B & F: subthreshold dose (100pg) of *slit2* mRNA; C & G: convergent extension defects caused by 300pg *slit2* mRNA; D & H: overexpression of *robo2* (200pg); I & M: convergent extension defects resulting from gain of function of *robo3v1* (200pg); J & N: overexpression of *robo3v2* (200pg); K & O: co-overexpression of *slit2* (100pg) and *robo2* (100pg); co-overexpression of *slit2* (100pg) and *robo3v2* (100pg).

Table 10; Appendix Two). Defective CE in both mesoderm and neurectoderm is reminiscent of zebrafish convergent extension mutants such as *silberblick/wnt11* (*slb*) (see Introduction: Figure 1.2H & L; Appendix Two; Heisenberg *et al.*, 1996; Heisenberg, Tada *et al.*, 2000).

Expression of *ntl* in the notochord reveals axial mesoderm to be expanded in the mediolateral axis due to reduced convergence and reduced in the anteroposterior axis due to reduced axial extension in *robo3v2* and *slit2* co-overexpressing embryos (4.5P) compared to the notochord of wildtype embryos (4.5E). Also, the notochord frequently deviates from the midline in *robo3v2* and *slit2* co-overexpressing embryos (4.5P). Anterior migration of the prechordal plate, highlighted by the mesodermal marker *hgg1*, is extremely reduced in embryos co-overexpressing 100pg of *robo3v2* and 100pg of *slit2* (4.5L) relative to wildtype embryos (4.5A) and *slit2* overexpressing embryos (4.5B) or *robo3v2* overexpressing embryos (4.5J) at the same dosage, remaining far behind of the border of the neural plate by the end of gastrulation. *dlx3* expression at the anterior border of the neural plate shows neurectodermal convergence to be impaired to a similar degree as in the mesoderm, causing severe mediolateral expansion and anteroposterior compression of the neural plate in *robo3v2* and *slit2* co-overexpressing embryos (4.5L & P) relative to wildtype embryos (4.5A & E) or gain of function of *slit2* (4.5B & F) or *robo3v2* (4.5J & N) alone.

Convergent extension movements are severely disrupted throughout the body axis in embryos co-overexpressing 100pg of *robo3v2* and 100pg of *slit2* (Fig. 4.4G; Table 10; Appendix Two) relative to wildtype embryos (4.4A) at 24hpf, suggesting *robo3v2* and *slit2* functionally interact. The body axis of *robo3v2* and *slit2* co-overexpressing embryos is considerably shorter in the anteroposterior axis (4.4G) than wildtype embryos (4.4A) and is frequently kinked or curled. The yolk extension is

malformed, thicker in diameter, shorter in the anteroposterior axis and less well separated from the body of the yolk than in wildtype. A proportion of *robo3v2* and *slit2* co-overexpressing embryos display mild defects in the separation of the eyes, reminiscent of *slit2* overexpression and the convergent extension mutant *slb/wnt11* (see Introduction: Figure 1.2B; Appendix Two) (Heisenberg *et al.*, 1996; Heisenberg, Tada *et al.*, 2000; Yeo *et al.*, 2001). These data provide evidence that *robo3v2* and *slit2* functionally interact during zebrafish gastrulation, and suggest that Robo3v2 is capable of acting as a receptor for the Slit2 ligand in the regulation of convergent extension.

Loss of function *robo2* and *robo3v1* does not affect convergent extension

I examined the effect of loss of function of zebrafish *robo* orthologues on convergent extension movements, both at 10hpf via *in situ* hybridisation for mesodermal, neurectodermal and dorsoventral patterning markers and via observation of gross morphology at 24hpf (Figure 4.6; Table 11; Appendix Two). To do this, I used three morpholinos: *robo2*-MO, *robo3v1*-MO and *robo3v2*-MO (Challa *et al.*, 2005; Hutson & Chien, 2002; see also Materials and Methods: Morpholino Preparation; Table 2). Of the morpholinos tested, *robo2*-MO and *robo3v1*-MO did not affect the anteroposterior extension of the body axis, formation of the yolk extension or bilateralisation of the eyefield at 24hpf, and no other morphological defects were apparent (Table 11; Appendix Two).

Convergent extension movements in *robo2* and *robo3v1* morphants at tailbud, assayed by *in situ* hybridisation for the mesodermal markers *ntl* and *hgg1* and the neurectodermal marker *dlx3*, were indistinguishable from wildtype (Table 11). Expression of *papc* in the paraxial mesoderm was unaltered in *robo2* and *robo3v1* morphants (*robo2*-MO: 100% similar to wildtype, n=14; *robo3v1*-MO:

100% similar to wildtype, n=13). Neither loss of function of *robo2* or loss of function of *robo3v1* had any effect on patterning in the developing brain. The expression patterns of the prospective eyefield marker *rx3* and the prospective MHB marker *pax2.1* were indistinguishable from wildtype in both *robo2* and *robo3v1* morphants (*robo2*-MO: 100% similar to wildtype where n=14; *robo3v1*-MO: 100% similar to wildtype where n=15). Furthermore, dorsoventral patterning was unaffected, assayed by the expression of the dorsal marker *chd* and the ventral marker *bmp2b* during early gastrulation (*robo2*-MO: *chd* expression 100% similar to wildtype where n=16 and *bmp2b* expression 100% similar to wildtype where n=20; *robo3v1*-MO: *chd* expression 100% similar to wildtype where n=12 and *bmp2b* expression 100% similar to wildtype where n=12). These observations are consistent with published data on the loss of function of *robo2* and *robo3v1* (Challa *et al.*, 2005; Fricke *et al.*, 2001).

ROBO MORPHANTS: 24HPF	AMT. (ng)	TOTAL	SEVERE CE DEFECT %	MILD CE DEFECT %	WT-LIKE %	DEAD %	MISC. %
WT+*robo2*-MO	2	11	-	-	91	9	-
WT+*robo2*-MO	4	31	-	-	81	16	3 non-specific
WT+*robo2*-MO	8	39	-	46	-	54	-
WT+*robo3v1*-MO	4	39	-	-	92	3	5 non-specific
WT-*robo3v1*-MO	8	38	-	92	-	8	-
WT+*robo3v2*-MO	4	55	-	96	-	4	-
WT+*robo3v2*-MO	8	42	12	-	-	88	-
WT+*robo3v1*-MO+ *robo3v2*-MO	1 each	60	-	-	100	-	-
ROBO MORPHANTS: 10HPF (*hgg1, ntl & dlx3*)							
WT+*robo2*-MO	4	17	-	-	100	-	-
WT+*robo3v1*-MO	4	15	-	-	100	-	-
WT+*robo3v2*-MO	4	13	-	100	-	-	-

Table 11. Loss of function of zebrafish *robo* orthologues.

Loss of function of *robo3v2* results in severe morphological disturbances

In contrast to loss of function of *robo2* and *robo3v1*, loss of function of *robo3v2* using the variant specific *robo3v2*-MO resulted in severe morphological disturbances at 24hpf (Figure 4.5; Table 11; Appendix Two). *robo3v2* morphant embryos were significantly shorter in the anteroposterior axis (4.6C) relative to wildtype embryos (4.6A). The body axis of *robo3v2* morphants (4.6C) is frequently curled or kinked and the yolk extension, although not thicker in diameter, is malformed compared to wildtype (4.6A). The somites appeared structurally normal with a normal horizontal myoseptum but were compressed in the anteroposterior axis in *robo3v2* morphants (4.6C) relative to wildtype (4.6A). These observations are typical in embryos where convergent extension movements are impaired. However, in combination with defects attributable to disturbed cell movements during gastrulation, *robo3v2* morphants exhibit defects that are less related to convergent extension defects. In the eye of *robo3v2* morphant embryos, the development of the layered structure of the retina is abnormal, visible as an area lacking pigment in the ventral portion of the eye (4.6C & D) relative to wildtype (4.6A & B). The eye also appears smaller in *robo3v2* morphants, and further evidence of patterning defects in the head is visible in the misshapen forebrain.

in situ hybridisation analysis using the neurectodermal marker *dlx3* and the mesodermal markers *ntl*, *hgg1* and *papc* reveals that mild convergent extension defects partially underlie the *robo3v2* morphant phenotype (Figure 4.6E-L). In the mesoderm, expression of *ntl* in axial mesoderm in *robo3v2* morphants (4.6J) is relatively normal compared to wildtype embryos (4.6I). *papc* expression in the pre-somitic mesoderm of *robo3v2* morphants also shows expansion in the mediolateral axis and reduction in the anteroposterior axis with a wider axial gap (4.6L; 69%, n=16) as compared to

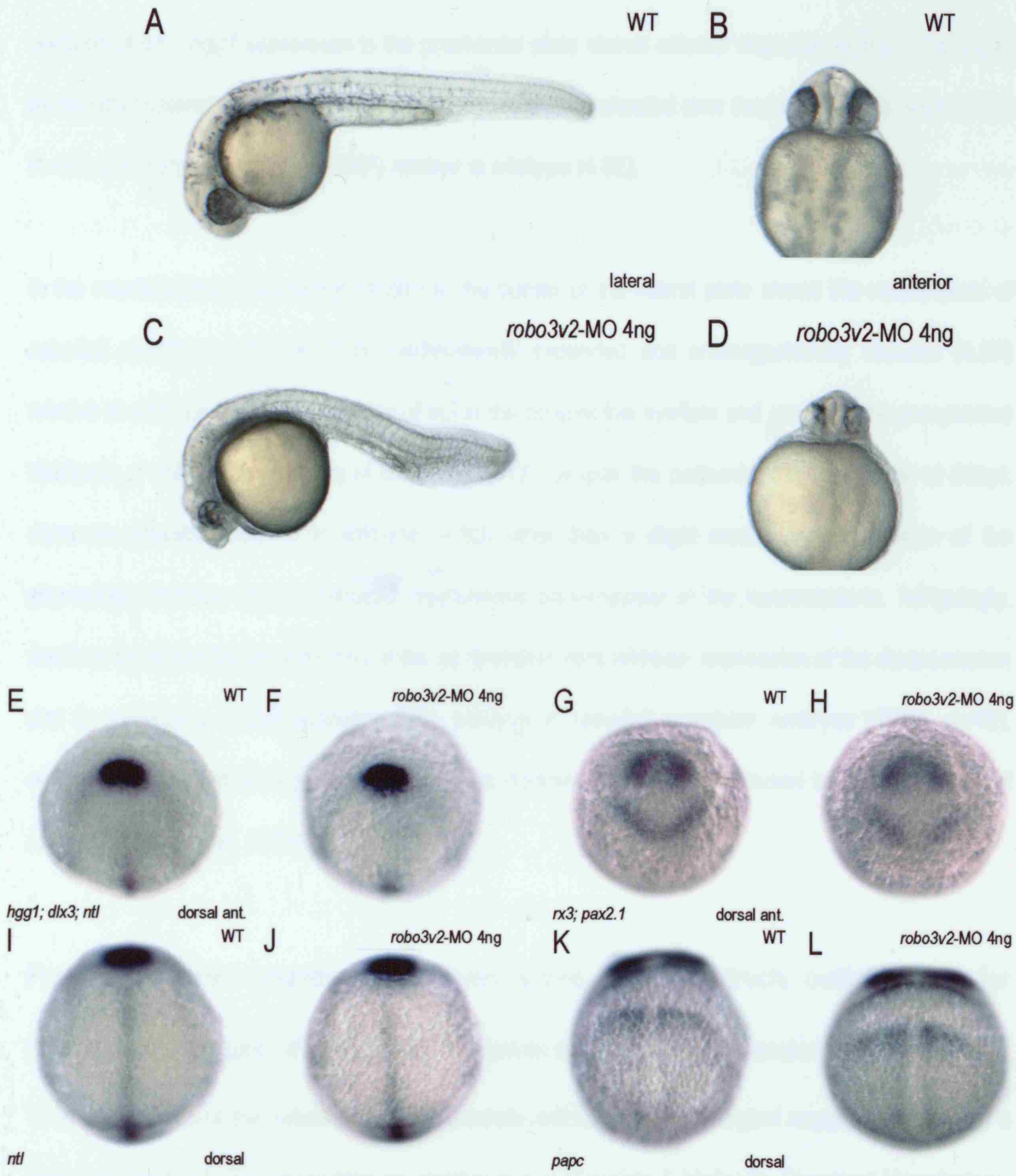

Figure 4.6

Loss of function of *robo3v2* causes mild convergent extension defects.

A: wildtype embryo at 24hpf, lateral view; B: wildtype embryo, anterior view; C: loss of function of *robo3v2* on the wildtype background (4ng *robo3v2*-MO), lateral view; D: loss of function of *robo3v2* (4ng *robo3v2*-MO), anterior view; E-J: *in situ* hybridisation analysis at 10hpf of the convergent extension defects arising from loss of function of r*obo3v2* (4ng *robo3v2*-MO), using the mesodermal markers *hgg1* and *ntl* and the neurectodermal marker *dlx3*. E & I: wildtype embryo; F & J: *robo3v2* morphant embryo (4ng *robo3v2*-MO). *in situ* hybridisation analysis of loss of function of *robo3v2* (4ng *robo3v2*-MO) on the expression of the mesodermal marker *papc* and the neurecto-dermal markers *rx3* and *pax2.1.* G & K: wildtype embryo; H & L: *robo3v2* morphant embryo (4ng *robo3v2*-MO).

wildtype (4.6K). *hgg1* expression in the prechordal plate shows anterior migration of this structure to be slightly impaired, leaving a misshapen prechordal plate situated over the border of the neural plate in *robo3v2* morphant embryos (4.6F) relative to wildtype (4.6E).

In the neurectoderm, expression of *dlx3* at the border of the neural plate shows the neural plate of *robo3v2* morphant embryos to be mediolaterally expanded and anteroposteriorly reduced (4.6F) relative to wildtype (4.6E). Expression of *rx3* in the prospective eyefield and *pax2.1* in the prospective hindbrain of *robo3v2* morphants (4.6H; 85%, n=13), despite the patterning defects visible at 24hpf, show no alteration relative to wildtype (4.6G) other than a slight mediolateral expansion of the expression domains due to reduced mediolateral convergence in the neurectoderm. Intriguingly, markers for dorsoventral patterning show no deviation from wildtype: expression of the dorsal marker *chd* is completely indistinguishable from wildtype in *robo3v2* morphant embryos (100%, n=15), contrary to published findings on disturbances to dorsoventral patterning caused by loss of function of *robo3v2* (Challa *et al.*, 2005).

Putative dominant negative/constitutively active Robo constructs outline a role for zebrafish orthologues of *robo* in the regulation of convergent extension movements.

To learn more about the nature of these structurally and functionally divergent receptors, I designed a series of constructs (for information on constructs see Materials & Methods: Construct Manufacture; Figure 2.2; Table 3; Appendix Two). Using "Lyn" (see Materials & Methods: Construct Manufacture for sequence of Lyn), a membrane localisation sequence derived from Lyn Tyrosine Kinase, I artificially membrane-tethered the intracellular domain (ICD) of Robo2 and the intracellular domain

common to Robo3v1 and Robo3v2 respectively, creating the Lyn-Robo2(ICD)-GFP, Lyn-Robo2(ICD) (unlabelled), Lyn-Robo3(ICD)-GFP and Lyn-Robo3(ICD) (unlabelled) constructs. With these ICD constructs, I aimed to create a situation where these functionally divergent Robo receptors lacking the extracellular domain and are both unable to receive to the secreted Slit signal and unable to change their subcellular localisation. For each, I ascertained that the GFP label does not artefactually enhance the resulting phenotypes (see Table 12).

I adopted a different approach in the creation of another construct Robo3v2(ECD/TM)-GFP. Here, I removed the intracellular domain and isolated and labelled the extracellular and transmembrane domains (ECD/TM) of Robo3v2 to create a truncated Robo3v2 receptor tethered to the external surface of the cell membrane but lacking the intracellular domains necessary for the transduction of the Slit signal. I confirmed that the Lyn-Robo2(ICD)-GFP and Lyn-Robo3(ICD)-GFP proteins are successfully translated via Western Blotting (data not shown; Materials & Methods: Western Blotting).

The Lyn-Robo3(ICD) construct severely impairs convergent extension movements

lyn-robo3(ICD)-GFP mRNA is successfully translated in living embryos and localises to the cell membrane (Figure 4.7A). Overexpression of 100pg of the putative dominant negative *lyn-robo3(ICD)-GFP* construct results in embryos that are severely shortened in the anteroposterior axis at 24hpf (4.7C) relative to wildtype (4.7B). In *lyn-robo3(ICD)-GFP* overexpressing embryos, the body axis is curled and the yolk extension has barely extended away from the body of the yolk (4.7C; Table 12) compared to wildtype controls (4.7B). These aspects of the *lyn-robo3(ICD)-GFP* overexpression phenotype are highly reminiscent of the zebrafish convergent extension mutant *tri/stbm* (Jessen *et*

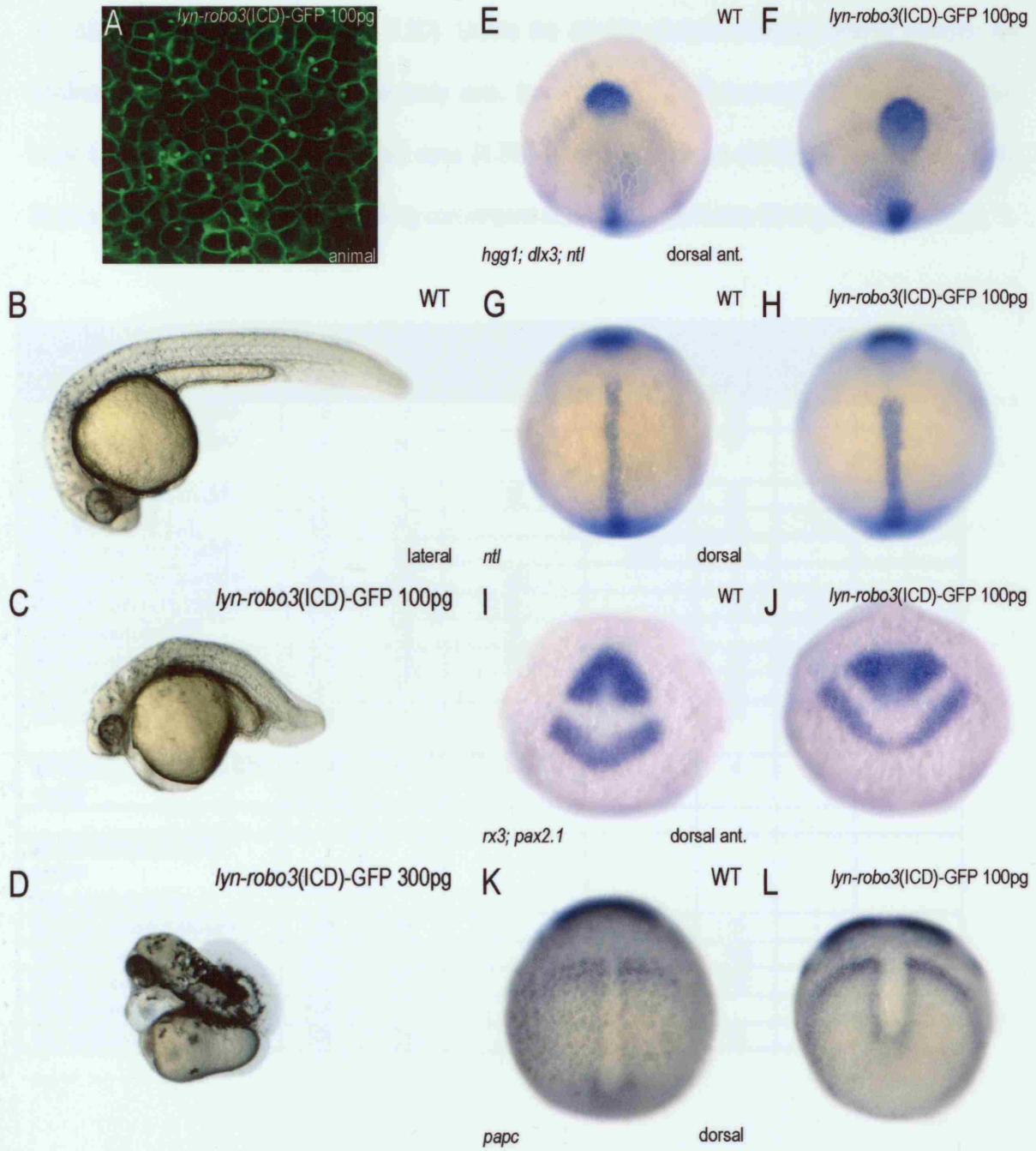

Figure 4.7

Lyn-Robo3(ICD)-GFP causes severe convergent extension defects.

A: localisation of Lyn-Robo3(ICD)-GFP to the cell membrane at 40% epiboly. B-D: the effect of overexpression of *lyn-robo3(ICD)-GFP* mRNA on extension of the body axis at 24hpf. A: wildtype embryo; B: 100pg *lyn-robo3(ICD)-GFP*; C: 300pg *lyn-robo3(ICD)-GFP*; E-H: *in situ* hybridisation analysis at 10hpf of *lyn-robo3(ICD)-GFP* overexpressing embryos using the markers *ntl*, *hgg1* and *dlx3*. E & G: wildtype embryo; F & H: 100pg *lyn-robo3(ICD)-GFP*. I-L: *in situ* hybridisation analysis of *lyn-robo3(ICD)-GFP* overexpressing embryos using the markers *rx3*, *pax2.1* and *papc*. I & K: wildtype embryo; J & L: *lyn-robo3(ICD)-GFP* overexpressing embryo.

al., 2002; see Introduction: Figure 1.2D). Unlike the *trilobite* mutant however, whose defects are confined to posterior regions of the body axis, *lyn-robo3(ICD)-GFP* overexpressing embryos also have smaller and less well separated eyes (4.7B) relative to wildtype (4.7B), suggesting that Lyn-Robo3(ICD)-GFP is capable of affecting convergent extension movements throughout the embryo.

ROBO CONSTRUCTS: 24HPF	AMT. (pg)	TOTAL	SEVERE CE DEFECTS %	MILD CE DEFECTS %	WT-LIKE %	DEAD %	MISC. %
WT+*lyn-robo2(ICD)-GFP*	100	77	-	19	78	3	-
WT+*lyn-robo2(ICD)-GFP*	200	39	-	8	87	-	5 non-specific
WT+*lyn-robo2(ICD)-GFP*	300	65	32	-	65	3	-
WT+*lyn-robo2(ICD)*	200	30	-	33	60	6	
WT+*lyn-robo3(ICD)-GFP*	50	30	-	100	-	-	-
WT+*lyn-robo3(ICD)-GFP*	100	145	100	-	-	-	-
WT+*lyn-robo3(ICD)-GFP*	300	58	80	-	10	10	-
WT+*lyn-robo3(ICD)*	100	72	8	88	-	4	-
WT+*lyn-robo3(ICD)*	200	33	42	21	21	16	
WT+*robo3v2(ECD/TM)-GFP*	100	37	-	16	81	3	
WT+*robo3v2(ECD/TM)-GFP*	300	31	-	16	81	-	3 non-specific
WT+*robo3v2(ECD/TM)-GFP* + *slit2*	R: 100 S: 300	69	71	-	4	12	13 non-specific
ROBO CONSTRUCTS: 10HPF (*ntl; hgg1 & dlx3*)							
WT+*lyn-robo2(ICD)-GFP*	100	19	-	5	95	-	-
WT+*lyn-robo2(ICD)-GFP*	200	14	-	-	100	-	-
WT+*lyn-robo2(ICD)-GFP*	300	21	-	-	100	-	-
WT+*lyn-robo3(ICD)-GFP*	100	25	20	80	-	-	-
WT+*robo3v2(ECD/TM)-GFP*	300	25	40	-	60	-	-

Table 12. The effect of Robo constructs on convergent extension.

in situ hybridisation analysis of embryos overexpressing 100pg of *lyn-robo3(ICD)-GFP* mRNA at tailbud stage confirms severe defects in convergent extension movements throughout the body axis

(Figure 4.7E-L; Table 12; Appendix Two). Expression of *ntl* in the notochord shows this structure to be greatly expanded in the mediolateral axis and shorter in the anteroposterior axis (4.7H) relative to wildtype (4.7G), reminiscent of the severe defects of the *silberblick/wnt11* (*slb*) mutant at tailbud stage (see Introduction: Figure 1.2H & L). However, expression of *hgg1* in the prechordal plate relative to expression of *dlx3* at the anterior border of the neural plate shows that while the neural plate is greatly expanded in the mediolateral axis, anterior migration of the prechordal plate is moderately reduced, leaving the prechordal plate across the border of the neural plate (4.7F) relative to wildtype (4.7E). This anterior situation is more typical of the *pk1a* morphant than the *slb* mutant (see Introduction: Figure 1.2J relative to H). Expression of *papc* in the pre-somitic mesoderm is greatly expanded in the mediolateral axis and reduced in the anteroposterior axis in *lyn-robo3(ICD)-GFP* overexpressing embryos (4.7L) relative to wildtype (4.7K), and the axial gap in *papc* expression is mediolaterally wider, mirroring the mediolateral expansion of the notochord (4.7H). While *rx3* expression in the prospective eyefield and *pax2.1* expression are present, indicating no change in the specification of these areas, severely defective convergent extension has widened their expression domains in the mediolateral axis and compressed them in the anteroposterior axis in *lyn-robo3(ICD)-GFP* overexpressing embryos (4.7J) as compared to wildtype (4.7I). Taken together, these findings imply that convergent extension is severely compromised throughout the body axis in both mesodermal and neurectodermal tissues as a result of *lyn-robo3(ICD)-GFP* overexpression.

I injected a higher dose of *lyn-robo3(ICD)-GFP* mRNA (300pg) to assess whether increasing the dose of my putative dominant negative construct would affect patterning as well as convergent extension. I found that a 300pg dose of *lyn-robo3(ICD)-GFP* failed to cause any truncation of posterior structures, but did result in a dose-dependent increase in the severity of convergent

extension defects (4.7D) relative to wildtype (4.7B). Embryos overexpressing 300pg *lyn-robo3(ICD)-GFP* mRNA were reminiscent of the *trilobite/knypek* double mutants, considered the most severe convergent extension mutants (Marlow *et al.*, 1998), severely shortened in the anteroposterior axis and displaying a curled body axis and no distinct separation between the yolk extension from the body of the yolk (4.7D) relative to wildtype embryos (4.7B). Many embryos overexpressing 300pg *lyn-robo3(ICD)-GFP* also exhibit cyclopia.

The Lyn-Robo2(ICD) construct weakly impairs convergent extension movements

The intensity of GFP expression in embryos overexpressing 100pg *lyn-robo2(ICD)-GFP* mRNA is comparable to embryos overexpressing 100pg *lyn-robo3*(ICD)-GFP mRNA (Figure 4.7A). Similarly, *lyn-robo2(ICD)-GFP* is localised to the cell membrane (4.8A). However, at this dose, overexpression of *lyn-robo2(ICD)-GFP* has a negligible effect on the extension of the body axis at 24hpf and creates no visible morphological disturbances (4.8C; Table 12; Appendix Two) relative to wildtype (4.8B).

in situ hybridisation analysis for the expression of mesodermal and neurectodermal markers at tailbud stage in 100pg *lyn-robo2(ICD)-GFP* overexpressing embryos reveals minimal and transient convergent extension defects (Fig. 4.8; Table 12; Appendix Two). Expression of *ntl* in axial mesoderm is indistinguishable from wildtype (4.8G). Expression of *dlx3* at the border of the neural plate shows it to be only marginally expanded in the mediolateral axis in *lyn-robo2(ICD)-GFP* overexpressing embryos (4.8F) relative to wildtype (4.8E). *hgg1* expression in the prechordal plate shows the anterior migration of this structure to be slightly retarded in *lyn-robo2(ICD)-GFP* overexpressing embryos(4.8F) relative to wildtype embryos (4.8E). The prechordal plate is situated

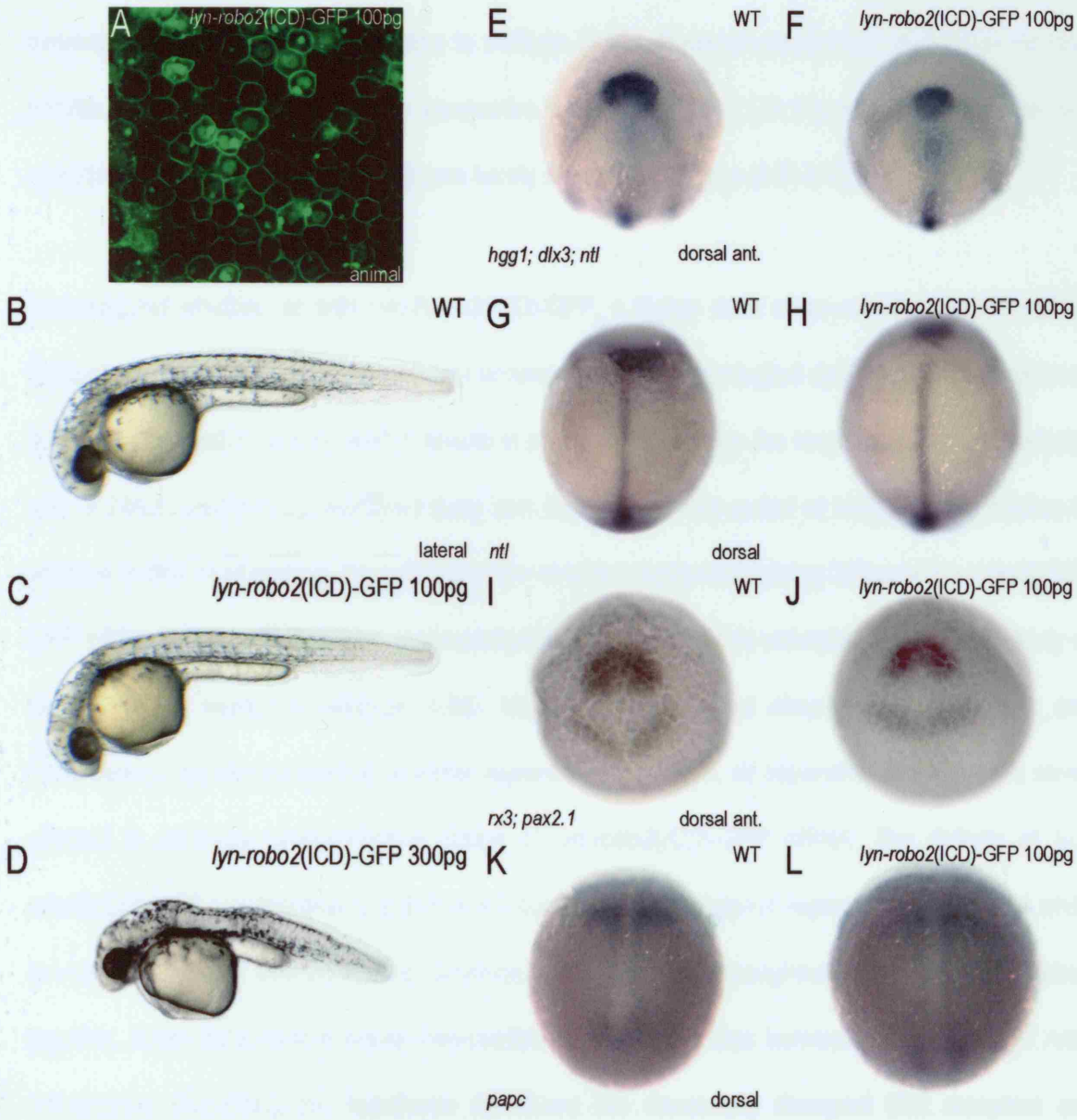

Figure 4.8

Lyn-Robo2(ICD)-GFP weakly impairs convergent extension movements.

A: localisation of Lyn-Robo2(ICD)-GFP to the cell membrane at 40% epiboly. B-D: the effect of overexpression of *lyn-robo2(ICD)-GFP* mRNA on extension of the body axis at 24hpf. A: wildtype embryo; B: 100pg *lyn-robo2(ICD)-GFP*; C: 300pg *lyn-robo2(ICD)-GFP*; E-H: *in situ* hybridisation analysis at 10hpf of embryos overexpressing 100pg of *lyn-robo2(ICD)-GFP* using the markers *ntl*, *hgg1* and *dlx3*. E & G: wildtype embryo; F & H: 100pg *lyn-robo2(ICD)-GFP*. I-L: *in situ* hybridisation analysis of *lyn-robo2(ICD)-GFP* overexpressing embryos using the markers *rx3*, *pax2.1* and *papc*. I & K: wildtype embryo; J & L: *lyn-robo2(ICD)-GFP* overexpressing embryo.

superior to the anterior border of the neural plate and is slightly misshapen in *lyn-robo2(ICD)-GFP* overexpressing embryos (4.8F) relative to wildtype (4.8E). However, expression of *papc* in the pre-somitic mesoderm (4.8L), *rx3* in the prospective eyefield and *pax2.1* in the prospective MHB of *lyn-robo2(ICD)-GFP* overexpressing embryos barely differ from wildtype (4.8I & K).

I investigated whether, as with Lyn-Robo3(ICD)-GFP, a higher dose of *lyn-robo2(ICD)-GFP* mRNA (300pg) was capable of a dose-dependent enhancement of morphological defects. Overexpression of 300pg of *lyn-robo2(ICD)-GFP* mRNA results in a further reduction in the length of the anteroposterior axis at 24hpf, producing a shortened body axis that is frequently curled or kinked (4.8D) relative to wildtype (4.8B). Furthermore, the yolk extension of embryos overexpressing 300pg of *lyn-robo2(ICD)-GFP* mRNA is thicker in diameter, anteroposteriorly reduced and has extended less from the body of the yolk (4.8D) relative to wildtype (4.8B). No other morphological disturbances are evident, and these defects appear confined to posterior regions of the embryo, as separation of the eyes is never affected in embryos overexpressing 300pg of *lyn-robo2(ICD)-GFP* mRNA. The defects of *lyn-robo2(ICD)-GFP* overexpressing embryos are confined to the posterior region of the body axis while *lyn-robo3(ICD)-GFP* overexpressing embryos exhibit defects throughout the body axis. Taken together, these data confirm earlier observations of the differences between the functions of *robo* orthologues, supporting the hypothesis that these two structurally divergent Slit2 receptors are functionally divergent in the context of the regulation of convergent extension movements.

The Robo3v2(ECD/TM)-GFP construct causes severe convergent extension defects

Given the contrast between Robo2 and Robo3v2 function, I anticipated that abrogation of Robo3v2 function using the Robo3v2(ECD/TM)-GFP construct would have severe consequences upon morphogenesis and the resulting phenotype prove informative about the role of Robo3v2 during zebrafish gastrulation. To judge whether the pCS2-Robo3v2(ECD/TM)-GFP construct was correctly manufactured, I injected pCS2-Robo3v2(ECD/TM)-GFP construct DNA into a single cell of 2-cell stage embryos, and by midgastrulation I was able to observe mosaic expression of GFP by UV fluorescence microscopy, suggesting that pCS2-Robo3v2(ECD/TM)-GFP is successfully transcribed and translated *in vivo*. As might be expected of a protein targeted to the cell membrane, pCS2-Robo3v2(ECD/TM)-GFP expression was evident in cytoplasmic vesicles *in vivo* (data not shown).

Overexpression of 100pg of *robo3v2(ECD/TM)-GFP* mRNA results in severe morphological defects at 24hpf (Fig. 4.9B; Appendix Two) relative to wildtype (4.9A). *robo3v2(ECD/TM)-GFP* overexpressing embryos are greatly reduced in the anteroposterior axis and exhibit dorsal curling of the body axis. The somites appear normally patterned, and exhibiting a normal horizontal myoseptum, but compressed in the anteroposterior axis due the reduced body length. The yolk extension is moderately thicker in diameter and shorter in the anteroposterior axis, although remaining distinct from the body of the yolk. Although cyclopia is not evident, the eye of *robo3v2(ECD/TM)-GFP* overexpressing embryos is smaller and irregularly shaped, reminiscently of, but to a lesser extent than, loss of function of *robo3v2*. These defects are reminiscent of *slit2* overexpression (Fig. 4.4C & D) to a greater extent than their resemblance to *lyn-robo3(ICD)-GFP* overexpressing embryos (Fig. 4.7C) or co-overexpression of *slit2* and *robo3v2* (Fig. 4.4G).

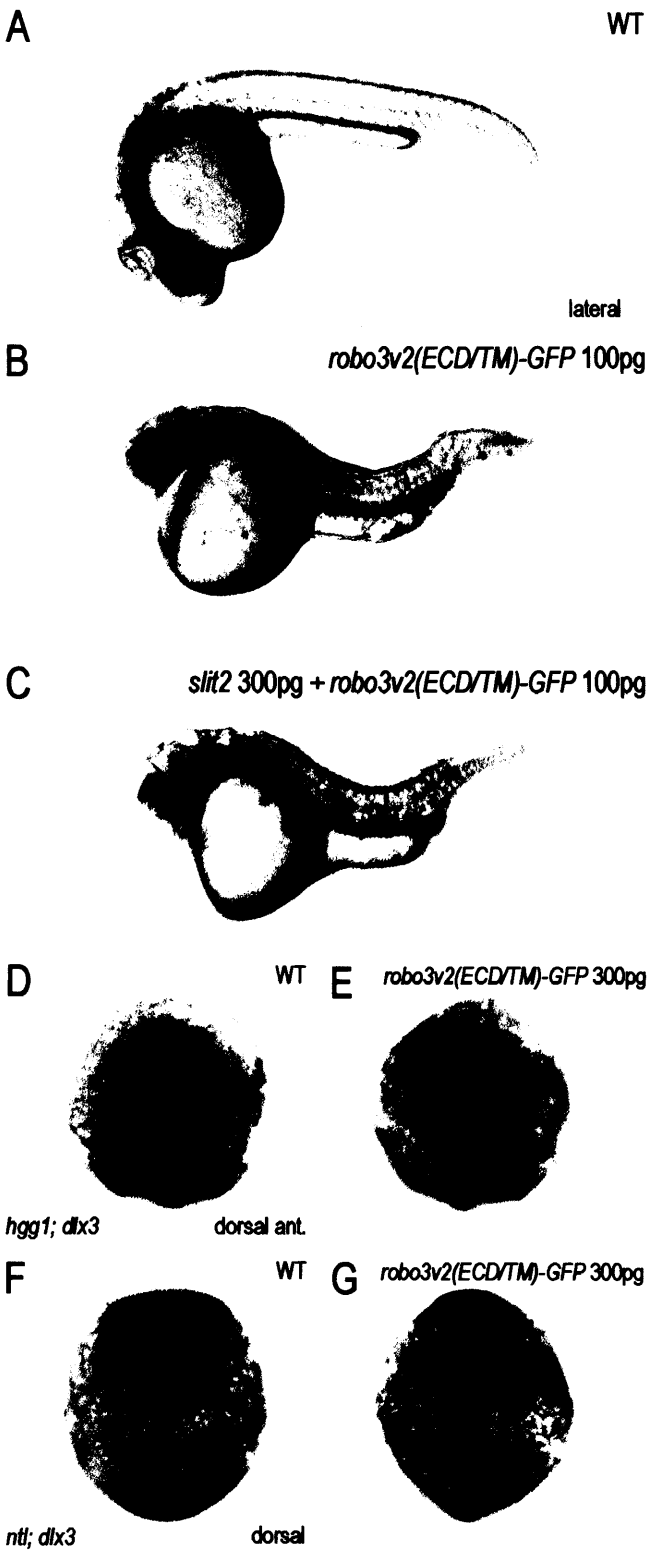

Figure 4.9

Robo3v2(ECD/TM)-GFP causes convergent extension defects and cannot rescue gain of function of *slit2*.

A: wildtype embryo at 24hpf; B: overexpression of 100pg of *robo3v2(ECD/TM)-GFP* causes a severe reduction in the extension of the anteroposterior axis; C: 100pg of *robo3v2(ECD/TM)-GFP* cannot rescue the convergent extension defects and cyclopia caused by gain of function of *slit2* (300pg). D-F: analysis of *robo3v2(ECD/TM)-GFP* (100pg) overexpressing emrbyos at tailbud stage via *in situ* hybridisation for the markers *hgg1*, *ntl* and *dlx3*. D & F: wildtype embryo; E & G; *robo3v2(ECD/TM)-GFP* (100pg) over-expressing embryo.

Overexpression of 300pg of *robo3v2(ECD/TM)-GFP* mRNA resulted in an identically severe phenotype to 100pg of *robo3v2(ECD/TM)-GFP* (Table 12).

At 10hpf, analysis of convergent extension defects resulting from the overexpression of 300pg of *robo3v2(ECD/TM)*-GFP mRNA via *in situ* hybridisation for the markers *hgg1*, *ntl* and *dlx3* shows convergent extension movements in both mesoderm and neurectoderm to be wholly unaffected (Fig. 4.9E & G) compared to wildtype (4.9D & F). The discrepancy between this phenotype and the severe defects evident at 24hpf most likely reflects pleiotropy of Robo3v2 function during embryogenesis.

However, despite only weakly impairing convergent extension movements, the Robo3v2(ECD/TM)-GFP construct clearly demonstrates the significance of the intracellular domain to Robo3v2 function. Furthermore, the striking resemblance between *robo3v2(ECD/TM)-GFP* and *slit2* overexpressing embryos suggests that Robo3v2 functions normally functions in opposition to authentic Robo receptors, potentially in an antagonistic manner. This is of particular interest given the structural similarities between Robo3v2 and the murine *robo* orthologue Rig-1, considered to function analogously to *Drosophila* Commissureless (Comm) in mammalian CNS development (Camurri *et al.*, 2004; Challa *et al.*, 2005; Sabatier *et al.*, 2004).

Robo3v2(ECD/TM)-GFP cannot rescue *slit2* gain of function

If Robo3v2 functions as an authentic receptor during gastrulation, then loss of function of *robo3v2*, disregarding for a moment the probable promiscuity in Slit-Robo interaction, should logically rescue the severe convergent extension defects resulting from gain of function of *slit2*. In this chapter, I have

showed that Robo3v2 expression and function contrasts greatly with that of Robo2, considered to function as an authentic receptor. Gain of function of *robo3v2* produces no detectable morphological defects, but loss of function of *robo3v2*, in contrast with loss of function of *robo2*, results in severe movement and patterning defects that imply that Robo3v2 functions pleiotropically during zebrafish development. Severe morphological defects caused by the Lyn-Robo3(ICD)-GFP construct exclusively affect convergent extension movements without producing the pleiotropic effects exhibited by *robo3v2* morphants, demonstrating that Robo3v2 function and mobility within the cell is critical for the regulation of convergent extension and suggesting that the extracellular domain of the protein mediates the pleiotropic functions of Robo3v2. The slight disturbance to the structure of the eye caused by expression of the Robo3v2(ECD/TM)-GFP construct, despite the ectopic localisation of this artificially secreted construct, supports this theory.

Most significantly, disruption of the intracellular domain-dependent functions of Robo3v2 using the Robo3v2(ECD/TM)-GFP construct causes severe morphological defects highly reminiscent of *slit2* overexpressing embryos. To answer definitively whether Robo3v2 acts as an authentic receptor in the regulation of convergent extension movements, I investigated the ability of 100pg of *robo3v2(ECD/TM)-GFP* mRNA to rescue the severe convergent extension defects caused by overexpression of 300pg of *slit2* mRNA (see Fig. 4.5C & D; Appendix Two). Rather than rescuing *slit2* gain of function, co-overexpression of *robo3v2(ECD/TM)-GFP* and *slit2* caused severe convergent extension defects and cyclopia (4.9C), an enhancement of convergent extension defects relative to *robo3v2(ECD/TM)-GFP* overexpressing embryos (4.9B).

Discussion & Conclusion

Summary

Gain of function of the repellent axon pathfinding ligand *slit2* in zebrafish was shown to cause severe convergent extension defects and cyclopia (Yeo *at al.*, 2001). In this chapter, I showed that, similarly to many known regulators of convergent extension movements, loss of function of *slit* orthologues also causes convergent extension defects. The subtle differences between the convergent extension defects arising from loss of function of *slit1a*, *slit2* and *slit3* suggest that zebrafish *slit* orthologues are not functionally redundant but function discretely in the regulation of convergent extension.

To understand how the Slit ligand is received by cells during gastrulation, I investigated the role of zebrafish orthologues of Roundabout (Robo), the receptor for Slit in commissure formation in the *Drosophila* CNS, in the regulation of convergent extension movements (Kidd *et al.*, 1998; Seeger *et al.*, 1993; Tear *et al.*, 1996). Gain of function of the *robo3* isoform *robo3v1* caused convergent extension defects, suggesting that Robo3v1 does not act as an authentic receptor. Conversely, I demonstrated that the authentic Robo receptor Robo2 and the Robo3 isoform Robo3v2 were capable of functionally interacting with the Slit2 ligand, implying that Robo2 and Robo3v2 act as receptors for Slits in the context of convergent extension movements. However, the phenotype given rise to as a result of the functional interaction between Slit2 and Robo2 contrasts from that of Slit2 and Robo3v2, suggesting that these Robo receptors function distinctly during embryogenesis. This functional distinction is supported by the observation that loss of function of *robo2* produces no detectable morphological defects at 24hpf, while loss of function of *robo3v2* causes both convergent extension defects and patterning defects affecting the development of the brain, eye and somites.

To dissect the discrete functions of Robo2 and Robo3v2 during gastrulation, I designed a series of putatively dominant negative/constitutively active constructs. By artificially membrane-tethering the intracellular domain of Robo2 and the intracellular domain common to both isoforms of Robo3, I aimed to create dominant negative/constitutively active Robo receptors lacking the capability to receive the Slit signal and forced to remain in one subcellular localisation. Overexpression of these constructs highlighted the distinction between the authentic receptor *robo2* and the isoforms of *robo3*: overexpression of the Lyn-Robo3(ICD)-GFP construct caused severe convergent extension defects reminiscent of the zebrafish convergent extension mutant *trilobite/stbm* (*tri*), while in comparison, overexpression of the Lyn-Robo2(ICD)-GFP construct caused mild convergent extension defects. To further explore divergent Robo3v2 function, I designed a second type of construct, the Robo3v2(ECD/TM)-GFP construct, using the extracellular and transmembrane domains unique to Robo3v2 with the aim of creating a dominant negative/constitutively active Robo3v2 receptor, able to bind the Slit ligand but lacking the intracellular domain and unable to transduce the Slit signal. Overexpression of the Robo3v2(ECD/TM)-Venus construct resulted in severe convergent extension defects, highly reminiscent of the overexpression of *slit2* (Yeo *et al.*, 2001). Indeed, the Robo3v2(ECD/TM)-GFP construct was unable to rescue and in fact enhanced the defects resulting from gain of function of *slit2*.

Discussion

The role of the Slit ligand in commissure formation in the *Drosophila* CNS is evolutionarily conserved in vertebrates: Slit ligands act through Robo receptors to repel commissural axons away from the midline after they have crossed, preventing errorial recrossing (Challa *et al.*, 201; Challa *et al.*, 2005;

Dalkic *et al.*, 2006; Brose *et al.*, 1999; Fricke *et al.*, 2001; Hutson & Chien, 2002; Kidd *et al.*, 1998a; Kidd *et al.*, 1998b; Kidd *et al.*, 1999; Lee *et al.*, 2001). Over the course of evolution, the functions of vertebrate Slit and Robo orthologues have also diversified to regulate other instances of directed cell migration. Some instances of Slit/Robo signalling outside the nervous system are analogous to their role in commissure formation: for example, zebrafish Robo4 is known to bind Slit ligands in the regulation of endothelial cell migration in the developing circulatory system (Bedell *et al.*, 2005; Huminiecki *et al.*, 2002; Park *et al.*, 2003). Conversely, some roles of vertebrate Slits relate less clearly to Slit/Robo signalling during commissure formation, such as the ability of Slit2 to stimulate axon branching in mammalian sensory neurons, an attractant role that contrasts sharply with the repellent role of Slit ligands in the developing nervous system (Wang *et al.*, 1999). Whether Slits act through Robo receptors in every instance is a fact yet to be determined.

To determine whether the function of Slit orthologues during gastrulation was mediated by orthologues of the Robo receptor during zebrafish gastrulation, I first undertook a detailed examination of the expression patterns of zebrafish *slits* and *robos*. Both *slit* and *robo* orthologues are expressed during gastrulation, before there are axons to guide. *slit2* overexpression is known to cause severe gastrulation defects in zebrafish (Yeo *et al.*, 2001): the expression of *slit* orthologues during gastrulation relates to their function in the regulation of cell movements at this time. Complementary expression of *robo* orthologues during gastrulation therefore suggests a hitherto unknown role for *robo* receptors in the regulation of cell movements during gastrulation. However, this investigation was hampered by a lack of isoform-specific probes, of particular importance in the case of the *robo3* isoforms *robo3v1* and *robo3v2*. RT PCR analysis demonstrated that both *robo3v1* and *robo3v2* are expressed during gastrulation, although *robo3v1* is most highly expressed during

early gastrulation, while *robo3v2* is most highly expressed during late gastrulation (Challa *et al.*, 2005). A generic *robo3* probe for regions common to both *robo3v1* and *robo3v2* revealed that the sum expression of these isoforms contrasted greatly with the expression of authentic *robo* receptors such as *robo1* and *robo2*. Expressed in the dorsal anterior mesoderm and neurectoderm but conspicuously absent from the dorsal midline, the sum expression of *robo3v1* and *robo3v2* is in some aspects reminiscent of *pk1a* expression at tailbud stage (see Fig. 3.2). This contrast with *robo* orthologues considered to function as authentic receptors is especially significant in light of the fact that, although both Robo3v1 and Robo3v2 localise to the cell membrane *in vivo*, Robo3v2 lacks a canonical signal sequence and is structurally similar to Rig-1 in mice (Challa *et al.*, 2005). The murine *robo* orthologue Rig-1 is believed to function to prevent inappropriate Slit/Robo repulsion of migrating axons in the development of the mammalian CNS (Camurri *et al.*, 2004; Sabatier *et al.*, 2004). This role is analogous to the function of *Drosophila* Commissureless (Comm) in the fly CNS and is intriguing because no homologues of Comm have been identified to date in vertebrates. The distinction between the expression of authentic *robo* receptors and *robo3* isoforms during gastrulation prompts speculation that the *robo3* isoforms are also functionally distinct. Without variant-specific probes, the probable distinctions between *robo3v1* and *robo3v2* during gastrulation will have to be explored using a different approach.

The lack of functional redundancy between zebrafish *slit* orthologues in the regulation of convergent extension is unsurprising given their distinct expression patterns during gastrulation (Hutson *et al.*, 2003; Yeo *et al.*, 2001). After confirmation of both specificity of morpholinos and lack of functional redundancy using a cross-rescue approach, future investigation of the relationship between the distinct expressions and functions of *slit* orthologues during gastrulation, using approaches such as

transplantation and *in vivo* time-lapse imaging, will prove extremely valuable in understanding the role of *slit* orthologues in the control of cell behaviour during gastrulation. As in *Drosophila*, vertebrate Slit ligands undergo post-translational proteolytic cleavage, and it is speculated that this proteolytic cleavage facilitates short- and long-range Slit function, short-range function mediated by the larger N-terminal cleavage product and long-range function mediated by the shorter, highly-diffusible C-terminal fragment (Brose *et al.*, 1999). No evidence exists to suggest that zebrafish *slit* orthologues have short- and long-range functions in the context of the regulation of convergent extension, but is tempting to speculate that expression of *slit* orthologues in the dorsal midline reflects a short-range effect of Slit on cell behaviour, while the effect of loss or gain of function of *slits* on the anterior migration of the prechordal plate represents long-range Slit activity.

It has proved challenging via the approaches used in this thesis to correlate the expression of *slit* orthologues with the phenotypes resulting from their loss of function. For example, *slit2* is expressed in the axial mesoderm and at the anterior border of the neural plate at 10hpf, and *slit2* overexpression causes severe mesodermal convergent extension defects that result in mediolateral expansion of the axial mesoderm and reduced anterior migration of the prechordal mesoderm (Yeo *et al.*, 2001). At 24hpf, *slit2* overexpression causes severe shortening of the anteroposterior axis and cyclopia (Yeo *et al.*, 2001). In this case, expression of *slit2* correlates well with the defects resulting from gain of function of a repellent ligand: reduced midline convergent extension movements cause shortening of the anteroposterior axis at 24hpf, while reduced anterior migration of the prechordal plate prevents inductive interactions between the prechordal plate and overlying neural tissues thought to assist in the separation of the retinae (England *et al.*, 2006; Heisenberg & Nüsslein-Volhard, 1997; Yeo *et al.*, 2001). Loss of function of *slit2* shows no such correlation. Although prechordal migration is not

severely impaired in *slit2* morphants, to be expected if a repellent influence on prechordal plate migration in the form of *slit2* expression at the anterior border of the neural plate migration is no longer present, convergent extension movements in the axial and paraxial mesoderm and to a lesser extent in the neurectoderm are still affected by loss of function of *slit2*. *slit1a* is expressed in the dorsal midline and not in the vicinity of the prechordal mesoderm, and yet loss of function of *slit1a* severely affects prechordal plate migration. *slit3* is expressed in the axial mesoderm and in the prechordal plate, and gain of function of *slit3* causes severe convergent extension defects and cyclopia, similar to gain of function of *slit2* (Yeo *et al.*, 2001), yet at 10hpf, neurectodermal convergent extension is severely compromised. I concluded from this that distinctive disturbances to convergent extension result from both gain of function and loss of function of *slit* orthologues in a manner highly reminiscent of *Drosophila* PCP genes and their vertebrate homologues, and I attempted to compare their defects further in Appendix Two of this thesis. Prior to further dissection of the functional differences between *slit* orthologues, it will be absolutely necessary to ascertain that loss of function is specific to individual orthologues: promiscuity can be eliminated by obtaining orthologue-specific mRNA for rescue of individual *slit* morphant phenotypes.

Divergence in expression and function is also evident in *robo* orthologues and their functional interaction with *slit* orthologues in the context of zebrafish gastrulation, although as with *slit* orthologues, a cross-rescue approach will be necessary in the future as a control for specificity and to explore the degree of functional redundancy between *robo* orthologues in the regulation of gastrulation movements. Gain of function of *robo3v1* resulted in convergent extension defects, suggesting it does not function as an authentic receptor. This is slightly unexpected, as of the two variants of Robo3, Robo3v2 is the most structurally divergent, lacking a canonical signal sequence

(Challa *et al.*, 2005). For this reason, I excluded Robo3v1 from my investigation into the functional interaction between the *slit2* ligand and zebrafish orthologues of the *robo* receptor in the regulation of convergent extension. However, the convergent extension defects resulting from gain of function of *robo3v1* strongly suggest that Robo3v1 is involved, albeit contrastingly relative to other Robo receptors, in the regulation of convergent extension movements and as such, the role of Robo3v1 must be addressed at a later date.

The severe convergent extension defects given rise to by overexpression of *slit2* (Yeo *et al.*, 2001) compared to those resulting from a functional interaction between *slit2* and *robo* orthologues suggests that Slit ligands bind promiscuously to multiple Robo receptors during convergent extension. At 10hpf, the functional interaction between *slit2* and *robo2* impairs neurectodermal convergent extension, but these defects are transient and at 24hpf *slit2* and *robo2* co-overexpressing embryos are indistinguishable from wildtype. Conversely, severe mesodermal, prechordal mesodermal and neurectodermal movement defects result from the functional interaction between *slit2* and *robo3v2*, the effects of which persist beyond 24hpf.

One possible explanation for this difference lies in the structural dissimilarity between authentic receptors such as Robo2 and the atypical Robo3v2 receptor, highly similar to the murine *robo* orthologue Rig-1 (Camurri *et al.*, 2004; Challa *et al.*, 2001; Challa *et al.*, 2005; Lee *et al.*, 2001; Sabatier *et al.*, 2004). The function of Rig-1 in the mouse CNS is thought to be analogous to the role of Comm during CNS development in *Drosophila*, physically sequestering authentic Robo receptors away from the cell membrane to prevent inappropriate Slit/Robo mediated axon repulsion (Sabatier *et al.*, 2004; Tear *et al.*, 1996). If Robo3v2 acts in zebrafish like Rig-1 in the mouse and Comm in the

fly, then it effectively functions to inhibit an inhibitor of cell migration: endogenous Robo3v2 expressed during late gastrulation is free to inhibit authentic Robo receptors, and may function to prevent inappropriate Slit/Robo signalling by repressing both endogenous and exogenous Robo2, compensating in part for the effect of *slit2* and *robo2* co-overexpression on convergent extension movements.

This could also explain the difference between loss of function of *robo2* and loss of function of *robo3v2* (see Appendix Two for further exploration of convergent extension defects). Loss of function of *robo2* only affects Robo2 function, which is probably compensated for by functionally redundancy with other authentic receptors such as Robo1. Potentially, loss of function of *robo3v2* abolishes a number of necessary inhibitory interactions, resulting in a multi-faceted phenotype. By this logic, gain of function of *robo3v2* should be equal to loss of function of everything Robo3v2 normally represses: while there is no evidence listing the full extent of these interactions, gain of function of *robo3v2* is phenotypically similar to loss of function of *robo2* in that neither yield detectable morphological defects. However, this explanation does not account for the genuine functional interaction between *slit2* and *robo3v2*, suggesting that Robo3v2 functions pleiotropically during embryogenesis.

I designed a series of putatively dominant negative/constitutively active Robo constructs to dissect the divergent roles of Robo2 and Robo3v2 during zebrafish gastrulation. Similarly to overexpression of *robo2* and co-overexpression of *slit2* and *robo2*, disruption of *robo2* function using the Lyn-Robo2(ICD)-GFP construct has a minimal impact upon convergent extension movements. In contrast, disruption of Robo3v2 function using the Lyn-Robo3(ICD)-GFP or Robo3v2(ECD/TM)-GFP constructs causes severe and characteristic morphological defects, although the fact that dominant

negative constructs have the potential to affect multiple processes non-specifically and unpredictably in practise must be taken into consideration. The severe defects arising from expression of the Lyn-Robo3(ICD)-GFP construct appear confined to convergent extension, in contrast with the multiple morphological defects arising from *robo3v2* loss of function. This suggests that the intracellular domain is particularly significant to Robo3v2 function during gastrulation and that the ability of Robo3v2 to move freely between intracellular compartments, abrogated in the artificially membrane-anchored Lyn-Robo3(ICD)-GFP protein, is critical to the role of Robo3v2 in the regulation of convergent extension movements.

The severe but distinct morphological defects resulting from expression of the Robo3v2(ECD/TM)-GFP construct affect convergent extension movements but also impinge upon the development of the eye, although much less severely than as a result of loss of function of *robo3v2* (4.6C & D). This expands upon the observation that in the absence of the extracellular domain, as with the Lyn-Robo3(ICD)-GFP construct, only convergent extension movements are affected and not patterning within the brain and eye. The Robo3v2(ECD/TM)-GFP construct demonstrates that the extracellular domain is important both for the regulation of convergent extension movements and the pleiotropic functions of Robo3v2, although further classification of Robo3v2(ECD/TM)-GFP-injected embryos, including analysis of the protein product of the construct via Western Blotting as for the Lyn-Robo(ICD) constructs and comparison with similar constructs manufactured from authentic Robo receptors such as Robo2, will be necessary to fully appreciate these aspects of Robo3v2 function.

If Slit/Robo signalling during zebrafish gastrulation is analogous to Slit/Robo signalling in the vertebrate CNS, then the receipt of Slit ligands by Robo receptors causes a repulsive change in cell

behaviour. Ligand overexpression enhances this repulsion, evident in the effect of *slit2* gain of function on convergent extension movements (Yeo *et al.*, 2001). Logically, overexpression of authentic receptors should cause no morphological defects, as endogenous ligand is theoretically the rate-limiting factor, while loss of function of authentic receptors should lessen the repulsive influence of the pathway on cell migration. The severe movement and patterning defects caused by loss of function of *robo3v2* set it apart from authentic receptors, despite evidence that Robo3v2 can interact with the Slit2 ligand in the regulation of convergent extension movements. The great similarity in the morphological defects of *robo3v2(ECD/TM)-GFP* and *slit2* overexpressing embryos suggests that Robo3v2 does not function identically to Robo2, as loss of function of this authentic receptor would rescue *slit2* gain of function. Moreover, the inability of the Robo3v2(ECD/TM)-GFP construct to rescue the *slit2* overexpression phenotype is confirmation that loss of function of *robo3v2* has the same effect on Slit/Robo signalling as overexpression of *slit2*. This finding is particularly significant in light of the structural similarity between Robo3v2 and the Robo3 homologue Rig-1 in mice, thought to act in the mammalian CNS similarly to Comm in the Drosophila CNS (Camurri *et al.*, 2004; Challa *et al.*, 2005; Sabatier *et al.*, 2004). This suggests that Robo3v2 acts analogously to Rig-1 in mice and Comm in *Drosophila* by antagonising Slit/Robo signalling in the regulation of convergent extension.

Chapter Five

Zebrafish slit and robo orthologues interact with pk1a and pk1b in the regulation of convergent extension movements.

Introduction

Slit/Robo signalling repels commissural neurons away from the midline as one of a number of mechanisms controlling axon migration in the construction of the *Drosophila* CNS scaffold (Kidd *et al.*, 1998a; Kidd *et al.*, 1998b; Seeger *et al.*, 1993; Tear *et al.*, 1996; Rothberg *et al.*, 1988). This role is evolutionarily conserved, as homologues of *Drosophila slit* act as chemorepellent ligands for homologues of the Robo receptor during vertebrate axon guidance (Brose *et al.*, 1999). However in zebrafish, both *slit* and *robo* orthologues begin to be expressed prior to axonogenesis during gastrulation, suggesting a role for Slit/Robo signalling in the regulation of gastrulation cell movements (Challa *et al.*, 2001; Challa *et al.*, 2005; Dalkic *et al.*, 2006; Hutson *et al.*, 2003; Lee *et al.*, 2001; Yeo *et al.*, 2001).

Gain of function of *slit2* was shown to induce severe convergent extension defects and cyclopia in zebrafish (Yeo *et al.*, 2001). In the preceding chapter, I demonstrated not only that loss of function of *slit1a*, *slit2* or *slit3* causes compromises convergent extension movements in both mesoderm and neurectoderm. However, there is no evidence that eyefield separation occurs abnormally in either *slit1a* or *slit2* morphant embryos, indicating that their defects are restricted to posterior regions of the body axis in a manner reminiscent of the convergent extension mutant *trilobite/stbm* (*tri*) or *pk1a*

morphant embryos than the *silberblick/wnt11* (*slb*) mutant (see Introduction: Fig. 1.2B, D & F). Furthermore, I showed that the axon guidance receptors Robo2 and Robo3v2 functionally interact with the Slit2 ligand in the regulation of discrete aspects of convergent extension movements, but that the nature of these interactions is divergent: the strong resemblance between *slit2* overexpression and abrogation of *robo3v2* function using the Robo3v2(ECD/TM)-GFP construct suggested that Robo3v2 opposes authentic Slit/Robo signalling during gastrulation in a manner analogous to the function of Commissureless (Comm) in Slit/Robo signalling in the *Drosophila* CNS (Tear *et al.*, 1996), intriguing as no vertebrate homologue of Comm has been identified to date.

The relationship between the axon pathfinding genes *slit* and *robo* and known regulators of convergent extension movements has yet to be elucidated, and no evidence exists to support a direct collaboration between Slit/Robo signalling and the non-canonical Wnt signalling pathway. However, PCP proteins considered to function in a pathway parallel to the non-canonical Wnt signalling such as Strabismus (Stbm), Prickle1a (Pk1a) or Flamingo2 (Fmi2/Celsr2) are known to regulate convergent extension movements and instances of cell migration outside the context of gastrulation (Carreira-Barbosa *et al.*, 2003; Wada *et al.*, 2006). Both convergent extension movements and the migration of hindbrain facial (nVII) branchiomotor neurons are impaired in *trilobite/stbm* (*tri*) mutant embryos and *pk1a* morphant embryos (Bingham *et al.*, 2002; Carreira-Barbosa *et al.*, 2003; Jessen *et al.*, 2002). Moreover, loss of function of *pk1a* on the *tri* mutant background greatly enhances these cell migration defects, suggesting that *stbm* and *pk1a* function in the same pathway: however, while *stbm* and *pk1a* are believed to modulate the non-canonical Wnt signalling pathway in the context of gastrulation movements, their role in the regulation of branchiomotor neuron migration is thought to be Wnt-independent (Carreira-Barbosa *et al.*, 2003). The tangential migration of facial (nVII) branchiomotor

neurons in the hindbrain is unaffected in the zebrafish convergent extension mutants *silberblick/wnt11* (*slb*) and *pipetail/wnt5b* (*ppt*), and loss of function of Dsh using the dominant negative construct *Xdd1* has no effect on branchiomotor neuron migration (Bingham *et al.*, 2002; Jessen *et al.*, 2002). However, recent evidence of an interaction between Frizzled3a (Fz3a) and Flamingo2/Celsr2 (Fmi2) in the regulation of branchiomotor neuron migration suggests that, rather than Wnt-independent, the control of axon pathfinding by vertebrate PCP proteins might be regulated by a pathway that diverges from Wnt/Fz signalling downstream of Wnt/Fz (Wada *et al.*, 2006).

At the end of gastrulation, expression of *pk1a* in the anterior neurectoderm and pre-somitic mesoderm and *pk1b* in the axial mesoderm is adjacent to the expression of *slit* orthologues in the dorsal midline, while the *robo* orthologues *robo1* and *robo2* are expressed ubiquitously (Fig. 3.2 & 4.1; Challa *et al.*, 2001; Challa *et al.*, 2005; Dalkic *et al.*, 2006; Hutson *et al.*, 2003; Lee *et al.*, 2001; Yeo *et al.*, 2001). The sum of expression of both *robo3* variants using a generic probe for *robo3* (reflecting *robo3v2* expression by majority, as this variant is most highly expressed at this time) highlighted a particular similarity between *pk1a* expression and *robo3* expression, both notably absent from the dorsal midline at tailbud stage (Fig. 3.2 & 4.1). In this chapter, I demonstrate that zebrafish orthologues of *slit* and *robo* collaborate with the *pk* orthologues *pk1a* and *pk1b* in the regulation of discrete aspects of convergent extension movements during zebrafish gastrulation.

Results

Loss of function of *slit* orthologues does not enhance the convergent extension defects of the *silberblick/wnt11* (*slb*) mutant

To assess whether the convergent extension phenotypes resulting from gain of function or loss of function of *slit* orthologues were mediated by the non-canonical Wnt signalling pathway, I examined the effect on convergent extension movements of loss of function of *slit1a* on the *silberblick/wnt11* (*slb*) mutant background. To achieve this, I injected *slit1a*-MO into homozygous *slb* embryos and analysed the effect on extension of the anteroposterior axis at 24hpf (see Materials & Methods: Morpholino Preparation & Table 2; Appendix Two). To ensure any enhancement of the defects of *slb* I observed were as a result of a functional interaction between *slit1a* and the non-canonical Wnt signalling pathway, I calibrated a dose of *slit1a*-MO subthreshold for the creation of convergent extension defects, and found 1ng to be suitable (Fig. 5.1D). Loss of function of *slit1a* on the *slb* mutant background using 1ng of *slit1a*-MO did not cause any detectable enhancement of the convergent extension defects of *slb* at 24hpf (100%, n=31). This suggests that the function of *slit* orthologues such as *slit1a* in the regulation of convergent extension movements during zebrafish gastrulation is mediated through a separate pathway to *wnt11*.

Loss of function of *slit* orthologues does not enhance the convergent extension defects of the *trilobite/stbm* (*tri*) mutant

The characteristically shortened and ventrally curled anteroposterior axis resulting from loss of function of *slit2* is highly reminiscent of convergent extension mutants such as *trilobite/stbm* (*tri*) (see Introduction: Fig. 1.2D; Appendix Two). I examined the effect of loss of function of *slit2* on the

convergent extension movements of the *trilobite* mutant. To achieve this, I injected *slit2*-MO into a mixture of wildtype, *tri+/-* and *tri-/-* embryos derived from heterozygous *tri* carrier incrosses, and analysed the effect on the extension of the anteroposterior axis at 24hpf (see Materials & Methods: Morpholino Preparation & Table 2). Prior to this experiment, I calibrated a dose of *slit2*-MO subthreshold for the creation of convergent extension defects to ensure that any phenotype resulting from the simultaneous loss of function of *slit2* and *stbm* was as a result of a functional interaction, not the addition of two unrelated phenotypes. I found a 1ng dose of *slit2*-MO insufficient to yield convergent extension defects alone (Fig. 5.1E). Loss of function of *slit2* on the *trilobite* background using 1ng of *slit2*-MO did not enhance the convergent extension defects of either heterozygous or homozygous *tri* embryos (100%, n=50). This suggests that *stbm* and *slit* orthologues are not epistatic in the regulation of convergent extension movements.

Simultaneous loss of function of *pk* and *slit* orthologues causes severe convergent extension defects

Given the similarities in the morphological defects that arise as a result of loss of function of *slit2* and *pk1a*, and in spite of the finding that loss of function *slit2* does not enhance the convergent extension defects of *trilobite*, I examined the effect of loss of function of the *pk* orthologues *pk1a* and *pk1b* in combination with loss of function of the *slit* orthologues *slit1a* and *slit2* on convergent extension movements. To do this, I firstly calibrated subthreshold doses of *pk1a*-MO and *pk1b*-MOa, to ensure any enhancement I observed was as a result of a genuine functional interaction between *slit* and *pk* orthologues. I found that a 1ng dose of *pk1a*-MO (Fig. 5.1B) was insufficient to cause the characteristic shortened body axis and curly tail down phenotype of *pk1a* morphants (see

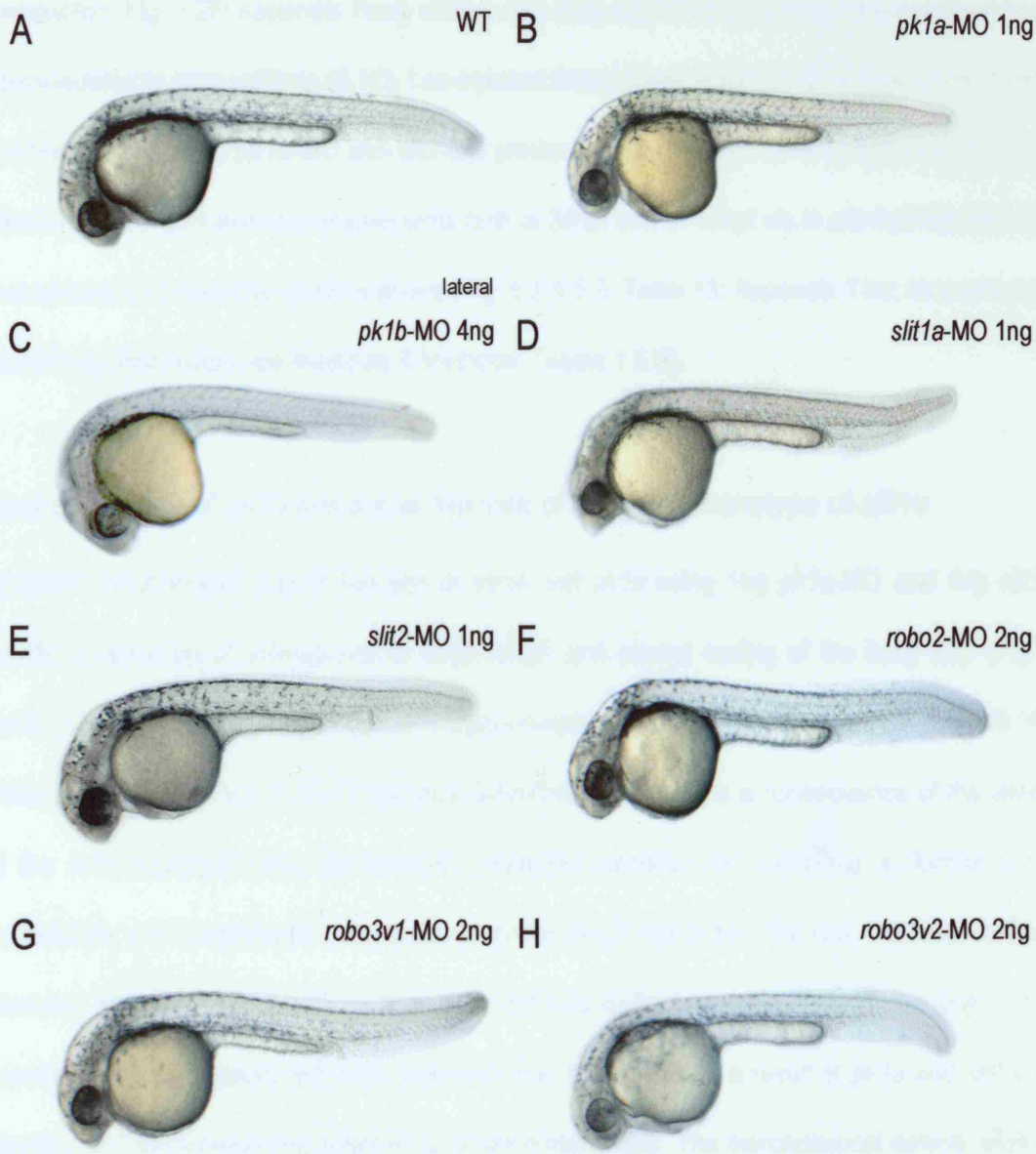

Figure 5.1

Individual *slit*, *robo* and *pk* morpholino dosages subthreshold for convergent extension defects.

A: wildtype embryo at 24hpf. B-H: doses of *slit*, *robo* and *pk* morpholinos insufficient to cause severe convergent extension defects at 24hpf on a wildtype background. B: *pk1a* morphant, 1ng dose *pk1a*-MO. C: *pk1b* morphant, 4ng dose *pk1b*-MOa. D: *slit1a* morphant, 1ng dose of *slit1a*-MO. E: *slit2* morphant, 1ng dose of *slit2*-MO. F: *robo2* morphant, 2ng dose of *robo2*-MO. G: *robo3v1* morphant, 2ng dose of *robo3v1* specific-MO. H: *robo3v2* morphant, 2ng dose of *robo3v2* specific-MO.

Introduction: Fig. 1.2F; Appendix Two), while a 4ng dose of *pk1b*-MOa yielded morphant embryos indistinguishable from wildtype (5.1C). I co-injected these doses of *pk1a*-MO and *pk1b*-MOa with subthreshold doses of *slit1a*-MO and *slit2*-MO previously described (5.1D & E) and analysed the effect on convergent extension movements both at 24hpf and at 10hpf via *in situ* hybridisation for key mesodermal and neurectodermal markers (Fig. 5.2 & 5.3; Table 13; Appendix Two; for probe and morpholino information see Materials & Methods: Tables 1 & 2).

Loss of function of *pk1a* enhances the loss of function phenotype of *slit1a*

At 24hpf, simultaneous loss of function of *slit1a* and *pk1a* using 1ng *pk1a*-MO and 1ng *slit1a*-MO results in reduction of anteroposterior body length and ventral curling of the body axis (Fig. 5.2B; Table 13; Appendix Two) compared to wildtype embryos (5.2A), *pk1a* morphant embryos (5.1B) and *slit1a* morphant embryos (5.1D) at identical subthreshold doses. As a consequence of the shortening of the anteroposterior axis, the normally patterned somites, and exhibiting a normal horizontal myoseptum, are compressed in the anteroposterior axis in the trunk. The yolk extension is thicker in diameter, shorter in the anteroposterior axis and less distinct from the body of the yolk. The eyes appear smaller and positioned more anteriorly than in wildtype as a result of *pk1a* and *slit1a* loss of function, and the surrounding forebrain is an abnormal shape. The morphological defects arising as a result of loss of function of both *slit1a* and *pk1a* are more severe than either *pk1a* or *slit1a* morphants alone, suggesting that *pk1a* and *slit1a* functionally interact.

To confirm that *slit1a* and *pk1a* interact in the regulation of convergent extension movements, I analysed the expression patterns of the mesodermal markers *hgg1* and *ntl* and the neurectodermal

marker *dlx3* in *pk1a:slit1a* double morphant embryos at 10hpf (Fig. 5.3; Table 13). Loss of function of *pk1a* using a subthreshold dose of *pk1a*-MO (1ng) has a minimal effect on convergent extension movements in both mesoderm and neurectoderm (5.3B & E). I showed in Chapter Four that loss of function of *slit1a* using 2ng of *slit1a*-MO mildly perturbed convergent extension movements, while a 1ng dose of *slit1a*-MO produces embryos indistinguishable from wildtype both at 10 and 24hpf (Fig. 4.2 & 4.3; Table 9). Simultaneous loss of function of *pk1a* and *slit1a* using 1ng *pk1a*-MO and 1ng *slit1a*-MO (Fig. 5.3C & F) disturbs convergent extension movements in both neurectoderm and mesoderm to a greater extent than in wildtype (5.3A & D), *pk1a* morphant or *slit1a* morphant embryos at identical subthreshold doses. In the axial mesoderm, expression of *ntl* shows the notochord to be expanded in the mediolateral axis and shorter in the anteroposterior axis (5.3F) relative to the notochord of wildtype (5.3D), *pk1a* morphant embryos (5.3E) and *slit1a* morphant embryos (data not shown) as a result of reduced convergent extension movements.

Expression of *hgg1* in the prechordal plate confirms the defect in mesodermal convergent extension movements arising from loss of function of both *pk1a* and *slit1a*. Strongly reduced anterior migration of the prechordal mesoderm results in the prechordal plate being situated less than halfway across the anterior border of the neural plate (5.3C), whereas the prechordal plate of wildtype embryos has migrated anterior to the border of the neural plate by the end of gastrulation (5.3A). In comparison, the anterior migration of the prechordal plate of *pk1a* morphant embryos is only slightly impaired at this subthreshold dose, leaving the prechordal plate of *pk1a* morphants one-third of the way across the border of the neural plate (5.3B), while prechordal plate migration in *slit1a* morphant embryos is indistinguishable from wildtype at this subthreshold dose (data not shown).

Neurectodermal convergent extension movements are most strongly affected by simultaneous loss of function of *pk1a* and *slit1a*: expression of *dlx3* at the border of the neural plate shows this structure to be greatly expanded in the mediolateral axis and shortened in the anteroposterior axis (5.3C & F) relative to wildtype (5.3A & D), *pk1a* morphant embryos (5.3 B & E) and *slit1a* morphant embryos (data not shown) at this subthreshold dose. These results suggest that *pk1a* and *slit1a* are epistatic in the context of the regulation of convergent extension movements in both the mesoderm and the neurectoderm.

PK:SLIT DOUBLE MORPHANTS: 24HPF	AMT. (ng)	TOTAL	SEVERE CE DEFECT %	MILD CE DEFECT %	WT-LIKE %	DEAD %	MISC. %
WT+*pk1a*-MO +*slit1a*-MO	1 each	99	2	94	4	-	-
WT+*pk1a*-MO +*slit2*-MO	1 each	90	3	92	-	5	-
WT+*pk1b*-MOa +*slit1a*-MO	*pk1b*: 4 *slit1a*: 2	58	88	-	8	2	2 non-specific
WT+*pk1b*-MOa +*slit2*-MO	*pk1b*: 4 *slit2*: 2	58	-	93	7	-	-
PK:SLIT DOUBLE MORPHANTS: 10HPF (*hgg1, ntl & dlx3*)							
WT+*pk1a*-MO +*slit1a*-MO	1 each	56	-	95	5	-	-
WT+*pk1a*-MO +*slit2*-MO	1 each	23	-	96	4	-	-
WT+*pk1b*-MOa +*slit1a*-MO	*pk1b*: 4 *slit1a*: 2	20	-	100	-	-	-
WT+*pk1b*-MOa +*slit2*-MO	*pk1b*: 4 *slit2*: 2	27	-	100	-	-	-

Table 13. Loss of function of *pk* orthologues in combination with *slit* orthologues.

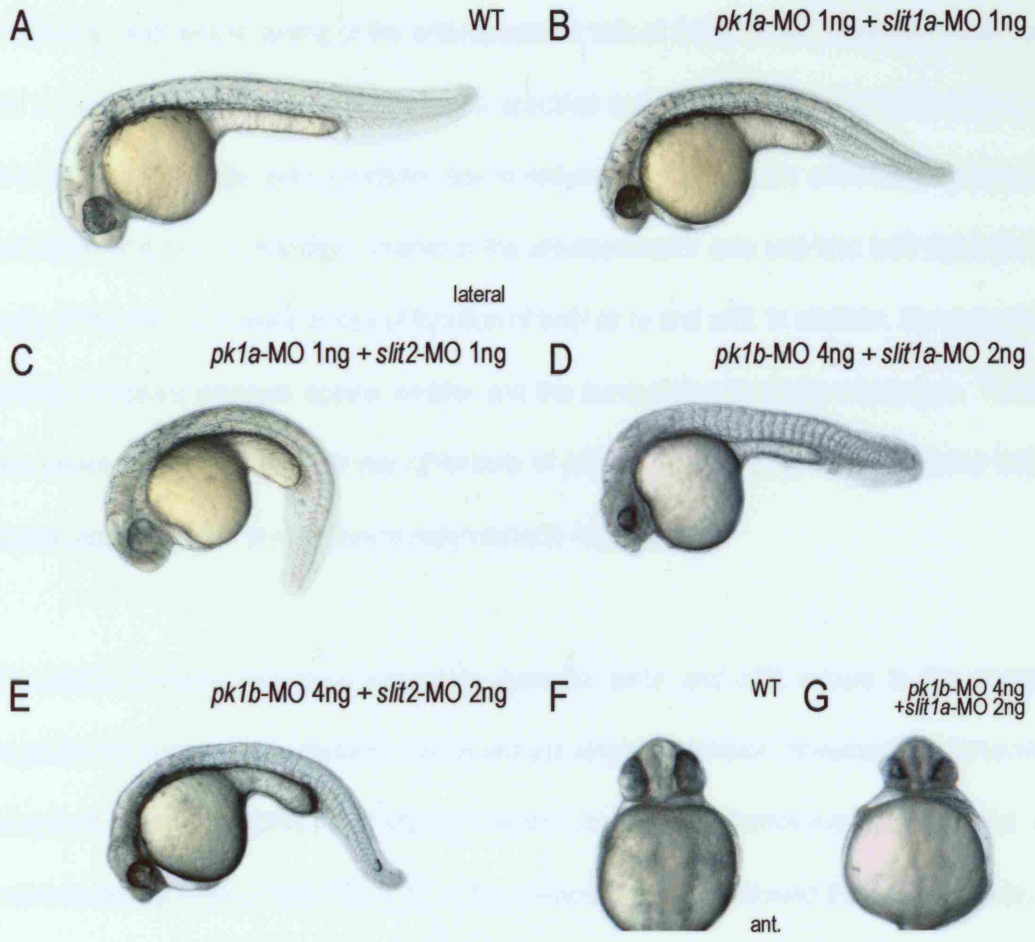

Figure 5.2

***slit* orthologues functionally interact with *prickle* orthologues in zebrafish.**

A: wildtype embryo at 24hpf; B-E: the effect of a genetic interaction between zebrafish *slit* and *pk* orthologues on convergent extension at 24hpf. B: simultaneous loss of function of *pk1a* (1ng *pk1a*-MO) and *slit1a* (1ng *slit1a*-MO); C: simultaneous loss of function of *pk1a* (1ng *pk1a*-MO) and *slit2* (1ng *slit2*-MO); D: simultaneous loss of function of *pk1b* (4ng *pk1b*-MO) and *slit1a* (2ng *slit1a*-MO); E: simultaneous loss of function of *pk1b* (4ng *pk1b*-MO) and *slit2* (2ng *slit2*-MO); G: anterior view of the defects in the development of the eye arising from loss of function of *pk1b* (4ng *pk1b*-MO) and *slit1a* (2ng *slit1a*-MO) relative to wildtype (F).

Loss of function of *pk1a* enhances the loss of function phenotype of *slit2*

Loss of function of both *pk1a* and *slit2*, using 1ng of *pk1a*-MO and 1ng of *slit2*-MO, causes severe shortening and ventral curling of the anteroposterior axis at 24hpf (5.2C; Appendix Two). As a result, the somites in the trunk, appearing normally specified and exhibiting a normal horizontal myoseptum, are compressed in the anteroposterior due to reduced anteroposterior extension. Likewise, the yolk extension is thicker in diameter, shorter in the anteroposterior axis and less well separated from the body of the yolk as a result of loss of function of both *pk1a* and *slit2*. In addition, the eyes of *pk1a:slit2* double morphant embryos appear smaller and the surrounding forebrain misshapen. These defects are severe relative to either the loss of function of *pk1a* (5.1B) or *slit2* (Table 9) at these subthreshold doses, and suggest that *pk1a* functionally interacts with *slit2*.

To confirm that the functional interaction between *pk1a* and *slit2* occurs in the context of the regulation of convergent extension, I analysed convergent extension movements in *pk1a:slit2* double morphant embryos at 10hpf via *in situ* hybridisation for the mesodermal markers *hgg1* and *ntl* and the neurectodermal marker *dlx3* (Fig. 5.3). In the previous section, I showed that loss of function of *pk1a* using 1ng of *pk1a*-MO is insufficient to cause severe convergent extension movements (5.3B & E), while in Chapter Four, I showed that loss of function of *slit2* using 1ng *slit2* has a minimal effect on convergent extension movements at both 10 and 24hpf (Table 9; Appendix Two).

Simultaneous loss of function of *pk1a* and *slit2* causes convergent extension defects in both mesoderm and neurectoderm of greater severity than either loss of function of *pk1a* or *slit2* alone at 10hpf. Expression of *ntl* in the notochord is mediolaterally expanded and anteroposteriorly shortened,

reflecting impaired convergent extension movements in the axial mesoderm of *pk1a:slit2* double morphants (5.3J) as compared to the notochord of wildtype (5.3D), *pk1a* morphant embryos (5.3E) and *slit2* morphant embryos (data not shown). However, expression of *hgg1* in the prechordal mesoderm shows this structure to have migrated across the anterior border of the neural plate to the same degree as *pk1a* morphant embryos (5.3B), suggesting that the collaboration between *slit2* and *pk1a* in the regulation of the anterior migration of the prechordal plate is less significant than *slit1a*. This confirms the findings of the previous chapter, where loss of function of *slit2* using a dose of *slit2*-MO sufficient to cause convergent extension defects in the neurectoderm and axial mesoderm (2ng) did not impair prechordal plate migration to the same degree as *slit1a* or *slit3* loss of function.

Neurectodermal convergent extension movements are perturbed in *pk1a:slit2* double morphants to a similar extent as in *pk1a:slit1a* double morphant embryos. Expression of *dlx3* at the border of the neural plate shows great expansion in the mediolateral axis and reduction in the anteroposterior axis of this structure, reflecting reduced convergent extension movements arising as a result of loss of function of both *pk1a* and *slit2* (5.3G & J). This mediolateral expansion is much more severe than caused by independent loss of function of *pk1a* (5.3B & E) or *slit2* (data not shown). Taken together, these results suggest that *pk1a* and *slit2* are epistatic in the regulation of convergent extension movements in the dorsal midline, but unlike *pk1a* and *slit1a*, *pk1a* and *slit2* do not collaborate in the regulation of the anterior migration of the prechordal plate, contributing significantly to the emerging picture of the discrete functions of zebrafish *slit* orthologues during the regulation of gastrulation movements.

Loss of function of *pk1b* enhances the loss of function phenotype of *slit1a*

I investigated the potential functional interaction between *pk1b* and zebrafish *slit* orthologues, firstly to confirm the contrast in function between *pk1a* and *pk1b*, and secondly, to further dissect the functional differences between *slit1a* and *slit2* during convergent extension. Loss of function of both *pk1b* and *slit1a*, using 4ng of *pk1b*-MOa and 2ng *slit1a*-MO, resulted in severe convergent extension and accompanying patterning defects at 24hpf (Fig. 5.2D & G; Table 13; Appendix Two) relative to wildtype controls (5.2A & F), or either loss of function of *pk1b* (5.1C) or *slit1a* (4.3B) alone. *pk1b:slit1a* double morphant embryos exhibit a severely shortened, curled and kinked anteroposterior axis. Not only are the somites compressed in the anteroposterior axis due to the reduced body length of *pk1b:slit1a* double morphant embryos, but also they appear misshapen, as if somitogenesis has not occurred correctly. While the yolk extension is shorter in the anteroposterior axis than that of wildtype, *pk1b* morphant or *slit2* morphant embryos, it is not significantly thicker in diameter and remains divided from the body of the yolk, in contrast with *pk1a:slit* double morphants and convergent extension mutants such as *trilobite* (see Introduction: Fig. 1.2D; Appendix Two).

The structure of the brain is visibly irregular and opaque due to cell death within, and the forebrain surrounding the eye is severely misshapen. The eye itself provides the greatest evidence of patterning defects separate to convergent extension defects in *pk1b:slit1a* double morphant embryos: not only are the eyes partially fused, but the laminar structure of the eye is disrupted, leading to an absence of pigment in the ventral half of the eye (5.2G) compared to wildtype (5.3F). Disruption of the formation of the eye in this way is reminiscent of loss of function of *robo3v2* (see Fig. 4.6; Appendix Two). Defects in eye development are not typical to *pk1b* or *slit1a* morphant embryos,

suggesting that *pk1b* and *slit1a* are epistatic and strongly interact in both the regulation of convergent extension and other, as yet unidentified developmental processes, critical for the development of the brain, eye and somites.

To examine the component of these defects resulting from impaired convergent extension defects, I analysed the effect of simultaneous loss of function of *pk1b* and *slit1a* on the relative positions of key mesodermal and neurectodermal markers at the end of gastrulation (Fig. 5.3; Table 13; Appendix Two). Surprisingly, given the severe reduction in the anteroposterior axis of *pk1b:slit1a* double morphant embryos at 24hpf, loss of function of *pk1b* and *slit1a* causes only mild perturbation of convergent extension movements. Expression of *ntl* in the undulating axial mesoderm reveals convergent extension in the notochord to be mildly reduced as a result of loss of function of both *pk1b* and *slit1a* (5.3K) compared the expression of *ntl* in the wildtype notochord (5.3D) and in *pk1b* morphant (3.3E) and *slit1a* morphant embryos (4.2F) at these doses. Defective anterior migration of the prechordal plate is not significantly enhanced (5.3H), while in the neurectoderm, mediolateral expansion of the neural plate as marked by the expression of *dlx3* is much less severe than *pk1a:slit* double morphants (5.3H & K).

As the impact upon convergent extension movements is minimal in comparison to *pk1a:slit* double morphants and many zebrafish convergent extension mutants, I must conclude that the strong functional interaction between *pk1b* and *slit1a* primarily affects developmental processes unrelated to the regulation of convergent extension. To investigate whether major patterning events initiated during gastrulation are disrupted as a result of loss of function of both *pk1b* and *slit1a*, I examined the expression of the dorsal marker *chordin* (*chd*) and the ventral marker *bmp2b* at 70% epiboly. Dorsal

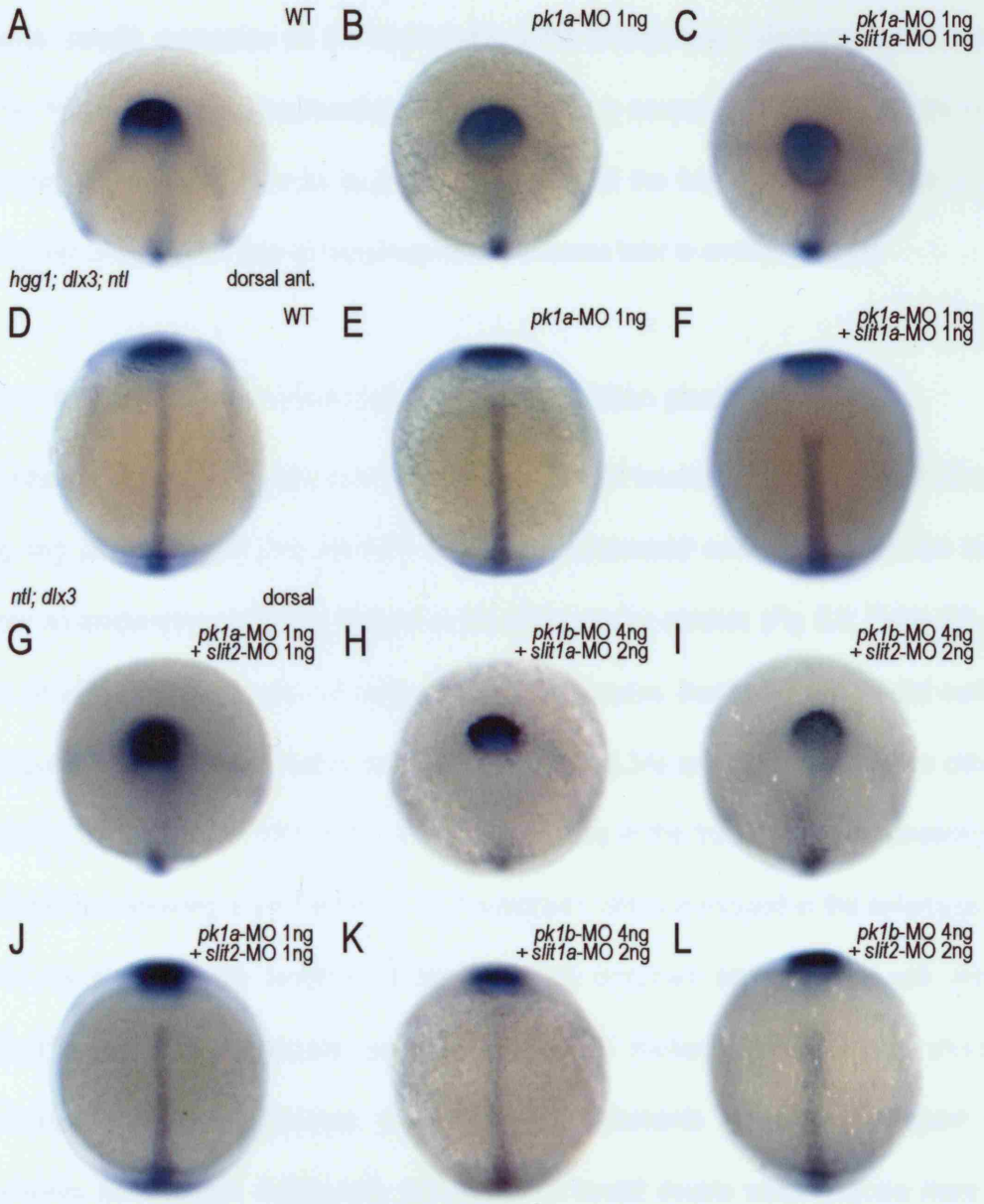

Figure 5.3

slit and _pk_ orthologues functionally interact in the regulation of convergent extension.

in situ hybridisation analysis of convergent extension movements at 10hpf using the mesodermal markers _hgg1_ and _ntl_ and the neurectodermal marker _dlx3_. A & D: wildtype embryo at 10hpf; B & E: minimal effect on convergent extension movements as a result of loss of function of _pk1a_ using a subthreshold dose of _pk1a_-MO (1ng); C & F: simultaneous loss of function of _pk1a_ (1ng _pk1a_-MO) and _slit1a_ (1ng _slit1a_-MO); G & J: simultaneous loss of function of _pk1a_ (1ng _pk1a_-MO) and _slit2_ (1ng _slit2_-MO); H & K: simultaneous loss of function of _pk1b_ (4ng _pk1b_-MOa) and _slit1a_ (2ng _slit1a_-MO); I & L: simultaneous loss of function of _pk1b_ (4ng _pk1b_-MOa) and _slit2_ (2ng _slit2_-MO).

expression of *chd* was unaltered in *pk1b:slit1a* double morphant embryos (100% where n=24). Likewise, *bmp2b* expression on the ventral side of the embryo was indistinguishable from wildtype (100%, n=24). Therefore, dorsoventral axis specification is normal in *pk1b:slit1a* double morphants, suggesting that the disturbances to patterning as a result the interaction between *pk1b* and *slit1a* during gastrulation affect distinct morphogenetic processes later in embryogenesis.

Loss of function of *pk1b* enhances the loss of function phenotype of *slit2*

In contrast to *pk1b:slit1a* double morphant embryos, loss of function of *pk1b* in combination with *slit2* using 4ng *pk1b*-MOa and 2ng *slit2*-MO results in compromised convergent extension movements without accompanying patterning defects in the brain, eye or somites (Fig 5.3; Table 13; Appendix Two). At 24hpf, loss of function of both *pk1b* and *slit2* causes shortening and ventral curling of the anteroposterior axis (5.3E) relative to wildtype embryos (5.3A) and more severe than either loss of function of *pk1b* (5.1C) or *slit2* (4.3C) alone. The somites in the trunk, although appearing normally structured and showing a normal horizontal myoseptum, are compressed in the anteroposterior axis due to the reduced body length of *pk1b:slit2* double morphant embryos. The yolk extension of *pk1a:slit1a* and *pk1a:slit2* double morphant embryos is thicker in diameter and shorter in the anteroposterior axis, characteristic of mutants and morphants in which convergent extension movements are impaired. Additionally, the eyes of *pk1b:slit2* double morphants are more anteriorly positioned and smaller in size than in wildtype or *pk1b* or *slit2* single morphant embryos, but show none of the defects in pigmentation that *pk1b:slit1a* double morphant embryos exhibit. This supports a functional interaction between *pk1b* and *slit2* reminiscent of the interaction between *pk1a* and zebrafish *slit* orthologues but contrasting in nature with that of *pk1b* and *slit1a*.

in situ hybridisation analysis for the markers *hgg1*, *ntl* and *dlx3* show that mild convergent extension defects underlie the *pk1b:slit2* double morphant phenotype (Fig. 5.3; Table 13; Appendix Two). These defects primarily affect convergent extension in the axial mesoderm. Expression of *ntl* in the notochord is mediolaterally expanded as a result of simultaneous loss of function of *pk1b* and *slit2* (5.3L), reflecting a reduction in convergent extension in the axial mesoderm relative to wildtype (5.3D), enhanced relative to loss of function of *pk1b* (3.3B) or *slit2* loss of function (4.2G) alone. Expression of *hgg1* in the prechordal plate shows the anterior migration of this structure to be relatively normal (5.3I), leaving the prechordal plate almost fully over the anterior border of the neural plate by the end of gastrulation compared to wildtype (5.3A). This adds support to the idea that *slit2* function does not contribute to prechordal plate migration during gastrulation movements to the same degree as *slit1a*.

Expression of *dlx3* at the border of the neural plate of *pk1b:slit2* double morphant embryos shows this structure to be mildly expanded in the mediolateral axis and reduced in the anteroposterior axis (5.3I & L), but still enhanced compared to the neural plate of *pk1b* (3.3B & E) and *slit2* (4.2C & G) single morphant embryos. In summary, these results suggest that *pk1b* and *slit2* functionally interact in the regulation of convergent extension movements in a manner contrasting with *pk1b* and *slit1a*.

Simultaneous loss of function of *pk* and *robo* orthologues causes severe convergent extension defects

Epistatis between *slit* and *pk* orthologues provides evidence of a hitherto unknown relationship between Slit/Robo signalling and pathways known to regulate convergent extension movements.

However, simultaneous loss of function of *pk1b* and *slit1a* yielded a complex and severe phenotype, only a small component of which was the result of impaired convergent extension movements. This implies that *slit1a* and *pk1b* function together in other pathways key to the development of the brain, eye and somites. Do the zebrafish *robo* orthologues *robo2* and *robo3v2* regulate the same processes as *pk1a* and *pk1b* in the regulation of convergent extension movements, or like *pk1b* and *slit1a*, are the functional interactions between *pk* and *robo* orthologues critical to multiple morphogenetic processes?

I examined the effect of simultaneous loss of function of *pk* orthologues and either *robo2* or *robo3v2* on movement and patterning, both at 24hpf and during gastrulation via *in situ* hybridisation analysis (Fig. 5.4, 5.5 & 5.6; Table 14; Appendix Two). I excluded loss of function of *robo3v1* from this analysis because in the previous chapter, overexpression of *robo3v1* yielded a transient but strong convergent extension phenotype, suggesting that despite localising to the cell membrane, *robo3v1* does not function as an authentic receptor (Challa *et al.*, 2005). To do this, I firstly calibrated suitable doses of *robo* morpholinos to co-inject that alone would be subthreshold to cause convergent extension defects. Of *robo2*, *robo3v1* and *robo3v2*, only loss of function *robo3v2*-MO using 4ng *robo3v2*-MO causes detectable morphological defects (see Chapter Four: Fig. 4.6; Table 11; Appendix Two). A 2ng dose of each *robo*-MO yielded no discernible effect on convergent extension, both at 24hpf (Fig. 5.1F, G & H) and at 10hpf (data not shown). I combined these subthreshold doses of *robo2*-MO and *robo3v2*-MO with 1ng of *pk1a*-MO or 2ng of *pk1b*-MO, doses of *pk* morpholinos insufficient to cause convergent extension defects (5.1B & C).

Loss of function of *pk1a* enhances the loss of function phenotype of *robo2*

Simultaneous loss of function of *pk1a* and *robo2* using 1ng *pk1a*-MO and 2ng *robo2*-MO acutely impairs the extension of the body axis (Fig. 5.4B) relative to wildtype embryos (5.4A) at 24hpf, in a manner reminiscent of the most severe zebrafish convergent extension mutants, such as *trilobite/stbm* (*tri*) (see Introduction: Fig. 1.2D; Appendix Two). Somites in the trunk, whilst normally patterned and exhibiting a normal horizontal myoseptum, are anteroposteriorly compressed due to the severity of the reduction in the extension of the anteroposterior axis. The eyes appear smaller and more anteriorly positioned in the misshapen forebrain. The yolk extension is thicker in diameter, greatly shortened in the anteroposterior axis, and poorly divided from the body of the yolk. The defects of *pk1a:robo2* double morphant embryos are greatly enhanced relative to loss of function of *pk1a* (5.1B) and loss of function of *robo2* (5.1F) alone, suggesting a functional interaction reminiscent of *pk1a:slit1a*, *pk1a:slit2* and *pk1b:slit2*, but not *pk1b:slit1a*, double morphant embryos.

I analysed *pk1a:robo2* double morphants through *in situ* hybridisation to confirm that *pk1a* and *robo2* interact in the regulation of convergent extension movements. Surprisingly, at 10hpf the relative positions of the expression domains of markers key to convergent extension movements in *pk1a:robo2* double morphant embryos are barely distinguishable from wildtype (Fig. 5.5; Table 14; Appendix Two). In the neurectoderm, expression of *dlx3* at the border of the neural plate of *pk1a:robo2* double morphant embryos (5.5B & E) does not display significant mediolateral expansion relative to wildtype (5.5A & D) or *robo2* morphant embryos (data not shown), while the neural plate of *pk1a* morphant embryos (5.3B & E) is considerably wider in the mediolateral axis despite the subthreshold dose of *pk1a*-MO. Unaltered expression of *rx3* in the prospective eyefield and

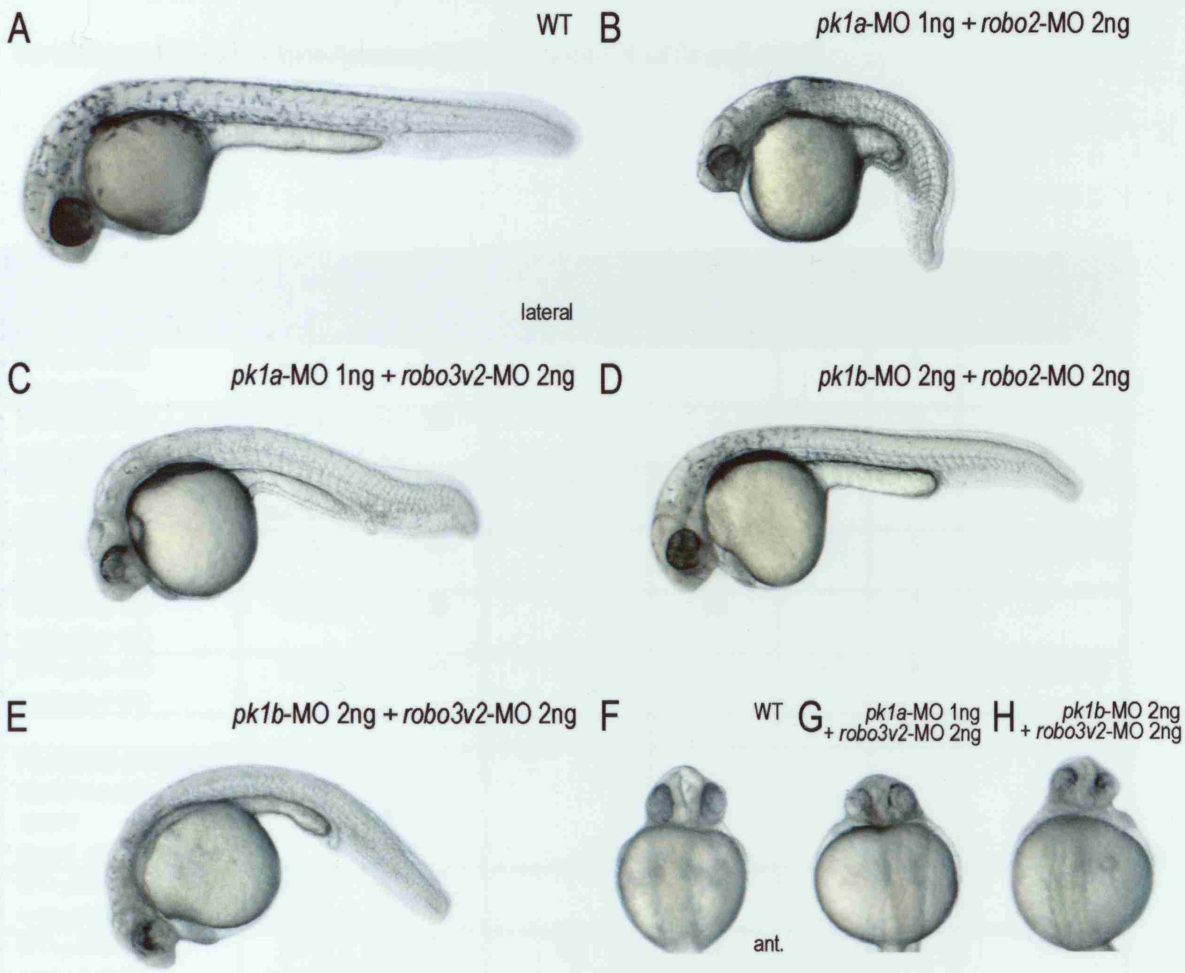

Figure 5.4

The zebrafish *robo* orthologues *robo2* and *robo3v2* functionally interact with *pk1a* and *pk1b*.

A: wildtype embryo at 24hpf. B-E: the genetic interaction between zebrafish *pk* and *robo* orthologues in lateral view at 24hpf. B: simultaneous loss of function of *pk1a* (1ng *pk1a*-MO) and *robo2* (2ng *robo2*-MO); C: loss of function of both *pk1a* (1ng *pk1a*-MO) and *robo3v2* (2ng *robo3v2*-MO); D: simultaneous loss of function of *pk1b* (2ng *pk1b*-MO) and *robo2* (2ng *robo2*-MO); E: loss of function of both *pk1b* (2ng *pk1b*-MO) and *robo3v2* (2ng *robo3v2*-MO). F-H: the effect on eyefield separation and the laminar structure of the eye at 24hpf, anterior view. F: wildtype embryo; G: simultaneous loss of function of *pk1a* (1ng *pk1a*-MO) and *robo3v2* (2ng *robo3v2*-MO); H: loss of function of both *pk1b* (2ng *pk1b*-MO) and *robo3v2* (2ng *robo3v2*-MO).

expression of *pax2.1* in the prospective MHB of *pk1a:robo2* double morphant embryos (5.5H; 100% where n=22) compared to wildtype embryos (5.5G) demonstrate that patterning in the brain occurs normally as a result of simultaneous loss of function of *pk1a* and *robo2*.

PK:ROBO DOUBLE MORPHANTS: 24HPF	AMT. (ng)	TOTAL	SEVERE CE DEFECT %	MILD CE DEFECT %	WT-LIKE %	DEAD %	MISC. %
WT+*pk1a*-MO +*robo2*-MO	*pk1a*: 1 *robo2*: 2	83	95	-	-	5	-
WT+*pk1a*-MO +*robo3v1*-MO	*pk1a*: 1 *robo3v1*: 2	24	-	-	88	12	-
WT+*pk1a*-MO +*robo3v2*-MO	*pk1a*: 1 *robo3v2*: 2	63	95	-	3	2	-
WT+*pk1b*-MOa +*robo2*-MO	2 each	96	3	-	94	1	2 non-specific
WT+*pk1b*-MO +*robo3v1*-MO	2 each	29	-	93	-	7	-
WT+*pk1b*-MO +*robo3v2*-MO	2 each	61	80	-	9	8	3 non-specific
PK:ROBO DOUBLE MORPHANTS: 10HPF (*hgg1, ntl & dlx3*)							
WT+*pk1a*-MO +*robo2*-MO	*pk1a*: 1 *robo2*: 2	19	-	100	-	-	-
WT+*pk1a*-MO +*robo3v2*-MO	*pk1a*: 1 *robo3v2*: 2	17	18	76	6	-	-
WT+*pk1b*-MOa +*robo2*-MO	2 each	20	-	100	-	-	-
WT+*pk1b*-MO +*robo3v2*-MO	2 each	24	-	96	4	-	-

Table 14. Loss of function of *pk* orthologues in combination with *robo* orthologues.

In the mesoderm, expression of *ntl* in the notochord shows the extension of the axial mesoderm of *pk1a:robo2* double morphants (5.5E; Table 14; Appendix Two) to be normal compared to wildtype (5.5D), *robo2* morphant embryos (data not shown) and *pk1a* morphant embryos (5.3E). Likewise, expression of *hgg1* in the prechordal plate shows the anterior migration of the prechordal mesoderm of *pk1a:robo2* double morphant embryos (5.5B) to be comparable to wildtype embryos (5.5A), leaving the prechordal plate situated fully anterior to the anterior border of the neural plate by the end of gastrulation. However, expression of *papc* in the pre-somitic mesoderm shows a mild expansion in the mediolateral axis and reduction in the anteroposterior axis, reflecting mildly impaired mesodermal convergent extension movements in the paraxial mesoderm (5.5K; 100% where n=20). It is unclear how this relates to the severe phenotype yielded by simultaneous loss of function of *pk1a* and *robo2* visible at 24hpf.

Loss of function of *pk1a* greatly enhances the loss of function phenotype of *robo3v2*

Loss of function of both *pk1a* and *robo3v2* results in a combination of movement and patterning defects at 24hpf (5.5C), greatly enhanced relative to the defects of loss of function of either *pk1a* (5.1B) or *robo3v2* (5.1H) alone, and highly reminiscent of *pk1b:slit1a* double morphant embryos (5.2D). Extension of the anteroposterior axis is reduced and the axis is both kinked and ventrally curled as a result of *pk1a* and *robo3v2* loss of function. Somites in the trunk appear abnormally shaped and are tightly compressed in the anteroposterior axis due to the reduction in body length. The forebrain is abnormally shaped relative to wildtype, while the eye itself appears smaller, the ventral portion of the eye lacking pigment (5.4G) in a manner highly reminiscent of the eyes of *pk1a:slit1a* double morphants (5.2G) or *robo3v2* morphants (4.6C & D). However, yolk extension

development is not significantly disrupted as a result of simultaneous loss of function of *pk1a* and *robo3v2*. These data suggest firstly that *pk1a* and *robo3v2* are epistatic and undergo strong functional interaction in a number of developmental processes, including the regulation of convergent extension and patterning within the brain, eye and somites. Striking similarities between *pk1b:slit1a* and *pk1a:robo3v2* double morphant embryos suggest that *robo3v2* and *slit1a* function together in the regulation of multiple morphogenetic processes.

The morphological defects of *pk1b:slit1a* and *pk1a:robo2* double morphant embryos seem disproportionately severe compared to the mild mesodermal and neurectodermal convergent extension defects visible at 10hpf via *in situ* hybridisation. The same is true of *pk1a:robo3v2* double morphants at 10hpf (Fig. 5.5; Table 14; Appendix Two). Expression of *dlx3* shows the neural plate to be mildly expanded in the mediolateral axis due to reduced convergent extension as a result of loss of function of *pk1a* and *robo3v2* (5.5C & F) compared to the wildtype neural plate (5.5A & D) or the neural plate of *pk1a* morphant embryos (5.3B & E) or *robo3v2* morphant embryos (data not shown). The specification of the eyefield and MHB, highlighted by the expression of *rx3* and *pax2.1* respectively, occurs normally in *pk1a:robo3v2* double morphant embryos (5.5I; 100% where n=18), but their expression domains are expanded in the mediolateral axis and compressed anteroposteriorly due to mildly impaired convergent extension movements.

Expression of *ntl* in the notochord shows mild mediolateral expansion due to mildly reduced convergent extension movements in the axial mesoderm of *pk1a:robo3v2* double morphant embryos (5.5F) relative to wildtype embryos (5.5D), *pk1a* morphant embryos (5.3E) and *robo3v2* morphant embryos (data not shown). The expression domain of *papc* in the paraxial mesoderm is also

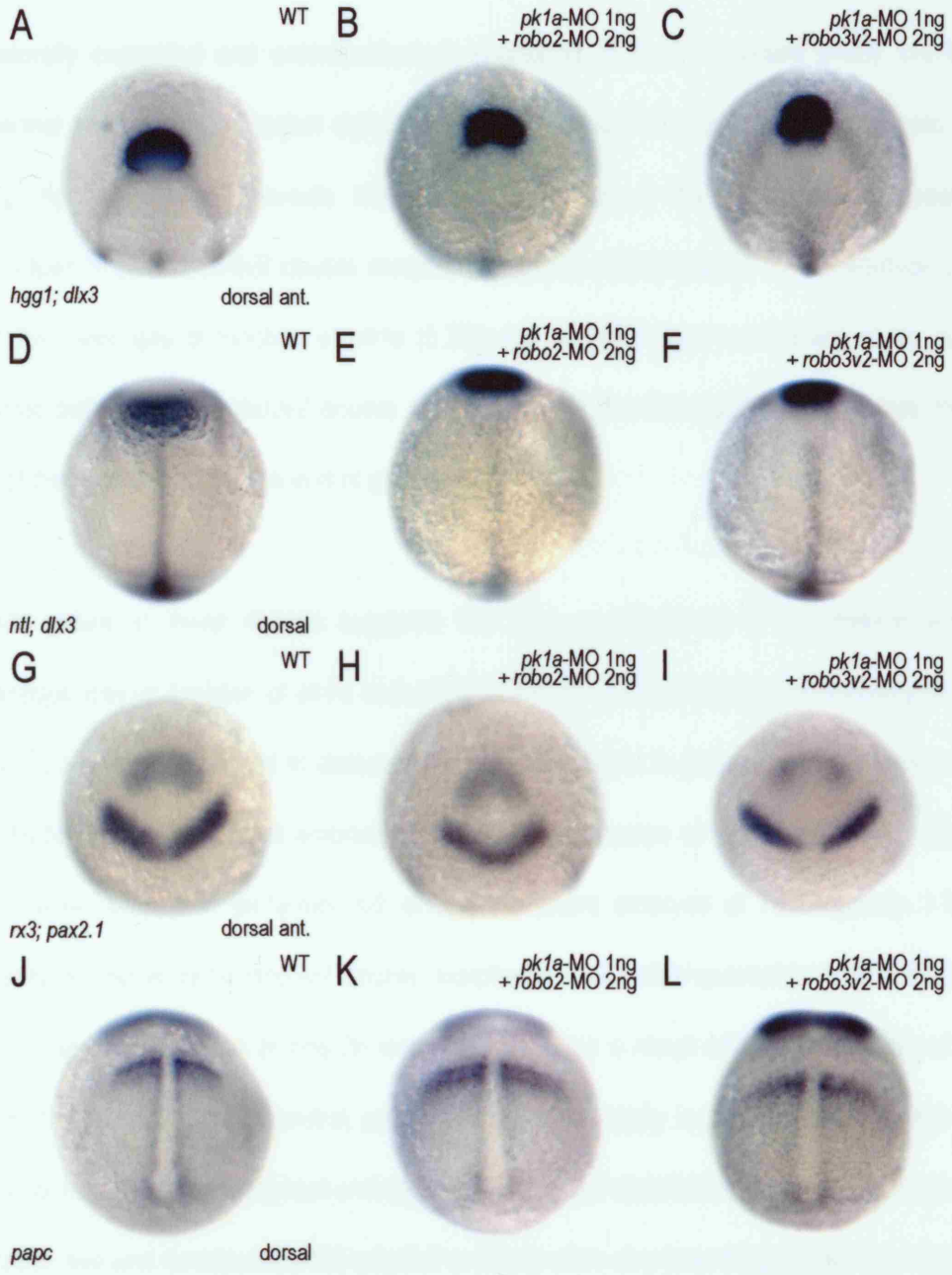

Figure 5.5

***robo2* and *robo3v2* functionally interact with *pk1a* in the regulation of convergent extension.**

5.5A-F: the relative convergent extension movements of the mesoderm and neurectoderm at 10hpf, highlighted by expression of the mesodermal markers *hgg1* and *ntl* and the neurectodermal marker *dlx3*. A & D: wildtype embryo; B & E: simultaneous loss of function of *pk1a* (1ng *pk1a*-MO) and *robo2* (2ng *robo2*-MO); C & F: loss of function of both *pk1a* (1ng *pk1a*-MO) and *robo3v2* (2ng *robo3v2*-MO). G-I: *rx3* expression in the future eyefield and *pax2.1* expression in the future MHB at 10hpf. G: wildtype embryo; H: loss of function of both *pk1a* (1ng *pk1a*-MO) and *robo2* (2ng *robo2*-MO); I: simultaneous loss of function of *pk1a* (1ng *pk1a*-MO) and *robo3v2* (2ng *robo3v2*-MO). J-L: expression of *papc* in the paraxial mesoderm at 10hpf. J: wildtype embryo; K: loss of function of both *pk1a* (1ng *pk1a*-MO) and *robo2* (2ng *robo2*-MO); L: loss of function of *pk1a* (1ng *pk1a*-MO) and *robo3v2* (2ng *robo3v2*-MO).

mediolaterally expanded and anteroposteriorly shortened (5.5L; 97% where n=29), confirming the mesodermal convergent extension defect arising as a result of loss of function of both *pk1a* and *robo3v2*. *hgg1* expression reveals the anterior migration of the prechordal mesoderm to be compromised in *pk1a:robo3v2* double morphant embryos (5.5C) relative to the wildtype prechordal plate (5.5A), and loss of function of *pk1a* (5.3B) and *robo3v2* (data not shown) alone, leaving the prechordal plate of *pk1a:robo3v2* double morphants only one-third of the way across the anterior border of the neural plate by the end of gastrulation.

The mild nature of these defects suggests that only a component of the defects arising from simultaneous loss of function of *pk1a* and *robo3v2* are as a result of impaired convergent extension defects. To see if disturbances to dorsoventral patterning were in part responsible for the defects of *pk1a:robo3v2* double morphant embryos, I examined expression of the dorsal marker *chd* and the ventral marker *bmp2b* in *pk1a:robo3v2* double morphant embryos at 70% epiboly. I found that expression of *chd* in *pk1a:robo3v2* double morphants was indistinguishable from wildtype (100%, n=19). Similarly, expression of *bmp2b* was unchanged as a result of loss of function of *pk1a* and *robo3v2* (100%, n=20). Dorsoventral patterning occurs normally in *pk1a:robo3v2* double morphant embryos as in *pk1b:slit1a* morphant embryos, and likewise, I conclude that the morphological defects in the brain, eye and somites of *pk1a:robo3v2* embryos arise at a later stage of development.

Loss of function of *pk1b* weakly enhances the loss of function phenotype of *robo2*

Further evidence of the divergent functions of *robo2* and *robo3v2* in the context of convergent extension movements is provided by simultaneous loss of function of *pk1b* and *robo2* (Fig. 5.4 & 5.6;

Table 14; Appendix Two). The contribution convergent extension defects make to the phenotype of *pk:robo3v2* double morphants is relatively small, and severe disturbances to patterning in the brain, eye and somites suggest that *pk1b* and *robo3v2* interact in a number of morphogenetic processes. Conversely, *robo2* function seems to relate more closely to the extension of the anteroposterior axis, confirmed by *pk1b:robo2* double morphant embryos: loss of function of *pk1b* and *robo2* causes a mild shortening of the anteroposterior axis and increase in the diameter of the yolk extension at 24hpf (5.4D) relative to wildtype embryos (5.4A) and *pk1b* morphant embryos (5.1C) or *robo2* morphant embryos (5.1F) at identical subthreshold doses. No other morphological defects are apparent in *pk1b:robo2* double morphant embryos.

An examination of mesodermal and neurectodermal markers at 10hpf via *in situ* hybridisation shows convergent extension defects to underlie the phenotype of *pk1b:robo2* double morphant embryos (Fig. 5.6; Table 14; Appendix Two). Expression of *ntl* in the axial mesoderm of *pk1b:robo2* double morphant embryos shows the notochord to be expanded in the mediolateral axis (5.6E) relative to the notochord of wildtype embryos (5.6D), *pk1b* morphant (3.3E) and *robo2* morphant embryos (data not shown), reflecting reduced convergent extension movements. Likewise, expression of *papc* in the paraxial mesoderm of *pk1b:robo2* double morphant embryos (5.6K) shows mediolateral expansion and anteroposterior reduction (100%, n=11) relative to the paraxial mesoderm of wildtype embryos (5.6J), *pk1b* morphant (3.3K) or *robo2* morphant embryos (data not shown). Expression of *hgg1* in the prechordal plate shows the anterior migration of the prechordal mesoderm to be mildly affected by simultaneous loss of function of *pk1b* and *robo2*: by the end of gastrulation, the prechordal plate has only migrated one-third of the way across the anterior border of the neural plate, in contrast to the prechordal plate of wildtype embryos (5.6A), *pk1b* morphant embryos (3.3B) and *robo2* morphant

embryos (data not shown) at the same subthreshold doses. Convergent extension movements are therefore affected throughout the mesoderm by loss of function of both *pk1b* and *robo2*.

In the neurectoderm, expression of *dlx3* shows the neural plate to be greatly expanded in the mediolateral axis (5.6B & E) relative to the neural plate in wildtype (5.6A & D) or that given rise to by loss of function of *pk1b* (3.3B & E) or *robo2* (data not shown) alone. Similarly, the expression domains of *rx3* in the prospective eyefield and *pax2.1* in the prospective MHB of *pk1b:robo2* double morphant embryos are mediolaterally expanded and compressed in the anteroposterior axis (5.6H; 100% where n=15) relative to wildtype (5.6G), *pk1b* morphants (*pax2.1* expression only: 3.3H) and *robo2* morphants (data not shown), demonstrating that convergent extension movements are impaired throughout the neurectoderm while patterning in the brain is unaltered by loss of function of *pk1b* and *robo2*. These data suggest that, in contrast with *pk1b:slit1a or pk:robo3v2* double mutants, the epistatic interaction between *pk1b* and *robo2* affects convergent extension movements in both the mesoderm and neurectoderm without visibly affecting other aspects of morphogenesis.

Loss of function of *pk1b* greatly enhances the loss of function phenotype of *robo3v2*

Loss of function of both *pk1b* and *robo3v2* acutely disturbs both movement and patterning (Fig. 5.4E; Table 14; Appendix Two) in a manner reminiscent of *pk1b:slit1a* (5.2D) and *pk1a:robo3v2* (5.4C) double morphant embryos. Of greater severity than loss of function of *pk1b* (5.1C) or *robo3v2* (5.1H) alone, *pk1b:robo3v2* double morphant embryos exhibit a severely anteroposteriorly shortened, ventrally curled body axis at 24hpf. The somites appear abnormal in shape and are compressed in the anteroposterior axis due to the reduction in body length. The yolk extension, whilst not greatly

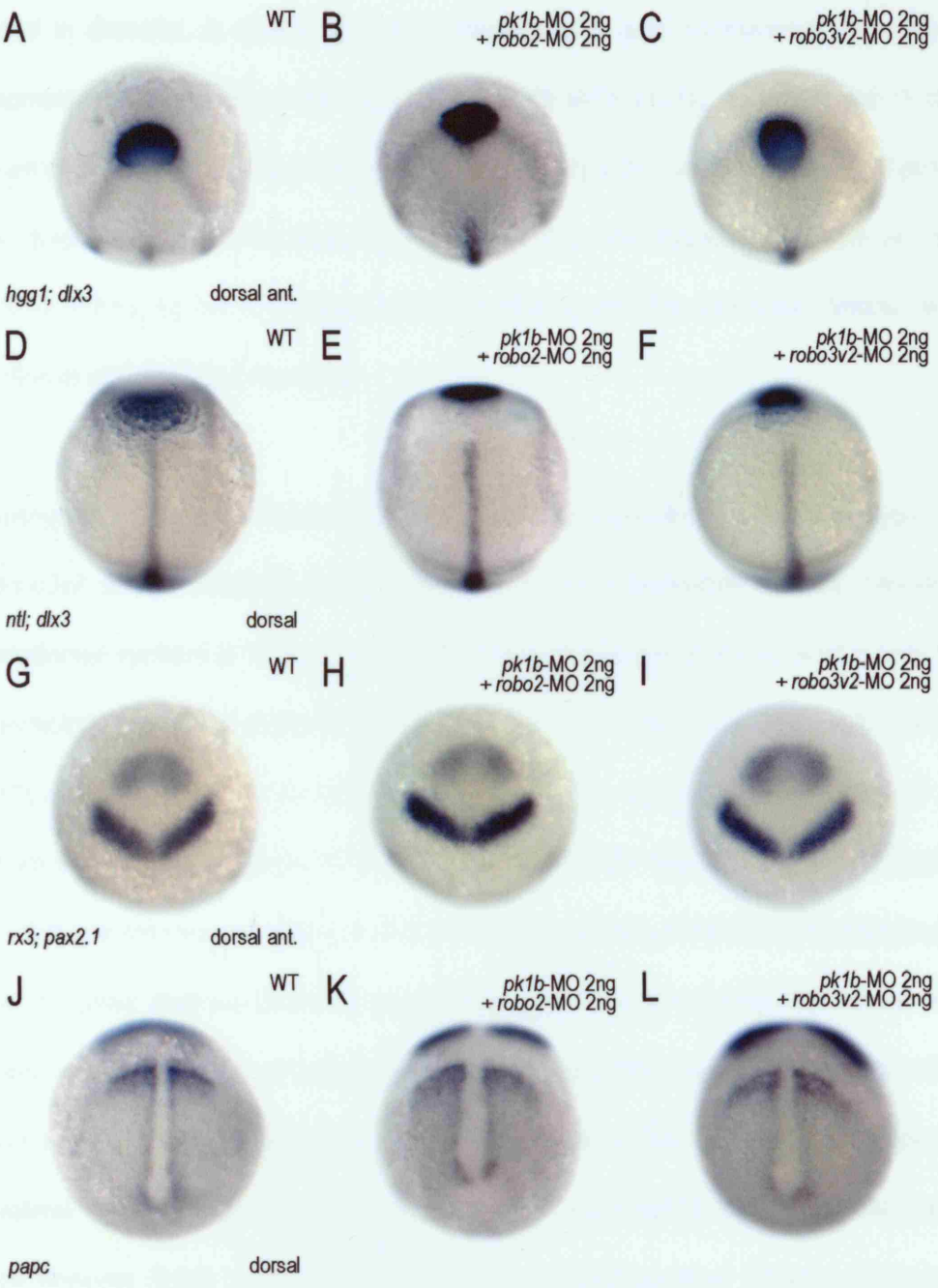

Figure 5.6

robo2 and _robo3v2_ functionally interact with _pk1b_ in the regulation of convergent extension.

5.6A-F: convergent extension movements in the mesoderm and neurectoderm at 10hpf, revealed by expression of the mesodermal markers *hgg1* and *ntl* and the neurectodermal marker *dlx3*. A & D: wildtype embryo; B & E: simultaneous loss of function of *pk1b* (2ng *pk1b*-MOa) and *robo2* (2ng *robo2*-MO); C & F: loss of function of both *pk1b* (2ng *pk1b*-MO) and *robo3v2* (2ng *robo3v2*-MO). G-I: expression of *rx3* in the prospective eyefield and *pax2.1* in the prospective MHB at 10hpf. G: wildtype embryo; H: loss of function of both *pk1b* (2ng *pk1b*-MO) and *robo2* (2ng *robo2*-MO); I: simultaneous loss of function of *pk1b* (2ng *pk1b*-MO) and *robo3v2* (2ng *robo3v2*-MO). J-L: expression of *papc* in the pre-somitic mesoderm at 10hpf. J: wildtype embryo; K: simultaneous loss of function of *pk1b* (2ng *pk1b*-MO) and *robo3v2* (2ng *robo3v2*-MO).

increased in diameter, is shortened in the anteroposterior axis. Furthermore, the defects in the development of the eye are more severe than *pk1b:slit1a* (5.2G), *pk1a:robo3v2* (5.4G) double morphant and *robo3v2*-morphant embryos (4.6C & D), only a tiny portion of the eye of *pk1b:robo3v2* double morphant embryos showing pigmentation (5.4H). This suggests that both *pk1* genes are capable of enhancing the convergent extension defects and the pleiotropic defects arising from abrogation of *slit1a/robo3v2* signalling.

To investigate to what extent convergent extension defects contribute to this phenotype, I analysed *pk1b:robo3v2* double morphant embryos through *in situ* hybridisation for key mesodermal and neurectodermal markers at 10hpf. Convergent extension movements are impaired in both mesoderm and neurectoderm, but the moderate nature of these defects cannot fully account for the severity of the *pk1b:robo3v2* phenotype at 24hpf. In the mesoderm, the expression domain of *ntl* in the notochord shows mild expansion in the mediolateral axis and reduction in the anteroposterior axis (5.6F) relative to the axial mesoderm of wildtype embryos (5.6D), *pk1b* morphant embryos (3.3E) and *robo3v2* morphant embryos (data not shown), reflecting impaired convergent extension movements as a result of loss of function of both *pk1b* and *robo3v2*. Similarly, expression of *papc* in the paraxial mesoderm of *pk1b:robo3v2* double morphant embryos (5.6L; 75% where n=16) is expanded in the mediolateral axis and reduced in the anteroposterior axis relative to the paraxial mesoderm of wildtype embryos (5.6J), *pk1b* morphant (3.3K) or *robo3v2* morphant embryos (data not shown), confirming that convergent extension movements are compromised in the mesoderm. The anterior migration of the prechordal plate is severely affected by simultaneous loss of function of *pk1b* and *robo3v2*: by the end of gastrulation, the prechordal mesoderm has failed to cross the anterior border

of the neural plate (5.6C), in contrast to wildtype embryos (5.6A) or loss of function of *pk1b* (3.3B) or *robo3v2* (data not shown) alone.

Convergent extension movements are also compromised in the neurectoderm as a result of loss of function of *pk1b* and *robo3v2*. Expression of *dlx3* at the border of the neural plate shows this structure to be expanded in the mediolateral axis (5.6C & F) to a much greater extent than in *pk1b* morphant embryos (3.3B & E) and *robo3v2* morphant embryos (data not shown). Mediolateral expansion and anteroposterior compression of the expression domains of *rx3* in the future eyefield and *pax2.1* in the future MHB of *pk1b:robo3v2* double morphant embryos (5.6I; 94% where n=17) relative to wildtype (5.6A & D), *pk1b* morphants (*pax2.1* expression only: 3.3H) and *robo3v2* morphants (data not shown) confirm this defect in neurectodermal convergent extension movements.

I also examined the expression of the dorsal marker *chd* and the ventral marker *bmp2b* in *pk1b:robo3v2* double morphant embryos at 70% epiboly. Dorsal expression of *chd* is unaltered as a result of loss of function of both *pk1b* and *robo3v2* (100%, n=21). Likewise, *bmp2b* expression in the ventral half of the embryo is indistinguishable from wildtype in *pk1b:robo3v2* double morphant embryos (100%, n=15). Dorsoventral patterning is unaffected as a result of simultaneous loss of function of *pk1b* and *robo3v2*: however, despite the fact that convergent extension defects are more significant in *pk1b:robo3v2* double morphants than in *pk1b:slit1a* and *pk1a:robo3v2* double morphant embryos, these defects do not fully account for the severe phenotype of *pk1b:robo3v2* double morphant embryos at 24hpf. Therefore the functional interaction between *pk1b* and *robo3v2* not only regulates convergent extension movements, but also regulates patterning events later in embryogenesis.

Discussion & Conclusion

Summary

In Chapter Four, I showed that, analogously to Slit/Robo signalling in commissure formation in the CNS, Robo receptors undergo a functional interaction with the Slit2 ligand in the context of the regulation of convergent extension movements. However, the divergent behaviour of the Robo2 and Robo3v2 receptors led me to conclude that while Robo2 functions as an authentic receptor, Robo3v2 acts antagonistically to Slit/Robo signalling during zebrafish gastrulation. This is especially significant when it is considered that Robo3v2 is structurally similar to the murine Robo3 orthologue Rig-1, thought to function to repress inappropriate Slit/Robo signalling in the mouse CNS in a manner reminiscent to the role of Comm in the *Drosophila* CNS (Camurri *et al.*, 2004; Challa *et al.*, 2005; Sabatier *et al.*, 2004; Tear *et al.*, 1996). To understand the relationship between Slit/Robo signalling and known regulators of convergent extension movements, in this chapter I first investigated the capability of Slit orthologues to interact with Wnt11, a component of the non-canonical Wnt signalling pathway, and Stbm, Pk1a, and Pk1b, components of a pathway considered parallel to but capable of modulating the non-canonical Wnt signalling pathway. I found that loss of function of *slit1a* failed to enhance the *silberblick/wnt11* (*slb*) mutant phenotype, while loss of function of *slit2* did not enhance the *trilobite/stbm* (*tri*) mutant phenotype, despite the morphological similarities between *slit2* morphants and homozygous *tri* embryos.

In contrast, I demonstrated a strong functional interaction between zebrafish orthologues of the *Drosophila* PCP gene *pk* and *slit* and *robo* orthologues in the context of the regulation of convergent extension movements. Furthermore, I showed that the epistatic interactions between *pk* and *slit* and

pk and *robo* fall into two classes. The first class primarily affects the regulation of convergent extension movements, while the second class disrupts convergent extension movements and the development of the somites, brain and eye later in embryogenesis (see Appendix Two for further exploration of convergent extension defects).

The enhancement of convergent extension defects given rise to by simultaneous loss of function of *pk1a* and *slit1a*, *pk1a* and *slit2*, *pk1b* and *slit2*, *pk1a* and *robo2*, and *pk1b* and *robo2* comprise the first class. *pk1a* collaborates with *slit1a*, *slit2* and *robo2* in the regulation of convergent extension movements: at 24hpf, extension of the anteroposterior axis and the formation of the yolk extension are impaired to a greater extent in *pk1a:slit1a*, *pk1a:slit2* and *pk1a:robo2* double morphant embryos than in their respective single morphants alone. Severe mesodermal and neurectodermal convergent extension defects visible at 10hpf via *in situ* hybridisation analysis account for the phenotypes of *pk1a:slit1a* and *pk1a:slit2* double morphant embryos to a greater extent than *pk1a:robo2* double morphant embryos. Likewise, *pk1b* collaborates with *slit2* and *robo2* in the regulation of convergent extension movements: *pk1b:slit2* and *pk1b:robo2* double morphant embryos are shorter in the anteroposterior axis than their respective single morphants, although the effect of loss of function of *pk1b* in combination with loss of function of *slit2* or *robo2* on the development of the yolk extension is less profound than in *pk1a:slit* or *pk1a:robo* double morphants. Moderate mediolateral expansion in the mesoderm and neurectoderm of *pk1b:slit1a*, *pk1b:slit2* and *pk1b:robo2* double morphant embryos at 10hpf demonstrate convergent extension defects to underlie their phenotypes at 24hpf.

A strong functional interaction between *pk1b* and *slit1a*, *pk1a* and *robo3v2*, and *pk1b* and *robo3v2* comprises the second class of double morphants. The anteroposterior axis of *pk1b:slit1a*,

pk1a:robo3v2 and *pk1b:robo3v2* double morphant embryos is shortened at 24hpf, although yolk extension development is largely unaffected in all three double morphants. Interestingly, multiple later aspects of patterning within *pk1b:slit1a*, *pk1a:robo3v2* and *pk1b:robo3v2* double morphant embryos appear strongly affected: the somites are misshapen, the structure of the brain is abnormal and, reminiscently of *robo3v2* morphant embryos, the ventral portion of the eye is missing. Dissimilarly to the first class of functional interactions, *in situ* hybridisation analysis of *pk1b:slit1a*, *pk1a:robo3v2* and *pk1b:robo3v2* double morphant embryos at 10hpf revealed only moderate convergent extension defects, disproportionate to the severe defects visible in these double morphants at 24hpf. The divergent nature of these interactions confirms the theory I proposed in Chapter Four of this thesis that *slit* and *robo* orthologues are not functionally redundant but instead have discrete and opposing functions in the regulation of convergent extension movements during zebrafish gastrulation.

Discussion

The discovery that overexpression of *slit2* causes severe convergent extension defects and cyclopia in zebrafish (Yeo *et al.*, 2001) proposed a role for *slit* orthologues in the regulation of cell movements during gastrulation. The function of Slit as a repellent ligand for the Robo receptor in the context of commissure formation in the *Drosophila* CNS is evolutionarily conserved in the vertebrate CNS (Challa *et al.*, 201; Challa *et al.*, 2005; Dalkic *et al.*, 2006; Brose *et al.*, 1999; Fricke *et al.*, 2001; Hutson & Chien, 2002; Kidd *et al.*, 1998a; Kidd *et al.*, 1998b; Kidd *et al.*, 1999; Lee *et al.*, 2001). Over the course of evolution, the roles of Slit ligands and Robo receptors have also diversified. The zebrafish *robo* orthologue, "Magic Roundabout" or Robo4, regulates endothelial cell migration in the forming circulatory system (Bedell *et al.*, 2005; Park *et al.*, 2003). Vertebrate orthologues of *slit* have

also proved capable of stimulating axon branching in a manner that may be Robo-independent (Wang *et al.*, 1999). It was necessary to address whether the role of *slit2* in the regulation of convergent extension, proposed by the severe defects resulting from *slit2* gain of function (Yeo *et al.*, 2001), was mediated through the Robo receptor or through an as yet unidentified pathway, reflecting diversification of Slit function. In Chapter Four of this thesis, I showed that *slit2* functionally interacts distinctly with *robo2* and *robo3v2* in the context of zebrafish gastrulation, suggesting that Slit/Robo signalling controls aspects of cell migration during convergent extension in a manner analogous to Slit/Robo signalling in the regulation of axon guidance.

The next challenge was to understand how Slit/Robo signalling during gastrulation related to known regulators of convergent extension movements such as the non-canonical Wnt signalling pathway (see Introduction: Fig. 1.1). The failure of loss of function of *slit* orthologues to enhance the convergent extension defect of the *silberblick/wnt11* (*slb*) mutant implies that the function of *slit* orthologues during gastrulation is independent of the non-canonical Wnt signalling pathway. A Wnt-independent role for the axon guidance genes *slit* and *robo* in the regulation of convergent extension is not implausible when it is considered that known regulators of both convergent extension and axon pathfinding, such as *strabismus* (*stbm*) or *pk1a*, are thought to act in a parallel pathway to non-canonical Wnt signalling; functioning Wnt-dependently in the context of the regulation of convergent extension movements, and Wnt-independently in the context of the regulation of facial (nVII) branchiomotor neuron migration in the hindbrain (Carreira-Barbosa *et al.*, 2003).

Stbm, a putative four-pass transmembrane protein known to be asymmetrically localised in the *Drosophila* wing and eye, was shown to bind and recruit both Pk and Dsh to the cell membrane in the

propagation of PCP, evidence of a physical link between the non-canonical Wnt signalling pathway and the parallel pathway from which *stbm* and *pk1a* are thought to modulate non-canonical Wnt signalling (Bastock *et al.*, 2003; Jenny *et al.*, 2003). The zebrafish convergent extension mutant *trilobite* (*tri*) encodes *stbm*, exhibiting severely impaired convergent extension movements and in collaboration with loss of function of *pk1a*, disruption to branchiomotor neuron migration (Carreira-Barbosa *et al.*, 2003; Jessen *et al.*, 2002). The convergent extension defects of homozygous *tri* embryos are confined to the posterior region of the body axis, strongly affecting the extension of the body axis and the development of the yolk extension (see Introduction: Fig. 1.2D). Loss of function of *slit* orthologues, particularly *slit2*, causes convergent extension defects in the posterior region of the body axis in a manner highly reminiscent of the *trilobite/stbm* (*tri*) mutant. The morphological resemblance between *slit2* morphants and homozygous *tri* embryos, coupled with the fact that *stbm* is considered to function in a parallel pathway to non-canonical Wnt signalling during gastrulation, prompted me to investigate whether *slit* orthologues interact with *stbm* in the context of the regulation of convergent extension movements. I found that loss of function of *slit2* did not enhance the convergent extension defects of *tri* embryos. This suggests that Slit/Robo signalling does not interact with Stbm, contrary to my expectations given that Slit/Robo signalling does not regulate convergent extension movements in collaboration with non-canonical Wnt signalling.

Loss of function of zebrafish *slit* and *robo* orthologues in combination with loss of function of the *pk* orthologues *pk1a* and *pk1b* demonstrated a strong functional interaction between Slit/Robo signalling and Pk, confirming that Slit/Robo signalling collaborates with pathways parallel but not linearly related to the non-canonical Wnt signalling pathway in the regulation of convergent extension. The defects arising from loss of function of *pk1a* affect posterior regions of the body axis similarly to loss of

function of *slit2*. However, *pk1a* and *stbm* are thought to collaborate both Wnt-dependently in the modulation of non-canonical Wnt signalling during convergent extension, and Wnt-independently in the regulation of branchiomotor neuron migration in the hindbrain, although recent evidence implicating Fz3a and Fmi2/Celsr2 in this process suggests that although divergent from the non-canonical Wnt signalling pathway beyond Fz, this pathway is not necessarily Wnt-independent (Carreira-Barbosa *et al.*, 2003; Wada *et al.*, 2006). It is unexpected that loss of function of *slit* orthologues should enhance the *pk1a* morphant phenotype and not the convergent extension defects of the *trilobite/stbm* (*tri*) mutant, suggesting that Pk and Stbm do not function together in all contexts. This is supported by evidence that XPk, but not XStbm, functions Fibronectin-independently in cell polarisation during convergent extension in *Xenopus* (Goto *et al.*, 2005). Defects unrelated to convergent extension evident in *pk1b:slit1a*, *pk1a:robo3v2* and *pk1b:robo3v2* double morphant embryos, such as the disruption of normal pigmentation in the eye, allow the roles of *stbm* and *pk* orthologues to be dissected, and suggest hitherto unidentified *stbm*-independent roles for *pk* in collaboration with *robo3v2* in the regulation of convergent extension movements and other processes such as the development of the brain, eye and somites later in embryogenesis.

The functional interaction between Slit/Robo signalling and *pk1a* and *pk1b* further defines the discrete functions of non-functionally redundant *slit* and *robo* orthologues during gastrulation proposed in Chapter Four. Loss of function of *slit1a* or *slit2* alone resulted in convergent extension defects at 10hpf that translated to subtly different convergent extension phenotypes at 24hpf (Fig. 4.2 & 4.3). In this chapter, I demonstrated that simultaneous loss of function of *pk1a* and *slit1a* or *pk1a* and *slit2* causes an enhancement of these convergent extension and yolk extension defects. However, loss of function of *pk1b* in combination with either *slit1a* or *slit2* highlights the contrast

between *slit1a* and *slit2* function. Loss of function of *pk1b* enhances the convergent extension defects, and to a lesser extent, the yolk extension defect of *slit2* morphant embryos. However, loss of function of *pk1b* and *slit1a* in combination causes severe morphological disturbances at 24hpf: while an element of this phenotype results from impaired convergent extension movements (although yolk extension development is largely normal), patterning defects underlie the brain, eye and somite abnormalities of *pk1b:slit1a* double morphant embryos. This suggests that *pk1b* and *slit1a* interact pleiotropically during embryogenesis, while *slit2* function during gastrulation relates more exclusively to the regulation of convergent extension movements.

These contrasting functions of *slit* orthologues during and beyond gastrulation appear to be mediated by different *robo* orthologues. The convergent extension defects resulting from loss of function of *pk1a* or *pk1b* in combination with *robo2* or *robo3v2* are less severe that the convergent extension defects of *pk:slit* double morphant embryos, implying that the Slit1a and Slit2 ligands bind promiscuously to Robo receptors in the regulation of convergent extension movements. The severe movement and patterning defects resulting from *pk1a:robo3v2* and *pk1b:robo3v2* double morphant embryos suggest that the divergent role of Slit1a in the patterning of the brain, eye and somites is mediated exclusively by the Robo3v2 receptor. In Chapter Four, I showed that loss of function of *robo3v2*, but not *robo2* or *robo3v1*, caused convergent extension defects and abnormal development of the eye (Fig. 4.6), uncharacteristic of an authentic receptor. Furthermore, while both the Robo2 and Robo3v2 receptors appear capable of functionally interacting with the Slit2 ligand in the regulation of convergent extension movements, abrogation of *robo3v2* function using the Robo3v2(ECD/TM)-GFP construct failed to rescue overexpression of *slit2*, suggesting that Robo3v2

acts antagonistically to Slit/Robo signalling during gastrulation and pleiotropically during embryogenesis.

While *pk1a* and *pk1b* are both capable of enhancing the pleiotropic defects arising from loss of function of *robo3v2*, functional interaction with *pk1b* is more critical to *robo3v2* function, firstly because *pk1b* enhances the *robo3v2* loss of function phenotype more severely than *pk1a*, and secondly because *pk1b:slit1a*, but not *pk1a:slit1a*, double morphant embryos exhibit the same, striking morphological defects as *pk:robo3v2* double morphant embryos. While severe convergent extension defects are caused by the functional interaction between *pk1a* and *robo2* and, to a lesser extent, *pk1b* and *robo2*, patterning defects do not result. This suggests that the interaction between Robo2 and Pk orthologues during gastrulation relates more exclusively to the regulation of convergent extension. Robo3v2 undergoes a functional interaction with *pk* orthologues in the regulation of convergent extension movements, but in contrast with Robo2, Robo3v2 also acts pleiotropically during zebrafish embryogenesis through interactions with Slit ligands and with *pk1b*.

Chapter Six

Characterisation of airbag (abg), a novel CE mutant.

Introduction

A number of mutants were isolated as part of an ENU mutagenesis screen for enhancers and suppressors of the *silberblick/wnt11* (*slb*) phenotype performed in collaboration with the Heisenberg lab in 2001/2002 (see Materials & Methods: Enhancers of *slb*: Screen Strategy & Fig. 2.1). e*nhC132*, a dominant enhancer of *slb*, was generated in this screen (see Fig. 6.1D & J; Appendix Two). While *enhC132-/-* embryos show only mild convergent extension defects, e*nhC132-/-:slb+/-* and e*nhC132-/-:slb-/-* embryos display a greater impairment of the extension of the anteroposterior axis and bilateralisation of the eyefield than *slb-/-* alone, additionally exhibiting features more reminiscent of severe convergent extension mutants such as the *trilobite/stbm* (*tri*) mutant or *pk1a* morphant embryos (see Introduction: Fig. 1.2D & F; Appendix Two), including ventral body curling and a severely misshapen yolk extension. At 24hpf, *enhc132-/-* embryos are easily identified by their large pericardial oedema, and because of this we provisionally named the mutant *airbag* (*abg*). This oedema begins to swell from 24hpf until their death at around 96hpf, and is accompanied by a weakly beating, unlooped heart and impaired circulation of the blood, a combination of defects unique amongst zebrafish convergent extension mutants. With the assistance of 2004 undergraduate project student Christine Yang, I confirmed that *enh132* genetically interacts with other Wnt/PCP genes known to regulate convergent extension movements, such as *stbm*, *pk1a* and *pk1b*.

Prior to the mapping of the *abg* mutation, I examined candidate mutants and morphants sharing features with *abg*. The zebrafish mutant *dackel* (*dak*^{to79c}), carrying a mutation in the heparin

sulphate (HS) synthesizing glycosyltranferase enzyme *exostosin2* (*ext2*), seemed a good candidate for complementation analysis with *abg*. Homozygous *dak* embryos exhibit impaired retinotectal axon pathfinding in combination with defects in jaw and branchial arch development (Karlstrom *et al.*, 1996; Lee *et al.*, 2004; Trowe *et al.*, 1996; van Eeden *et al.*, 1996b). The *dak* jaw phenotype is reminiscent of the *ppt/wnt5b* mutant (Hammerschmidt *et al*, 1996; Killian *et al.*, 2003; Rauch *et al.*, 1997; Schilling *et al.*, 1996; Stoick-Cooper *et al.*, 2007), while impaired retinotectal axon pathfinding is reminiscent of *tri* and *pk1a* morphant embryos (Carreira-Barbosa *et al.*, 2003; Jessen *et al.*, 2002). These morphological similarities were especially interesting given that HSPGs function is required both for Slit/Robo signalling and for normal function of known modulators of Wnt/PCP signalling such as *knypek/glypican4/6* and *syndecan4* (Inatani *et al.*, 2003; Lee *et al.*, 2004; Munoz *et al.*, 2006), particularly relevant in light of the hitherto unknown interaction between axon guidance genes and known regulators of convergent extension presented in this thesis. However, *abg* and *dak* complement each other, and since undertaking this analysis, a better understanding of the *dak* mutant has been reached that excludes a role for non-canonical Wnt signalling (Lee *et al.*, 2004). However, HSPGs are known to function Slit/Robo signalling-dependently, for instance during in axon sorting in the optic tract in zebrafish (Inatani *et al.*, 2003; Lee *et al.*, 2004).

abg embryos are also phenotypically reminiscent of morphants for *duboraya* (*dub*), a zebrafish homologue of a mammalian phosphorylation-dependent cytoskeletal reorganisation gene (Oishi *et al.*, 2006). Cytoskeletal reorganisation during ciliogenesis in Kupffer's Vesicle, a ciliated organ situated in the prospective tailbud whose chirality dictates the flow of determinants of left-right asymmetry around the early embryo, occurs abnormally in the *duboraya* (*dub*) morphant (Oishi *et al.*, 2006). As a result, fluid flow in Kupffer's Vesicle is disrupted and hypothetical determinants of

left/right asymmetry are abnormally distributed in the early embryo with the consequence that left/right asymmetry and organogenesis are perturbed (Oishi et al., 2006). Heart looping is abnormal, and *dub* morphant embryos develop a large pericardial oedema, highly reminiscent of homozygous *abg* embryos (Oishi *et al.*, 2006). Furthermore, *fz2* morphant embryos were shown to have abnormal left/right asymmetry that subsequently affected the development and looping of the heart (Oishi *et al.*, 2006). Given the similarities between *abg* and *dub*, I examined left-right asymmetry in the *abg* mutant through the expression of *foxA3/fkd2* in the pancreas: however, left-right asymmetry is normal in *abg* embryos, their centralised heart possibly an artefact of oedema formation.

Although *abg* and *dub* appear to be unrelated, convergent extension defects in combination with *cardia bifida* in the zebrafish mutant *miles apart* (*mil*) demonstrate a link between convergent extension and cardiogenesis (Matsui *et al.*, 2005; Matsui *et al.*, 2006). During the development of the zebrafish heart and circulatory system, the musculature of the heart or *myocardium* is formed from two bilateral mesodermal precursor cell populations that migrate and fuse at the midline to form the primitive heart tube, while the endothelial lining of heart and vasculature and the blood are given rise to by cells of the *intermediate cell mass* (*ICM*), a dorsally situated population of cells of ventral marginal mesodermal origin (Detrich *et al.*, 1995; Stainier *et al.*, 1995). Precursor cells in the ICM are capable of giving rise to both *endocardial cells*, which give rise to the endothelial lining of the heart, and *haematopoietic stem cells*, which give rise to the blood and migrate anteriorly from the ICM to the yolk to join the circulation (Detrich *et al.*, 1995; Stainier *et al.*, 1995). Mutations that affect the ICM impact upon the circulatory system in two ways: firstly, a trade off between cardiac and blood lineages in ICM precursor cell differentiation means that heart and blood development are inextricably linked; and secondly, disruption of differentiation

within the ICM has consequences upon subsequent inductive interactions crucial to the development of the heart and major vessels (Detrich *et al.*, 1995; Brutsaert & Andries, 1992, Shah & Lewis, 1993, and Markwald *et al.*, 1990: cited in Stanier *et al.*, 1995). At 24hpf, the bHLH transcription factor *scl* is expressed in both endothelial and haematopoietic precursor cells in the ICM, although *scl* function is not required for endothelial differentiation (Gering *et al.*, 1998). Interestingly, *scl* overexpression causes an overproduction of haematopoietic precursors, but many *scl* overexpressing embryos fail to develop normal circulation of the blood, exhibit a characteristic pericardial oedema and die between 6 and 7dpf (Gering *et al.*, 1998). However, although aberrant haematopoiesis could account for the abnormal circulation and characteristic pericardial oedema of *abg-/-* embryos as in the case of gain of function of *scl*, the hearts of *scl* overexpressing embryos beat normally (Gering *et al.*, 1998), while the hearts of *abg-/-* mutants are severely deformed.

Recently, a mutation in an enzyme key to the isoprenoid synthesis pathway, known as *3-hydroxy-3-methylglutaryl-Coenzyme A reductase 1b* (*hmgcr1b*), was shown to affect heart morphogenesis in zebrafish (D'Amico *et al.*, 2007). *hmgcr1b* functions upstream of protein prenylation, a type of post-translational modification thought to target CAAX box-containing proteins, including the small GTP-ase Rho, to the cell membrane (D'Amico *et al.*, 2007; Thorpe *et al.*, 2004). *hmgcr1b* mutants exhibit a delay in the migration of heart precursor cells to the midline, a failure of heart looping morphogenesis, characteristic pericardial oedema, a thickened, malformed yolk extension and convergent extension defects, highly reminiscent of the *abg* mutant (D'Amico *et al.*, 2007). In this chapter, I explore the relationships between the *abg* mutant and non-canonical Wnt signalling in the regulation of convergent extension movements, and in light of the *hmgcr1b* mutant, the development of the heart and circulatory system.

Results

airbag (*abg*) is an enhancer of the *silberblick/wnt11* (*slb*) phenotype

airbag (*abg*) was isolated in a screen for enhancers and suppressors of the *silberblick/wnt11* (*slb*) phenotype (see Materials & Methods for screen strategy). The majority of *abg* carriers were of the genotype *abg+/-*, however, due to the way the screen was performed, a small proportion of our carriers were of the genotype *abg+/-:slb+/-*, contaminated with one copy of the *slb* gene during the course of segregation of the *abg* locus from the *slb+/-* background. Prior to characterising the *abg* phenotype, it was necessary to perform identifying incrosses and backcrosses with *slb* with our *abg* carriers, both to confirm the original findings of the screen and to separate the *abg+/-* carriers from the *abg+/-:slb+/-* carriers. With the assistance of Masa Tada and 2004 undergraduate project student Christine Yang, I isolated four pairs of carriers, designated C1, C2, C6 and C7. By crossing carriers of different genotypes, we were able to correlate genotype with phenotype and reveal the dose dependent nature of *abg*'s epistatic enhancement of the *silberblick* phenotype (Fig. 6.1 & 6.2; Appendix Two; Appendix Three).

Incrossing the C1 male and C1 female resulted in progeny 75% of which were phenotypically wildtype at 24hpf (Fig. 6.1E & F compared to A & B; Appendix Two). 25% of the progeny showed a slight reduction in the extension of the anteroposterior axis, slight pericardial oedema and a shorter, thicker, deformed yolk extension, defects characteristic of homozygous *abg-/-* embryos (6.1G & H; Appendix Two; Appendix Three: C1 Incross). At first glance, this suggested that both C1 parents were of the genotype *abg+/-* and that *abg* undergoes standard Mendelian inheritance. But many of the genotypes created in *abg* carrier crosses are phenotypically wildtype, and a phenotypic ratio of 3:1 can arise not only as a result of incrossing two *abg+/-* carriers but also as a result of an incross between an *abg+/-* carrier with a carrier of the genotype *abg+/-:slb+/-*

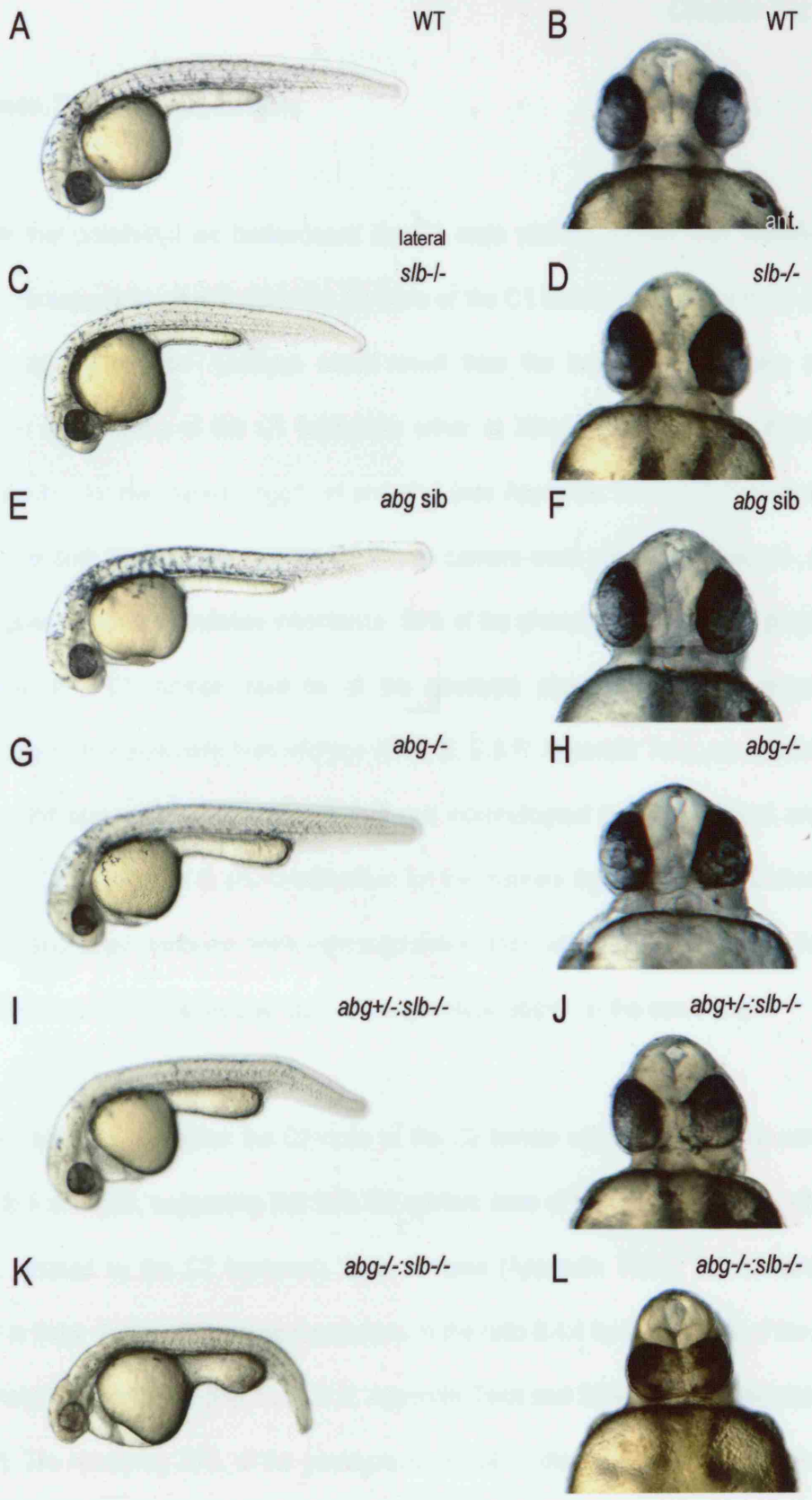

Figure 6.1

Correlating genotype with phenotype in *airbag* (*abg*) identification crosses.

Dose-dependent enhancement of morphological defects at 24hpf as a result of a genetic interaction between *slb* and *abg*, lateral and anterior views. A & B: wildtype embryo, 24hpf; C & D:*slb*-/-; E & F: sibling from *abg*+/- carrier incross; G & H: *abg*-/- embryo; I & J: *slb*-/- enhanced by one copy of the *abg* gene (*abg*+/-:*slb*-/-); K & L: *slb*-/- enhanced by two copies of the *abg* gene (*abg*-/-:*slb*-/-).

(see Appendix Three: C7 x C6 Incross).

To exclude this possibility, we backcrossed the C1 male and C1 female with identified *slb-/-* carriers in the expectation that if either the C1 male or the C1 female carried one copy of the *slb* gene, a proportion of *slb-/-* embryos would result from the backcross. However, no *slb-/-* presented in the progeny of the C1 backcross either at 30hpf or at via *in situ* hybridisation analysis at 10hpf for the markers *hgg1*, *ntl* and *dlx3* (see Appendix Three: C1 Backcross). This confirmed that both the C1 male and the C1 female carriers were genotypically *abg+/-*, and that *abg* undergoes standard Mendelian inheritance. 50% of the phenotypically wildtype proportion of the progeny of a C1 incross must be of the genotype *abg+/-*, but as this proportion is phenotypically indistinguishable from wildtype (6.1A, B, E & F; Appendix Two), we concluded that one copy of the *abg* mutation is insufficient to cause morphological defects. At 10hpf, analysis of progeny of a C1 incross via *in situ* hybridisation for the markers *hgg1*, *ntl* and *dlx3* showed that both *abg+/-* and *abg-/-* embryos were indistinguishable from wildtype (100%, n=45). At a later date, we identified the C7 carrier pair, both of the genotype *abg+/-*, in the same way.

Conversely, backcrossing either the C2 male or the C2 female with identified *slb-/-* carriers did produce *slb-/-* embryos, suggesting that both C2 carriers were of the genotype *abg+/-:slb+/-*. The genotypes created by the C2 backcross were complex (Appendix Three: C2 Backcross), but translated to three distinct phenotypic populations in the ratio 8:4:4 by 24hpf. 50% of the progeny were phenotypically wildtype (Fig. 6.1A & B; Appendix Two) and 25% were phenotypically *slb-/-* (6.1C & D). The remaining 25%, of the genotype *abg+/-:slb-/-*, displayed a further reduction of the extension of the anteroposterior axis and abnormal yolk extension development relative to *slb-/-* embryos (6.1I). Furthermore, *abg+/-:slb-/-* embryos displayed partial failure of eyefield separation

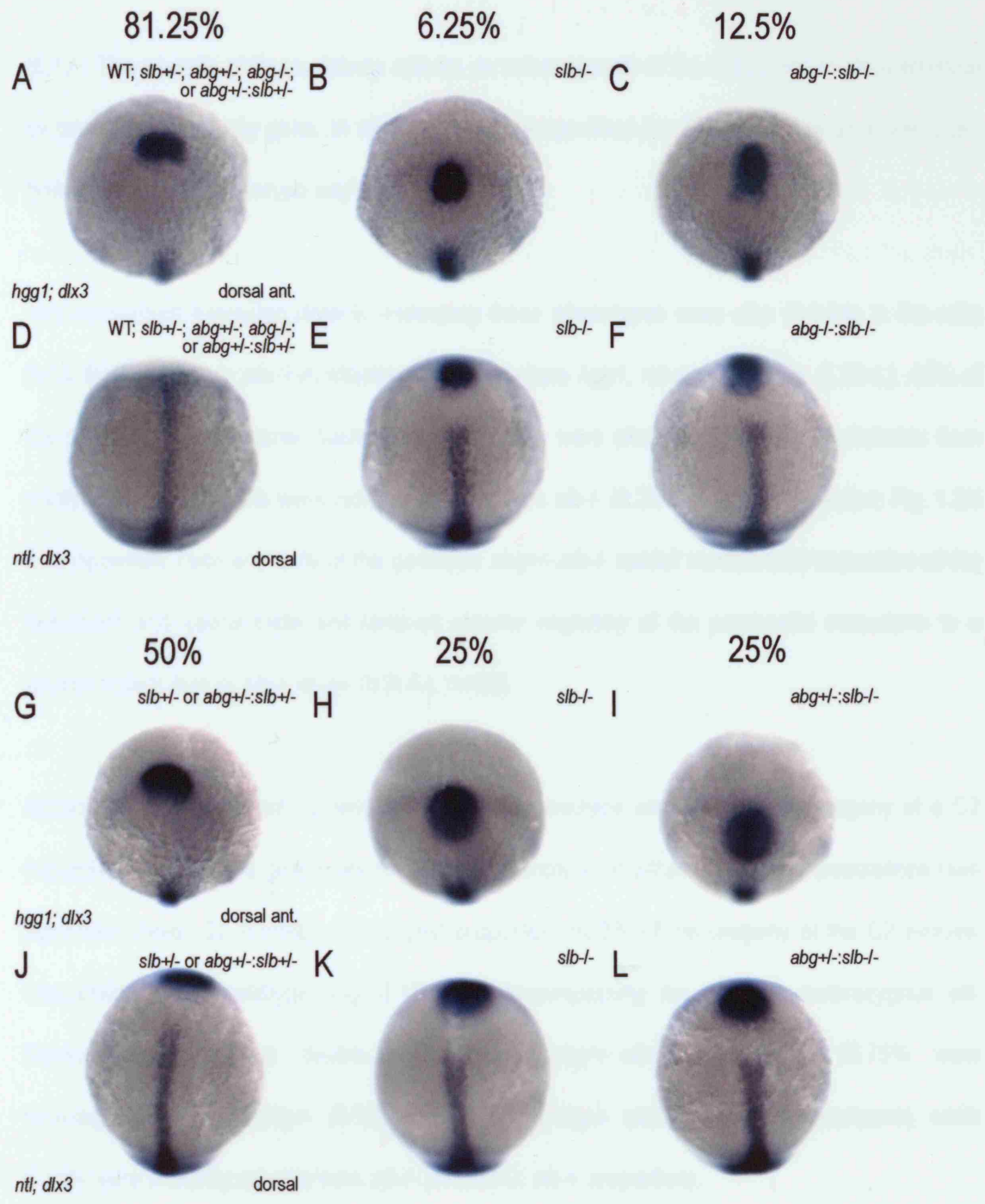

Figure 6.2

in situ hybridisation analysis of the typical phenotypic proportions generated by an *abg+/-:slb+/-* carrier incross and an *abg+/-:slb+/-* x *slb-/-* backcross.

A-F: phenotypes and proportions resulting froman *abg+/-:slb+/-* carrier incross. A & D: phenotypically wildtype proportion (81.25%), encompassing the wildtype, *slb+/-*, *abg+/-*, *abg-/-* and *abg+/-:slb+/-* genotypes; B & E: *slb-/-* proportion (6.25%); C & F: *abg* enhancement of the convergent extension defects of *slb-/-*, encompassing the *abg+/-:slb-/-* and *abg-/-:slb-/-* genotypes (12.5%). G-L: phenotypes and proportions resulting from backcrossing *abg+/-:slb+/-* carriers with identified *slb-/-* carriers. G & J: phenotypically wildtype proportion (50%), including the *slb+/-* and *abg+/-:slb+/-* genotypes; H & K: *slb-/-* proportion (25%); I & L: *abg* enhancement of the convergent extension defects of *slb-/-* (*abg+/-:slb-/-* genotype).

(6.1J). The severity of these defects reflects an enhancement of the homozygous *slb* phenotype by one copy of the *abg* gene. In the same way, we identified the C6 carrier pair at a later date, both carriers of the genotype *abg+/-:slb+/-*.

The convergent extension defects underlying these phenotypes were also divisible in the ratio 8:4:4 at 10hpf, via *in situ* hybridisation for the markers *hgg1*, *ntl* and *dlx3* (Fig. 6.2G-L). 46% of the progeny of a C2 carrier backcrossed with *slb-/-* were phenotypically indistinguishable from wildtype (6.2G & J); 30% were indistinguishable from *slb-/-* (6.2H & K; see Introduction: Fig. 1.2H & L; Appendix Two) and 24% of the genotype *abg+/-:slb-/-* exhibit mediolateral expansion of the notochord and neural plate and reduced anterior migration of the prechordal mesoderm to a greater extent than in *slb-/-* alone (6.2I & L; n=80).

As both the C2 male and C2 female were of the genotype *abg+/-:slb+/-*, the progeny of a C2 incross yielded multiple genotypes divisible by phenotype at 24hpf into several populations (see Appendix Three: C2 Incross). The largest proportion, 62.5% of the progeny of the C2 incross, was phenotypically wildtype (Fig. 6.1E & F), encompassing the wildtype, heterozygous *slb*, heterozygous *abg* and double heterozygous (*abg+/-:slb+/-*) genotypes. 18.75% were indistinguishable from *abg-/-* (6.1G & H; including *abg-/-* and *abg-/-:slb+/-* genotypes), while 6.25% were indistinguishable from *slb-/-* (6.1C & D; *slb-/-* proportion).

6.25% of the embryos generated by C2 carrier incross were of the genotype *abg+/-:slb-/-*, and as a result of the addition of one copy of the *abg* mutation, reduction in the extension of the anteroposterior axis and thickening of the yolk extension is enhanced (6.1I) relative to *slb-/-* alone (6.1C). Furthermore, failure of eyefield bilateralisation typical to *slb-/-* but almost outbred in our

slb-/- carriers (6.1D) was moderately enhanced by the addition of one copy of *abg* (6.1J). A further 6.25% of C2 incross embryos were of the genotype *abg-/-:slb-/-*, and the addition of two copies of the *abg* mutation severely enhanced the defects in axis extension and yolk extension formation (6.1K) relative to *slb-/-* (6.1C) and *abg+/-:slb-/-* (6.1I) embryos. Confirming the dose-dependent nature of this enhancement, failure of eyefield separation in *slb-/-* was severely enhanced in *abg-/-:slb-/-* embryos (6.1L) relative to *slb-/-* (6.1D) and *abg+/-:slb-/-* (6.1I) embryos.

in situ hybridisation analysis of the progeny of a C2 incross at 10hpf using the markers *hgg1*, *ntl* and *dlx3* confirmed the increasing severity of convergent extension defects in these populations (6.2A-F). 81.25% of the embryos resulting from a C2 incross were phenotypically indistinguishable from wildtype (6.2A & D), while 6.25% were indistinguishable from homozygous *slb* (6.2B & E; see Introduction: Fig. 1.2H & L). 12.5% of the embryos, corresponding to the *abg+/-:slb-/-* and *abg-/-: slb-/-* proportions of the progeny of a C2 incross, showed an enhancement of the convergent extension defects of *slb* (6.2C & F), but it was not possible to differentiate between the phenotypes given rise to by the *abg+/-:slb-/-* and *abg-/-:slb-/-* genotypes at 10hpf.

Convergent extension movements are weakly impaired in *airbag* (*abg*) embryos

abg-/- embryos are indistinguishable from their wildtype and heterozygous siblings until 24hpf, when reduced extension of the anteroposterior axis results in a shortened anteroposterior axis and a shorter, thicker yolk extension (Fig. 6.1G; Appendix Two). The body axis of homozygous *abg* embryos remains ventrally curled relative to their wildtype and heterozygous siblings, although *abg-/-* embryos do not exhibit any degree of retinal fusion (6.1H), indicating that the defects resulting from the *abg* mutation are confined to posterior regions of the body axis.

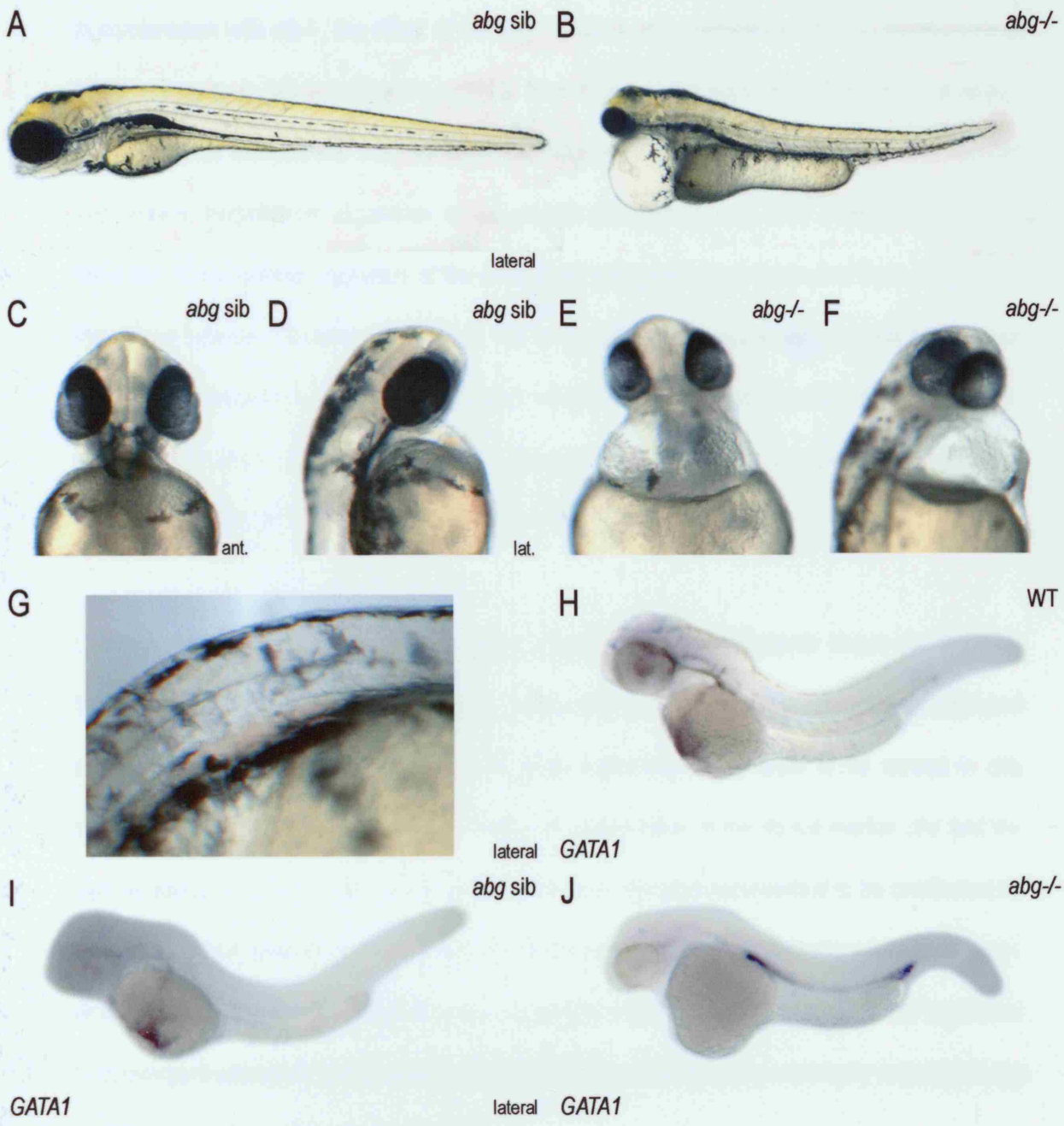

Figure 6.3

Investigation of the defects in heart and blood formation in of *airbag* (*abg*).

A & B: characteristic phenotype of the abg mutant at 72hpf. A: wildtype/heterozygous *abg* sibling; B: *abg-/-* embryo. C-F: heart morphology at 36hpf, anterior and lateral views. C & D: wildtype/heterozygous *abg* sibling; E & F: *abg-/-* embryo. G: blood pooling in major blood vessels in the trunk in *abg-/-* embryos at 36hpf; H-J: *in situ* hybridisation analysis of *GATA1* expression in haemopoeitic precursor cells in 36hpf embryos obtained from an *abg+/-* carrier incross. H: wildtype *GATA1* expression on the body of the yolk; I: expression of *GATA1* in a wildtype/heterozygous *abg* sibling embryo, indistinguishable from wildtype; J: *GATA1* expression in an *abg-/-* embryo, showing the delayed anterior migration of blood cell precursors from the ICM to the yolk as a result of the *abg* mutation.

In combination with *slb-/-*, the effect of the *abg* mutation on convergent extension movements at 10hpf is severe. *in situ* hybridisation analysis of embryos of the genotype *abg+/-:slb-/-* or *abg-/-: slb-/-* using the mesodermal markers *hgg1* and *ntl* and the neurectodermal marker *dlx3* showed that severe mediolateral expansion of the neural plate (*dlx3*) and axial mesoderm (*ntl*) and reduction in the anterior migration of the prechordal mesoderm (*hgg1*) resulted from the genetic interaction between *slb* and *abg* (6.2C, F, I & L; Appendix Two). However, analysis of *hgg1*, *ntl* and *dlx3* expression in the progeny of *abg+/-* carrier incrosses demonstrated that, in isolation, homozygous *abg-/-* embryos exhibit no detectable disturbances to convergent extension movements (6.2A, D G & J; 100% wildtype where n=59).

Likewise, expression of *papc* in the paraxial mesoderm of *abg-/-* mutants shows no deviation from wildtype (100% wildtype where n=41), while *rx3* expression in the prospective eyefield and *pax2.1* expression in the prospective MHB show patterning in the brain to be normal in *abg* embryos (100% wildtype where n=40). Finally, an examination of the dorsal marker *chd* and the ventral marker *bmp2b* in *abg-/-* embryos at 70% epiboly showed dorsoventral to be unaffected by the *abg* mutation (data not shown). The mild nature of the convergent extension defects of *abg-/-* embryos at 10hpf reflects the dependency on genetic interaction with *slb/wnt11* in the regulation of convergent extension, but could also reflect partial compensation by maternally expressed *abg* protein as our *abg* carriers are not MZ null.

The *abg* phenotype is enhanced by loss of function of *pk1a*

I examined the effect of loss of function of *pk1a* on the *abg* background to see if *abg* genetically interacts with components of pathways parallel to the non-canonical Wnt signalling pathway in the regulation of convergent extension movements (Fig. 6.4 & 6.5; Table 15; Appendix Two). I

injected a subthreshold dose of *pk1a*-MO (1ng; see Fig. 5.1B) into embryos generated by *abg*+/- carrier incross. At 24hpf, the wildtype and heterozygous *abg* proportion were indistinguishable (see Table 15), exhibiting a reduction of anteroposterior body length, ventral body curling and a mild disturbance to yolk extension development reminiscent of *pk1a* morphant embryos (6.4C) relative to uninjected siblings (6.4A). In contrast, the *abg*-/- proportion of embryos showed strongly enhanced convergent extension defects as a result of loss of function of *pk1a* (6.4D) compared to uninjected homozygous *abg* embryos (6.4B), suggestive of a genetic interaction between *abg* and *pk1a*.

An examination of mesodermal and neurectodermal markers via *in situ* hybridisation at the end of gastrulation demonstrates that the interaction between *abg* and *pk1a* severely impairs convergent extension movements. At 10hpf, expression of *ntl* in notochord, *hgg1* in the prechordal plate and *dlx3* at the border of the neural plate is indistinguishable in the wildtype, heterozygous and homozygous *abg* proportions of uninjected control embryos resulting from *abg*+/- carrier incross (6.5A & E). Although impossible to know the genotype of the injected embryos at 10hpf, the effect of loss of function of *pk1a* clearly separates the embryos into two distinct populations (Fig. 6.5; Table 15; Appendix Two). The wildtype and *abg*+/- proportions are indistinguishable from each other and constitute approximately 75% of the *pk1a*-MO-injected progeny of embryos derived from *abg*+/- carrier incrosses. Expression of *ntl* in the axial mesoderm (6.5F) and *papc* in the paraxial mesoderm (6.5N; 79% where n=14) shows convergent extension movements to be impaired in the mesoderm of wildtype and *abg*+/- embryos in which *pk1a* function is lacking. Expression of *hgg1* in the prechordal mesoderm (6.5B) shows anterior migration of the prechordal plate to be largely unaffected by loss of function of *pk1a* in *abg* siblings, although this structure is misshapen relative to wildtype embryos (6.5A). However, expression of *dlx3* at the

border of the neural plate reveals mediolateral expansion of the neural plate resulting from impaired convergent neurectodermal extension movements (6.5B & F). Expression of *rx3* in the prospective eyefield and *pax2.1* in the prospective MHB confirm the mediolateral expansion of the neurectoderm but show patterning in the future brain to be undisturbed by loss of function of *pk1a* in *abg* siblings (6.5J; 73% where n=30). These defects are reminiscent of and no worse than *pk1a* morphant embryos (see Introduction: Fig. 1.2J & N; Appendix Two).

The *abg-/-* proportion is clearly identifiable, as approximately 25% of the embryos derived from *abg+/-* carrier incrosses exhibiting severe disturbances to convergent extension movements as a result of loss of function of *pk1a*. Expression of *ntl* in the axial mesoderm shows severe mediolateral expansion of the notochord, indicating that convergent extension is acutely impaired as a result of loss of function of *pk1a* in *abg-/-* embryos (6.5G). This severe defect in mesodermal convergent extension is also evident in the paraxial mesoderm, marked by expression of *papc* (6.5O; 21% where n=14). Anterior migration of the prechordal mesoderm is also severely impaired by loss of function of *pk1a* in *abg-/-* embryos, resulting in the prechordal plate being situated posterior to the anterior border of the neural plate by the end of gastrulation (6.5C) compared to *abg* siblings injected with *pk1a*-MO (6.5B) and wildtype controls (6.5A). In the neurectoderm, expression of *dlx3* shows the neural plate to be expanded the mediolateral axis (6.5C & G) more severely than either *pk1a* morphant embryos (Fig. 1.2J & N) or *abg* siblings injected with *pk1a*-MO (6.5B & F). Reduced neurectodermal convergent extension movements are also evident in the expression of *rx3* in the future eyefield and *pax2.1* in the future MHB (6.5K; 27% where n=30). Together these results suggest that loss of function of *pk1a* on the *abg* background strongly enhances the convergent extension defects of *abg-/-* embryos but not their wildtype or *abg+/-* siblings. This suggests that *abg* not only genetically interacts with components

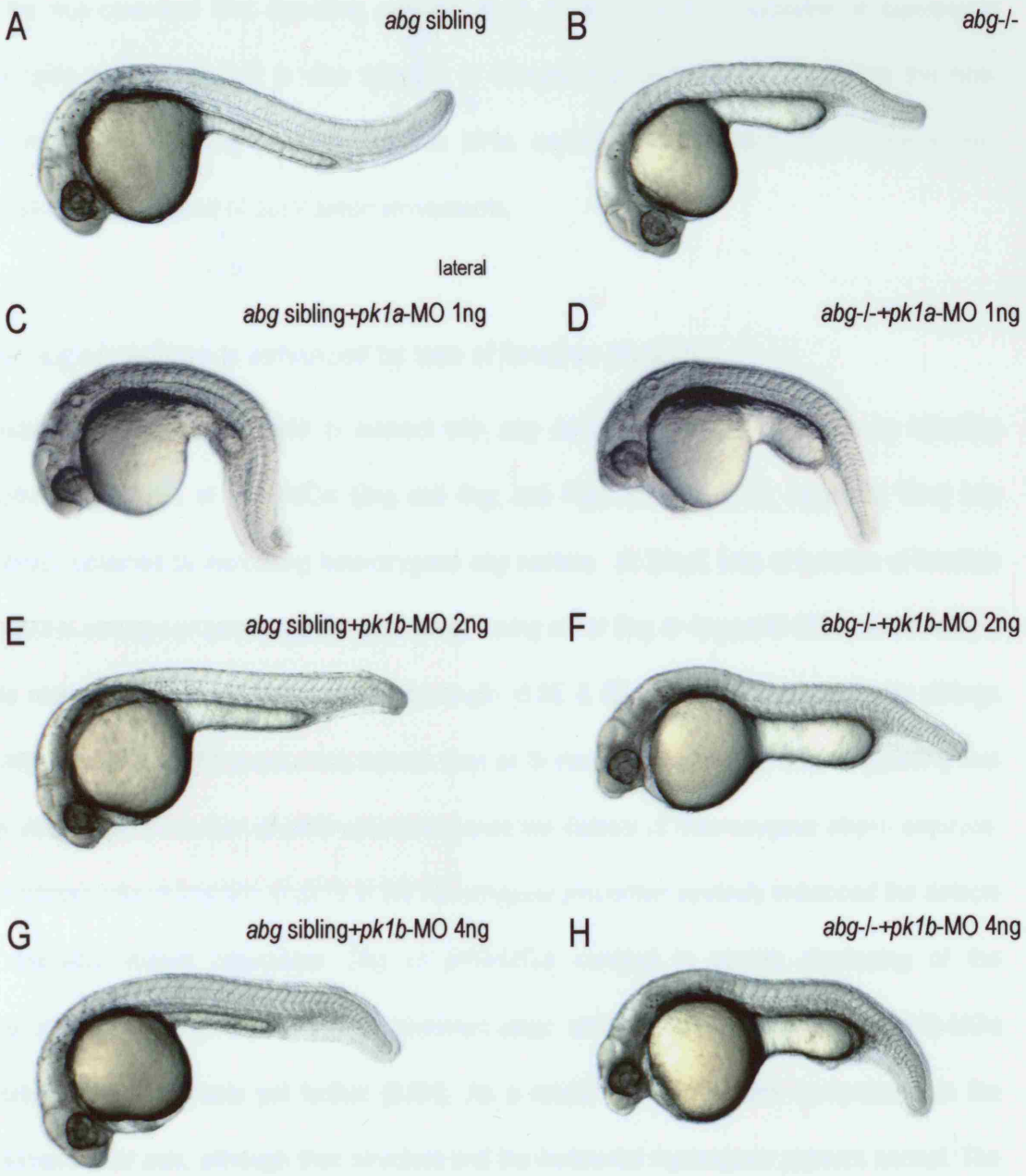

Figure 6.4

Loss of function of *pk1a* and *pk1b* enhances the *abg-/-* phenotype at 24hpf.

A: wildtype or heterozygous *abg* sibling; B: *abg-/-* embryo; C: loss of function of *pk1a* (1ng *pk1a*-MO) in a wildtype or heterozygous *abg* sibling; D: loss of function of *pk1a* (1ng *pk1a*-MO) in an *abg-/-* embryo; E: loss of function of *pk1b* (2ng *pk1b*-MO) in a wildtype or heterozygous *abg* sibling; F: loss of function of *pk1b*-MO (2ng *pk1b*-MO) in an *abg-/-* embryo; G: loss of function of *pk1b* (4ng *pk1b*-MO) in a wildtype or heterozygous *abg* sibling; H: loss of function of *pk1b*-MO (4ng *pk1b*-MO) in an *abg-/-* embryo.

of the non-canonical Wnt signalling pathway such as *wnt11* in the regulation of convergent extension movements, but is also epistatic to components of pathways parallel to the non-canonical Wnt signalling pathway such as *pk1a*, capable of modulating non-canonical Wnt signalling in the context of gastrulation movements.

The *abg* phenotype is enhanced by loss of function of *pk1b*

I examined the ability of *pk1b* to interact with *abg* during convergent extension by injecting subthreshold doses of *pk1b*-MOa (2ng and 4ng: see Figs. 3.2 and 5.1C; Appendix Two) into embryos obtained by incrossing heterozygous *abg* carriers. At 24hpf, loss of function of function of *pk1b* in wildtype or heterozygous *abg* siblings using either 2ng or 4ng *pk1b*-MOa caused only a mild reduction in the anteroposterior body length (6.5E & G) relative to uninjected *abg* siblings (6.4A), reminiscent of but not more severe than *pk1b* morphants (see Fig. 3.2), suggesting that like *pk1a*, loss of function of *pk1b* cannot enhance the defects of heterozygous *abg+/-* embryos. In contrast, loss of function of *pk1b* in the homozygous proportion severely enhanced the defects of the *abg* mutant phenotype: 2ng of *pk1b*-MOa resulted in severe shortening of the anteroposterior axis (6.4F) relative to uninjected *abg-/-* embryos (6.5B), while 4ng of *pk1b*-MOa shortened the body axis yet further (6.5H). As a result, the somites are compressed in the anteroposterior axis, although their structure and the horizontal myoseptum appears normal. The eye is smaller but complete, more anteriorly situated in the misshapen forebrain than in uninjected *abg-/-* embryos. Interestingly, the yolk extension defects of *abg* are greatly enhanced by loss of function of *pk1b*, and while extension of the anteroposterior axis is decreased by *pk1b*-MOa in a dose-dependent manner, the yolk extension phenotype is not. Enhancement of the characteristic yolk extension defect by *pk1b* in this way suggests on the *abg* background, convergent extension and the development of the yolk extension may be separated.

LOSS OF FUNCTION OF PK IN ABG: 24HPF	AMT (ng)	TOTAL	SEVERE CE DEFECTS %	MILD CE DEFECTS %	WT-LIKE %	DEAD %	MISC. %
WT or *abg+/-* + *pk1a*-MO	1	37	-	100	-	-	-
***abg-/-* + *pk1a*-MO**	1	15	100	-	-	-	-
WT or *abg+/-* + *pk1b*-MOa	2	44	-	100	-	-	-
***abg-/-* + *pk1b*-MOa**	2	12	75	-	-	25	-
WT or *abg+/-* + *pk1b*-MOa	4	39	-	100	-	-	-
***abg-/-* + *pk1b*-MOa**	4	13	77	-	-	23	
WT, *abg+/-* and *abg-/-* + *pk1a*-MO	1	29	14	86	-	-	-
WT, *abg+/-* and *abg-/-* + *pk1b*-MOa	2	41	-	-	41	-	-

Table 15. Loss of function of *pk1a* and *pk1b* on the *airbag* (*abg*) background.

These data support a strong genetic interaction between *pk1b* and *abg*. However, *in situ* hybridisation analysis of the effects of loss of function of *pk1b* on the *abg* mutant background on convergent extension movements at 10hpf show this strong interaction to be unrelated to convergent extension (Fig. 6.5; Table 15; Appendix Two). Expression of *ntl* in the axial mesoderm (6.5H) and *papc* in the paraxial mesoderm (6.5P; 96% where n=25) show mesodermal convergent extension movements to be indistinguishable from wildtype (6.5E) in the wildtype, heterozygous and homozygous proportions of embryos derived by *abg+/-* carrier incross. Likewise, anterior migration of the prechordal plate, marked by expression of *hgg1*, is indistinguishable from wildtype (6.5A) in the wildtype, heterozygous and homozygous proportions of the progeny of an *abg+/-* incross injected with 2ng *pk1b*-MOa (6.5D). The same is true of neurectodermal convergent extension: expression of *dlx3* at the border of the neural plate demonstrates that no detectable effects of convergent extension movements result from loss of function of *pk1b* in the wildtype, heterozygous or homozygous proportions of obtained by *abg+/-*

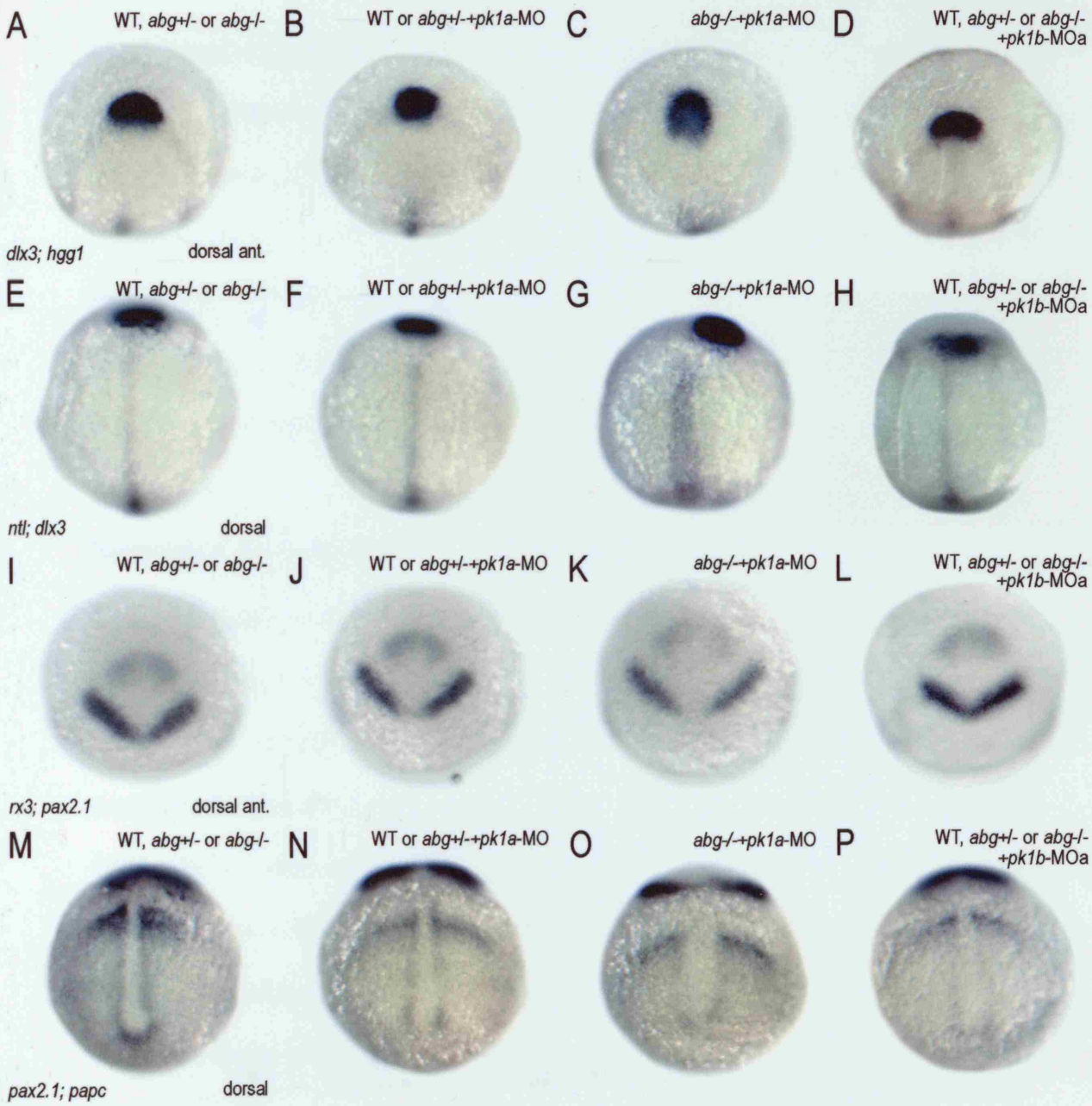

Figure 6.5

Loss of function of *pk1a*, but not *pk1b*, enhances the gastrulation phenotype of *abg-/-*..

A-H: expression of the mesodermal markers *ntl* and *hgg1* and the neurectodermal marker *dlx3* highlights convergent extension defects at 10hpf in the *abg* mutant enhanced by loss of function of *pk1a* or *pk1b*. A & E: wildtype embryo; B & F: loss of function of *pk1a* (1ng *pk1a*-MO) in wildtype or heterozygous *abg* sibling; C & G: loss of function of *pk1a* (1ng *pk1a*-MO) in *abg-/-* embryo; D & H: loss of function of *pk1b* (2ng *pk1b*-MO) in a wildtype, *abg+/-* or *abg-/-* embryo. I-L: effect of convergent extension defects on expression of *rx3* and *pax2.1* resulting from loss of function of *pk1a* or *pk1b* in the *abg* mutant at 10hpf. I: wildtype embryo; J: loss of function of *pk1a* (1ng *pk1a*-MO) in wildtype or heterozygous *abg* sibling; K: loss of function of *pk1a* (1ng *pk1a*-MO) in the *abg-/-* mutant; L: loss of function of *pk1b* (2ng *pk1b*-MO) in a wildtype, *abg+/-* or *abg-/-* embryo. M-P: expression of *papc* at 10hpf highlights convergent extension defects resulting from loss of function of *pk1a* or *pk1b* on the *abg* mutant background. M: wildtype embryo; N: loss of function of *pk1a* (1ng *pk1a*-MO) in wildtype or heterozygous *abg* sibling; O: loss of function of *pk1a* (1ng *pk1a*-MO) in *abg-/-* embryos; P: loss of function of *pk1b* (2ng *pk1b*-MO) in a wildtype, *abg+/-* or *abg-/-* embryo.

carrier incross. Similarly, expression of *rx3* in the future eyefield and *pax2.1* in the future MHB show no detectable alteration in convergent extension or patterning in wildtype, heterozygous *abg* or and homozygous *abg* embryos lacking *pk1b* function (6.5L; 100% where n=17). From this, I conclude that while both *pk1a* and *pk1b* are epistatic to *abg*, *pk1a* and *abg* function in the regulation of convergent extension movements, while *pk1b* and *abg* function in the regulation of processes either unrelated to convergent extension, or as in the case of yolk extension formation, of as yet undetermined relationship to convergent extension.

Retinotectal axon pathfinding is normal in *abg* embryos

During my search for candidate mutants to potentially complement with the *abg* mutant, I observed a marked morphological similarity between *abg-/-* embryos and the zebrafish *dackel* (*dak*) mutant, encoding the heparin sulphate (HS) synthesizing glycosyltranferase enzyme *exostosin2* (*ext2*) (Karlstrom *et al.*, 1996; Lee *et al.*, 2004; Trowe *et al.*, 1996; van Eeden *et al.*, 1996b). To investigate the potential relationship between HSPG synthesis, Slit/Robo signalling and the interaction between *abg* and *pk* homologues, I examined the effect of loss of function of *pk1a* or *pk1b*, using subthreshold doses of *pk1a*-MO (1ng) or *pk1b*-MOa (2ng; see Fig. 5.1B & C), on retinotectal axon pathfinding in 72hpf *abg-/-* embryos, visualised via the expression of acetylated tubulin.

In uninjected wildtype or heterozygous *abg* siblings, the morphology of the optic chiasm was indistinguishable from wildtype (100%, n=51). Likewise, in uninjected homozygous *abg* embryos, the optic chiasm was indistinguishable from wildtype (100%, n=35), implying that the *abg* mutation does not affect pathfinding in retinotectal axons independently. Loss of function of *pk1a* causes no detectable alteration to pathfinding in the formation of the optic chiasm in either

wildtype or heterozygous *abg* sibling embryos (100%, n=21) or in *abg-/-* embryos (100%, n=6), suggesting that the interaction between *abg* and *pk1a* is not relevant to axon pathfinding in the optic chiasm. Likewise, loss of function of *pk1b* causes no visible alteration in optic chiasm formation in either wildtype or heterozygous *abg* siblings (100%, n=6) or in homozygous *abg* mutants (100%, n=6), suggesting that the severe morphological defects resulting from the interaction between *abg* and *pk1b* are unrelated to either convergent extension or retinotectal pathfinding. Concurrently, I performed complementation analysis with dak^{to79c} and *abg*, and they failed to complement. A preliminary examination of the expression of HSPG (HSPG antibody kindly supplied by Chi-Bin Chien, Utah) in *abg-/-* embryos, indistinguishable from wildtype (data not shown), confirmed that *dak* and *abg* are unrelated.

Left/right asymmetry is normal in *abg* embryos

Given the similarity in morphological defects between *abg* mutants and *dub* morphants and that *abg* genetically interacts with the non-canonical Wnt signalling pathway of which *fz* orthologues are a component, I investigated the relationship between *abg* and *dub*. Expression of the TGF-ß *south-paw* (*spaw*) on the left side of the embryo during somitogenesis is classically considered a good indicator of left/right asymmetry in the brain and visceral organs of zebrafish (for information on the *spaw* probe, see Long *et al.*, 1998). However, as *abg-/-* embryos are indistinguishable from their siblings until 24hpf at the earliest, *spaw* expression was not a reliable option for the examination of left/right asymmetry in the progeny of *abg+/-* carrier incrosses. I also ruled out the heart as a reliable indicator of left/right asymmetry when considering a marker for an unpaired, asymmetric visceral organ at a later stage of development, as the hearts of *abg-/-* embryos are severely deformed (6.3E & F).

To investigate left/right asymmetry reliably, I instead examined the expression of *foxA3/fkd2* in the pancreas of *abg* mutant embryos. In wildtype controls at 36hpf, *foxA3/fkd2* was expressed on the left side of the body in 100% of the embryos examined (n=65). Expression of *foxA3/fkd2* on the left side of the body was evident in the majority of wildtype/heterozygous *abg* siblings generated by *abg*+/- carrier incrosses (92% where n=83). Expression of *foxA3/fkd2* on the left side of the body was also evident in the majority of homozygous *abg* embryos generated by *abg*+/- carrier incrosses (97% where n=64). Only 8% of wildtype/heterozygous *abg* siblings and 3% of *abg*-/- embryos showed *foxA3/fkd2* on the right side of the body. This suggests that, unlike *dub* morphant embryos, left/right asymmetry is unaffected by the *abg* mutation and that *dub* and *abg* are not related.

In *abg* mutants, the heart and vasculature develops abnormally

While many of the defects of *abg*-/- embryos are highly reminiscent of impaired convergent extension movements, aspects of the *abg* phenotype are not shared with established zebrafish convergent extension mutants. The characteristic pericardial oedema of *abg*-/- embryos begins to form between 24 and 30hpf (Fig. 6.3B, E & F). This oedema pulls the forming heart ventrally into straight tube (6.3E & F), abolishing looping morphogenesis and heart laterality. Over time, the beating of the heart grows weaker, and forming blood pools in the major vessels as the circulatory system fails to function (6.3G). The oedema continues to enlarge until the death of homozygous *abg* embryos at around 96hpf, while in contrast, their wildtype and heterozygous siblings continue to thrive (6.3A, C & D).

The hearts of *abg*-/- embryos are pulled by the forming oedema into a straight, median tube between 24 and 36hpf (100%, n=13), meaning it was impossible to score laterality defects in the

looping morphogenesis of the heart. Instead, I undertook a preliminary examination of markers for the development of the heart and blood via *in situ* hybridisation (Fig. 6.3). At the 18-somite stage, *cardiac myosin light chain 2* (*cmlc2*) is expressed bilaterally over the yolk in fields of myocardial precursor cells that will later migrate to the midline and form the heart. Zebrafish mutants for 3-*hydroxy-3-methylglutaryl-Coenzyme A reductase 1b* (*hmgcr1b*), a component of the isoprenoid synthesis pathway, are of great morphological similarity to *abg-/-* embryos (D'Amico *et al.*, 2007). It was recently shown that abrogation of the function of *hmgcr1b*, visualised on the *cmlc2*-eGFP transgenic background, resulted in the delayed migration of myocardial precursor cells to the midline (D'Amico *et al.*, 2007). Expression of *cmlc2* at the 18-somite stage in embryos derived from *abg+/-* carrier incrosses showed no discernible differences between the wildtype, heterozygous and homozygous proportions (100%, n=27). However, due to the poor quality of the staining, I could not satisfactorily identify both right and left progenitor populations in wildtype controls, leaving me uncertain about *cmlc2* expression in the *abg* mutant. Given the great resemblance between *hmgcr1b* and *abg* mutants, a thorough examination of *cmlc2* expression is a priority for the future characterisation of the *abg* mutant.

Expression of *scl* in haematopoietic cells migrating towards the yolk at 24hpf is indistinguishable between the wildtype, *abg+/-* and *abg-/-* progeny of an *abg+/-* carrier incross (data not shown; 100%, n=62), suggesting that *scl* expression is unaffected by the *abg* mutation. However, the expression of markers for haematopoietic differentiation downstream of *scl* is altered in *abg-/-*. At 36hpf, *GATA1* expression in wildtype control embryos is restricted to cells of ICM origin that have adopted a haematopoietic fate and migrated to the yolk to join the circulation (Fig. 6.3H; 100% where n=45; Detrich *et al.*, 1995). *GATA1* expression in precursor cells that have migrated anteriorly from the ICM to the yolk is evident in the wildtype and heterozygous populations of an

abg+/- carrier incross at 36hpf identically to wildtype controls (6.3I; 77% where n=64). Conversely in *abg-/-* embryos at 36hpf, clearly identifiable by their morphology, *GATA1* is expressed superior to the yolk extension but has not reached the body of the yolk, suggesting that the anterior migration of haematopoietic precursors from the ICM to the yolk is delayed (6.3J; 23% where n=64). This suggests that the *abg* mutation affects haematopoietic differentiation downstream of *scl* through *GATA1*. However, although aberrant haematopoiesis could account for the abnormal circulation and characteristic pericardial oedema of *abg-/-* embryos as in the case of gain of function of *scl*, the hearts of *scl* overexpressing embryos beat normally (Gering *et al.*, 1998), while the hearts of *abg-/-* mutants are severely deformed. From this, it is possible to speculate that multiple aspects of cardiovascular development are affected by the *abg* mutation.

Discussion & Conclusion

Summary

In this chapter, I introduced the *airbag* (*abg*) mutant, a novel enhancer of the convergent extension defects of the *silberblick/wnt11* (*slb*) mutant. I demonstrated the dose-dependent epistatic enhancement of *slb* by *abg* through a number of identifying genetic crosses, but also showed that in isolation, the *abg* mutation has a negligible effect on convergent extension, suggesting *abg* is dependent upon genetic interaction with *wnt11* in the regulation of convergent extension movements.

Moreover, I demonstrated that loss of function of *pk1a* or *pk1b* enhances the convergent extension and yolk extension defects of *abg-/-* embryos, suggesting that *pk1a* and *pk1b* are capable of genetically interacting with *abg*. I showed in Chapter Three of this thesis that *pk1a* and *pk1b* can cooperate in the regulation of convergent extension. However, the differences between

pk1a and *pk1b* in terms of expression and interaction with the Slit/Robo signalling pathway propose divergent functions for these *pk1* genes. This is supported by the interactions between *abg* and *pk1a* or *pk1b*: while loss of function of *pk1a* in *abg-/-* embryos affects convergent extension movements, loss of function of *pk1b* in *abg-/-* embryos results in a severe phenotype apparently unrelated to convergent extension.

In view of the morphological similarity between *abg-/-* and the *dackel* mutant, encoding a component of the HSPG synthesis pathway necessary for Slit/Robo signalling in the nervous system (Inatani *et al.*, 2003; Lee *et al.*, 2004), and given the strong functional interaction between Slit/Robo signalling and *pk* orthologues presented in Chapter Five, I investigated whether the interaction between *abg* and *pk* orthologues was related to HSPG synthesis and Slit/Robo signalling, but this was not the case. Despite considerable morphological similarities between *abg-/-* and the *dub* morphant, in which ciliogenesis in Kupffer's Vesicle is disturbed with consequences for left/right asymmetry, and despite the discovery of corresponding defects in *fz2* morphants (Oishi *et al.*, 2006), no detectable disturbances to left/right asymmetry were evident in *abg-/-* embryos, suggesting that *abg* is also unrelated to *dub.*

Further to the convergent extension defects resulting from loss of function of *wnt11* or *pk1a* in combination with the *abg* mutation, homozygous *abg* embryos exhibit severe cardiovascular defects that prove lethal at 96hpf. This combination of defects is unique amongst zebrafish convergent extension mutants, although convergent extension and cardiogenesis are not unrelated, as both convergent extension movements and the migration of bilateral myocardial precursor cells to the midline in the formation of the heart are disrupted in the mutant *miles apart* (*mil*) (Matsui *et al.*, 2005; Matsui *et al.*, 2006). However, alteration of the expression of

haematopoietic markers, coupled with abnormal circulation of the blood, suggests that the cardiovascular defects of *abg-/-* are multi-faceted.

Discussion

The impaired convergent extension movements and incomplete eyefield separation characteristic of the *silberblick/wnt11* (*slb*) mutant are of variable severity within and between generations, suggesting *silberblick* is sensitive to enhancement or suppression by different genetic backgrounds. An ENU mutagenesis screen was designed and undertaken in collaboration by the Heisenberg and Tada labs in 2002 to identify potential enhancers and suppressors of the *slb* phenotype (see Materials & Methods: Fig. 2.1; Enhancers of *slb*: screen strategy). The screen isolated a number of enhancers and suppressors of the *slb* phenotype: in this chapter, I introduced *enhc132*, a dominant enhancer of the *silberblick* phenotype provisionally named *airbag* (*abg*) because of its characteristic pericardial oedema. *abg-/-* embryos do not exhibit convergent extension defects independently of loss of function of known regulators of gastrulation movements such as *wnt11* or *pk1a*, but do display severe defects in the formation of the yolk extension, the heart and the circulatory system, a combination of defects unique amongst established zebrafish convergent extension mutants. Discovering the relationship between the complex phenotype of *abg-/-* embryos and the control of convergent extension movements could further our understanding of the genetic interactions underpinning cell behaviour during convergent extension. Potentially, disruption of the migration of bilateral populations of myocardial precursor cells to midline in the formation of the heart and the anterior migration of haematopoietic cells to the yolk to join the circulatory system in *abg-/-* embryos could provide evidence that *abg* participates in the regulation of other all instances of directed cell migration during embryogenesis.

abg was identified on the basis of its interaction with a component of the non-canonical Wnt signalling pathway in the regulation of convergent extension movements, although *abg-/-* embryos are phenotypically dissimilar to every zebrafish Wnt/PCP mutant identified to date. As *abg-/-* has little effect on convergent extension movements alone, it must be concluded that the function of *abg* during convergent extension is non-canonical Wnt signalling-dependent: however, the mild phenotype may reflect compensation by maternal contribution of the gene, as our *abg* carriers are not MZ null. Loss of function of *pk1a* is known to enhance the convergent extension defects of the *slb* mutant (Carreira-Barbosa *et al.*, 2003). Stbm and Pk1a are thought to function in a pathway parallel to non-canonical Wnt signalling, capable of genetically interacting in the modulation of non-canonical Wnt signalling during convergent extension in a manner considered non-canonical Wnt-dependent (Carreira-Barbosa *et al.*, 2003). I showed in this chapter that loss of function of *pk1a* in *abg-/-* embryos strongly enhances their convergent extension defects, implying that *abg* can interact with *pk1a* in the context of the regulation of convergent extension movements. Moreover, Tada lab undergraduate project student Christine Yang demonstrated in her dissertation in 2004 that loss of function of *stbm* on the *abg* mutant background enhanced the convergent extension defects of *abg-/-* embryos (data not shown). This evidence proposes a non-canonical Wnt-dependent role for *abg* in the regulation of convergent extension movements, bridging non-canonical Wnt signalling and non-linearly related modulators of non-canonical Wnt signalling situated in a parallel pathway. Dissimilarly to the *trilobite/stbm* (*tri*) mutant background however, where loss of function of *pk1a* is sufficient to enhance the convergent extension defects of *tri+/-* embryos and effectively abolish the effects of the single remaining copy of *stbm* (Carreira-Barbosa *et al.*, 2003), loss of function of *pk1a* on the *abg* mutant background appears insufficient to enhance the *abg+/-* phenotype. This suggests that, unlike Stbm, Abg does not function in a linear pathway with Pk1a in the context of the regulation of convergent extension movements.

The ability of *abg* to interact with *pk1a* in the context of convergent extension raised the question of whether *abg* can also participate in other processes that *pk* orthologues are known to regulate. Pk1a and Stbm are also thought to function Wnt and Dsh-independently in the regulation of facial (nVII) branchiomotor neuron migration in the hindbrain (Carreira-Barbosa *et al.*, 2003), although recent evidence implicating Frizzled3a (Fz3a) and Flamingo2 (Fmi2/Celsr2) in the regulation of branchiomotor neuron migration suggests that the Wnt-independent status of this process may have to be reconsidered (Wada *et al.*, 2006). Loss of function of *pk1b*, using *pk1b*-MOa and *pk1b*-MOb in combination, blocks the tangential migration of branchiomotor neurons (personal communication, V. Prince; Rohrschneider *et al.*, 2007), as does loss of function of *pk1a* (Carreira-Barbosa *et al.*, 2003). While a genuine genetic interaction is evident between *abg* and *pk1b* at 24hpf, no disturbance to convergent extension movements is visible at 10hpf, suggesting that this interaction affects processes outside the context of convergent extension. Furthermore, the divergent nature of the interactions of *pk1a* and *pk1b* with the Slit/Robo signalling pathway presented in Chapter Five of this thesis suggested that while *pk1a* function relates more specifically to the regulation of convergent extension movements, perhaps *pk1b* mediates the pleiotropic functions of Slit/Robo signalling outside the context of gastrulation movements. Analysis of the participation of *abg* in concert with *pk1a* or *pk1b* in the regulation of branchiomotor neuron migration in order to clarify the relationship between *abg*, *pk1a*, *pk1b* and *stbm* is necessary in the immediate future.

To gain insight into the contribution of *abg* to non-canonical Wnt signalling and its modulators in the control of cell behaviour during convergent extension, I compared and attempted to complement *abg* mutants with mutants or morphants that exhibited similar phenotypes. The *dackel* (*dak*) mutant was originally identified in the 1996 Tübingen screen for mutants in which fin

development and retinotectal axon pathfinding are disrupted (Lee *et al.*, 2004; Karlstrom *et al.*, 1996; Trowe *et al.*, 1996; van Eeden *et al.*, 1996b). *dak* encodes the heparin sulphate (HS) synthesizing glycosyltranferase enzyme Exostosin2 (Ext2) and exhibits defects in the development of the jaw and branchial arches reminiscent of *ppt/wnt5b* (Schilling *et al.*, 1996) and impaired retinotectal axon guidance (Lee *et al.*, 2004), significant given the interaction between the axon pathfinding genes *slit* and *robo* and *pk* orthologues presented in Chapter Five of this thesis. HSPGs are known to be important for axon sorting in the optic tract and this role is considered to be dependent upon Slit/Robo signalling in zebrafish as in *Drosophila* (Inatani *et al.*, 2003; Lee *et al.*, 2004). Due to the parallels between *dak* and Wnt/PCP mutants, I investigated expression of HSPG protein in *abg-/-* embryos via antibody staining, but found HSPG expression unaltered in *abg* mutants (data not shown). Concurrently, I undertook complementation analysis of *abg* and *dak* and found that these mutants did complement one another (data not shown). This suggested that the function of *abg* is unrelated to Slit/Robo and HSPGs, and a relationship between zebrafish *pk* orthologues, Slit/Robo signalling and *abg* in the regulation of convergent extension remains unclear.

The *duboraya* (*dub*) morphant, encoding a zebrafish homologue of a mammalian phosphorylation-dependent cytoskeletal reorganisation gene, develops a large pericardial oedema reminiscent of a Japanese lantern after which it is named (Oishi *et al.*, 2006). Loss of function of *dub* disrupts ciliogenesis in Kupffer's Vesicle, a ciliated organ responsible for the flow of fluid bearing determinants of left-right asymmetry around the early embryo (Oishi *et al.*, 2006). As a result of the defective cilia generated in the Kupffer's Vesicle of *dub* morphant embryos, left-right asymmetry is disturbed with consequences for the morphogenesis of the heart and visceral organs (Oishi *et al.*, 2006). Reorganisation of the actin cytoskeleton in the generation of cell

polarity and migratory behaviour during gastrulation is a fundamental cellular response to the genetic regulation of convergent extension movements, although the exact mechanisms by which the non-canonical Wnt signalling and parallel modulating pathways communicate with cytoskeletal regulators such as GTPases remains unclear (Eaton *et al.*, 1996; Krasnow & Adler, 1994; Lee & Adler, 2002; Wong & Adler, 1993). Despite the discovery that left-right asymmetry is aberrant in *fz2* morphant embryos, causing defects in somitogenesis and organogenesis as a consequence (Oishi *et al.*, 2006), left-right asymmetry is normal in *abg-/-* embryos, meaning that the *abg* and *dub* phenotypes are unrelated. However, the link between impaired convergent extension movements and organogenesis is a valid one when it is considered that the zebrafish mutant *miles-apart* (*mil*) exhibits defects in cardiogenesis and convergent extension movements (Matsui *et al.*, 2005; Matsui *et al.*, 2006).

The *abg* mutant shares considerable morphological similarities with *hmcgr1b* mutants at 24hpf, including severe cardiovascular abnormalities and a characteristic pericardial oedema (D'Amico *et al.*, 2007). Hmcgr1b is also maternally provided, making it a good candidate for *abg*, as the mild convergent extension phenotype of *abg-/-* embryos at 10hpf could reflect compensation by maternally contributed protein. *hmcgr1b*, a component of the isoprenoid synthesis pathway, lies upstream of post-translational protein prenylation critical to the subcellular localisation of cytoskeletal regulators such as Rho (D'Amico *et al.*, 2007). Loss of function of *hmcgr1b* causes Rho to be mislocated to the cytoplasm instead of the cell surface membrane, with the result that the migration of bilateral populations of myocardial precursor cells to the midline in the formation of the primitive heart tube is delayed, causing severe defects in heart morphology (D'Amico *et al.*, 2007). Prenylation is also known to be significant in the migration of primordial germ cells from their site of origin to the developing zebrafish gonad (Thorpe *et al.*, 2004). Rab-GTPases, known

to function in vesicular transport, rely on prenylation by *Rab escort proteins* (*REP*s) to function (Zerial & McBride, 2001: cited in Starr *et al.*, 2004). Degeneration of the mechanosensory hair cells of the vestibular system, the product of vertebrate PCP signalling in the inner ear, results if the prenylation of Rab-GTPases by REPs is abolished, as in the zebrafish *choroideremia* (*chm*) mutant (Davies *et al.*, 2005; Lewis & Davies, 2002; Starr *et al.*, 2004). Compellingly, Wnt11 and Rab5c interact in the vesicular transport of E-cadherin (Ulrich *et al.*, 2005). Although evidence demonstrating the asymmetric subcellular localisation of vertebrate Wnt/PCP proteins during CE is lacking, the interaction between Wnt11 and Rab5c, coupled with the significance of protein prenylation both to Rab function and to the directed cell migration of myocardial precursors and primordial germ cells, suggests that non-canonical Wnt signalling regulates convergent extension movements by controlling vesicular trafficking and subcellular localisation of Wnt/PCP proteins or their downstream effectors, such as the cytoskeletal regulator Rho (Ulrich *et al.*, 2005; Starr *et al.*, 2004; Thorpe *et al.*, 2004). Indeed, zebrafish *pk* orthologues bear a CIIS prenylation motif at their C-terminus: while it is known that the CIIS motif does not contribute to the function of *pk* orthologues in the regulation of convergent extension movements (Veeman *et al.*, 2003), it has yet to be elucidated whether this prenylation motif targets *pk* orthologues to subcellular locations.

Due to constraints of time, only a preliminary examination of the expression of cardiovascular markers in *abg-/-* embryos was possible. This analysis did however reveal that the anterior migration of haematopoietic precursor cells from their point of origin in the ICM to the yolk in order to join the circulatory system was delayed in *abg-/-* embryos, supported by the observation that the circulation of the blood in *abg-/-* embryos is weak, leading to the dorsal pooling of blood *in vivo*. The bHLH transcription factor *scl* is expressed in haematopoietic precursor cells, and gain of function of *scl* was shown to cause malfunction of the circulatory system and a large pericardial oedema, finally resulting in the death of *scl* overexpressing embryos at 6-7dpf (Gering *et al.*,

1998). However, although the defects of *scl* overexpressing embryos are superficially reminiscent of *abg-/-* embryos, gain of function of *scl* did not result in defects in the formation of the heart (Gering *et al.*, 1998). A more thorough investigation of the defects in the cardiogenesis of the *abg* mutant is necessary in the future, particularly in light of the great morphological similarity between *abg-/-* embryos and the *hmcgr1b* mutant. Multiple processes requiring directed cell migration, including convergent extension, heart tube formation and blood cell precursor migration, are disrupted in homozygous *abg* mutants: in view of the fact that prenylation is key to vesicular transport (Zerial & McBride, 2001: cited in Starr *et al.*, 2004) and the migration of primordial germ cells in zebrafish (Thorpe *et al.*, 2004), that non-canonical Wnt signalling regulates vesicular transport in the orchestration of convergent extension, and that *abg* is capable of undergoing genetic interaction with *pk* orthologues bearing C-terminal prenylation motifs, there is considerable evidence to suggest that future characterisation and mapping of the *abg* mutation will significantly increase our understanding of the regulation of cell movements during embryogenesis.

Chapter Seven

General Discussion & Future Directions

Discussion:

pk1b: a novel *pk1* gene with multiple functions during zebrafish embryogenesis

Asymmetric subcellular localisation of the *Drosophila* PCP protein Prickle (Pk) at the distal vertex of wing hair cells restricts Fz activity and downstream actin prehair formation to the proximal vertex of wing hair cells in a manner that non-autonomously propagates asymmetry in the plane of the epithelium, generating a polarised array of wing hairs (Axelrod, 2001; Strutt, 2001; Tree *et al.*, 2002). Homologues of *Drosophila* PCP genes are evolutionarily conserved in vertebrates (Carreira-Barbosa *et al.*, 2003; Formstone & Mason, 2005; Jessen *et al.*, 2002; Sumanas *et al.*, 2001; Sumanas & Ekker, 2001; Veeman *et al.*, 2003; Wallingford, 2000; Wallingford *et al.*, 2002b). They function in the regulation of processes analogous to the establishment of PCP in the eye, wing and thorax of *Drosophila*, such as the generation of polarised arrays of mechanosensory stereocilia in the mouse and chick inner ear (Davies *et al.*, 2005; Lewis & Davies 2002). They also function in the regulation of processes that superficially appear less clearly related to PCP but are in fact reliant upon the generation and propagation of cell polarity integral to PCP, such as the directed migration of neurons in the developing nervous system or mesodermal and neurectodermal cells during gastrulation.

The novel zebrafish *pk1* gene *pk1b* was cloned from a gastrula cDNA library by Masa Tada in 2005 according to the protocol described in Carreira-Barbosa *et al.*, 2003. Pk1b is of great structural similarity to Pk1a in terms of the conserved PET/LIM domains but bears a longer N-terminus region

and is divergent at the C-terminus. The expression of *pk1b* is more reminiscent of *pk2* than *pk1a*, and dissimilarly to the dynamic shift in expression of *pk1a* from midline mesoderm at 90% epiboly to a conspicuous absence from the midline at tailbud, *pk1b* expression remains axial during late gastrulation (Thesis: Carreira-Barbosa F., 2005; Carreira-Barbosa *et al.*, 2003; Veeman *et al.*, 2003). This contrast extends to the function of *pk1b*: gain of function of *pk1b* has no effect on convergent extension movements, whereas gain of function of *pk1a* causes severe convergent extension defects (Carreira-Barbosa *et al.*, 2003). Likewise, loss of function of *pk1b* has an almost negligible effect on convergent extension, while loss of function of *pk1a* moderately compromises convergent extension movements (Carreira-Barbosa *et al.*, 2003).

pk1a and *pk1b* appear functionally redundant in the regulation of convergent extension movements, in contrast to *pk1a* and *pk2*, although cross-rescue will be necessary to confirm this (Carreira-Barbosa *et al.*, 2003; Veeman *et al.*, 2003). However, evidence of epistasis between *pk1b* and established zebrafish convergent extension mutants presented in this thesis proposes divergent functions for Pk1a and Pk1b in zebrafish development. Loss of function of *pk1a* strongly enhances the convergent extension defects of *silberblick/wnt11* (*slb*) suggesting that Pk1a functions Wnt-dependently in the regulation of convergent extension movements (Carreira-Barbosa *et al.*, 2003). Loss of function of *pk1a* also enhances convergent extension and branchiomotor neuron migration defects in the *trilobite/stbm* (*tri*) mutant, suggesting that Pk1a modulates convergent extension movements in collaboration with Stbm in a Wnt-dependent manner, and branchiomotor neuron migration in collaboration with Stbm through a divergent pathway (Carreira-Barbosa *et al.*, 2003). Loss of function of *pk1b* mildly enhances the convergent extension defects *silberblick* and *trilobite*, confirming a Wnt-dependent function in the regulation of convergent extension. However, loss of

function of *pk1a* in heterozygous *trilobite* embryos is sufficient to negate the function of the remaining functional copy of Stbm (Carreira-Barbosa *et al.*, 2003), while loss of function of *pk1b* cannot enhance the defects of *tri+/-* embryos. Although loss of function of *pk1b* purportedly abolished branchiomotor neuron migration in the hindbrain (personal communication, V. Prince; Rohrschneider *et al.*, 2007), loss of function of *pk1b* in the *off-road/fmi2/celsr2* (*ord*) mutant does not support a functional interaction between *pk1b* and *fmi2*, both of which are known to function in the regulation of branchiomotor neuron migration (although it is yet to be elucidated whether *pk1b* and *fmi2* function cooperatively in this context) (Formstone & Mason, 2005; Wada *et al.*, 2006). Conversely, loss of function of *pk1a*, known to regulate branchiomotor neuron migration in collaboration with Stbm (Carreira-Barbosa *et al.*, 2003), strongly enhances the convergent extension defects of *ord-/-* mutants. If *pk1b* genuinely functions in the regulation of branchiomotor neuron migration, then it is through a separate pathway to Pk1a, Stbm and Fmi2. In conclusion, *pk1b* function contrasts greatly with that of *pk1a* during the regulation of convergent extension movements.

Slit/Robo signalling in convergent extension and beyond

Zebrafish orthologues of the *Drosophila* axon pathfinding genes *slit* and *robo* are expressed during gastrulation, before there are axons to guide. Gain of function of *slit2* was shown to induce severe convergent extension movements and cyclopia in zebrafish (Yeo *et al.*, 2001), defects highly reminiscent of zebrafish convergent extension mutants such as *silberblick/wnt11* (*slb*) (Heisenberg *et al.*, 1996; Heisenberg, Tada *et al.*, 2000), suggesting a role for Slit/Robo signalling in the regulation of cell migration during gastrulation analogous to the evolutionarily conserved role of Slit/Robo signalling in the nervous system of *Drosophila* and vertebrates (Brose *et al.*, 1999; Challa *et al.*,

2005; Fricke *et al.*, 2001; Kidd *et al.*, 1998a, Kidd *et al.*, 1998b; Hutson & Chien, 2002; Rothberg *et al.*, 1988; Seeger *et al.*, 1993; Tear *et al.*, 1996).

The role of the Slit ligand has diversified over the course of evolution (Wang *et al.*, 1999), but Slit function independently of the Robo receptor was eliminated by evidence of functional interactions between the Slit2 ligand and Robo2 and Robo3v2 receptors in the context of convergent extension. However, divergent phenotypes resulting from the interaction between Slit2 and Robo2 and Slit2 and Robo3v2, coupled with the fact that overexpression of *robo3v1* yielded convergent extension defects dissimilarly to an authentic receptor, suggested that the function of the zebrafish Robo3 variants Robo3v1 and Robo3v2 contrasts with that of authentic receptors such as Robo2 in the context of the regulation of convergent extension movements. Indeed, loss of function of *robo3v2* yielded a combination of movement and patterning defects, suggestive of multiple roles during zebrafish development. Finally, the morphological similarities between *slit2* overexpressing embryos and abrogation of Robo3v2 function using the Robo3v2(ECD/TM)-GFP construct suggested that Robo3v2 functions to antagonise inappropriate Slit/Robo signalling, much as Comm functions to repress inappropriate Slit/Robo mediated repulsion of axons during commissure formation in the *Drosophila* CNS (Tear *et al.*, 1996). This is especially interesting in view of the structural similarities between Robo3v2 and Rig-1, a mammalian *robo3* orthologue thought to function analogously to *Drosophila* Comm during the development of the mouse CNS (Camurri *et al.*, 2004; Sabatier *et al.*, 2004).

Taken together, these facts suggest that Slit/Robo signalling functions analogously to its function in the nervous system in the regulation of convergent extension movements during zebrafish gastrulation. Moreover, the divergent functions of the Robo3v2 receptor suggest that, as in the

mouse, zebrafish get around the fact that no vertebrate homologues of Comm exist by adapting the function of a Robo receptor to repress Slit/Robo signalling where appropriate. Similarly to Comm expression in the CNS midline of *Drosophila*, the restricted expression of Robo3v2 during gastrulation could provide insight into the boundaries within which Slit/Robo signalling is free to act upon migrating cells during convergent extension and beyond which Slit/Robo signalling is inhibited (see Dickson & Gilestro, 2006).

However, the severe phenotype resulting from co-overexpression of *robo3v2* and *slit2* is suggestive of a functional interaction between Robo3v2 and the Slit2 ligand, possibly separable from the role of Robo3v2 as an antagonist of canonical Slit/Robo signalling and more related to the pleiotropic functions of Robo3v2, evident in *robo3v2* morphant and *pk1b:slit1a*, *pk1a:robo3v2* and *pk1b:robo3v2* double morphant embryos. Overexpression of two very different Robo constructs suggested that the multiple roles of Robo3v2 are mediated by different parts of the Robo3v2 protein. The Lyn-Robo3(ICD)-GFP construct artificially tethers the intracellular domain common to both variants of Robo3 to the cell membrane, abolishing both the capability to bind the Slit ligand and to move between intracellular compartments, aspects critical to the evolutionarily conserved function of Robo receptors in the nervous system of *Drosophila* and vertebrates (Brose *et al.*, 1999; Challa *et al.*, 2005; Fricke *et al.*, 2001; Kidd *et al.*, 1998a, Kidd *et al.*, 1998b; Hutson & Chien, 2002; Rothberg *et al.*, 1988; Seeger *et al.*, 1993; Tear *et al.*, 1996). The severe phenotype that results is reminiscent of *knypek/trilobite* double mutant embryos, considered the most severe convergent extension mutants (Marlow *et al.*, 1998). This suggests that the intracellular domain of Robo3v2 and the ability of Robo3v2 protein to move freely inside the cell are of particular significance to the element of Robo3v2 function related to the regulation of convergent extension movements. The

Robo3v2(ECD/TM)-GFP construct effectively tethers the extracellular domain of Robo3v2 to the membrane on the outside of the cell, free to bind but unable to transduce the Slit signal. The severe phenotype that results, a combination of convergent extension defects and patterning defects in the brain, eye and somites, suggests that the extracellular domain of Robo3v2 and transduction of the Slit signal is important for both the convergent extension and pleiotropic roles of Robo3v2.

The multi-faceted collaboration between *pk* orthologues and Slit/Robo signalling

Divergence in the interaction of *pk1* genes with components of the Slit/Robo signalling pathway proposes a difference in the focus of *pk1a* and *pk1b* function during embryogenesis. Loss of function of *pk1b*, in combination with loss of function of *slit1a* and *robo3v2*, causes severe disturbances to convergent extension movements and specific patterning events in the development of the eye and somites. Abrogation of *robo3v2* function using the Robo3v2(ECD/TM)-GFP construct results in a phenotype highly reminiscent of *slit2* overexpression, suggesting that *robo3v2* acts in opposition to canonical Slit/Robo signalling during gastrulation. However, the genuine functional interaction between Robo3v2 and Slit2 evident from gain of function analysis, coupled with the similarity between *pk1b:slit1a* and *pk1b:robo3v2* double morphants, suggests that *robo3v2* is capable of functionally interacting with *slit1a* and *slit2* in contexts separate to the antagonism of authentic Robo receptors during convergent extension. Insight into these developmental processes and their consequences upon, for instance, the development of the eye and somites, can perhaps be gained through an examination of the expression of *robo3v2* later in development (Challa *et al.*, 2005).

pk1a is known to regulate the migration of branchiomotor neurons in the hindbrain, and loss of function of *pk1a* enhances both the convergent extension and branchiomotor neuron migration defects of the *trilobite/stbm* (*tri*) (Carreira-Barbosa *et al.*, 2003) and *off-road/fmi2/celsr2* (*ord*) mutants (the effect of loss of function of *pk1a* on branchiomotor neuron migration in *ord-/-*: personal communication, M. Tada). Conversely, *pk1b* does not interact with *trilobite* identically to *pk1a*, and does not visibly interact with the *off-road* mutant in the context of gastrulation movements, despite evidence that loss of function of *pk1b* blocks the tangential migration of branchiomotor neurons (personal communication, V. Prince; Rohrschneider *et al.*, 2007). It is surprising therefore that epistasis between *pk1a* and the axon pathfinding genes *slit* and *robo* is restricted to the regulation of convergent extension movements while epistasis between *pk1b*, *slit* and *robo* appears to influence many developmental processes. In view of this however, the divergent nature of the interaction between *pk1b* and the *silberblick*, *trilobite* and *off-road* mutants seem less surprising, the strong functional interaction between *pk1b*, *slit1a* and *robo3v2* revealing the focus of *pk1b* function to be outside the context of gastrulation. The great morphological similarities between *pk1b:slit1a*, *pk1a:robo3v2* and *pk1b:robo3v2* double morphants suggests that Slit1a, Slit2, Pk1b, and to a much lesser extent Pk1a, are involved in the regulation of processes unrelated to convergent extension dependent upon the extracellular domain of Robo3v2. Indeed, *pk1b* expression was recently observed in retinal ganglion cells (RGCs) later in development, where *robo2* also functions in axon guidance (personal communication, M. Carl; Hutson & Chien, 2002). Zebrafish *pk* orthologues are cytoplasmic proteins (Carreira-Barbosa *et al.*, 2003; Veeman *et al.*, 2003), suggesting that they might act downstream of the Robo3v2 receptor to transduce the Slit signal outside the context of the regulation of gastrulation movements.

Pk1b and Slit/Robo signalling: potential interaction with Hedgehog signalling

The next step is to discover the developmental context of the epistatic interaction between *pk1b*, *slit1a* and *robo3v2*. *robo3v2* morphant embryos and *pk1b:slit1a*, *pk1a:robo3v2* and *pk1b:robo3v2* double morphant embryos exhibit disturbances to the patterning of the brain, eye and somites extra to convergent extension defects. In the fly, Hh signalling regulates boundary formation during segmentation by interrupting repression of the Smoothened (Smo) receptor by the Patched (Ptc) transmembrane protein, transduction of Hh activating downstream Gli transcription factors (van den Heuvel & Ingham, 1996; Hammerschmidt *et al.*, 1997). Likewise, vertebrate components of the Hh signalling pathway act through Smo/Ptc and Gli transcription factors, but the roles of Hh signalling have diversified considerably over the course of evolution to include patterning within the central nervous system and a variety of other tissues throughout embryogenesis (Baressi *et al.*, 2000; Chen *et al.*, 2001; Hammerschmidt *et al.*, 1997). Vertebrate Hh signalling also functions in the regulation of directed cell migration, thought to be mediated by a pathway distinct from Ptc/Smo: cells in the ventral neural tube experience higher levels of Hh and as a result behave cohesively and do not migrate; conversely, cells in the dorsal neural tube such as neural crest cells are subject to lower levels of Hh, correlating with migratory behaviour (Testaz *et al.*, 2001). Highly reminiscent of the *robo3v2* loss of function and *pk1b:slit1a*, *pk1a:robo3v2* and *pk1b:robo3v2* double morphant phenotypes, U-shaped somites, reduction and ventral curling of the anteroposterior axis, thickening of the yolk extension and partial fusion of the retinae result from mutations in the Hedgehog (Hh) signalling pathway in zebrafish (Baressi *et al.*, 2000; Chen *et al.*, 2001). Moreover, it was demonstrated that abrogation of Hh signalling disrupts the development of the *retinal pigment epithelium* (*RPE*) of the eye in *Xenopus* (Perron *et al.*, 2003).

In the past, I investigated the effect of loss of function of *pk1a* in the zebrafish *slow-muscle-omitted* (*smu*) mutant, but despite evidence that certain LIM proteins interact with the Hh signalling pathway (Bach, 2000; Dawid *et al.*, 1998; Hunter & Rhodes, 2005), I found no convincing evidence to suggest that Pk1a and Hh signalling interact (data not shown). Given that the interaction between *pk1b* and Slit/Robo signalling affects eye and somite development while the interaction between *pk1a* and Slit/Robo signalling relates to the regulation of convergent extension, it would perhaps be more relevant to investigate the potential interaction between *pk1b* and the Hh signalling pathway. However, the epistasis between *pk* orthologues and Slit/Robo signalling was discovered on the basis of their function in the regulation of multiple instances of directed cell migration during embryogenesis: if Hh signalling influences neural crest migration through a pathway independent of Patched and Smoothened, then an alternative approach to the loss of function of *pk* orthologues on the *smoothened* mutant background may be necessary to satisfactorily re-investigate the interaction between *pk* orthologues and Hh signalling.

airbag and the interaction between Pk1b, Slit/Robo signalling and Hh signalling

The interaction between *pk1b* and the novel enhancer of the *silberblick* phenotype, *airbag* (*abg*), may shed light on the relationship between the putative *pk1b/slit1a/robo3v2* pathway in eye and somite development and Hh signalling. *abg-/-* embryos bear considerable morphological similarity to the zebrafish 3-*hydroxy-3-methylglutaryl-Coenzyme A reductase 1b* (*hmcgr1b*) mutant, in which the directed migration of myocardial precursor cells to the midline during heart tube formation is delayed due to disrupted protein prenylation and consequential mislocalisation of the cytoskeletal regulator, Rho (D'Amico *et al.*, 2007). Similarly, abolishing the prenylation of the vesicular transport proteins

Rab-GTPases by Rab escort proteins (REPs) causes localisation of Ras and Rho to the cytoplasm instead of the cell membrane, resulting in the degeneration of stereocilia in the vertebrate inner ear (Starr *et al.*, 2004). Hh signalling also relies upon intracellular trafficking: Hh activity recruits the Smo receptor from vesicles within the cell to the cell membrane, and disruption of the trafficking of Smo by dominant negative Rab-GTPases perturbs Hh signalling (Zhu *et al.*, 2003). More recently, it was suggested that *hmgcr* is responsible for sequestering Hh in intracellular vesicles, thereby modulating Hh signalling in the regulation of germ cell migration in *Drosophila* (Deshpande & Schedl, 2005). If *abg* is in fact related to the *hmcgr1b* mutant then the significance of protein prenylation to vesicular trafficking in the context of the regulation of convergent extension movements will be undisputed: although the *abg-/-* phenotype is dissimilar to Hh signalling mutants, the speculative relationship between pleiotropic functions of *pk1b/slit1a/robo3v2* in the patterning of the eye and somites and Hh signalling may prove a reality.

Future Directions:

Constraints of time unfortunately mean that many avenues remain unexplored. The largest deficiency of this thesis is the absence of quantification, and future characterisation of *pk1b* function, the role of Slit/Robo signalling in the regulation of convergent extension and the epistatic interaction between non-canonical Wnt signalling and the Slit/Robo signalling pathway must overcome this deficiency. In an attempt to validate my qualitative observations, I have constructed a database of phenotypic characteristics of the mutants and morphants presented in this thesis (see Appendix Two) but in the future, it will be necessary to implement measurement of morphological characteristics in the collection of data. Phenotypic aspects such as anteroposterior body length, angle of extension of the

head, angle of body axis or tail kinking and curling could be collected by examination of gross morphology at 24hpf. 3- and 4-Dimensional confocal microscopy could yield quantifiable information on the dimensions of and cells comprising the notochord, neural plate and prechordal plate and the cell movements underlying the morphogenesis of these features (see Materials & Methods: *in vivo* Time-lapse Movies for details): however, measurement of the dimensions these features is possible immediately in 10hpf embryos stained via *in situ* hybridisation.

In the following sections, I outline specific directions for progression in the continued characterisation of *pk1b*, investigation of the role of Slit/Robo signalling during gastrulation and the relationship between this signalling pathway and non-canonical Wnt signalling, and identification of the novel enhancer of *silberblick/wnt11* (*slb*), *airbag* (*abg*).

The function of *pk1b* in the regulation of convergent extension

pk1b functions pleiotropically during zebrafish development but is still able to cooperate with *pk1a* in the context of the regulation of convergent extension. Therefore, a complete characterisation of the function of *pk1b* both in comparison to and in collaboration with *pk1a* in the context of convergent extension is necessary to fully understand these divergent *pk1* genes. As a priority, it is necessary to ascertain that loss of function of *pk1b* using *pk1b*-MOa and *pk1b*-MOb is both effective and specific. Verification of efficacy could be ascertained by the ability of *pk1b* mRNA to rescue *pk1b* loss of function via morpholino, and in tandem, confirmation of reduced *pk1b* expression in *pk1b* morphant embryos could be achieved through RT PCR. Similarly, verification of the specificity of *pk1b*-MOs to

pk1b could be achieved through rescue and cross-rescue with other *pk* genes, such as *pk1a*, and monitoring expression of all *pk* genes by RT PCR.

To continue characterisation of *pk1b* function, the ability of *pk1b* loss of function to rescue *wnt11* overexpression must be investigated. *pk1a* loss of function can rescue the gain of function phenotype of *wnt11* (Carreira-Barbosa *et al.*, 2003) and this may clarify the contrast I observed between loss of function of *pk1a* and loss of function of *pk1b* on the *silberblick/wnt11* (*slb*) mutant background. Likewise, an investigation of the effect of loss of function of *pk1b* on facial (nVII) branchiomotor neuron migration on the *trilobite/stbm* (*tri*) and *off-road/fmi2/celsr2* (*ord*) mutant backgrounds could eliminate the involvement of Pk1b in the regulation of branchiomotor neuron migration via a Pk1a/Stbm/Fmi2 pathway, committing Pk1b to a Wnt-dependent role in the regulation of convergent extension.

Further to this, and in view of the contrast between *pk1a* and *pk1b* in their interaction with *trilobite* and the strong implication that functions of Pk1b outside the context of gastrulation may be mediated through a pathway unrelated to Pk1a, Stbm or Fmi2, the question of the subcellular localisation of *pk1b* in response to the presence of PCP proteins must be answered definitively. Development of a technique similar to the visualisation of the subcellular localisation of *pk1b* with respect to notochord-somite boundary is vital, as evidence of a functional asymmetry in the subcellular localisation of any components of the Wnt/PCP pathway in vertebrate analogues of PCP is extremely desirable. Repetition of the analysis of changes to the subcellular localisation of *pk1b* in the presence of Stbm, or lack thereof, may increase our understanding of the interaction between Pk1b and Stbm in the context of gastrulation but not branchiomotor neuron migration. As described in Carreira-Barbosa *et*

al., 2003, an examination of the effect of loss of function or gain of function of *pk1b* on the subcellular localisation of Dsh-GFP could help elucidate the relationship between Pk1b and the non-canonical Wnt signalling pathway during gastrulation. Our current technique of visualising the subcellular localisation of *pk1b* through the overexpression of labelled mRNA may not reflect the endogenous situation: creation a zebrafish *pk1b*-GFP transgenic line could help to address these limitations.

Finally, revision of the potential interaction of *pk* orthologues with the Hh signalling pathway, bearing in mind that Hh may act through a pathway distinct from Smo, may define the pleiotropic functions of Pk1b but also yield information relating to gastrulation and other instances of directed cell migration during embryogenesis. Loss of function of *pk1b* in zebrafish mutants for Hh signalling such as *smoothened* (*smu*) or in the presence of the drug cyclopamine, an inhibitor of Hh signalling, is a starting point for dissecting this potential interaction. Examination of the expression of *engrailed* (*en*), a transcription factor known to activate Hh signalling, in the horizontal myoseptum of *pk1a* and *pk1b* morphant embryos might prove informative about the relationship between Hh signalling and *pk1* genes and even provide an opportunity for understanding the basis of the somite defects of *robo3v2* single morphant and *pk1b:slit1a*, *pk1a:robo3v2* and *pk1b:robo3v2* double morphant embryos.

Slit/Robo signalling in the regulation of convergent extension

In this thesis, I have shown that Slit/Robo signalling functions with known regulators of convergent extension in the context of gastrulation movements. To better understand the relationship between Robo receptors during convergent extension movements, their functional redundancy between must be investigated. Confirmation of the efficacy and specificity of *slit* and *robo* morpholinos is a

necessary first step: efficacy of loss of function could be ascertained through the ability of mRNA to rescue the development of morphants for specific *slit* and *robo* orthologues, while specificity of morpholinos and functional redundancy between orthologues could be assessed by cross-rescue. Analysis of the level of expression of *slit* and *robo* orthologues via RT PCR following loss of function could add a further level of verification to these assays.

Robo3v1 and Robo3v2 were shown to contrast in expression and function later in development, and the possibility of their functional redundancy was not discussed (Challa *et al.*, 2005). Robo3v2 appears to act in opposition to canonical Slit/Robo signalling during gastrulation, while gain of function of *robo3v1* causes convergent extension defects: as both Robo3v1 and Robo3v2 are expressed at the cell surface, the relationship between their function must be elucidated. Generation of a common *robo3* morpholino may be practical for this analysis. Likewise, although the similarity in the phenotype given rise to by the Robo3v2(ECD/TM)-GFP construct and overexpression of *slit2* strongly suggested that Robo3v2 acts in opposition to canonical Wnt signalling, I showed evidence of a functional interaction between Slit2 and both Robo2 and Robo3v2, implying that both can act as receptors for the Slit2 ligand. Potential redundancy between Robo2 and Robo3v2 function must be explored through the simultaneous loss of function of *robo2* and *robo3v2*. Despite many failed attempts to manufacture an ECD/TM construct that disrupts the function of an authentic receptor, e.g. Robo2(ECD/TM)-GFP, contrasting the Robo3v2(ECD/TM)-GFP phenotype with such a construct is a further necessary step in this process. As an essential component of this analysis, the protein products of both Robo2(ECD/TM)-GFP and Robo3v2(ECD/TM)-GFP must be visualised by Western Blotting as for the Lyn-Robo(ICD) constructs. Finally, co-immunoprecipitation could build upon the functional interactions I have described in this thesis and elucidate potential promiscuity of ligand

specificity by providing evidence of the physical interactions between Robo receptors and Slit ligands during gastrulation.

Discovery of a reliable readout of convergent extension cell behaviour in response to the interaction between canonical Slit/Robo signalling, the inhibitory control of canonical Slit/Robo signalling by Robo3v2 and known regulators of convergent extension, is an immediate priority. It must be considered however, that the presence of an endogenous inhibitor of Slit/Robo signalling may mask the effects of Slit/Robo signalling on cell behaviour: furthermore, due to the pleiotropic functions of Robo3v2, attempts to study the effect of canonical Slit/Robo signalling in the absence of Robo3v2, either through loss of function of *robo3v2* or through the targeted mutation of *robo3v2*, will result in severe morphological defects. In view of the fact that loss of function analysis excluded a direct interaction between Slit/Robo signalling and the non-canonical Wnt pathway, Slit/Robo signalling is unlikely to share the same readout as activation of the non-canonical Wnt signalling pathway in the context of convergent extension, such as recruitment of Dsh to the cell membrane (Carreira-Barbosa *et al.*, 2003). I attempted to discover a readout for cell behaviour during gastrulation in response to Slit/Robo signalling based upon the epistasis between zebrafish *pk* orthologues and components of the Slit/Robo signalling pathway. However, the subcellular localisation of Venus-Pk1b showed no alteration in response to the overexpression of canonical Slit/Robo signalling components such as *robo2* or components antagonistic to canonical Slit/Robo signalling such as *robo3v2* (data not shown), suggesting an alternate approach must be found. Performing sections for whole-mount *in situ* hybridisation analysis of the expression of *slit* and *robo* orthologues during gastrulation may help me correlate this readout with the discrete domains of ligand and receptor expression in mesoderm and neurectoderm in the future.

My results have also shown that Slit/Robo signalling functions in multiple other developmental contexts of undetermined relationship to either gastrulation or Slit/Robo signalling in the nervous system. Many of these contexts are out of the scope of this thesis, but confirmation or elimination of a relationship between Slit/Robo signalling, Pk1a, Pk1b and the regulation of facial (nVII) branchiomotor neuron migration could prove useful in the construction of the pathways reliant upon Slit/Robo signalling both within and outside of the context of gastrulation. Generation of zebrafish *robo* mutants/morphants in which branchiomotor neuron migration is easily visualised would facilitate analysis of the effect upon branchiomotor neuron migration of loss of function of *pk* orthologues in concert with loss of function of *robo* orthologues. For instance, crossing MZ *astray/robo2* (*ast*) with the Islet-1-GFP transgenic line would yield *ast*+/- progeny 50% of which carried Islet-1-GFP, allowing the visualisation of Islet-1-GFP expression in branchiomotor neurons either by confocal fluorescence microscopy of antibody staining against GFP.

Identification of *airbag*

In the context of the role of *abg* in the regulation of convergent extension, further characterisation of the dose-dependency of the interaction between *abg* and *pk1a* or *pk1b* is necessary. 75% of the progeny of *abg*+/- carrier incrosses injected with a subthreshold dose (1ng) of *pk1a*-MO (Fig. 5.1B), corresponding to the wildtype and heterozygous proportions, exhibited a curly tail down phenotype reminiscent of *pk1a* morphant embryos (Fig. 6.5C; Table 15; see also Carreira-Barbosa *et al.*, 2003). Either the amount of *pk1a*-MO used in this instance was not subthreshold or there was an unusually low population of wildtype embryos and the visible phenotype of this proportion reflected heterozygous *abg* embryos enhanced by loss of function of *pk1a*. To exclude this possibility, injection

of 3ng of *pk1a*-MO, sufficient to cause a severe *pk1a* morphant phenotype (Carreira-Barbosa *et al.*, 2003), into embryos generated from *abg+/-* carrier incrosses, would test the ability of loss of function of *pk1a* to abolish the function of the remaining functional copy of the *abg* gene in *abg+/-* embryos. If 25% of the embryos are *pk1a* morphant like, 50% are greatly enhanced and 25% are acutely affected by loss of function of *pk1a* using 3ng of *pk1a*-MO, then dose-dependency will be confirmed.

Mapping of the *abg* mutation is a necessity. In the mean time, given the great similarity between *abg* and *hmgcr1b* mutants and the potential significance of prenylation to our understanding of the effect of non-canonical Wnt signalling on cell behaviour during convergent extension, either complementation analysis with the *hmgcr1b* mutant, and/or loss of function analysis of *hmcgr1b* on wildtype, *abg+/-* and convergent extension mutant backgrounds using the published *hmgcr1b*-MO (D'Amico *et al.*, 2007) should be undertaken as a priority. Further to this, characterisation of the phenotype of homozygous *abg* embryos must continue, including a definitive examination of *cmlc2* expression compared to the *hmgcr1b* mutant (D'Amico *et al.*, 2007). Secondarily to this, in view of the fact that the migration of haematopoietic cells is affected by the *abg* mutation, and that a trade off exists between the adoption of haematopoietic or endothelial lineages in cells of the ICM, the corresponding effect of the *abg* mutation on endothelial differentiation, and the consequential effect on heart morphology, must be investigated via analysis of the expression of endothelial markers such as *flk-1* or *tie* (see Liao *et al.*, 1997).

Finally, in avian embryos, loss of function of *fibronectin* (*fn*) yields defective precardiac cell migration (Linask & Lash, 2004), and as the significance of FN function to gastrulation movements in *Xenopus* is well established (Davidson *et al.*, 2006; Marsden & DeSimone, 2001), discovery of an equivalent

relationship in zebrafish might prove enlightening in the quest to relate the defects of *abg-/-* embryos to the regulation of convergent extension.

Literature Cited

Adler PN. (2002).
Planar signalling and morphogenesis in *Drosophila*.
Developmental Cell **2**: 525–535.

Agius E, Oelgeschlager M, Wessely O, Kemp C & De Robertis EM. (2000).
Endodermal Nodal-related signals and mesoderm induction in *Xenopus*.
Development **127**: 1173–1183.

Amaya E, Stein PA, Musci TJ & Kirschner MW. (1993).
FGF signalling in the early specification of mesoderm in *Xenopus*.
Development **118**: 477–487.

Arber S, Barbayannis FA, Hanser H, Schneider C, Stanyon CA, Bernard O & Caroni P. (1998).
Regulation of actin dynamics through phosphorylation of cofilin by LIM-kinase.
Nature **393**: 805–809.

Axelrod JD. (2001).
Unipolar membrane association of Dishevelled mediates Frizzled planar cell polarity signaling.
Genes & Development **15**: 1182–1187.

Axelrod JD, Miller JR, Shulman JM, Moon RT & Perrimon N. (1998).
Differential recruitment of Dishevelled provides signaling specificity in the planar cell polarity and Wingless signaling pathways.
Genes & Development **12**: 2610–2622.

Bach I. (2000).
The LIM domain: regulation by association.
Mechanisms of Development **91**: 5–17.

Barresi MJ, Stickney HL & Devoto SH. (2000).
The zebrafish *slow-muscle-omitted* gene product is required for Hedgehog signal transduction and the development of slow muscle identity.
Development **127**: 2189–2199.

Bastock R, Strutt H & Strutt D. (2003).
Strabismus is asymmetrically localised and binds to Prickle and Dishevelled during Drosophila planar polarity patterning.
Development **130**: 3007–3014.

Battye R, Stevens A & Jacobs JR. (1999).
Axon repulsion from the midline of the *Drosophila* CNS requires *slit* function.
Development **126**: 2475–2481.

Bedell VM, Yeo SY, Park KW, Chung J, Seth P, Shivalingappa V, Zhao J, Obara T, Sukhatme VP, Drummond IA, Li DY & Ramchandran R. (2005).
roundabout4 is essential for angiogenesis *in vivo*.
PNAS **102**: 6373–6378.

Bingham S, Higashijima S, Okamoto H & Chandrasekhar A. (2002).
The zebrafish *trilobite* gene is essential for tangential migration of branchiomotor neurons.
Developmental Biology **242**: 149–160.

Boutros M, Paricio N, Strutt DI & Mlodzik M. (1998).
Dishevelled Activates JNK and Discriminates between JNK Pathways in Planar Polarity and *wingless* Signaling.
Cell **94**: 109–118.

Brose K, Bland KS, Wang KH, Arnott D, Henzel W, Goodman CS, Tessier-Lavinge M & Kidd T. (1999).
Slit proteins bind Robo receptors and have an evolutionarily conserved role in repulsive axon guidance.
Cell **96**: 795–806.

Brutsaert DL & Andries LJ. (1992).
The endocardial endothelium.
American Journal of Physiology **263**: 985–1002.

Cadigan KM & Nusse R. (1997).
Wnt signaling: a common theme in animal development.
Genes & Development **11**: 3286–3305.

Caneparo L, Huang YL, Staudt N, Tada M, Ahrendt R, Kazanskaya O, Niehrs C & Houart C. (2007).
Dickkopf-1 regulates gastrulation movements by coordinated modulation of Wnt/ß-catenin and Wnt/PCP activities, through interaction with the Dally-like homolog Knypek.
Genes & Development **21**: 465–480.

Camurri L, Mambetisaeva E & Sundaresan V. (2004).
Rig-1, a new member of Robo family genes, exhibits a distinct pattern of expression during mouse development.
Gene Expression Patterns **4**: 99–103.

Carmany-Rampey A & Schier AF. (2001).
Single-cell ingression during zebrafish gastrulation.
Current Biology **11**: 1261–1265.

Carreira-Barbosa, F.
Thesis: Regulation of gastrulation movements by planar cell polarity genes in zebrafish.
UCL, 2005.

Carreira-Barbosa F, Concha ML, Takeuchi M, Ueno N, Wilson SW & Tada M. (2003).
Prickle1 regulates cell movements during gastrulation and neuronal migration in zebrafish.
Development **130**: 4037–4046.

Chae J, Kim MJ, Goo JH, Collier S, Gubb D, Charlton J, Adler PN & Park WJ. (1999).
The *Drosophila* tissue polarity gene *starry night* encodes a member of the protocadherin family.
Development **126**: 5421–5429.

Challa AK, Beattie CE & Seeger MA. (2001).
Identification and characterisation of *roundabout* orthologs in zebrafish.
Mechanisms of Development **101**: 249–253.

Challa AK, McWhorter ML, Wang C, Seeger MA & Beattie CE. (2005).
Robo3 isoforms have distinct roles during zebrafish development.
Mechanisms of Development **122**: 1073–1086.

Chen W, Burgess S & Hopkins N. (2001).
Analysis of the zebrafish *smoothened* mutant reveals conserved and divergent functions of *hedgehog* activity.
Development **128**: 2385–2396.

Chen HW, Marinissen MJ, Oh SW, Chen X, Melnick M, Perrimon N, Gutkind JS, Hou SX. (2002).
CKA, a novel multidomain protein, regulates the JUN N-terminal kinase signal transduction pathway in *Drosophila*.
Molecular Cell Biology **22**: 1792–1803.

Christian JL, Olson DJ & Moon RT. (1992).
Xwnt-8 modifies the character of mesoderm induced by FGF in isolated *Xenopus* ectoderm.
EMBO Journal **11**: 33–41.

Chung CY, Potikyan G & Firtel RA. (2001).
Control of cell polarity and chemotaxis by Akt/PKB and PI3 kinase through the regulation of PAKa.
Molecular Cell **7**: 937–947.

Ciruna B, Jenny A, Lee D, Mlodzik M & Schier AF. (2006).
Planar cell polarity signalling couples cell division and morphogenesis during neurulation.
Nature **439**: 220–224.

Collier S & Gubb D. (1997).
Drosophila tissue polarity requires the cell-autonomous activity of the *fuzzy* gene, which encodes a novel transmembrane protein.
Development **124**: 4029–4037.

Concha ML & Adams RJ. (1998).
Oriented cell divisions and cellular morphogenesis in the zebrafish gastrula and neurula: a time-lapse analysis.
Development **125**: 983–994.

Conlon FL, Sedgwick SG, Weston KM & Smith JC. (1996).
Inhibition of Xbra transcription activation causes defects in mesodermal patterning and reveals autoregulation of Xbra in dorsal mesoderm.
Development **122**: 2427–2435.

Conlon FL & Smith JC. (1999).
Interference with brachyury function inhibits convergent extension, causes apoptosis, and reveals separate requirements in the FGF and activin signalling pathways.
Developmental Biology **213**: 85–100.

Cooke J. (1973).
Properties of the primary organization field in the embryo of *Xenopus laevis.* IV. Pattern formation and regulation following early inhibition of mitosis.
Journal of Embryology & Experimental Morphology **30**: 49–62.

Copp AJ, Greene ND & Murdoch JN. (2003).
The genetic basis of mammalian neurulation.
Nature Reviews Genetics **4**: 784–793.

Cunliffe V & Smith JC. (1992).
Ectopic mesoderm formation in *Xenopus* embryos caused by widespread expression of a Brachyury homologue.
Nature **358**: 427–430.

Curtin JA, Quint E, Tsipouri V, Arkell RM, Cattanach B, Copp AJ, Henderson DJ, Spurr N, Stanier P, Fisher EM, Nolan PM, Steel KP, Brown SD, Gray IC & Murdoch JN. (2003).
Mutation of *celsr1* disrupts planar polarity of inner ear hair cells and causes severe neural tube defects in the mouse.
Current Biology **13**: 1129–1133.

D'Amico L, Scott IC, Jungblut B & Stanier DY. (2007).
A mutation in zebrafish *hmgcr1b* reveals a role for Isoprenoids in vertebrate heart-tube formation.
Current Biology **17**: 252–259.

Dale L, Matthews G & Coleman A. (1993).
Secretion and mesoderm-inducing activity of the TGF-β-related domain of *Xenopus* Vg1.
EMBO Journal **12**: 4471–4480.

Dalkic E, Kuscu C, Sucularli C, Aydin IT, Akcali KC & Kono O. (2006).
Alternatively spliced Robo2 isoforms in zebrafish and rat.
Development Genes & Evolution **216**: 555–563.

Davidson LA, Marsden M, Keller R & DeSimone DW. (2006).
Integrin α5ß1 and Fibronectin regulate polarized cell protrusions required for *Xenopus* convergence and extension.
Current Biology **16**: 833–844.

Davies A, Formstone C, Mason I & Lewis J. (2005).
Planar cell polarity of hair cells in the chick inner ear is correlated with polarised distribution of c-Flamingo-1 protein.
Developmental Dynamics **233**: 998–1005.

Dawid IB, Breen JJ & Toyama R. (1998).
LIM domains: multiple roles as adapters and functional modifiers in protein interactions.
Trends in Genetics **14**: 156–162.

Deshpande G & Schedl P. (2005).
HMGCoA reductase potentiates *hedgehog* signalling in *Drosophila melanogaster.*
Developmental Cell **9**: 629–638.

Detrich III HW, Kieran MW, Chan FY, Barone LM, Yee K, Rundstadler JA, Pratt S, Ransom D & Zon LI. (1995).
Intraembryonic haemopoeitic cell migration during vertebrate development.
PNAS **92**: 10713–10717.

Dickson BJ & Gilestro GF. (2006).
Regulation of commissural axon pathfinding by Slit and its Robo receptors.
Annual Review of Cell & Developmental Biology **22**: 651–675.

Driever W, Solnica-Krezel L, Schier AF, Neuhauss SC, Malicki J, Stemple DL, Stainier DY Zwartkruis F, Abdelilah S, Rangini Z, Belak J & Boggs C. (1996).
A genetic screen for mutations affecting embryogenesis in zebrafish.
Development **123**: 37–46.

Du SJ, Purcell SM, Christian JL, McGrew LL & Moon RT. (1995).
Identification of distinct classes and functional domains of Wnts through expression of wild-type and chimeric proteins in *Xenopus* embryos.
Molecular & Cellular Biology **15**: 2625–2634.

Dyson S & Gurdon JB. (1997).
Activin signalling has a necessary function in *Xenopus* early development.
Current Biology **7**: 81–84.

Eaton S. (1997).
Planar polarisation of *Drosophila* and vertebrate epithelia.
Current Opinion in Cell Biology **9**: 860–866.

Eaton S, Wepf R & Simons K. (1996).
Roles for Rac1 and Cdc42 in planar polarization and hair outgrowth in the wing of *Drosophila*.
Journal of Cell Biology **135**: 1277–1289.

El-Messaoudi S & Renucci A. (2001).
Expression pattern of the *frizzled 7* gene during zebrafish embryonic development.
Mechanisms of Development **102**: 231–234.

Elul T & Keller R. (2000).
Monopolar protrusive activity: a new morphogenetic cell behaviour in the neural plate dependent on vertical interactions with the mesoderm in *Xenopus*.
Developmental Biology **224**: 3–19.

Elul T, Koehl MA & Keller R. (1997).
Cellular mechanism underlying neural convergent extension in *Xenopus laevis* embryos.
Developmental Biology **191**: 243–258.

England SJ, Blanchard GB, Mahadevan L & Adams RJ. (2006).
A dynamic fate map of the forebrain shows how vertebrate eyes form and explains two causes of cyclopia.
Development **133**: 4613–4617.

Erter CE, Wilm TP, Basler N, Wright CV & Solnica-Krezel L. (2001).
Wnt8 is required in lateral mesendodermal precursors for neural posteriorization *in vivo*.
Development **128**: 3571–3583.

Essner JJ, Amack JD, Nyholm MK, Harris EB & Yost HJ. (2005).
Kupffer's vesicle is a ciliated organ of asymmetry in the zebrafish embryo that initiates left-right development of the brain, heart and gut.
Development **132**: 1247–1260.

Formstone CJ & Mason I. (2005).
Combinatorial activity of Flamingo proteins directs convergence and extension within the early zebrafish embryo via the planar cell polarity pathway.
Developmental Biology **15**: 320–335.

Fricke C, Lee JS, Geiger-Rudolph S, Bonhoeffer F & Chien CB. (2001).
astray, a zebrafish *roundabout* homolog required for retinal axon guidance.
Science **292**: 507–510.

Genova JL, Jong S, Camp JT & Fehon RG. (2000).
Functional analysis of Cdc42 in actin filament assembly, epithelial morphogenesis, and cell signaling during *Drosophila* development.
Developmental Biology **221**: 181–194.

Gering M, Rodaway AR, Göttgens B, Patient RK & Green AR. (1998).
The *SCL* gene specifies haemangioblast development from early mesoderm.
EMBO Journal **17**: 4029–4045.

Gilbert S. (2000).
Developmental Biology (6th Ed.)
Sinauer Associates INC. Publishers, USA.

Glickman NS, Kimmel CB, Jones MA & Adams RJ. (2003).
Shaping the zebrafish notochord.
Development **130**: 873–887.

Glinka A, Wu W, Delius H, Monaghan AP, Blumenstock C & Niehrs C. (1998).
Dickkopf-1 is a member of a new family of secreted proteins and functions in head induction.
Nature **391**: 357–362.

Gong Y, Mo C & Fraser SE. (2004).
Planar cell polarity signaling controls cell division orientation during zebrafish gastrulation.
Nature **430**: 689–693.

Goto T, Davidson L, Asashima M & Keller R. (2005).
Planar cell polarity genes regulate polarized extracellular matrix deposition during frog gastrulation.
Current Biology **15**: 787–793.

Green JBA, New HV & Smith JC. (1990).
Responses of embryonic *Xenopus* cells to activin and FGF are separated by multiple dose thresholdsand correspond to distinct axes of the mesoderm.
Cell **71**: 731–739.

Green JBA & Smith JC. (1992).
Graded changes in dose of a *Xenopus* activin A homologue elicit stepwise transitions in embryonic cell fate.
Nature **347**: 391–394.

Grevengoed EE, Loureiro JJ, Jesse TL & Peifer M. (2001).
Abelson kinase regulates epithelial morphogenesis in *Drosophila*.
Journal of Cell Biology **155**: 1185–98.

Habas R, Kato Y & Xe H. (2001).
Wnt/Frizzled activation of Rho regulates vertebrate gastrulation and requires a novel Formin homology protein Daam1.
Cell **107**: 843–854.

Haffter P, Granato M, Brand M, Mullins MC, Hammerschmidt M, Kane DA, Odenthal J, van Eeden FJ, Jiang YJ, Heisenberg CP, Kelsh RN, Furutani-Seiki M, Vogelsang E, Beuchle D, Schach U, Fabian C & Nüsslein-Volhard C. (1996).
The identification of genes with unique and essential functions in the development of the zebrafish, *Danio rerio*.
Development **123**: 1–36.

Hammerschmidt M, Brook A & McMahon AP. (1997).
The world according to hedgehog.
Trends in Genetics **13**: 14–21.

Hammerschmidt M, Pelegri F, Mullins MC, Kane DA, Brand M, van Eeden FJ, Furutani-Seiki M, Granato M, Haffter P, Heisenberg CP, Jiang YJ, Kelsh RA, Odenthal J, Warga RM & Nüsslein-Volhard C. (1996).
Mutations affecting morphogenesis during gastrulation and tail formation in the zebrafish, *Danio rerio*.
Development **123**: 143–151.

Hardin J & Keller R. (1988).
The behaviour and function of bottle cells during gastrulation of *Xenopus laevis*.
Development **103**: 211–230.

Harland R & Gerhart J. (1997).
Formation and function of Spemann's organiser.
Annual Review of Cell & Developmental Biology **13**: 611–667.

Heisenberg CP, Brand M, Jiang YJ, Warga RM, Beuchle D, van Eeden FJ, Furutani-Seiki M, Granato M, Haffter P, Hammerschmidt M, Kane DA, Kelsh RN, Mullins MC, Odenthal J & Nüsslein-Volhard C. (1996).
Genes involved in forebrain development in the zebrafish, *Danio rerio*.
Development **123**: 191–203.

Heisenberg CP & Nüsslein-Volhard C. (1997).
The function of *silberblick* in the positioning of the eye anlage in the zebrafish embryo.
Developmental Biology **184**: 85–94.

Heisenberg CP, Tada M, Rauch GJ, Saúde L, Concha ML, Geisler R, Stemple DL, Smith JC & Wilson SW (2000).
Silberblick/Wnt11 mediates convergent extension movements during zebrafish gastrulation.
Nature **405**: 76–81.

Heasman J. (1997).
Patterning the *Xenopus* blastula.
Development **124**: 4179–4191.

Heasman J. (2006).
Patterning the early *Xenopus* embryo.
Development **133**: 1205–1217.

Hirose Y, Varga ZM, Kondoh H & Furutani-Seiki M. (2004).
Single cell lineage and regionalization of cell populations during *Medaka* neurulation.
Development **131**: 2553–2563.

Holtfreter J. (1943).
A study of the mechanics of gastrulation. Part I.
The Journal of Experimental Zoology **94**: 261–318.

Hou XS, Goldstein ES & Perrimon N. (1997).
Drosophila Jun relays the Jun amino-terminal kinase signal transduction pathway to the Decapentaplegic signal transduction pathway in regulating epithelial cell sheet movement.
Genes & Development **11**: 1728–1737.

Huminiecki L, Gorn M, Suchting S, Poulsom R & Bicknell R. (2002).
Magic Roundabout is a new member of the Roundabout receptor family that is endothelial specific and expressed at sites of active angiogenesis.
Genomics **79**: 547–552.

Hunter CS & Rhodes SJ. (2005).
LIM-homeodomain genes in mammalian development and human disease.
Molecular Biology Reports **32**: 67–77.

Hutson LD & Chien CB. (2002).
Pathfinding and error correction by retinal axons: the role of *astray/robo2*.
Neuron **33**: 205–217.

Hutson LD, Jurynec MJ, Yeo SY, Okamoto H & Chien CB. (2003).
Two divergent *slit1* genes in zebrafish.
Developmental Dynamics **228**: 358–369.

Inatani M, Irie F, Plump AS, Tessier-Lavigne M & Yamaguchi Y. (2003).
Mammalian brain morphogenesis and midline axon guidance require heparan sulfate.
Science **302**: 1044–1046.

Jacinto A, Martinez-Arias A & Martin P. (2001).
Mechanisms of epithelial fusion and repair.
Nature Cell Biology **3**: E117–123.

Jacinto A. & Martin P. (2001)
Morphogenesis: unravelling the biology of hole closure.
Current Biology **11**: R705–707.

Jacinto A, Woolner S. & Martin P. (2002)
Dynamic analysis of dorsal closure in Drosophila: from genetics to cell biology.
Developmental Cell **3**: 9–19.

Jenny A, Darken RS, Wilson PA & Mlodzik M. (2003).
Prickle and Strabismus form a functional complex to generate a correct axis during planar cell polarity signalling.
EMBO Journal **22**: 4409–4420.

Jessen JR, Topczewski J, Bingham S, Sepich DS, Marlow F, Chandrasekhar A & Solnica-Krezel L. (2002).
Zebrafish *trilobite* identifies new roles for Strabismus in gastrulation and neuronal movements.
Nature Cell Biology **4**: 610–615.

Kane DA, Hammerschmidt M, Mullins MC, Maischein HM, Brand M, van Eeden FJ, Furutani-Seiki M, Granato M, Haffter P, Heisenberg CP, Jiang YJ, Kelsh RN, Odenthal J, Warga RM & Nüsslein-Volhard C. (1996).
The zebrafish epiboly mutants.
Development **123**: 47–55.

Kane DA, McFarland KN & Warga RM. (2005).
Mutations in *half baked*/E-cadherin block cell behaviors that are necessary for teleost epiboly.
Development **132**: 1105–1116.

Kanki JP & Ho RK. (1997).
The development of the posterior body in zebrafish.
Development **124**: 881–893.

Karlstrom RO, Trowe T, Klostermann S, Baier H, Brand M, Crawford AD, Grunewald B, Haffter P, Hoffmann H, Meyer SU, Müller BK, Richter S, van Eeden FJ, Nüsslein-Volhard C & Bonhoeffer F. (1996).
Zebrafish mutations affecting retinotectal axon pathfinding.
Development **123**: 427–438.

Kaltschmidt JA, Lawrence N, Morel V, Balayo T, Fernández BG, Pelissier A, Jacinto A & Martinez Arias A. (2002).
Planar polarity and actin dynamics in the epidermis of *Drosophila*.
Nature Cell Biology **4**: 937–944.

Kawano Y & Kypta R. (2003).
Secreted antagonists of the Wnt signalling pathway.
Journal of Cell Science **116**: 2627–2634.

Keller R, Davidson LA, Edlund A, Elul T, Ezin M, Shook DR & Skoglund P. (2000).
Mechanisms of convergence and extension by cell intercalation.
Philos. Trans. R. Soc. Lond. B Biol. Sci. **355**: 897–922.

Keller R, Davidson LA & Shook DR. (2003).
How we are shaped: the biomechanics of gastrulation.
Differentiation **71**: 171–205.

Keller R, Shih J & Domingo C. (1992).
The patterning and functioning of protrusive activity during convergence and extension of the *Xenopus* organizer.
Development **(Suppl.)**: 81–91.

Kessel RG. (1960).
The role of cell division in gastrulation of *Fundulus heteroclitus*.
Experimental Cell Research **20**: 277–282.

Kibar Z, Vogan KJ, Groulx N, Justice MJ, Underhill DA & Gros P. (2001).
Ltap, a mammalian homolog of *Drosophila Strabismus/Van Gogh*, is altered in the mouse neural tube mutant Loop-tail.
Nature Genetics **28**: 251–255.

Kidd T, Brose K, Mitchell KJ, Fetter RD, Tessier-Lavigne M, Goodman CS & Tear G. (1998a).
Roundabout controls axons crossing of the CNS midline and defines a novel subfamily of evolutionarily conserved guidance receptors.
Cell **92**: 205–215.

Kidd T, Russell C, Goodman CS & Tear G. (1998b).
Dosage-sensitive and complementary functions of Roundabout and Commissureless control axon crossing of the midline.
Neuron **20**: 25–33.

Kidd T, Bland KS & Goodman CS. (1999).
Slit is the midline repellent for the Robo receptor in *Drosophila*.
Cell **96**: 785-794.

Kiecker C & Niehrs C. (2001).
A morphogen gradient of Wnt/ß-catenin signalling regulates anteroposterior neural patterning in *Xenopus*.
Development **128**: 4189–4201.

Kilian B, Mansukoski H, Barbosa FC, Ulrich F, Tada M & Heisenberg CP. (2003).
The role of Ppt/Wnt5 in regulating cell shape and movement during zebrafish gastrulation.
Mechanisms of Development **120**: 467–476.

Kimelman D, Christian JL & Moon RT. (1992).
Synergistic principles of development: overlapping patterning systems in *Xenopus* mesoderm induction.
Development **116**: 1–9.

Kofron M, Birsoy B, Houston D, Tao Q, Wylie C & Heasman J. (2007).
Wnt11/ß-catenin signalling in both oocytes and early embryos acts through LRP6-mediated regulation of axin.
Development **134**: 503–513.

Kofron M, Demel T, Xanthos J, Lohr J, Sun B, Sive H, Osada S, Wright C, Wylie C & Heasman J. (1999).
Mesoderm induction in *Xenopus* is a zygotic event regulated by maternal VegT via TGFbeta growth factors.
Development **126**: 5759–5770.

Kramer-Zucker AG, Olale F, Haycraft CJ, Yoder BK, Schier AF & Drummond IA. (2005).
Cilia-driven fluid flow in the zebrafish pronephros, brain and Kupffer's vesicle is required for normal organogenesis.
Development **132**: 1907–1921.

Krasnow RE & Adler PN. (1994).
A single *frizzled* protein has a dual function in tissue polarity.
Development **120**: 1883–1893.

Krasnow RE, Wong LL & Adler PN. (1995).
disheveled is a component of the *frizzled* signaling pathway in *Drosophila*.
Development **121**: 4095–4102.

Ku M & Melton DA. (1993).
Xwnt-11: a maternally expressed *Xenopus wnt* gene.
Development **119**: 1161–1173.

Kühl M, Sheldahl LC, Malbon CC & Moon RT. (2000).
Ca^{2+}/Calmodulin-dependent Protein Kinase II is stimulated by Wnt and Frizzled homologs and promotes ventral cell fates in *Xenopus*.
Journal of Biological Chemistry **275**: 12701–12711.

Kurth T & Hausen P. (2000).
Bottle cell formation in relation to mesodermal patterning in the *Xenopus* embryo.
Mechanisms of Development **97**: 117–131.

Lee H & Adler PN. (2002).
The function of the *frizzled* pathway in the *Drosophila* wing is dependent on *inturned* and *fuzzy*.
Genetics **160**: 1535–1547.

Lee JS, Ray R & Chien CB. (2001).
Cloning and expression of three zebrafish Roundabout homologues suggest roles in axon guidance and cell migration.
Developmental Dynamics **221**: 216–230.

Lee JS, von der Hardt S, Rusch MA, Stringer SE, Stickney HL, Talbot WS, Geisler R, Nüsslein-Volhard C, Selleck SB, Chien CB & Roehl H. (2004).
Axon sorting in the optic tract requires HSPG synthesis by *ext2* (*dackel*) and *extl3* (*boxer*).
Neuron **44**: 947–960.

Leptin M. (1995).
Drosophila gastrulation: from pattern formation to morphogenesis.
Annual Review of Cell & Developmental Biology **11**: 189–212.

Lekven AC, Thorpe CJ, Waxman JS & Moon RT. (2001).
Zebrafish *wnt8* encodes two Wnt8 proteins on a bicistronic transcript and is required for mesoderm and neurectoderm patterning.
Developmental Cell **1**: 103–114.

Lewis J & Davies A.
Planar cell polarity in the inner ear: how do hair cells acquire their orientated structure?
Journal of Neurobiology **53**: 190–201.

Liao W, Bisgrove BW, Sawyer H, Hug B, Bell B, Peters K, Grunwald DJ & Stanier DY. (1997).
The zebrafish gene *cloche* acts upstream of a *flk-1* homologue to regulate endothelial cell differentiation.
Development **12**: 381–389.

Linask KK & Lash JW. (2004)
A role for fibronectin in the migration of avian precardiac cells. I. Dose dependent effects of fibronectin antibody.
Developmental Biology **129**: 315–323.

Lustig KD, Kroll KL, Sun EE & Kirschner MW. (1996).
Expression cloning of a *Xenopus* T-related gene (Xombi) involved in mesodermal patterning and blastopore lip formation.
Development **122**: 4001–4012.

MacDonald R, Barth KA, Xu Q, Holder N, Mikkola I & Wilson SW. (1995).
Midline signalling is required for Pax gene regulation and patterning of the eyes.
Development **121**: 3267–3278.

Mao B, Wu W, Li Y, Hoppe D, Stannek P, Glinka A & Niehrs C. (2001).
LDL-receptor-related protein 6 is a receptor for Dickkopf proteins.
Nature **411**: 321–325.

Markwald RR, Mjaatvedt CH, Krug EL & Sinning AR. (1990).
Inductive interactions in heart development. Role of cardiac adherons in cushion tissue formation.
Annals of the New York Academy of Sciences **588**: 13–25.

Marlow F, Gonzalez EM, Yin C, Rojo C & Solnica-Krezel L. (2004).
No-tail co-operates with non-canonical Wnt signaling to regulate posterior body morphogenesis in zebrafish.
Development **131**: 203–216.

Marlow F, Topczewski J, Sepich DS & Solnica-Krezel L. (2002).
Zebrafish Rho kinase 2 acts downstream of Wnt11 to mediate cell polarity and effective convergence and extension movements.
Current Biology **12**: 876–884.

Marlow F, Zwartkruis F, Malicki J, Neuhauss SC, Abbas L, Weaver M, Driever W & Solnica-Krezel L. (1998).
Functional interactions of genes mediating convergent extension, *knypek* and *trilobite*, during the partitioning of the eye primordium in zebrafish.
Developmental Biology **203**: 382–399.

Marsden M & DeSimone DW. (2001).
Regulation of cell polarity, radial intercalation and epiboly in *Xenopus*: novel roles for integrin and fibronectin.
Development **128**: 3625–3647.

Matsui T, Raya Á, Kawakami Y, Callol-Massot C, Capdevila J, Rodríguez-Esteban C & Izpisúa Belmonte JC. (2005).
Noncanonical Wnt signaling regulates midline convergence of organ primordia during zebrafish development.
Genes & Development **19**: 164–175.

Matsui T, Raya Á, Callol-Massot C, Kawakami Y, Oishi I, Rodríguez-Esteban C & Izpisúa Belmonte JC. (2006).
miles-apart-mediated regulation of cell–fibronectin interaction and myocardial migration in zebrafish.
Nature Clinical Practice Cardiovascular Medicine **4**: S77–82.

Miyagi C, Yamashita S, Ohba Y, Yoshizaki H, Matsuda M & Hirano T. (2004).
STAT3 non cell autonomously controls planar cell polarity during convergence and extension.
Journal of Cell Biology **166**: 975–981.

Mizuno T, Tsutsui, K & Nishida Y. (2002).
Drosophila myosin phosphatase and its role in dorsal closure.
Development **129**: 1215–1223.

Montero JA, Carvalho L, Wilsch-Bräuninger M, Kilian B, Mustafa C & Heisenberg CP. (2005).
Shield formation at the onset of zebrafish gastrulation.
Development **132**: 1187–1198.

Montero JA, Kilian B, Chan J, Bayliss PE & Heisenberg CP. (2003).
Phosphoinositide 3-Kinase is required for process outgrowth and cell polarization of gastrulating mesendodermal cells.
Current Biology **13**: 1279–1289.

Mullins MC, Hammerscmidt M, Haffter P & Nüsslein-Volhard C. (1994).
Large-scale mutagenesis in the zebrafish: in search of genes controlling development in a vertebrate.
Current Biology **4**: 189–202.

Muñoz R, Moreno M, Oliva C, Orbenes C & Larraín J. (2006).
Syndecan-4 regulates non-canonical Wnt signalling and is essential for convergent and extension movements in *Xenopus* embryos.
Nature Cell Biology **8**: 492–500.

Nasevicius A & Ekker SC. (2000).
Effective targeted gene 'knockdown' in zebrafish.
Nature Genetics **26**: 216–220.

Nieuwkoop P. & Florschütz P. (1950).
Quelque caracteres speaciaux de la gastrulation et de la neurulation de l'oeuf de *Xenopus laevis*, Daud. et de quelque autres Anoures.
Arch. Biol. **61**: 113–150.

Ober EA, Olofsson B, Mäkinen T, Jin SW, Shoji W, Koh GY, Alitalo K & Stainier DY. (2004).
Vegfc is required for vascular development and endoderm morphogenesis in zebrafish.
EMBO Reports **5**: 78–84.

Oishi I, Kawakami Y, Raya Á, Callol-Massot C & Izpisúa-Belmonte JC. (2006).
Regulation of primary cilia formation and left-right patterning in zebrafish by a noncanonical Wnt signaling mediator, *duboraya*.
Nature Genetics **38**: 1316–1322.

Park KW, Morrison CM, Sorensen LK, Jones CA, Rao Y, Chien CB, Wu JY, Urness LD & Li DY. (2003).
Robo4 is a vascular-specific receptor that inhibits endothelial migration.
Developmental Biology **261**: 251–267.

Park WJ, Liu J, Sharp EJ & Adler PN. (1996).
The *Drosophila* tissue polarity gene *inturned* acts cell autonomously and encodes a novel protein.
Development **122**: 961–969.

Park M & Moon RT. (2002).
The planar cell-polarity gene *stbm* regulates cell behaviour and cell fate in vertebrate embryos.
Nature Cell Biology **4**: 20–25.

Perron M, Boy S, Amato MA, Viczian A, Koebernick K, Pieler T & Harris WA. (2003).
A novel function for Hedgehog signalling in retinal pigment epithelium differentiation.
Development **130**:1565–1577.

Piepenburg O, Grimmer D, Williams PH & Smith JC. (2004).
Activin redux: specification of mesodermal pattern in *Xenopus* by graded concentrations of endogenous *activin B*.
Development **131**: 4977–4986.

Ponting CP & Bork P. (1996).
Plekstrin's repeat performance: A novel domain in G-protein signaling?
Trends in Biochemical Science **21**: 245–246.

Ramos JW, Whittaker CA & DeSimone DW. (1996).
Integrin-dependent adhesive activity is spatially controlled by inductive signals at gastrulation.
Development **122**: 2873–2883.

Rauch GJ, Hammerschmidt M, Blader P, Schauerte HE, Strähle U, Ingham PW, McMahon AP & Haffter P. (1997).
Wnt5 is required for tail formation in the zebrafish embryo.
Cold Spring Harbor Symposia on Quantitative Biology **62**: 227–234.

Ricos MG, Harden N, Sem KP, Lim L & Chia W. (1999).
Dcdc42 acts in TGF-beta signaling during *Drosophila* morphogenesis:
distinct roles for the Drac1/JNK and Dcdc42/TGF-beta cascades in cytoskeletal regulation.
Journal of Cell Science **112**: 1225–1235.

Riesgo-Escovar JR & Hafen E. (1997).
Common and distinct roles of DFos and DJun during Drosophila development.
Science **278**: 669–672.

Rohrschneider MR, Elson GE & Prince VE. (2007).
Zebrafish Hoxb1a regulates multiple downstream target genes including *prickle1b*.
Developmental Biology **307**: 358–372.

Rothberg JM, Hartley DA, Walther Z & Artavanis-Tsakonas S. (1988).
slit: an EGF-homologous locus of *D. melanogaster* involved in the development of the embryonic central nervous system.
Cell **55**: 1047–1059.

Sabatier C, Plump AS, Le MA, Brose K, Tamada A, Murakami F, Lee EY & Tessier-Lavigne M. (2004).
The divergent Robo family protein Rig-1/Robo3 is a negative regulator of Slit responsiveness required for midline crossing by commissural axons.
Cell **117**: 157–169.

Saka Y & Smith JC. (2001).
Spatial and temporal patterns of cell division during early *Xenopus* embryogenesis.
Developmental Biology **229**: 307–318.

Saka Y, Tada M & Smith J. (2000).
A screen for targets of the *Xenopus* T-box gene *Xbra*.
Mechanisms of Development 93: 27-39.

Sambrook J, Fritsch E & Maniatis T. (1989).
Molecular Cloning.
Cold Spring Harbor Laboratory Press, USA.

Sampath K, Rubinstein AL, Cheng AM, Liang JO, Fekany K, Solnican-Krezel L, Korzh V, Halpern ME & Wright CV. (1998).
Induction of the zebrafish ventral brain and floorplate requires *cyclops/nodal* signalling.
Nature **395**: 185–189.

Schilling TF, Piotrowski T, Grandel H, Brand M, Heisenberg CP, Jiang YJ, Beuchle D, Hammerschmidt M, Kane DA, Mullins MC, van Eeden FJ, Kelsh RN, Furutani-Seiki M, Granato M, Haffter P, Odenthal J, Warga RM, Trowe T & Nüsslein-Volhard C. (1996).
Jaw and branchial arch mutants in zebrafish I: branchial arches.
Development **123**: 329–344.

Schülte-Merker S, Smith JC & Dale L. (1994).
Effects of truncated *activin* and FGF receptors and of *follistatin* on the inducing activities of BVgI and *activin*: does *activin* play a role in mesoderm induction?
EMBO Journal **13**: 3533–3541.

Seeger MA, Tear G, Ferres-Marco D & Goodman CS. (1993).
Mutations affecting growth cone guidance in *Drosophila*: genes necessary for guidance toward or away from the midline.
Neuron **10**: 409–426.

Sepich DS, Calmelet C, Kiskowski M & Solnica-Krezel L. (2005).
Initiation of convergent and extension movements of lateral mesoderm during zebrafish gastrulation.
Developmental Dynamics **234**: 279–292.

Sepich DS, Myers DC, Short R, Topczewski J, Marlow F & Solnica-Krezel L. (2000).
Role of the zebrafish *trilobite* locus in gastrulation movements of convergence and extension.
Genesis **27**: 159–173.

Shah AM & Lewis MJ. (1993).
Modulation of myocardial contraction by endocardial and coronary vascular endothelium.
Trends in Cardiovascular Medicine **3**: 98–103.

Sheldahl LC, Park M, Malbon CC & Moon RT. (1999).
Protein Kinase C is differentially stimulated by Wnt and Frizzled homologs in a G-protein-dependent manner.
Current Biology **9**: 695–698.

Sheldahl LC, Slusarski DC, Pandur P, Miller JR, Kühl M & Moon RT. (2003).
Dishevelled activates Ca^{2+} flux, PKC and CamKII in vertebrate embryos.
Journal of Cell Biology **161**: 769–777.

Shih J & Keller R. (1992a).
Cell motility driving mediolateral intercalation in explants of *Xenopus laevis*.
Development **116**: 901–914.

Shih J & Keller R. (1992b).
Patterns of cell motility in the organiser and dorsal mesoderm of *Xenopus laevis*.
Development **116**: 915–930.

Shimizu T, Yabe T, Muraoka O, Yonemura S, Aramaki S, Hatta K, Bae YK, Nojima H & Hibi M. (2005).
E-cadherin is required for gastrulation cell movements in zebrafish.
Mechanisms of Development **122**: 747–763.

Slack J. (1991).
From Egg to Embryo (2nd Ed.).
Cambridge University Press, UK.

Slusarski DC, Corces VG & Moon RT. (1997a)
Interaction of Wnt and a Frizzled homologue triggers phophatidylinositol signalling.
Nature **390**: 410–413.

Slusarski DC, Yang-Snyder J, Busa WB & Moon RT. (1997b).
Modulation of intracellular Ca^{2+} signalling by XWnt5a.
Developmental Biology **182**: 114–120.

Sluss HK & Davis RJ. (1997).
Embryonic morphogenesis signaling pathway mediated by JNK targets the transcription factor JUN and the TGF-beta homologue decapentaplegic.
Journal of Cellular Biochemistry **67**: 1–12.

Smith JC, Conlon FL, Saka Y & Tada M. (2000).
XWnt11 and the regulation of gastrulation in *Xenopus*.
Philos. Trans. R. Soc. Lond. B Biol. Sci. **355**: 923–930.

Sokol SY. (1996).
Analysis of Dishevelled signaling pathways during *Xenopus* development.
Current Biology **6**: 1456-1467.

Solnica-Krezel L, Stemple DL, Mountcastle-Shah E, Rangini Z, Neuhauss SC, Malicki J, Schier AF, Stainier DY, Zwartkruis F, Abdelilah S & Driever W. (1996).
Mutations affecting cell fates and cellular rearrangements during gastrulation in zebrafish.
Development **123**: 67–80.

Solnica-Krezel L. (2005).
Conserved patterns of cell movements during vertebrate gastrulation.
Current Biology **15**: R213–228.

Stainier DY, Weinstein BM, William Detrich III H, Zon LI & Fishman MC. (1995).
cloche, an early acting zebrafish gene, is required by both the endothelial and haematopoeitic lineages.
Development **121**: 3141–3150.

Starr CJ, Kappler JA, Chan DK, Kollmar R & Hudspeth AJ. (2004).
Mutation of the *choroideremia* gene encoding Rab escort protein 1 devastates hair cells.
PNAS **101**: 2572–2577.

Stephens L, Ellson C & Hawkins P. (2002).
Roles of PI3Ks in leukocyte chemotaxis and phagocytosis.
Current Opinion in Cell Biology **14**: 203–213.

Stoick-Cooper CL, Weidinger G, Riehle KJ, Hubbert C, Major MB, Fausto N & Moon RT. (2007).
Distinct Wnt signalling pathways have opposing roles in appendage regeneration.
Development **134**: 479–489.

Strutt D. (2001).
Asymmetric localization of Frizzled and the establishment of cell polarity in the *Drosophila* wing.
Molecular Cell **7**: 367–375.

Sumanas S & Ekker SC. (2001).
Xenopus frizzled-7 morphant displays defects in dorsoventral patterning and convergent extension movements during gastrulation.
Genesis **30**: 119–122.

Sumanas S, Kim HJ, Hermanson S & Ekker SC. (2001).
Zebrafish *frizzled-2* morphant displays defects in body axis elongation.
Genesis **30**: 114–118.

Symes K & Smith JC. (1987).
Gastrulation movements provide an early marker of mesoderm induction in *Xenopus laevis*.
Development **101**: 339–349.

Tada M, Concha ML & Heisenberg CP. (2002).
Non-canonical Wnt signalling and regulation of gastrulation movements.
Seminars in Cell & Developmental Biology **316**: 1–10.

Tada M & Smith JC. (2000).
Xwnt11 is a target of *Xenopus* Brachyury: regulation of gastrulation movements via Dishevelled, but not through the canonical Wnt pathway.
Development **127**: 2227–2238.

Takeuchi M, Nakabayashi J, Sakaguchi T, Yamamoto TS, Takahashi H, Takeda H & Ueno N. (2003).
The prickle-related gene in vertebrates is essential for gastrulation cell movements.
Current Biology **13**: 674–679.

Tao Q, Yokota C, Puck H, Kofron M, Birsoy B, Yan D, Asashima M, Wylie C, Lin X & Heasman J. (2005).
Maternal Wnt11 activates the canonical Wnt signalling pathway required for axis formation in *Xenopus* embryos.
Cell **120**: 857–871.

Taylor J, Abramova N, Charlton J & Adler PN. (1998).
Van Gogh: a new *Drosophila* tissue polarity gene.
Genetics **150**: 199–210.

Tear G, Harris R, Sutaria S, Kilomanski K, Goodman CS & Seeger MA. (1996).
commissureless controls growth cone guidance across the CNS midline in *Drosophila* and encodes a novel membrane protein.
Neuron **16**: 501–514.

Testaz S, Jarov A, Williams KP, Ling LE, Koteliansky VE, Fournier-Thibault C & Duband JL. (2001).
Sonic hedgehog restricts adhesion and migration of neural crest cells independently of the Patched-Smoothened-Gli signalling pathway.
PNAS **98**: 12521–12526.

Thorpe JL, Doitsidou M, Ho SY, Raz E & Farber SA. (2004).
Germ cell migration in zebrafish is dependent on HMGCoA reductase activity and prenylation.
Developmental Cell **6**: 295–302.

Topczewski J, Sepich DS, Myers DC, Walker C, Amores A, Lele Z, Hammerschmidt M, Postlethwait J & Solnica-Krezel L. (2001).
The zebrafish glypican Knypek controls cell polarity during gastrulation movements of convergent extension.
Developmental Cell **1**: 251–264.

Tree DR, Shulman JM, Rousset R, Scott MP, Gubb D & Axelrod JD. (2002).
Prickle mediates feedback amplification to generate asymmetric planar cell polarity signaling.
Cell **109**: 371–381.

Trowe T, Klostermann S, Baier H, Granato M, Crawford AD, Grunewald B, Hoffmann H, Karlstrom RO, Meyer SU, Müller B, Richter S, Nüsslein-Volhard C & Bonhoeffer F. (1996).
Mutations disrupting the ordering and topographic mapping of axons in the retinotectal projection of the zebrafish, *Danio rerio*.
Development **123**: 439–450.

Ulrich F, Concha ML, Heid PJ, Voss E, Witzel S, Roehl H, Tada M. Wilson SW, Adams RJ, Soll DR & Heisenberg CP. (2003).
Slb/Wnt11 controls hypoblast cell migration and morphogenesis at the onset of zebrafish gastrulation.
Development **130**: 5375–5384.

Ulrich F, Krieg M, Schötz EM, Link V, Castanon I, Schnabel V, Taubenberger A, Mueller D, Puech PH & Heisenberg CP. (2005).
Wnt11 functions in gastrulation by controlling cell cohesion through Rab5c and E-cadherin.
Developmental Cell **9**: 555–564.

Usui T, Shima Y, Shimada Y, Hirano S, Burgess RW, Schwarz TL, Takeichi M & Uemura T. (1999).
Flamingo, a seven-pass transmembrane Cadherin, regulates planar cell polarity under the control of Frizzled.
Cell **98**: 585–595.

van den Heuvel M & Ingham PW. (1996).
smoothened encodes a receptor-like serpentine protein required for *hedgehog* signalling.
Nature **382**: 547–551.

van Eeden FJ, Granato M, Schach U, Brand M, Furutani-Seiki M, Haffter P, Hammerschmidt M, Heisenberg CP, Jiang YJ, Kane DA, Kelsh RN, Mullins MC, Odenthal J, Warga RM, Allende ML, Weinberg ES & Nüsslein-Volhard C. (1996a).
Mutations affecting somite formation and patterning in the zebrafish, *Danio rerio*.
Development **123**: 153–164.

van Eeden FJ, Granato M, Schach U, Brand M, Furutani-Seiki M, Haffter P, Hammerschmidt M, Heisenberg CP, Jiang YJ, Kane DA, Kelsh RN, Mullins MC, Odenthal J, Warga RM & Nüsslein-Volhard C. (1996b).
Genetic analysis of fin formation in the zebrafish, *Danio rerio*.
Development **123**: 255–262.

Varga ZM, Wegner J & Westerfield M. (1999).
Anterior movement of ventral diencephalic precursors separates the primordial eye field in the neural plate and requires *cyclops*.
Development **126**: 5533–5546.

Veeman MT, Slusarski DC, Kaykas A, Louie SH & Moon RT. (2003).
Zebrafish *prickle*, a modulator of non-canonical *wnt/fz* signalling, regulates gastrulation movements.
Current Biology **13**: 680–685.

Vinson CR & Adler PN. (1987).
Directional non-cell autonomy and the transmission of polarity information by the *frizzled* gene of *Drosophila*.
Nature **329**: 549–551.

von der Hardt S, Bakkers J, Inbal A, Carvalho L, Solnica-Krezel L, Heisenberg CP & Hammerschmidt M. (2007).
The Bmp gradient of the zebrafish gastrula guides migrating lateral cells by regulating cell-cell adhesion.
Current Biology **17**: 1–13.

Wada H, Tanaka H, Nakayama S, Iwasaki M & Okamato H. (2006)
Frizzled3a and Celsr2 function in the neurepithelium to regulate migration of facial motor neurons in the developing zebrafish hindbrain.
Development **133**: 4749–4759.

Wallingford JB, Fraser SE & Harland RM. (2002a).
Convergent extension: the molecular control of polarized cell movement during embryonic development.
Developmental Cell **2**: 695–706.

Wallingford JB, Goto T, Keller R & Harland RM (2002b).
Cloning and expression of *Xenopus* Prickle, an orthologue of a *Drosophila* planar cell polarity gene.
Mechanisms of Development **116**: 183–186.

Wallingford JB, Rowning BA, Vogeli KM, Rothbächer U, Fraser SE & Harland RM. (2000).
Dishevelled controls cell polarity during *Xenopus* gastrulation.
Nature **405**: 81–85.

Wang J, Hamblet NS, Mark S, Dickinson ME, Brinkman BC, Segil N, Fraser SE, Chen P, Wallingford JB & Wishaw-Boris A. (2006).
Dishevelled genes mediate a conserved mammalian PCP pathway to regulate convergent extension during neurulation.
Development **133**: 1767–1778.

Wang KH, Brose K, Arnott D, Kidd T, Goodman CS, Henzel W & Tessier-Lavigne M. (1999).
Biochemical purification of a mammalian Slit protein as a positive regulator of sensory axon elongation and branching.
Cell **96**: 771–784.

Warga RM & Nüsslein-Volhard C. (1999).
Origin and development of the zebrafish endoderm.
Development **126**: 827–838.

Wehrli M & Tomlinson A. (1995).
Epithelial planar polarity in the developing *Drosophila* eye.
Development **121**: 2451–2459.

Westerfield M. (2000).
The Zebrafish Book. A guide for the laboratory use of zebrafish (Danio rerio) (4th Ed.).
University of Oregon Press, USA.

Westfall TA, Brimeyer R, Twedt J, Gladon J, Olberding A, Furutani-Seiki M & Slusarski DC. (2003).
Wnt-5/*pipetail* functions in vertebrate axis formation as a negative regulator of Wnt/ß-catenin activity.
Journal of Cell Biology **162**: 889–898.

Wilson P & Keller R. (1991).
Cell rearrangement during gastrulation in *Xenopus*: direct observation of cultured explants.
Development **112**: 289–300.

Wilson SW, Ross LS, Parrett T & Easter SS Jr. (1990).
The development of a simple scaffold of axon tracts in the brain of the embryonic zebrafish.
Development **108**: 121–145.

Winklbauer R & Keller RE. (1996).
Fibronectin, mesoderm migration, and gastrulation in *Xenopus.*
Developmental Biology **177**: 413–426.

Winklbauer R & Schürfeld M. (1999).
Vegetal rotation, a new gastrulation movement involved in the internalization of the mesoderm and endoderm in *Xenopus.*
Development **126**: 3703–3713.

Winter CG, Wang B, Ballew A, Royou A, Karess R, Axelrod JD & Luo L. (2001).
Drosophila Rho-associated kinase (Drok) links Frizzled-mediated planar cell polarity signaling to the actin cytoskeleton.
Cell **105**: 81–91.

Witzel S, Zimyanin V, Carreira-Barbosa F, Tada M & Heisenberg CP. (2006).
Wnt11 controls cell contact persistence by local accumulation of Frizzled7 at the plasma membrane.
Journal of Cell Biology **175**: 791–802.

Wolpert L, Beddington R., Brockes J, Jessell T, Lawrence P & Meyerowitz E. (1998).
Principles of Development (1st Ed.).
Oxford University Press, UK.

Wong LL & Adler PN. (1993).
Tissue polarity genes of *Drosophila* regulate the subcellular location for prehair initiation in pupal wing cells.
Journal of Cell Biology **123**: 209–221.

Woo K & Fraser SE. (1995).
Order and coherence in the fate map of the zebrafish nervous system.
Development **121**: 2595–2609.

Xanthos JB, Kofron M, Wylie C & Heasman J. (2001).
Maternal VegT is the initiator of a molecular network specifying endoderm in *Xenopus laevis.*
Development **128**: 167–180.

Yamashita S, Miyagi C, Carmany-Rampey C, Shimizu T, Fujii R, Schier AF & Hirano T. (2002).
Stat3 controls cell movements during zebrafish gastrulation.
Developmental Cell **2**: 363–375.

Yamashita S, Miyagi C, Fukada T, Kagara N, Che YS & Hirano T. (2004).
Zinc transporter LIV1 controls epithelial-mesenchymal transistion in zebrafish gastrula organizer.
Nature **429**: 298–302.

Ybot-Gonzalez P, Savery D, Gerelli D, Signore M, Mitchell CE, Faux CH, Greene ND & Copp AJ. (2007).
Convergent extension, planar–cell-polarity signalling and initiation of mouse neural tube closure.
Development **134**: 789–799.

Yeo SY, Little MH, Yamada T, Miyashita T, Halloran MC, Kuwada JY, Huh TL & Okamoto H. (2001).
Overexpression of a *slit* homologue impairs convergent extension of the mesoderm and causes cyclopia in embryonic zebrafish.
Developmental Biology **230**: 1–17.

Yuan SS, Cox LA, Dasika GK & Lee EY. (1999).
Cloning and functional studies of a novel gene aberrantly expressed in RB-deficient embryos.
Developmental Biology **207**: 62–75.

Zallen JA, Yi BA & Bargmann CI. (1998).
The conserved Immunoglobulin superfamily member SAX-3/Robo directs multiple aspects of axon guidance in *C. elegans*.
Cell **92**: 217–227.

Zerial M & McBride H. (2001).
Rab proteins as membrane organizers.
Nature Reviews Molecular Cell Biology **2**: 107–117.

Zhu AJ, Zheng L, Suyama K & Scott MP. (2003).
Altered localization of *Drosophila* Smoothened protein activates Hedgehog signal transduction.
Genes & Development **17**: 1240–1252.

Appendix One

Reagents & Solutions

General Fish Maintenance

Fish Medium

Aquarium water + few drops of Methylene Blue

Dissection Plates

1% Agarose (for everyday use) in H_2O (see below for 1X PBS recipe).

Approx. 2ml set in 10ml Sterilin plates

Paraformaldehyde Fix (PFA) for In Situ Hybridisation

4% Paraformaldehyde (PFA) dissolved in 1X PBS

DMSO Fix for Antibody Staining

20% DMSO	(100% stock)
80% Methanol	(100% stock)

Detection of mRNA & Protein

1X Phosphate Buffered Saline (PBS) for In Situ Hybridisation/ Antibody Staining

Dissolve 1 PBS tablet (OXOID BR0014G) per 100ml pure H_2O and autoclave.

- add 500µl of 10% Tween-20 to 50ml 1X PBS for PBS Tween (0.1%)
- add 500µl of 10% Triton to 50ml 1X PBS for PBS Triton (0.1%)
- add 2.5ml of 10% Triton to 50ml 1X PBS for PBS Triton (0.5%)

Methanol in PBS (50ml) for In Situ Hybridisation/Antibody Staining

75% 37.5ml Methanol (100% stock) + 12.5ml 1X PBS

50% 25ml Methanol (100% stock) + 25ml 1X PBS

25% 12.5% Methanol (100% stock) + 37.5ml 1X PBS

Proteinase K in PBS for In Situ Hybridisation/Antibody Staining

10μg/ml PK in 1X PBS (1.5μl/ml stock)

Hyb+ for In Situ Hybridisation	For 50ml:	
50% Formamide	25ml	(100% stock)
5X SSC (pH6)	12.5ml	(20X stock)
200μg/ml t-RNA	100μl	(100mg/ml stock)
100μg/ml Heparin	50μl	(100mg/ml stock)
1X Denhardt's Solution	1ml	(50X stock)
5mM EDTA	0.5ml	(500mM stock)
Autoclaved pure H_2O	10.35ml	

Hyb- for In Situ Hybridisation	For 20ml:	
50% Formamide	10ml	(100% stock)
2X SSC	2ml	(20X stock)
0.1% Tween-20	500μl	(10% stock)
Autoclaved pure H_2O to 20ml		

20X SSC (500ml) for In Situ Hybridisation

77.6g NaCl

44.1g $Na_3C_6H_5O_7.2H_2O$

400ml H_2O

Adjust to pH6

Autoclaved pure H_2O to 500ml

- 5ml 20X SSC + 500µl of 10% Tween-20 in 50ml H_2O = 2X SSCT
- 500µl 20X SSC + 500µl of 10% Tween-20 in 50ml H_2O = 0.2X SSCT

Maleic Acid Buffer for In Situ Hybridisation

0.1M Maleic Acid pH 7.5 (1X stock)

150mM NaCl (stock)

- add 500µl of 10% Triton for MABT (0.1% Triton)

Boerringer Blocking Solution for In Situ Hybridisation

2% BBR in MABT

Staining Buffer (50ml) for In Situ Hybridisation

2.5ml Tris.Cl pH9.5 (2M stock)

1ml NaCl (5M stock)

2.5ml $MgCl_2$ (1M stock)

100µl Levamisol (1M stock)

500µl Tween-20 (10% stock)

Autoclaved pure H_2O to 50ml

3,3' Diaminobenzidine (DAB) liquid for Antibody Staining

Inactive:

25µl DAB in 1.5ml 1X PBS

Active:

25µl DAB + 2.5µl H_2O_2 (30% stock) in 1.5ml 1X PBS

Pre-Antibody Staining Bleach Solution for Antibody Staining

1ml Methanol (100% stock) + 10µl H_2O_2 (30% stock)

Post-Antibody Staining Bleach Solution for Antibody Staining

0.4ml KOH (10% stock)

0.15ml H_2O_2 (30% stock)

in 5ml H_2O

Visualisation, Photography & Confocal

Glycerol in PBS for Visualisation & Photography

30% 15ml Glycerol (100% stock) + 35ml 1X PBS

50% 25ml Glycerol (100% stock) + 25ml 1X PBS

75% 37.5ml Glycerol (100% stock) + 12.5ml 1X PBS

80% 40ml Glycerol (100% stock) + 10ml 1X PBS

90% 45ml Glycerol (100% stock) + 10ml 1X PBS

Methyl Cellulose for Live Photography

2.5% Methyl Cellulose (100% stock) in fish water.

Hank's Embryonic Medium for Live Confocal Imaging

Solution 1:	Solution 2:	Solution 4:
4g NaCl	0.179g Na_2HPO_4	0.72g $CaCl_2$
0.2g KCl	0.3g $K_2H_2PO_4$	in 50ml pure H_2O
in 50ml pure H_2O	in 50ml pure H_2O	

Solution 5:	Solution 6 (made fresh on day of use):
1.23g $MgSO_4.7H_2O$	0.35g $NaHCO_3$
in 50ml pure H_2O	in 10ml pure H_2O

Final Solution (500ml):

Solution 1: 50ml

Solution 2: 5ml

Solution 4: 5ml

430ml H_2O

Solution 5: 5ml

Solution 6: 5ml

Adjust pH to 7.4

Make up to 500ml with pure H_2O

Agarose Aliquots in Hank's Embryonic Medium for Live Confocal Imaging

0.5% Low-Melt (Sigma Type VII) in Hank's Embryonic Medium

0.8% Low-Melt (Sigma Type VII) in Hank's Embryonic Medium

1% Low-Melt (Sigma Type VII) in Hank's Embryonic Medium

Agarose Dissection Plates for Live Confocal Imaging

1% Agarose (for everyday use) in Hank's Embryonic Medium

Approx. 2ml set in 10ml Sterilin plates

Molecular Work

50X Stock TAE Electrophoresis Buffer (500ml)

121g TRIZMA base

28.55ml Acetic Acid

9.3g EDTA

in 500ml pure H_2O

- dilute to 1X with autoclaved pure H_2O

0.8% Agarose Gel for Gel Electrophoresis (makes 2 gels)

0.64g Agarose (for everyday use)

in 80ml TAE

2μl Ethidium Bromide

NTP Cap Mix for In Vitro Transcription of mRNA

5μl ATP	(100mM stock)
5μl UTP	(100mM stock)
5μl CTP	(100mM stock)
5μl GTP	(10mM stock)
25μl RNA cap	(100mM stock)

1X HEPES Buffer for dilution of morpholinos

5mM HEPES pH7

200mM KCl

5X Running Buffer for Western Blotting

7.5g Trizma base (Tris.Cl)

47g Glycine

20% SDS (0.94ml)

in 500ml pure H_2O

1X Blotting Buffer for Western Blotting

1.57g Tris.Cl

14.48g Glycine

20% SDS (0.94ml)

200ml Methanol

in 500ml pure H_2O

10% SDS PAGE 2-Layered Gel for Western Blotting

	Upper Gel (10ml)	Lower Gel (10ml)
30% Acrylamide	1.6ml	3.3ml
0.5M Tris.Cl (pH6.8)	2.5ml	-
1.5M Tris.Cl (pH8.8)	-	2.5ml
H_2O	5.7ml	4ml
20% SDS	0.05ml	0.05ml
10% APS	0.1ml	0.1ml
TEMED	10µl	10µl

Appendix Two

Phenotypes

One of the greatest challenges facing those studying convergent extension is how to quantify the effects of gain or loss of function of genes known to regulate aspects of cell behaviour during gastrulation. Future characterisation of the role of *pk1b*, Slit/Robo signalling and *airbag* (*abg*) in the regulation of gastrulation movements will have to satisfy this need for quantification. Measurement of phenotypic aspects at 24hpf, such as length of anteroposterior body axis, angle of curvature of the body axis, angle of eversion of the tail, dimensions of yolk extension, in concert with measurement of phenotypic aspects at 10hpf such as notochord dimensions, neural plate dimensions and position of the prechordal plate will be useful for the creation of a benchmark database of phenotypes to render results less subjective and more meaningful. Due to constraints of time, I was unfortunately unable to measure phenotypic aspects of the mutants and morphants presented in this thesis in this way.

However, in an attempt to make my observations less qualitative and more quantitative, I have constructed a pictorial scoring system for their major characteristics. Examination of the relative severity of defects resulting from impaired convergent extension in this way has allowed me to more than qualitatively differentiate between the 'mild', 'moderate', 'severe' and 'very severe' CE defects cited throughout this thesis.

Key to 24hpf scoring chart:

Body length: 0 = indistinguishable from WT; 1 = body axis slightly shorter than WT; 2 = body axis noticeably shorter than WT; 3 = strong shortening of body axis; 4 = severely shortened body axis.
Body curvature: 0 = indistinguishable from WT; 1 = gentle curvature or kinking in part; 2 = axis curling throughout body; 3 = strong curling of body axis; 4 = extreme curvature of body axis.
Yolk extension: 0 = indistinguishable from WT; 1 = slightly thicker than WT but not shorter; 2 = thicker and shorter than WT; 3 = very thick and short; 4 = poorly defined from body of yolk.
Eye fusion: 0 = indistinguishable from WT; 1 = slightly smaller eyes than WT; 2 = eyes medially closer together than WT; 3 = partial fusion; of the eyes; 4 = cyclopia.

24hpf scoring chart:

Mutant/Morphant	Score	Body Length	Body Curvature	Yolk Extension	Eye Fusion
WT 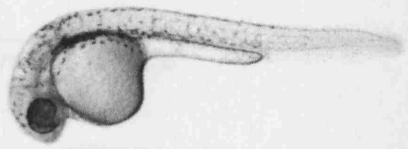	N/A	N/A	N/A	N/A	N/A
WT + *slit3*-MO 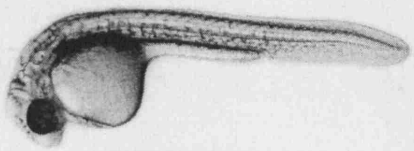	WT-like	0	0	0	0
abg sibling 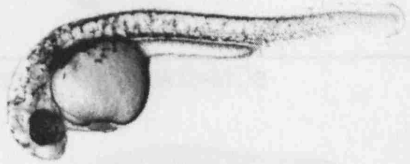	WT-like	0	0	0	0
WT + *robo3v1*-MO 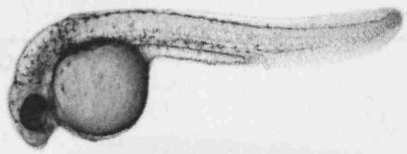	WT-like	0	0	0	0
WT + *slit2* + *robo2* 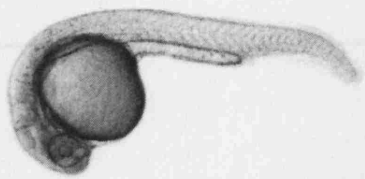	WT-like	0	0	0	0

WT + *slit2* + *robo3v1* 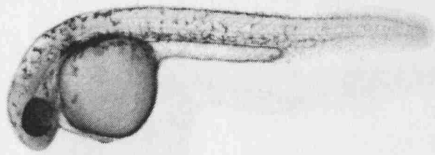	WT-like	0	0	0	0
ord + *pk1b*-MOa 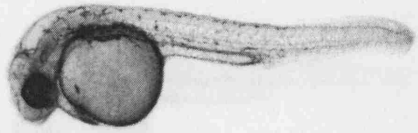	WT-like	0	0	0	0
WT + *pk1b*-MO 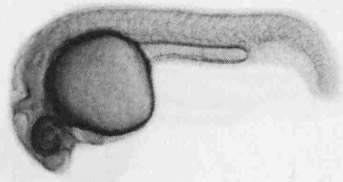	mild	1	0	0	1
abg sibling + *pk1b*-MOa 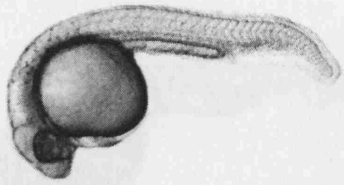	mild	1	0	0	1
slb 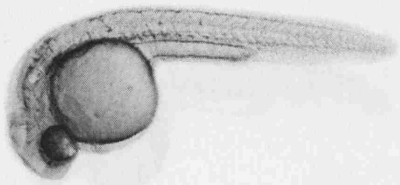	mild	1	0	0	2

slb + *pk1b*-MOa 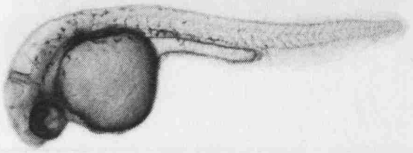	mild	1	0	0	3
WT + *lyn-robo2(ICD)-GFP* 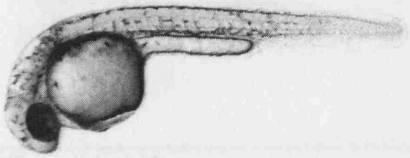	mild	1	0	1	0
WT + *robo2* 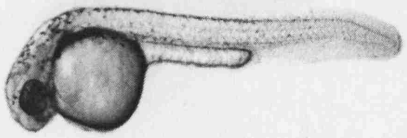	mild	1	0	1	0
WT + *robo3v2* 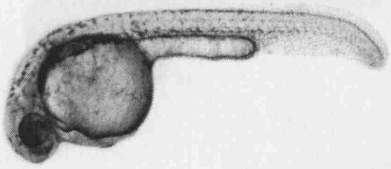	mild	1	0	2	0
WT + *robo2*-MO + *pk1b*-MOa 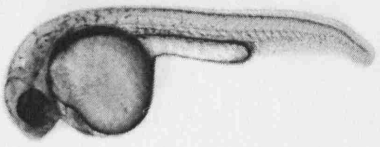	mild	1	0	2	0

tri sibling + *pk1b*-MO 	mild	1	0	1	1
abg 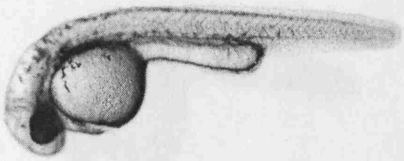	mild	1	0	2	1
WT + *slit1a*-MO 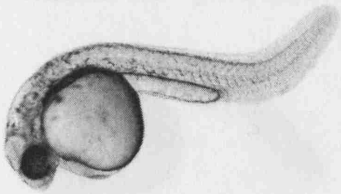	mild	1	1	1	0
WT + *slit2* + *robo3v2* 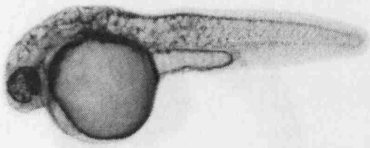	mod	2	0	2	1
WT + *robo3v2* + *pk1a* 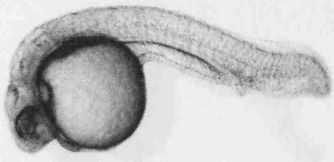	mod	2	1	0	1

WT + *robo3v2*-MO 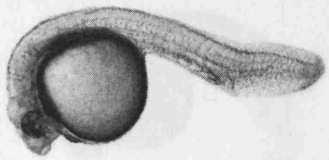	mod	2	1	0	1
WT + *slit1a*-MO + *pk1b*-MOa 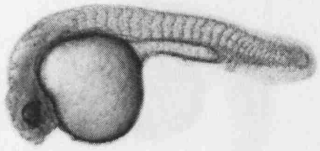	mod	2	1	1	1
WT + *robo3v2*-MO + *pk1b*-MOa 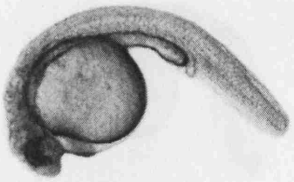	mod	2	1	1	1
WT + *slit2*-MO 	mod	2	1	2	1
WT + *slit2*-MO + *pk1b*-MOa 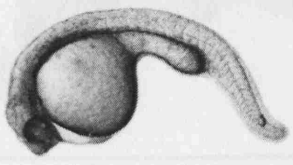	mod	2	1	2	1

WT + *pk1a*-MO 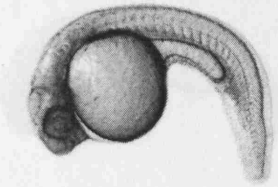	mod	2	2	2	1
ord + *pk1a*-MO 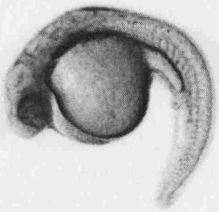	mod	2	2	2	1
abg sibling + *pk1a*-MO 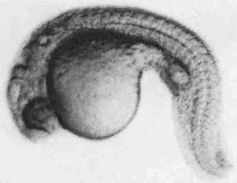	mod	2	2	2	1
WT + *slit1a*-MO + *pk1a*-MO 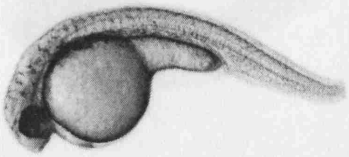	mod	2	1	3	0
abg-/-;slb+/- 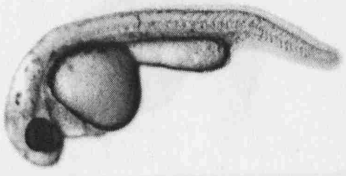	mod	2	1	3	0

abg + *pk1b*-MOa 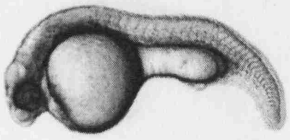	severe	3	2	3	1
abg-/-;slb-/- 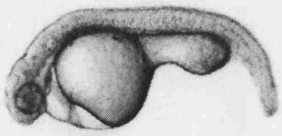	severe	3	2	3	1
WT + *robo3v2(ECD/TM)-GFP* 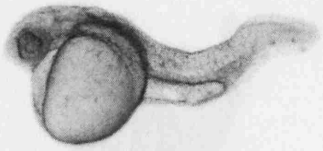	severe	3	3	2	1
WT + *slit2* + *robo3v2(ECD/TM)-GFP* 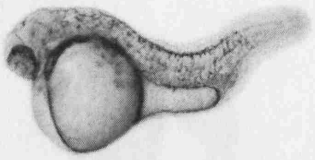	severe	3	3	2	4
WT + *slit2*-MO + *pk1a*-MO 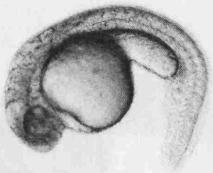	severe	3	3	3	1

abg + *pk1a*-MO 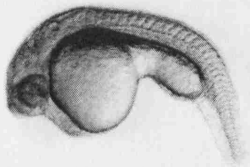	severe	3	3	3	1
WT + *pk1a*-MO + *pk1b*-MOa 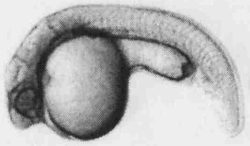	severe	3	3	3	1
WT + *slit2* 	severe	3	3	3	4
WT + *robo2*-MO + *pk1a*-MO 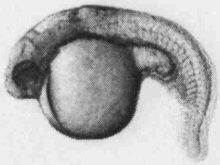	very severe	4	4	4	1
ppt 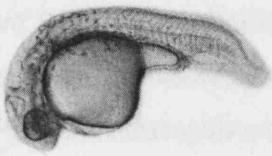	very severe	4	4	4	1

tri 	very severe	4	4	4	0
kny 	very severe	4	4	4	1
tri + *pk1b*-MOa 	very severe	4	4	4	1
WT + *lyn-robo3(ICD)-GFP* 	very severe	4	4	4	1

<u>*Key to 10hpf scoring chart*</u>:

Notochord: 0 = indistinguishable from WT; 1 = slightly thicker than WT; 2 = thicker still and shorter than WT; 3 = moderately severe thickening/shortening; 4 = severe thickening/shortening.

Neural Plate: 0 = indistinguishable from WT; 1 = slightly wider than WT; 2 = both wider and shorter than WT; 3 = moderately severely wider and shorter than WT; 4 = extremely wide/short.

Prechordal Plate: 0 = indistinguishable from WT; 1 = misshapen relative to WT; 2 = only halfway across anterior border of neural plate; 3 = only one-third across anterior border of neural plate; 4 = totally behind anterior border of neural plate.

10hpf scoring chart:

Mutant/Morphant	Score	Notochord	Neural Plate	Prechordal Plate
WT 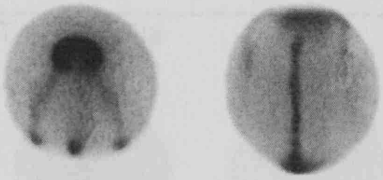	N/A	N/A	N/A	N/A
abg sibling 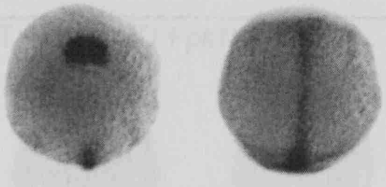	WT-like	0	0	0
abg sibling + *pk1b*-MOa 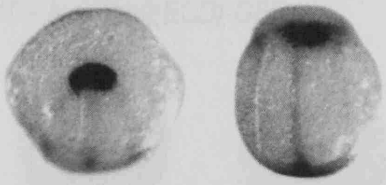	WT-like	0	0	0
WT + *robo3v2(ECD/TM)-GFP* 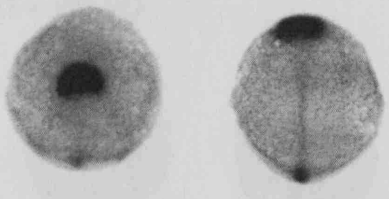	WT-like	0	0	0
WT + *robo3v2* 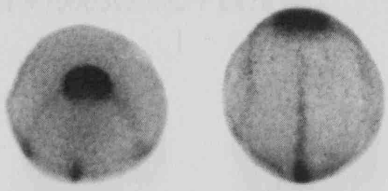	WT-like	0	0	0

WT + *robo2* 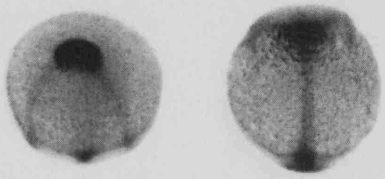	WT-like	0	0	0
WT + *pk1b*-MOa 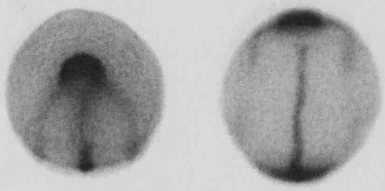	WT-like	0	0	0
WT + *robo2*-MO + *pk1a*-MO 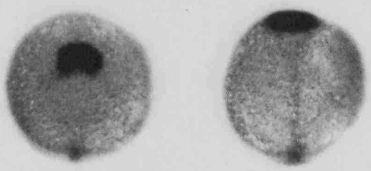	mild	0	1	0
WT + *lyn-robo2(ECD)-GFP* 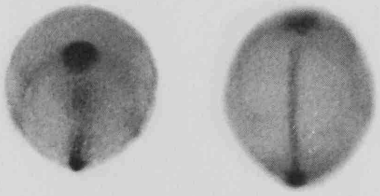	mild	0	1	1
WT + *slit2*-MO 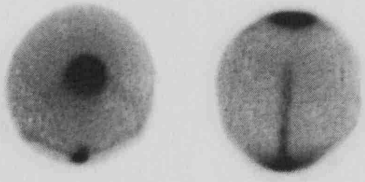	mild	1	0	1
WT + *robo3v2*-MO + *pk1a*-MO 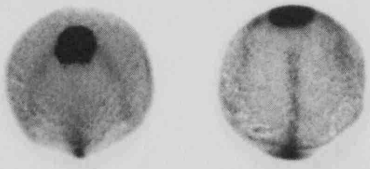	mild	1	0	2

WT + *robo3v2*-MO 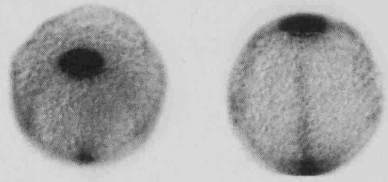	mild	1	1	1
WT + *slit2* + *robo2* 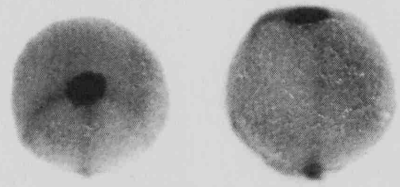	mild	1	2	1
abg sibling + *pk1a*-MO 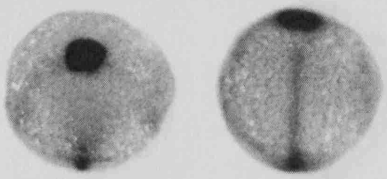	mild	1	2	1
WT + *robo2*-MO + *pk1b*-MOa 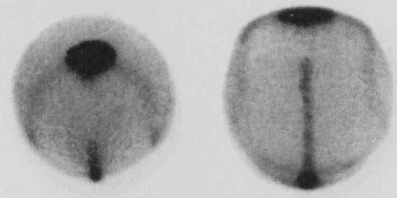	mild	1	2	1
WT + *slit1a*-MO + *pk1b*-MOa 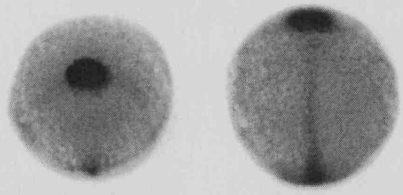	mild	1	2	1
WT + *slit2*-MO + *pk1b*-MOa 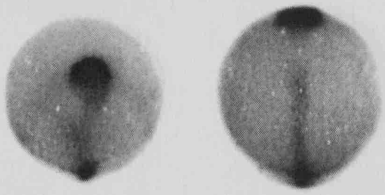	mild	2	2	1

WT + *pk1a*-MO 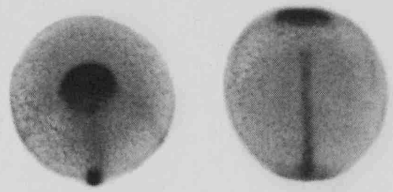	mod	2	2	2
WT + *slit1a*-MO 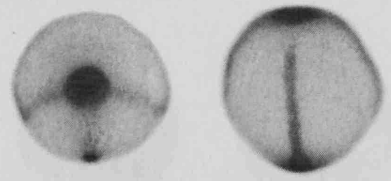	mod	2	3	2
WT + *slit2*-MO + *pk1a*-MO 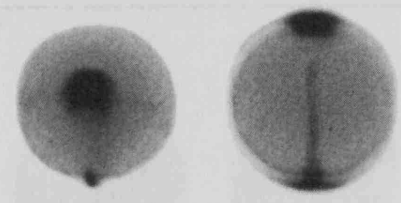	mod	2	3	2
lyn-robo3(ICD)-GFP GOF 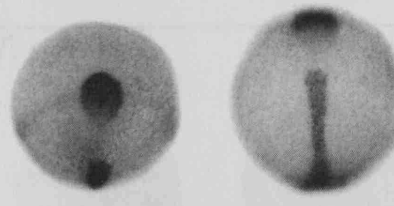	mod	3	3	2
WT + *slit1a*-MO + *pk1a*-MO 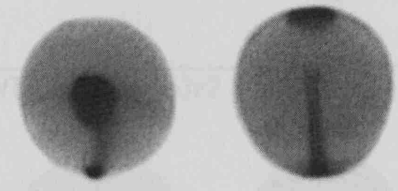	mod	3	3	2
WT + *slit3*-MO 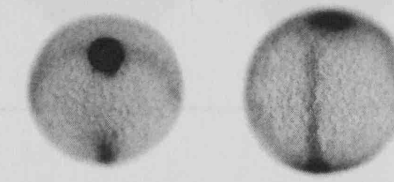	severe	3	4	3

WT + *robo3v2*-MO + *pk1b*-MOa 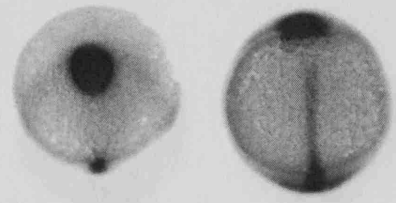	severe	3	4	3
WT + *robo3v1* 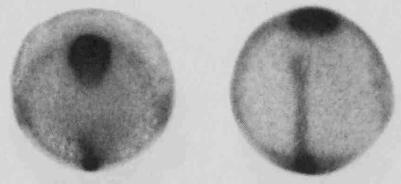	severe	3	4	3
tri 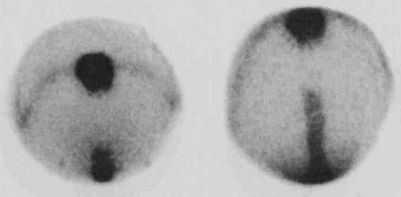	severe	4	4	3
WT + *slit2* 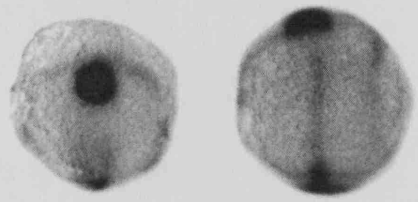	very severe	3	4	4
WT + *slit2* + *robo3v2* 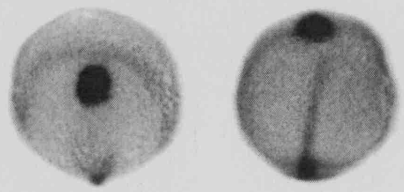	very severe	3	4	4

slb 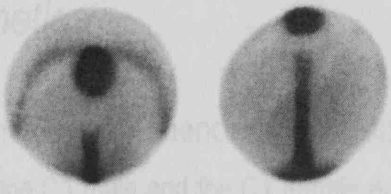	very severe	4	4	4
abg-/-;slb-/- 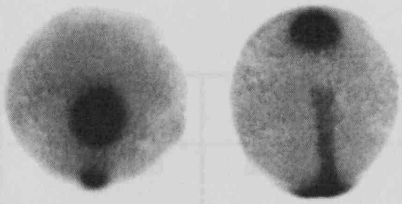	very severe	4	4	4
abg + *pk1a*-MO 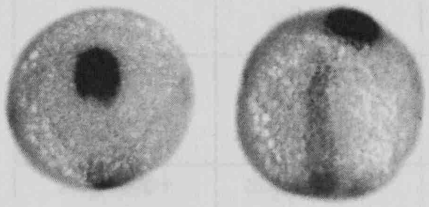	very severe	4	4	4

Appendix Three

Genetics

C1 Incross: 3/4 phenotypically wildtype and 1/4 phenotypically *abg-/-*.

Both the C1 male and the C1 female are of the genotype *abg+/-*:(*slb+/+*). The possible combinations of alleles in the gametes of both parents are therefore: *abg+*:*slb+*, *abg+*:*slb+*, *abg-*:*slb+* and *abg-*:*slb+*.

		C1 PARENT: *abg+/-*:(*slb+/+*)			
	GAMETES	***abg+*:*slb+***	***abg+*:*slb+***	***abg-*:*slb+***	***abg-*:*slb+***
C1 PARENT: *abg+/-*:(*slb+/+*)	***abg+*:*slb+***	*abg+/+*:*slb+/+* wildtype	*abg+/+*:*slb+/+* wildtype	*abg+/-*:*slb+/+* *abg* het	*abg+/-*:*slb+/+* *abg* het
	abg+*:*slb+	*abg+/+*:*slb+/+* wildtype	*abg+/+*:*slb+/+* wildtype	*abg+/-*:*slb+/+* *abg* het	*abg+/-*:*slb+/+* *abg* het
	abg-*:*slb+	*abg+/-*:*slb+/+* *abg* het	*abg+/-*:*slb+/+* *abg* het	*abg-/-*:*slb+/+* *abg* hom	*abg-/-*:*slb+/+* *abg* hom
	abg-*:*slb+	*abg+/-*:*slb+/+* *abg* het	*abg+/-*:*slb+/+* *abg* het	*abg-/-*:*slb+/+* *abg* hom	*abg-/-*:*slb+/+* *abg* hom

Genotypes resulting:

25% wildtype; 50% heterozygous *abg* and 25% homozygous *abg*.

Phenotypes at 24hpf:

75% indistinguishable from wildtype: (wildtype and *abg+/-* proportions) 25% *abg-/-* (*abg-/-* proportion).

Phenotypes at 10hpf:

100% indistinguishable from wildtype (wildtype, *abg+/-* and *abg-/-* proportions)

C1 Backcross: 100% phenotypically wildtype.

Backcrossing either C1 parent of the genotype *abg+/-:slb+/+* with (*abg+/+*):*slb-/-* carriers does not produce embryos of the genotype *slb-/-*, confirming that C1 *abg* carriers do not carry one copy of the *slb* gene. The possible combinations of alleles in the gametes of the C1 parent are: *abg+:slb+*, *abg+:slb+*, *abg-:slb+* and *abg-:slb+*. The possible combinations of alleles in the gametes of the *slb-/-* parent are: *abg+:slb-*, *abg+:slb-*, *abg+:slb-* and *abg+:slb-*.

		slb* PARENT: (*abg+/+*):*slb-/-			
	GAMETES	***abg+:slb-***	***abg+:slb-***	***abg+:slb-***	***abg+:slb-***
C1 PARENT: *abg+/-:(slb+/+)*	***abg+:slb+***	*abg+/+:slb+/-* *slb* het	*abg+/+:slb+/-* *slb* het	*abg+/+:slb+/-* *slb* het	*abg+/+:slb+/-* *slb* het
	abg+:slb+	*abg+/+:slb+/-* *slb* het	*abg+/+:slb+/-* *slb* het	*abg+/+:slb+/-* *slb* het	*abg+/+:slb+/-* *slb* het
	abg-:slb+	*abg+/+:slb+/-* *slb* het	*abg+/+:slb+/-* *slb* het	*abg+/-:slb+/-* double het	*abg+/-:slb+/-* double het
	abg-:slb+	*abg+/+:slb+/-* *slb* het	*abg+/+:slb+/-* *slb* het	*abg+/-:slb+/-* double het	*abg+/-:slb+/-* double het

Genotypes resulting:

75% heterozygous *slb* and 25% double heterozygote (*abg+/-:slb+/-*).

Phenotypes resulting at 24hpf:

100% indistinguishable from wildtype (*slb+/-* and *abg+/-:slb+/-* proportions).

Phenotypes at 10hpf:

100% indistinguishable from wildtype (*slb+/-* and *abg+/-:slb+/-* proportions).

C2 Incross: several distinct populations, divisible by phenotype.

Both the C2 male and the C2 female are of the genotype *abg+/-:slb+/-*. The possible combinations of alleles in the gametes of both parents are therefore: *abg+:slb+*, *abg+:slb-*, *abg-: slb+* and *abg-:slb-*.

		C2 PARENT: *abg+/-:slb+/-*			
	GAMETES	***abg+:slb+***	***abg+:slb-***	***abg-:slb+***	***abg-:slb-***
C2 PARENT: *abg+/-:slb+/-*	***abg+:slb+***	*abg+/+:slb+/+* wildtype	*abg+/+:slb+/-* *slb* het	*abg+/-:slb+/+* *abg* het	*abg+/-:slb+/-* double het
	abg+:slb-	*abg+/+:slb+/-* *slb* het	*abg+/+:slb-/-* *slb* hom	*abg+/-:slb+/-* double het	*abg+/-:slb-/-* *slb* hom+
	abg-:slb+	*abg+/-:slb+/+* *abg* het	*abg+/-:slb+/-* double het	*abg-/-:slb+/+* *abg* hom	*abg-/-: slb+/-* *abg* hom+
	abg-:slb-	*abg+/-:slb+/-* double het	*abg+/-:slb-/-* *slb* hom+	*abg-/-: slb+/-* *abg* hom+	*abg-/-:slb-/-* double hom

Genotypes resulting:

6.25% wildtype; 12.5% *slb+/-*; 6.25% *slb+/-*; 12.5% *abg+/-*; 6.25% *abg-/-*; 25% double heterozygote (*abg+/-:slb+/-*); 12.5% *abg-/-* plus one copy of the *slb* gene (*abg-/-:slb+/-*); 12.5% *slb-/-* plus one copy of the *abg* gene (*abg+/-:slb-/-*); 6.25% double homozygote (*abg-/-: slb-/-*).

Phenotypes at 24hpf:

In the ratio 10:3:1:1:1, 62.5% are phenotypically wildtype (wildtype, *slb+/-*, *abg+/-* and *abg+/-:slb+/-* proportions); 18.75% phenotypically *abg-/-* (*abg-/-* and *abg-/-:slb+/-* proportions); 6.25% phenotypically *slb-/-* (*slb-/-* proportion); 6.25% *slb-/-* enhanced by one copy of the *abg* gene (*abg+/-:slb-/-* proportion) and 6.25% *slb-/-* enhanced by two copies of the *abg* gene (*abg-/-:slb-/-* proportion).

Phenotypes at 10hpf:

81.25% are phenotypically wildtype (wildtype, *slb+/-*, *abg+/-*, *abg+/-:slb+/-*, *abg-/-* and *abg-/-:slb+/-* proportions), 6.25% *slb-/-* (*slb-/-* proportion) and 12.5% enhanced *slb-/-* (*abg+/-:slb-/-* and *abg-/-:slb-/-* proportions).

C2 Backcross: several distinct populations, divisible by phenotype.

Backcrossing either C2 parent of the genotype *abg+/-:slb+/-* with (*abg+/+*):*slb-/-* carriers produces embryos of the genotype *slb-/-*, confirming that C2 *abg* carriers each carry one copy of the *slb* gene. The possible combinations of alleles in the gametes of the C2 parent are: *abg+:slb+*, *abg+:slb-*, *abg-:slb+* and *abg-:slb-*. The possible combinations of alleles in the gametes of the *slb-/-* parent are: *abg+:slb-*, *abg+:slb-*, *abg+:slb-* and *abg+:slb-*.

		slb* PARENT: (*abg+/+*):*slb-/-			
	GAMETES	***abg+:slb-***	***abg+:slb-***	***abg+:slb-***	***abg+:slb-***
C2 PARENT: *abg+/-:slb+/-*	***abg+:slb+***	*abg+/+:slb+/-* *slb* het	*abg+/+:slb+/-* *slb* het	*abg+/+:slb+/-* *slb* het	*abg+/+:slb+/-* *slb* het
	abg+:slb-	*abg+/+: slb-/-* *slb* hom	*abg+/+: slb-/-* *slb* hom	*abg+/+: slb-/-* *slb* hom	*abg+/+: slb-/-* *slb* hom
	abg-:slb+	*abg+/-:slb+/-* double het	*abg+/-:slb+/-* double het	*abg+/-:slb+/-* double het	*abg+/-:slb+/-* double het
	abg-:slb-	*abg+/-:slb-/-* *slb* hom+	*abg+/-:slb-/-* *slb* hom+	*abg+/-:slb-/-* *slb* hom+	*abg+/-:slb-/-* *slb* hom+

Genotypes resulting:

25% heterozygous *slb*; 25% homozygous *slb*; 25% double heterozygous (*abg+/-:slb+/-*) and 25% homozygous *slb* enhanced by one copy of the *abg* gene (*abg+/-:slb-/-*).

Phenotypes at 24hpf:

In the ratio 8:4:4, 50% are wildtype (*slb+/-* and *abg+/-:slb+/-*proportions); 25% homozygous *slb* (*slb-/-* proportion) and 25% homozygous *slb* enhanced by one copy of the *abg* gene (*abg+/-:slb-/-*).

Phenotypes at 10hpf:

In the ratio 8:4:4, 50% are wildtype (*slb+/-* and *abg+/-:slb+/-*proportions); 25% homozygous *slb* (*slb-/-* proportion) and 25% homozygous *slb* enhanced by one copy of the *abg* gene (*abg+/-:slb-/-*).

C6 x C7 Incross: several distinct genotypes.

C7 *abg* carriers are of the genotype *abg+/-*:(*slb+/+*), identical to the C1 carrier pair, while C6 *abg* carriers are of the genotype *abg+/-*: *slb-/-*, identical to the C2 carrier pair. Incrossing these carriers yields several different genotypes, translating into two distinct phenotypes at 24hpf. The possible combinations of alleles in the gametes of the C7 parent are: *abg+*:*slb+*, *abg+*:*slb+*, *abg-*:*slb+* and *abg-*:*slb+*. The possible combinations of alleles in the gametes of the C6 parent are: *abg+*:*slb+*, *abg+*:*slb-*, *abg-*: *slb+* and *abg-*:*slb-*.

		C6 PARENT: *abg+/-:slb+/-*			
	GAMETES	***abg+:slb+***	***abg+:slb-***	***abg-:slb+***	***abg-:slb-***
C7 PARENT: *abg+/-:(slb+/+)*	***abg+:slb+***	*abg+/+:slb+/+* wildtype	*abg+/+:slb+/-* *slb* het	*abg+/-:slb+/+* *abg* het	*abg+/-:slb+/-* double het
	abg+:slb+	*abg+/+:slb+/+* wildtype	*abg+/+:slb+/-* *slb* het	*abg+/-:slb+/+* *abg* het	*abg+/-:slb+/-* double het
	abg-:slb+	*abg+/-:slb+/+* *abg* het	*abg+/-:slb+/-* double het	*abg-/-:slb+/-* *abg* hom	*abg-/-:slb+/-* *abg* hom+
	abg-:slb+	*abg+/-:slb+/+* *abg* het	*abg+/-:slb+/-* double het	*abg-/-:slb+/-* *abg* hom	*abg-/-:slb+/-* *abg* hom+

Genotypes resulting:

12.5% wildtype; 12.5% heterozygous *slb*; 25% heterozygous *abg*; 25% double heterozygous (*abg+/-*: *slb+/-*); 12.5% homozygous *abg* and 12.5% homozygous *abg* plus one copy of the *slb* gene.

Phenotypes at 24hpf:

75% wildtype (wildtype; *slb+/-*; *abg+/-* and *abg+/-*:*slb+/-* proportions); 25% *abg-/-* (*abg-/-* and *abg-/-*: *slb-/-* proportions).

Phenotypes at 10hpf:

100% wildtype (wildtype; *slb+/-*; *abg+/-*; *abg+/-*:*slb+/-*; *abg-/-* and *abg-/-*:*slb+/-* proportions) .